Faculty of Science and Engineering

Analysis of Various Complex Flows of Micropolar Fluids in the Slip Flow Regime

Muhammad Kamran

This thesis is presented for the Degree of
Doctor of Philosophy
of
Curtin University

November 2018

Declaration

I, *Muhammad Kamran*, certify that this thesis has been substantially accomplished during enrolment in the degree. This thesis does not contain material which has been accepted for the award of any other degree or diploma in my name, in any university or other tertiary institution.

No part of this work will, in future, be used in a submission with my name, for any other degree or diploma in any university or other tertiary institution without the prior approval of the **Curtin University** and where applicable, any partner institution responsible for the joint-award of this degree.

This thesis does not contain any material previously published or written by another person, except where due acknowledgment/reference has been made in the text. The presented research has been published during my PhD studies and cited with Digital Object Identifiers (DOIs) at the beginning of chapters contained in. Where applicable, a permission has been granted from the respective editor(s) to reproduce (use as it is) the material in this thesis. For detailed information, please see the appendix B.

Muhammad Kamran

Signature:

Date: November 2, 2018 at 15:14:24

Abstract

This thesis comprises a body of work that investigates heat and mass transfer of micropolar fluids over a stretching/shrinking sheet with slip and the Newtonian heating conditions at the boundary. Various aspects of the complex flows such as heat source/sink, thermal radiation and the Hall effect on the magneto-micropolar fluid flow, and the transfer of mass with chemical reaction are investigated. Four mathematical models are formulated and transformed into systems of nonlinear differential equations with mixed derivative boundary conditions.

The system of governing flow equations is solved by using a semi-analytical technique called Homotopy Analysis Method (HAM). Under some special cases, the obtained solutions are found to be in an excellent agreement with the analytical and numerical solutions in the literature.

The presented analytical study reveals that when sheet stretches, the first and second order slip parameters significantly enhances the slip effects in the micropolar fluid flow with radiation and chemical reactions, respectively. In case of shrinking sheet, slip effect considerably increases with an increase in the first and second order slip parameters in heat source/sink and the radiative magneto-micropolar fluid flow models. A steady state heat transfer model for the Hall current shows a dramatic enhancement in the thermal boundary layer thickness of the micropolar fluid flow over a stretching/shrinking sheet with an increase in the Newtonian heating parameter.

Acknowledgments

I am thankful to my supervisor, Associate Professor Benchawan Wiwatanapataphee and co-supervisor Professor Yong Hong Wu for their guidance and support. Their helpful suggestions and encouragement have been of the great value to me in the research and the thesis preparation. I would also like to thank associate Professor Grant Keady for his helpful discussion. I am very grateful to the Curtin University for the financial support during the period of my study. I would also like to thank the Department of Mathematics and Statistics for providing me with the necessary facilities. Furthermore, It is my pleasure to mention about my lab-mates named as Samira Shaban Albrbar, Mehdi Ghasem Moghadam, Kobamelo Mashaba, Shican Liu, Yu Yang, Chong Lai and Rui Li for their moral support and fruitful research discussion. Lastly, I would like to share my gratitudes to my family specially my father (late: He passed away during my second year of PhD, may his soul rest in peace), my mother and my wife who gave me moral and emotional support during the period of my study at Curtin University, Australia.

List of Publications

This thesis contains work that has been published and/or in press for publication. Approval from the respective authorities has been granted and attached in the appendix B.

- Muhammad Kamran, Heat source/sink and Newtonian heating effects on convective micropolar fluid flow over a stretching/shrinking sheet with slip flow model. International Journal of Heat and Technology, Vol. 36, No. 2 (2018), 473-482. https://doi.org/10.18280/ijht.360212

- Muhammad Kamran and Benchawan Wiwatanapataphee, Radiative magneto-micropolar fluid flow over a stretching/shrinking sheet with slip flow model. Journal of Physics: Conference Series Vol. 1123, No. 1 (2018) 012034 (9 pages). https://doi.org/10.1088/1742-6596/1123/1/012034

- Muhammad Kamran, Benchawan Wiwatanapataphee and Kuppalapalle Vajravelu, Hall current, Newtonian heating and second order slip effects on convective magneto-micropolar fluid flow over a sheet. International Journal of Modern Physics C, Vol. 29, No. 9 (2018) 1850090 (24 pages). https://doi.org/10.1142/S0129183118500900

- M. Kamran and Benchawan Wiwatanapataphee, Chemical reaction and Newtonian heating effects on steady convection flow of a micropolar fluid with second order slip at the boundary. European Journal of Mechanics-B/Fluids, 71 (2018): 138-150. https://doi.org/10.1016/j.euromechflu.2018.04.005

Contents

List of Figures

List of Tables

Nomenclature

A	constant coefficient for mean free path
a	positive dimensional constant, s^{-1}
$\mathfrak{A}$	constant coefficient
$\mathbf{B}$	magnetic field vector
$\mathfrak{B}$	constant coefficient
B	square of constant mean free path, m^2
B_o	transverse magnetic field, Wb m^{-1}
C	concentration of the species
C_∞	ambient concentration of the species
C_{f_x}	local skin friction coefficient
C_m	dimensionless chemical reaction parameter
c_p	specific heat at constant pressure, $JK^{-1}Kg^{-1}$
$\mathfrak{C}$	constant coefficient
$\frac{D}{Dt}$	material derivative
D_m	mass diffusivity, m$^2s^{-1}$
d	molecular mean free path, m
$\mathfrak{D}$	constant coefficient
$\mathbf{E}$	electric field vector
e	electric charge, C
$\mathfrak{E}$	constant coefficient
$\mathbf{f}$	body force
f	dimensionless velocity
f_w	dimensionless suction/injection parameter
g	gravitational acceleration, ms^{-2}
Gr_x	dimensionless local Grashof number
h_s	surface heat transfer coefficient, Wm$^{-2}K^{-1}$
h	dimensionless microrotational velocity
$\mathbf{J}$	electric current density vector
j	microinertia per unit mass, m^2
K	dimensionless material parameter
k	thermal conductivity, Wm$^{-1}K^{-1}$

k_n	Knudsen number
$\mathbf{l}$	body couple per unit mass
l	constant
M	dimensionless Magnetic field parameter
m	Hall parameter
M_x	local wall couple stress
n_e	number of charge on the electron density
Nu_x	local Nusselt number
p	pressure
Pr	dimensionless Prandtl number
Q_o	dimensional heat source/sink parameter
Q	dimensionless heat source/sink parameter
q_r	radiative heat flux
R	dimensionless thermal radiation parameter
Re_x	dimensionless local Reynolds number
s	constant for stretching(> 0)/shrinking(< 0) sheet
Sc	Schmidt number
T	fluid temperature, K
T_∞	temperature of the ambient fluid, K
u	horizontal velocity component, ms^{-1}
v	transverse velocity component, ms^{-1}
w	normal to u and v velocity component, ms^{-1}
$\mathbf{V}$	velocity vector
v_o	suction/injection velocity, ms^{-1}
x	horizontal direction, m
y	transverse directions, m
z	perpendicular to x and y, m

Greek Letters

α	dimensionless first order slip parameter
α_ν	constants material properties
β	dimensionless second order slip parameter
β_T	coefficient of thermal expansion, K^{-1}
β_c	coefficient of thermal expansion with concentration
β_ν	constants material properties
γ	spin gradient viscosity coefficient, $Kgms^{-1}$
γ_ν	constants material properties
δ	dimensionless Newtonian heating parameter
ϵ	momentum accommodation coefficient

θ	dimensionless temperature
λ	dimensionless buoyancy parameter
λ_ν	constants material properties
Λ	concentration to thermal buoyancy ratio parameter
μ	dynamic viscosity, Nsm^{-2}
ν	kinematic viscosity, m^2s^{-1}
ψ	stream function, m^2s^{-1}
ρ	fluid density, Kgm^{-3}
χ	microrotation viscosity,$Kgm^{-1}s^{-1}$
ω	microrotational velocity (cartesian), ms^{-1}
σ	electrical conductivity
ξ	first order homogeneous constant reaction rate, s^{-1}

Sub Scripts

w	wall
∞	free stream

Chapter 1

Introduction

1.1 Background of Research

Over the last two decades, a great deal of research has been carried out to study the micropolar fluid flows. Micropolar fluids belong to a subclass of simple microfluids with non-symmetric stress tensor and present the micro-rotational inertia and micro-rotational effects. Geometrically, they consist of randomly oriented rigid spherical micro-particles suspended in a viscous medium where the deformation of these particles is not considered. The physical properties and behaviour of this viscous medium are affected by the prescribed micro-particles contained in each of its volume element. The theory of simple microfluids and micropolar fluids was proposed by Eringen [1–3]. Various concepts, which are not given in the classic fluid mechanics, were introduced including the inertial spin, body moments, micro-stress averages and stress moments. The effects of micro-structured particles are modelled with the help of an additional transport equation by representing the local angular momentum and in addition to some extra constitutive parameters, which are not reported in the classical Navier-Stokes theory of fluid mechanics. Eringen [4] later extended the existed theory to thermo micropolar fluids to study the heat conduction and heat dissipation effects. He explained other aspects of this theory in [5, 6]. For instant, he reported the exposition of microcontinuum field theories such as micropolar, microstretch, and micromorphic for different fluid media as exemplified by anisotropic fluids, liquid crystals, polymeric melts, suspensions, slurries, biological fluids, dusty gases, etc.

1.2 Some Applications

It is well known that the theory of micropolar fluids explains the particular characteristics of polymeric fluids, concrete with sand, muddy fluids, liquid crystal

with rigid molecules, colloidal fluid, fluids with certain additives, rigid suspensions, chopped fibre composites or animal blood with non-deformable cells [5]. Heat transfer boundary layer flow over the stretching/shrinking sheet involves in various industrial processes such as manufacturing of glass sheets, polymer extrusion, wire coating, continuous steel casting and crystal growing. Detailed treatises on various features of the micropolar fluids were investigated and reported by Lukaszewicz [7].

Understanding the influence of the heat source/sink on the micropolar fluid flow is important for industrial processes such as paper production, crystal growing, tinning and annealing of metals. The effects of heat generation/absorption, thermal radiation, magnetohydrodynamics, the Hall current and the first order homogeneous chemical reaction parameters have significant applications in the diverse fields of science and engineering.

The study of magneto-micropolar fluid flow has received great attention in heat transfer literature due to bioengineering and industrial applications such as the analysis of the electrically conducting blood flow in the cardiovascular system and the crystallisation of fluids with certain additives. Moreover, electrically conducting micropolar fluids are used in oil and gas extraction, in chemical processing of dyeing, Hall and MHD generators. Furthermore, the presence of the chemical reaction plays a key role in some chemical processes such as polymer production, the manufacturing of ceramics or glassware, modelling and design of drug delivery robots, dyeing in cloth industry and the cooling of the tower.

1.3   Flow over a Stretching/Shrinking Sheet

Generally, governing equations of the micropolar fluid flow consist of a set of partial differential equations (Equations (1.1)–(1.3)) subject to a set of appropriate initial and boundary conditions [3]:

$$\frac{D\rho}{Dt} + \rho \bigtriangledown .\mathbf{V} = 0, \tag{1.1}$$

$$\rho\frac{D\mathbf{V}}{Dt} = -\bigtriangledown p + (\lambda_\nu + 2\mu + \chi)\bigtriangledown(\bigtriangledown.\mathbf{V}) - (\mu + \chi)(\bigtriangledown \times \bigtriangledown \times \mathbf{V}) + \chi(\bigtriangledown \times \boldsymbol{\omega})$$
$$+ \rho\mathbf{f}, \tag{1.2}$$

$$j\rho\frac{D\boldsymbol{\omega}}{Dt} = (\alpha_\nu + \beta_\nu + \gamma_\nu)\bigtriangledown\bigtriangledown.\boldsymbol{\omega} - \gamma_\nu \bigtriangledown \times \bigtriangledown \times\boldsymbol{\omega} + \chi \bigtriangledown \times\boldsymbol{\omega} - 2\chi\boldsymbol{\omega} + \rho\mathbf{l}, \tag{1.3}$$

where $\mathbf{V} = (u, v, w)$ is the velocity field and $\boldsymbol{\omega} = (\omega_x, \omega_x, \omega_z)$ is the microrotation velocity vector of the micro-particles.

This thesis focuses on the mixed convective heat and mass transfer micropolar

fluid flow over a linearly stretching/shrinking sheet in the slip flow regime under the influence of the Newtonian heating. Under the Boussinesq approximation and the boundary layer assumptions (see Chapters 2 and 4 in [8]), respectively. The system of Equations (1.1)–(1.3) then reduces to the system of partial differential equations (Equation (1.4)) [9, 10],

$$
\left.
\begin{aligned}
&\frac{\partial u}{\partial x} + \frac{\partial v}{\partial y} = 0, \\
&u\frac{\partial u}{\partial x} + v\frac{\partial u}{\partial y} = \frac{\mu + \chi}{\rho}\left(\frac{\partial^2 u}{\partial y^2}\right) + \frac{\chi}{\rho}\left(\frac{\partial \omega}{\partial y}\right) + g\beta_T\left(T - T_\infty\right) + \\
&\qquad\qquad \mathfrak{A}g\beta_C\left(C - C_\infty\right) - \mathfrak{B}\frac{\sigma B_o^2}{\rho}u - \mathfrak{C}\frac{B_o}{\rho}J_z, \\
&u\frac{\partial w}{\partial x} + v\frac{\partial w}{\partial y} = \frac{\mu + \chi}{\rho}\left(\frac{\partial^2 w}{\partial y^2}\right) + \frac{B_o}{\rho}J_x, \\
&u\frac{\partial \omega}{\partial x} + v\frac{\partial \omega}{\partial y} = \frac{\gamma}{\rho j}\left(\frac{\partial^2 \omega}{\partial y^2}\right) - \frac{\chi}{\rho j}\left(2\omega + \frac{\partial u}{\partial y}\right), \\
&u\frac{\partial T}{\partial x} + v\frac{\partial T}{\partial y} = \frac{k}{\rho c_p}\left(\frac{\partial^2 T}{\partial y^2}\right) + \mathfrak{D}\frac{Q_o}{\rho c_p}\left(T - T_\infty\right) - \mathfrak{E}\frac{1}{\rho c_p}\frac{\partial q_r}{\partial y}, \\
&u\frac{\partial C}{\partial x} + v\frac{\partial C}{\partial y} = D_m\left(\frac{\partial^2 C}{\partial y^2}\right) - \xi\left(C - C_\infty\right),
\end{aligned}
\right\}
\tag{1.4}
$$

along with the pertaining boundary conditions as follows:

$$
\left.
\begin{aligned}
&u = su_{\mathrm{w}}(x) + u_{\mathrm{slip}};\ v = v_o;\ \omega = -n\frac{\partial u}{\partial y};\ k\frac{\partial T}{\partial y} = -h_s T;\ C = C_w \text{ at } y = 0, \\
&\qquad\qquad u \to 0;\ \omega \to 0;\ T \to T_\infty;\ C \to C_\infty \text{ as } y \to \infty.
\end{aligned}
\right\}
\tag{1.5}
$$

Based on Wu's slip flow model [11], the slip flow velocity u_{slip}, valid for every Knudsen number, is given by

$$
u_{\mathrm{slip}} = \frac{2}{3}\left(\frac{3 - \epsilon l^3}{\epsilon} - \frac{3}{2}\frac{1 - l^2}{k_n}\right)d\frac{\partial u}{\partial y} - \frac{1}{4}\left(l^4 + \frac{2}{k_n^2}(1 - l^2)\right)d^2\frac{\partial^2 u}{\partial y^2},
\tag{1.6}
$$

where l is chosen from $min[1/k_n, 1]$ which leads to $0 < l \leqslant 1$ for any value of the Knudsen (k_n) number and ϵ is the momentum accommodation coefficient which is defined as $0 < \epsilon \leqslant 1$. We rewrite Equation (1.6) as

$$
u_{\mathrm{slip}} = A\frac{\partial u}{\partial y} + B\frac{\partial^2 u}{\partial y^2},
\tag{1.7}
$$

where A and B are defined in Equation (1.6). In Equations (1.6)–(1.7), the molecular mean free path d and A are always positive and B is consequently

3

negative in magnitude.

1.4   Aim and Objectives

The aim of the thesis is to investigate the micropolar fluid flow behaviour in the slip flow regime under the influence of the Newtonian heating. Several different physical effects are present in the model, given by Equations (1.4)–(1.5). We investigate these as follows:

- chapter three treats the influence of the heat generation/absorption parameter on the micropolar fluid flow with the second order slip and the Newtonian heating at the boundary,

- chapter four focuses on the MHD micropolar fluid flow under the impact of thermal radiation parameter in the slip flow regime affected by the Newtonian heating,

- chapter five describes the Hall current effect on the micropolar fluid flow over a stretching/shrinking sheet under the slip and the Newtonian heating conditions,

- chapter six deals with the heat and mass transfer flow of the micropolar fluid influenced by first order chemical reaction, slip and the Newtonian heating parameters.

In this thesis, objectives are designed to

- formulate a system of equations describing the micropolar fluid flow under the influences of the Hall current, heat generation/absorption, thermal radiation and the first order chemical reaction parameters,

- derive a dimensionless non-linear system of coupled equations incorporating with physical flow parameters by using a suitable similarity transform,

- develop an efficient algorithm for simulation which is based on a semi-analytical technique called Homotopy Analysis Method and conduct the validation tests for the current research in comparison with the exact and numerical results in the literature,

- discuss the effects of the model parameters on the prescribed velocities, temperature and concentration profiles near and away from the sheet.

1.5   Significance

In this thesis, the behaviours of the micropolar fluid flow under various effects have been investigated with the second order slip and the Newtonian heating conditions at the boundary. In the slip flow regime, the fluid particle, close to the boundary, slips towards the boundary of the surface due to their finite tangential velocity. This effect can not be ignored due to its numerous applications in engineering and biomedical sciences, e.g., refrigerating coils, polishing artificial heart valves and internal cavities.

In Newtonian heating, heat transfer rate from the bounding surface with finite heat capacity is directly proportional to the local surface temperature. When the micropolar fluid flow over a stretching/shrinking sheet, the Newtonian heating condition plays an important role in the slip effect. Magnetic field contributes significantly to control the convective micropolar fluid flow. Since the micropolar fluids are the fluids with certain additives, e.g., dusty/suspension fluids and their use in the science and engineering applications is significant. The results found here could also be useful in the applications relating to pumping and levitation of liquids and gases, separation of contaminants from gases and frictional electrification in chemical reactions.

1.6   Outlines of the Thesis

This thesis is divided into seven chapters. Chapter one explains the essential features of the micropolar fluid flow, problem statement, aim and scope of the present research project.

Chapter two elaborates the previously published work on the micropolar fluid flow and highlights the areas which require further research and analysis. Moreover, it also describes a brief introduction to the methodology that is to be used to solve the coupled nonlinear system of equations with mixed derivative boundary conditions.

Chapter three presents the effect of heat transfer flow of micropolar fluid with heat source/sink condition in the slip flow regime. In the first part, we formulated the governing system of equations and secondly, derived a dimensionless nonlinear system of ordinary differential equations by using a suitable similarity transform. Thirdly, we applied HAM to get the semi-analytical series solution and validated the results with the published work. Lastly, an analysis of the obtained results is reported with the graphical illustrations.

Chapter four concerns with the thermal radiation impact on the magneto-micropolar fluid flow over linearly stretching/shrinking sheet. Based on the

analysis of the MHD micropolar fluid flow, a proposed set of partial differential equations is formulated and then solved by using HAM after converting it into a non-dimensional form. Results and discussion section are followed by the validation of the obtained results.

Chapter five deals with the study of the Hall current. Based on the Ohm's law with Maxwell's equations, a heat transfer mathematical model of the mixed convective micropolar fluid flow is derived which is incorporated with the Hall current effect. A dimensionless coupled system of differential equations is solved by Optimal Homotopy Analysis Method (OHAM). An optimal convergence control parameter is then tabulated along with its graphical representations. Obtained solutions are validated with the exact analytical solutions by using these optimal values. Then a comparison with numerical results is presented before the results and discussion section.

Chapter six explains the influence of the first order chemical reaction parameter on the heat and mass transfer in micropolar fluid flows. A two-dimensional system of steady state coupled partial differential equations is formulated and then solved by applying rigorous mathematical steps of the HAM in non-dimensional form. Proceedings sections contain the results validation and discussion.

Chapter seven describes the conclusion obtained from the present study and directions for future work.

Chapter 2

Literature Review

This chapter presents the literature review on the complex flows of micropolar fluids over a stretching/shrinking sheet in the slip flow regime. We particularly focus on the impacts of heat generation and absorption, magnetohydrodynamics (MHD), thermal radiation, Hall current and first order chemical reaction on the flow of a micropolar fluid.

2.1   Essence of the Micropolar Fluid

It is well known that theories of classical fluid mechanics could not adequately explain certain characteristics of polymeric fluids, fluids with additives or the animal blood. Such fluids exhibit micro-rotational effects and micro-rotational inertia, and later they were named as micropolar fluids in the theory of Eringen [3]. This describes the effects of micro-structured particles with the help of an additional transport equation by representing the local angular momentum, and, in addition, to some extra constitutive parameters, which are not included in the classical Navier-Stokes theory of fluid mechanics [1–3, 5, 6].

Later on, this theory has been applied to some basic viscous micropolar fluid flows such as Couette and Poiseuille flow [12], heat conducting micropolar fluid flows [4, 13], through concentric cylinders [14, 15] and the boundary-layer [9] micropolar fluid flow. An experimental study by Ariman *et al.* [16] established a good comparison with the exact solution of a steady and pulsatile micropolar fluid flow through a circular tube. Migun [17] proposed an experimental method to determine parameters which characterize the micro-particles of the micropolar fluid. He examined the volumetric flow rate of the micropolar fluid when it passes through the two circular cylinders of different cross section and the obtained results are good in agreement with the already published results. Kolpashchikov *et al.* [18] experimentally calculated the viscosity coefficients of the micropolar fluid flow with the help of specific viscometric and thermal measurements along with the concrete

form of the boundary conditions for the microrotation. They quantitatively examined the governing flow parameters of the steady state micropolar fluid flow through any constant cross section of the capillary tube.

Recently, many investigations on the micropolar fluid flows have been carried out by analysing various other effects. These effects include to variable heat flux [19], magnetohydrodynamics (MHD) flow [20,21], non-linear power-law diffusion flow over a stretching sheet [22], nonlinearly shrinking/stretching sheet [23], flow in a differentially heated irregular cavity [24], square and wavy cavities [25,26] free convective flow over a circular cylinder [27], and flow over a permeable vertical cone [28].

The following subsections explain a literature review on the previously published work closely related to the present research by elaborating the importance of heat generation and absorption, thermal radiation, MHD, the Hall effect and the first order homogeneous chemical reaction parameters on the micropolar fluid flow passing over a continuously stretching/shrinking sheet under the influences of second order slip and the Newtonian heating conditions at the boundary.

2.1.1 Micropolar Fluid Flow with Heat Source/Sink

In the past few decades, the flow of micropolar fluid past over a sheet attracted many researchers because of its numerous applications in industry, for example, paper production, crystal growing, tinning and annealing of metals.

Kelson and Farrell [29] examined suction and injection effects on the porous stretching sheet. They observed that suction and injection parameters have direct influence on the microrotation boundary and coupling parameters even if the mass transfer through the surface was high. The effect of surface condition on the micropolar fluid flows over a porous stretching surface was investigated by Kelson and Desseaux [30]. They found that in the presence of smaller values of the pertaining parameters, low injection rate through the surface could lead to an effective decrease in the wall stress in industrial applications. Bhargava *et al.* [31] extended the work of Kelson and Desseaux [30] to mixed convective incompressible micropolar fluid flow by using a numerical method. They found that suction parameter caused to enhance the heat transfer rate which may increase the cooling effect at the plate while injection rate reduced it. Heat generation and absorption (source/sink) effect of water-based nanofluid flow through a permeable stretching tube was analysed by Ahmed *et al.* [32]. In their study, suction/injection parameter played a direct role to enhance the heat transfer rate in the fluid flow. An exact analytical solution for the heat transfer micropolar fluid flow over permeable shrinking/stretching sheets was reported by Turkyilmazoglu [33,34]. The influence

of thermal radiation on the nano magneto-micropolar fluid flow over a permeable stretching sheet with a non-uniform heat source/sink was numerically investigated by Pal and Mandal [21]. In their proposed model, they analysed that higher values of the heat source/sink parameter made a sudden fall in the nanofluid temperature near the wall. A numerical study was used to analyse the impact of the heat generation and absorption on the MHD micropolar fluid flow over a moving porous plate by Rahman and Sattar [35]. They used a volumetric heat generation rate (see in [36]) with the following expression

$$Q = \begin{cases} Q_o(T - T_\infty), & \text{for} \quad T \geq T_o, \\ 0, & \text{for} \quad T < T_o, \end{cases}$$

in the conservation of energy equation. This relation is valid as an approximation of the state of some exothermic processes along with the T_o as an onset temperature. When the temperature of the main stream fluid is not less than T_o, $Q_o(T - T_\infty)$ is considered and investigated its influence on the heat transfer phenomenon in the steady state non-Newtonian fluid flow.

Furthermore, Ziabakhsh et $al.$ [37] conducted an analytical study of the uniform heat generation/absorption effect on the non-Newtonian micropolar fluid flow over a permeable wall. They reported that heat generation/absorption parameter enhanced the temperature of the micropolar fluid flow in the presence of constant pertaining parameters. The effects of the heat source/sink and the first order chemical reaction on the heat and mass transfer in micopolar fluid flow over a uniformly stretching sheet were reported by Damseh et $al.$ [38]. It was mentioned that heat generation parameter rose thermal boundary layer thickness and the negative temperature gradient of the micropolar fluid flow while heat absorption parameter had reverse impact on the flow regime. Analytical and numerical techniques have been used to examine the heat and mass transfer MHD micropolar fluid flows [39–41]. Mohamed and Abo-Dahab [39] studied the impacts of the heat generation, thermal radiation and first order chemical reaction on the MHD micropolar fluid flow over a vertical permeable plate. They found that in heat and mass transfer flow of the micropolar fluid, heat generation parameter slightly effected on the translation velocity. The influence of heat generation on MHD heat and mass transfer micropolar fluid flow in the presence of thermal diffusion and chemical reaction was reported by Olajuwon and Oahimire [40]. It was revealed that higher values of the heat generation parameter were resulted in a fall of the velocity component and the temperature of the micropolar fluid flow. Mishra et $al.$ [41] investigated the impact of the heat generation and double stratification on the MHD heat and mass transfer flow of a micropolar fluid over a semi infinite

vertical plate. They observed that heat source parameter enhances the boundary layer fluid flow by diffusing the heat between the stratified fluid layers.

Hence, it is up to best of our knowledge, the research of the heat generation/absorption effect on the mixed convective micropolar fluid flow passing over a stretching/shrinking sheet in the presence of seond order slip and the Newtonian heating conditions at the boundary has never been examined before.

2.1.2 Radiative MHD Micropolar Fluid Flow

The study of magneto-micropolar fluid flow has received great attention in heat transfer literature due to its bio-engineering and industrial applications such as the analysis of the electrically conducting blood flow [42–44] in the cardiovascular system and the crystallization [45] of fluids with certain additives.

In the literature, many investigations [19,21,35,40,46–54] have been reported on varying behaviours of the magneto-micropolar fluid flow over different geometries. Olajuwon and Oahimire [40] studied the influence of thermal radiation parameter on unsteady MHD heat and mass transfer micropolar fluid flow over a permeable moving plate in the presence of heat generation and chemical reaction. Malga and Naikoti [51] analysed the MHD micropolar fluid flow over a porous plate present in porous media under the influence of heat generation and thermal diffusion by using a numerical technique. Bakr *et al.* [52] examined the Newtonian heating, thermal radiation and mass diffusion effects on one dimensional unsteady MHD micropolar fluid flow over a semi-infinite vertical plate embedded in porous medium. They studied the Navier slip condition on the flow regime.

Moreover, a numerical investigations have been carried out to investigate the thermal radiation effect on MHD micropolar fluid flow over a curved stretching sheet by Naveed *et al.* [53]. They found that higher values of the dimensionless radiation parameter increased the heat transfer rate when the fluid passed over a curved stretching sheet. Impact of thermal radiation on MHD micropolar nanofluid flow over a stretching sheet under the influence of non-uniform heat generation and absorption conditions was reported by Pall and Mandal [21]. They observed that due to a decrease in the mean Rosseland absorption coefficient, thermal radiation parameter rose the thermal boundary layer thickness. Sabeel *et al.* [54] analysed the influences of thermal relaxation time and internal material parameters on MHD viscoelastic micropolar fluid flow over a semi-infinite surface by using the Cattaneo-Christov heat flux equation in the presence of chemical reaction. They applied the finite difference method to studied the effects of the pertaining parameters on the MHD fluid flow.

From the literature review, we can conclude that a few attempts have been

carried out to study the micropolar fluid flow in the slip flow regime. The influences of the thermal radiation and the Newtonian heating parameters on the mixed convective magneto-micropolar fluid flow over a linearly stretching/shrinking sheet in the slip flow regime using second order slip condition were not investigated and reported before.

2.1.3 Impact of Hall Current on MHD Fluid Flow

The theory of micropolar fluids has also been extended to the electrically conducting fluids in a magnetic field which has numerous engineering applications in oil and gas extraction, in chemical processing, Hall and MHD generators [55]. More specifically, when an electric current passes through a conductor under the influence of a strong transverse magnetic field, the moving charged particles under the influence of the magnetic force causes to lean them to either side of the conducting material. Due to this drift or gyration of charged particles, the electric conductivity is reduced to produce another transverse current named as Hall current, and this phenomenon is called the Hall effect. The Hall effect usually occurs in conducting solids, liquids as well as ionised gases.

Over the last few decades, various mathematical models have been proposed to study the influence of the Hall current on the flow pattern of the micropolar fluid over various shapes of geometries [56–63]. Eldahab and El-Aziz [56] analysed the impact of the Ohmic heating and the Hall current on a rotating cone immersed in a magneto-micropolar fluid flow. They found that in the presence of the strong magnetic field, the Hall parameter yields an increase in the surface heat transfer rate. Thermal instability of the micropolar fluid flow under the influence of the Hall current was reported by Rani and Tomar [57]. In this investigation, they observed that Hall parameter causes to increase the critical Rayleigh number in stationary convection of the micropolar fluid flow. On the other hand, in overstationay convection flow, the critical Rayleigh number increased initially and then it decreased with further increase in the Hall parameter. The combined effects of the Hall current and the thermal radiation on the heat and mass transfer of the micropolar fluid flow in the rotating system within the influence of heat generation and chemical reaction were studied by Pal *et al.* [58]. They found that higher value of the Hall parameter rose the resultant and angular velocity distributions in an oscillatory mixed convection flow of a micropolar fluid over a semi-infinite plate.

In addition to further literature survey, Yang and Wang [59] investigated the magnetic field effect on a power-law non-Newtonian fluid flow passing through a rectangular channel by using a multiple-relaxation-time lattice Boltzmann method.

Anika *et al.* [60] examined the Hall and Ion-slip current on the unsteady MHD micropolar fluid flow over an impermeable vertical plate with thermal diffusion effect. Othman *et al.* [61] reported the Hall current and gravity effects on the MHD micropolar fluid flow within the thermoelastic medium which is possessing the microtemperatures property. Wahed and Akl [62] studied the Hall current on the MHD nanofluid flow over a rotating disk present under the influence of viscous dissipation and the nonlinear thermal radiation effects. Bilal *et al.* [63] examined the Hall and Ion-slip effect on the MHD heat and mass transfer micropolar fluid flow over a permeable linearly stretching sheet present in the porous medium. They considered the suction and injection effects with variable thermal diffusivity.

It can be observed, from the above mentioned literature, the study of the Hall current on the MHD micropolar fluid flow has not been conducted and published before under the impacts of the second order slip and the Newtonian heating conditions at the boundary.

2.1.4 Micropolar Fluid Flow with Chemical Reaction

In the study of heat and mass transfer, many reactions involve the simultaneous diffusion of molecular species. These species appear or disappear through a chemical reaction either within or at the boundary of the phase. Categorically, there are two types of chemical reactions. The one is uniform throughout a given phase named as the homogeneous chemical reaction. Another takes place within or at the boundary of the phase of interest, called heterogeneous chemical reaction. Chemical reaction is greatly important in some industrial processes such as polymer production, to design the chemical processing equipment, for example, to design the machine which is used to spray on the agriculture fields, food processing, the manufacturing of ceramics or glassware, dying in cloth industry and the cooling of the tower.

The effect of chemical reaction on magneto-micropolar fluid flow over a porous plate in the porous medium has been investigated and reported by various researchers [54, 58, 64–67]. The impact of the chemical reaction on MHD micropolar fluid flow over a porous plate in the porous medium has been analyzed by Mohamed and Dahab [64]. In their analysis, the influence of thermal radiation and heat generation has also been conducted. They noticed that with an increase in the chemical reaction parameter, concentration profile decreased in the heat and mass transfer flow. Chamkha *et al.* [65] studied the influence of the chemical reaction on the radiating magneto-micropolar fluid flow over a vertical heated plate with the ohmic heating. It was observed that with these parameters, an increase in the chemical reaction caused a decrease in the concentration profile

and its boundary layer thickness. A numerical investigation of chemical reaction on MHD free convective heat and mass transfer micropolar fluid flow past over an oscillatory plate in the rotating frame of reference has been investigated by Bakr [66]. Hayat *et al.* [67] reported a study of the chemical reaction on mixed convective radiating magneto-micropolar fluid flow past over a stretching sheet. They observed that when chemical reaction parameter was $\gamma > 0$ then the concentration profile decreased with higher values of it and the concentration profile increased with $\gamma < 0$. Pal *et al.* [58] analysed a combined study of the chemical reaction and the Hall effects on the thermally radiating micropolar fluid flow past over a semi-infinite vertical impermeable plate. They reported that when the first order homogeneous chemical reaction parameter increased then the concentration profile decreased in the magneto-micropolar fluid flow. Sabeel *et al.* [54] analysed the influences of chemical reaction, thermal relaxation time and internal material parameters on MHD viscoelastic micropolar fluid flow over a semi-infinite surface by using the Cattaneo-Christov heat flux equation.

In last few decades, the study of heat and mass transfer in micropolar fluids has received significant attention due to their applications in various industrial processes such as oil extraction, solidification of liquid crystals, polymeric suspensions, etc.

In the literature, many investigations of the micropolar fluid flow have been reported under different kinds of conditions [46, 68–74]. For example, Eldabe and Ouaf [68] numerically investigated the heat and mass transfer magnetohydrodynamics (MHD) micropolar fluid flow over a linear stretching surface in the presence of viscous dissipation and the Joule heating. They found that an increase in the viscous dissipation and the Joule heating caused to rose the micropolar fluid temperature. Ishak *et al.* [69] studied the boundary layer micropolar fluid flow over a moving and fixed porous surface with the dilute concentration of microelements. They investigated one of the cases in which plate and free stream fluid flow moved in opposite direction, and the dual solutions have been calculated and reported. Ishak [70] reported a numerical solution of an incompressible radiating micropolar fluid flow over a stretching sheet. Ishak reported that the thermal boundary layer thickness increased with the higher value of the radiation parameter. Bachok *et al.* [71] examined the unsteady thermal boundary layer flow of an incompressible micropolar fluid over an impulsively stretching sheet. Zheng *et al.* [72] reported the dual solutions of the heat transfer micropolar fluid flow past over a stretching/shrinking sheet with the condition of power-law surface velocity and the temperature distribution. They investigated that both solutions are physically meaningful and closely related to each other. An investigation of magneto-micropolar fluid flow through a pipe has been investigated by Sherief *et*

al. [73]. An exact analytical investigation of magneto-micropolar fluid flow has been reported by Ezzat and Shreen [74]. Chaudhary and Jain [46] investigated the slip effect on the heat and mass transfer MHD radiative micropolar fluid flow past over a vertical porous plate.

From the above cited work, it can be seen that combined effects of first order chemical reaction, second order slip and the Newtonian heating parameters on the mixed convective micropolar fluid flow over a stretching/shrinking sheet have not been studied before.

2.1.5 Second Order Slip and the Newtonian Heating Conditions

In the analysis of the boundary layer of the viscous fluids, it is well known that the velocity of fluid particles matches with the velocity of the solid surface. This effect is known as a no-slip effect. On the other hand, some fluid particles no longer take the velocity of the solid surface and slip along the surface due to their finite tangential velocity. This effect can not be ignored and resulting flow behaviour is called as a slip-flow regime. In heat and mass transfer, the slip flow effect has important engineering applications such as transmission lines, refrigerating coils, polishing artificial heart valves and internal cavities. Wu [11] derived a slip flow model with the help of the kinetic theory for arbitrary Knudsen number. He found that it is a preferable approach to investigate the slip flow behaviour other than that of the Maxwell slip model [75], second-order slip model [76], 1.5th order slip model [77] and Fukui–Kaneko slip model [78]. Recently, Wu's slip flow model has been used in many investigations of flow patterns of the Newtonian [79–83] and non-Newtonian micropolar [84–88] fluids over different geometries by using analytical and numerical techniques to analyse the fluid flow behaviour.

In literature, there are four commonly used heating processes, specified as i) wall to ambient temperature distribution, ii) surface heat flux distribution, iii) conjugate condition and iv) the Newtonian heating [89–94]. The concept of the Newtonian heating was presented by [89], in which the heat transfer rate from the bounding surface is directly proportional to the local surface temperature of the fluid. The Newtonian heating effect usually called as conjugate convective flow occurs in many engineering applications, e.g. in heat exchangers; where the conduction at the wall of the solid cylindrical tube was influenced by convection of the moving fluid around it. Around the blade of the wind turbine; where the conduction in the blade and convection in the surrounding fluid helps to analyse and model the vital design of the blade [91, 92].

2.2 Homotopy Analysis Method

In this section, a brief introduction of the Homotopy Analysis Method (HAM) is presented. The Homotopy Analysis Method was developed by Liao [95–97] which produces approximately analytical series solution of the nonlinear ordinary differential equations. It has a great advantage to control the convergence of the HAM series solution. It is preferable to apply the HAM on the nonlinear ordinary differential equation(s) as compared to the perturbation and non-perturbation, Adomian decomposition, artificial small parameter and the δ-expansion methods (see reference in [96]).

The basic features of the HAM solution in accordance with the nonlinear ordinary differential equation are presented here in a general form as follows:

$$\mathcal{N}[f(\eta)] = 0, \tag{2.1}$$

where $\mathcal{N}$ represents the nonlinear operator, $f(\eta)$ is a unknown function with an independent variable η. Let f_0 denotes the initial solution of the above $f(\eta)$ which satisfies the initial and boundary conditions of the Equation (2.1) and $\mathcal{L}$ denotes the auxiliary linear operator satisfying the property $\mathcal{L}f = 0$ when $f = 0$. For this HAM solution, a mapping is defined as

$$f(\eta) \rightarrow \phi(\eta, q). \tag{2.2}$$

Liao [96] derived a so-called zero order Homotopy deformation equation as follows:

$$(1 - q)\mathcal{L}[\phi(\eta, q) - f_0(\eta)] = q\hbar H(\eta)\mathcal{N}(\phi(\eta, q))], \tag{2.3}$$

in which auxiliary parameter ($\hbar \neq 0$) and the auxiliary function ($H(\eta) \neq 0$) are chosen to be wisely enough so that when the embedding parameter q varying from 0 to 1 generates the sequence of the HAM solution which leads to change the $\phi(\eta, q)$ from the initial solution (guess) to the actual solution ($f(\eta)$) of the Equation (2.1).

From literature, it is observed that the basic features of HAM has great freedom such as the choice of the initial approximation (guess/solution) [96], auxiliary parameter or convergence control parameter ($\hbar$) [98–100] and the auxiliary function [101–103], which play an important role in the desired series solution. Furthermore, a Taylor's series expansion of $\phi(\eta, q)$ can be written as

$$\phi(\eta, q) = \phi(\eta, 0) + \sum_{n=1}^{\infty} \mathbb{D}_n(\phi(\eta, q))q^n, \tag{2.4}$$

15

where the nth order deformation derivative, $\mathbb{D}_n(\phi)$, is defined by

$$\mathbb{D}_n(\phi(\eta, q)) = \frac{1}{n!} \left. \frac{d^n \phi(\eta, q)}{dq^n} \right|_{q=0}.$$

It is assumed that with the proper choice of the basic features of the HAM, the homotopy solution, $\phi(\eta, q)$, exists for all $q \in [0, 1]$ and the solution expanded by the Taylor's series (in Equation (2.4)) converges at $q = 1$ which is given by

$$f(\eta) = f_0(\eta) + \sum_{n=1}^{\infty} f_n(\eta). \tag{2.5}$$

To obtain the value of $f_n(\eta)$, with the help of Equation (2.3), Liao [96] proposed an nth-order deformation equation by differentiating the n times with respect to q and then setting $q = 0$ before dividing by $n!$, which reads as

$$\mathcal{L}[f_n(\eta) - \mathcal{X}_n f_{n-1}(\eta)] = \hbar H(\eta) \mathfrak{R}_n(f_{n-1}(\eta)), \tag{2.6}$$

where

$$\mathcal{X}_p = \begin{cases} 0 & \text{for } p \le 1, \\ 1 & \text{for } p > 1, \end{cases} \tag{2.7}$$

and

$$\mathfrak{R}(f_{n-1}(\eta)) = \mathbb{D}_{n-1}(\mathcal{N}(\phi(\eta, q)))|_{q=0}, \tag{2.8}$$

where, $\mathfrak{R}(f_{n-1}(\eta))$ depends upon the following

$$f_0(\eta), \ f_1(\eta), \ f_2(\eta), \ f_3(\eta), \ \cdots, \ f_{n-1}(\eta),$$

which are obtained from the nth-order of deformation equation (Equation (2.6)). Thus, the final m^{th}-order approximated series solution reads

$$f(\eta) \approx \sum_{n=0}^{m} f_n(\eta). \tag{2.9}$$

Furthermore, Optimal Homotopy Analysis Method (OHAM) is based on the deformation-functions with some unknown convergence-control parameters. The values of these optimal convergence control parameters (optimal auxiliary parameters) are computed by the minimum of the squared residual of given nonlinear differential equations which play an important role in the convergence of the series solution, and the obtained solutions are much more accurate in general.

Usually, a single convergence control parameter produces good enough approximate solution within short computation time. However, the higher the number of the optimal convergence control parameters; higher will be the computation time with possible better approximations. The brief explanation with rigorous examples can be seen in [97].

2.3   Chapter Summary

By reviewing the development in the literature of the micropolar fluid flow and analyzing the published work on heat and mass transfer in micropolar fluid flow influenced by the heat source/sink, MHD, thermal radiation, first order chemical reaction and the Hall effects, we conclude that these effects are not studied in the slip flow regime under the influence of the Newtonian heating condition. Homotopy Analysis Method is welknown method for the solution of the nonlinear system of differential equations. The use of this method will be helpful to get the novel results due to the complex nature of the system of nonlinear coupled differential equations along with the pertaining mixed derivative boundary conditions.

Chapter 3

Heat Transfer Flow with Heat Source/Sink[1]

In this chapter, we consider the problem given in [84] to examine the influences of the Newtonian heating and the heat source/sink parameters on the mixed convective micropolar fluid flow over a permeable stretching/shrinking sheet in the presence of the slip flow regime. The problem in [84] was based on the analytical work of Fang *et al.* [79] to study the boundary layer flow of the micropolar fluid over a permeable shrinking sheet with the second order slip at the boundary by ignoring the heat transfer analysis. In contrast with the already published work, the study in this chapter has two new features. Firstly, the flow behaviour considering the effects of the heat source/sink (generation/absorption) at the weak concentration of microelements is studied. Secondly, the Newtonian heating effect on the mixed convective micropolar fluid flow over the stretching/shrinking permeable sheet with the second order slip flow model [11] is tackled which, to the best of our knowledge, has never been investigated and reported before.

3.1   Governing Equations

We consider a two-dimensional steady state incompressible micropolar fluid flow over a vertical permeable stretching/shrinking sheet with velocity $u_w(x) = sax$ for a positive dimensional constant $(a > 0)$. The flow is taken along the x–axis, and the y–axis is normal to the surface, as shown in Figure 3.1. The acceleration due to gravity (g) is acted in the downward direction and Newtonian heating [89, 90] is introduced in the thermal boundary condition. To study the only heat

---

[1]Copyright permission: please see in Appendix B.
Muhammad Kamran, Heat source/sink and Newtonian heating effects on convective micropolar fluid flow over a stretching/shrinking sheet with slip flow model. International Journal of Heat and Technology, 36(2), 473-482. https://doi.org/10.18280/ijht.360212
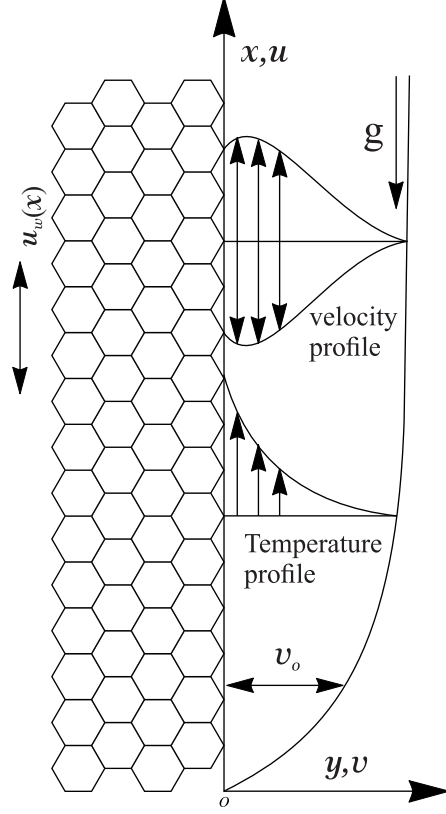
Figure 3.1: Flow model.

transfer micropolar fluid flow, the system of equations (Equations (1.4)–(1.5)) with $\mathfrak{A} = \mathfrak{B} = \mathfrak{C} = \mathfrak{E} = 0$, $\mathfrak{D} = 1$ and in the absence of the Hall effect can be reduces to:

$$\frac{\partial u}{\partial x} + \frac{\partial v}{\partial y} = 0, \tag{3.1}$$

$$u\frac{\partial u}{\partial x} + v\frac{\partial u}{\partial y} = \frac{\mu + \chi}{\rho}\left(\frac{\partial^2 u}{\partial y^2}\right) + \mathrm{g}\beta_T\left(T - T_\infty\right) + \frac{\chi}{\rho}\left(\frac{\partial \omega}{\partial y}\right), \tag{3.2}$$

$$u\frac{\partial \omega}{\partial x} + v\frac{\partial \omega}{\partial y} = \frac{\gamma}{\rho j}\left(\frac{\partial^2 \omega}{\partial y^2}\right) - \frac{\chi}{\rho j}\left(2\omega + \frac{\partial u}{\partial y}\right), \tag{3.3}$$

$$u\frac{\partial T}{\partial x} + v\frac{\partial T}{\partial y} = \frac{k}{\rho c_p}\left(\frac{\partial^2 T}{\partial y^2}\right) + \frac{Q_o}{\rho c_p}\left(T - T_\infty\right), \tag{3.4}$$

with the second order slip (u_{slip} defined in Equations (1.6)–(1.7)) and the Newtonian heating $((3.5)_4)$ conditions at the boundary,

$$\left.\begin{array}{c} u = su_w(x) + u_{\text{slip}}, v = v_o, \omega = -n\dfrac{\partial u}{\partial y}, k\dfrac{\partial T}{\partial y} = -h_s T \text{ at } y = 0, \\[2mm] u \to 0,\ \omega \to 0,\ T \to T_\infty \text{ as } y \to \infty. \end{array}\right\} \tag{3.5}$$

where u and v are the velocity components in the x and y direction, respectively. The spin gradient viscosity is considered as $\gamma = (\mu + \chi/2)\,j = \mu\,(1 + K/2)\,j$ for $K = \chi/\mu$ and $j = \nu/a$ which are the material parameter and microinertia density [104], respectively. In $(3.5)_2$, $v_o > 0$ is the suction and $v_o < 0$ is the injection velocities of the permeable stretching/shrinking sheet. The constant n, in $(3.5)_3$, has the range $0 \leq n \leq 1$, in which $n = 0$ represents the strong concentration of micro-elements near the sheet which are unable to rotate [105, 106], $n = 0.5$ shows the vanishing of anti–symmetric stress tensor which represents the weak concentration, and $n = 1$ can be used for the turbulent flow. However, $n = 0.5$ which corresponds to the dilute micropolar fluid and this dilute fluid is considered in the present study.

By introducing the non-dimensional similarity variables with velocity components $u = \partial \psi / \partial y$ and $v = -\partial \psi / \partial x$ as follow:

$$
\eta = \sqrt{u_w(x)}(\nu x)^{-\frac{1}{2}}y,\ \psi = \sqrt{x\nu u_w(x)}f(\eta),
$$
$$
\omega = \sqrt{xu_w(x)}(\nu)^{-\frac{1}{2}}ah(\eta)\ \text{and}\ \theta(\eta) = \frac{T - T_\infty}{T_\infty}.
$$

The stream function (ψ) usually satisfies the equation of the conservation of mass (Equation (3.1)), governing equations (Equations (3.2)–(3.4)) are transformed into a set of non-linear coupled ordinary differential equations (see in Section A.1 of appendix) as follow:

$$
(1 + K)f''' - (f')^2 + ff'' + \lambda\theta + Kh' = 0, \tag{3.6}
$$
$$
(1 + K/2)h'' - f'h + fh' - K(2h + f'') = 0, \tag{3.7}
$$
$$
\theta'' + Prf\theta' + QPr\theta = 0, \tag{3.8}
$$

with the boundary conditions,

$$
\left.\begin{array}{l}
f = f_w,\ f' = s + \alpha f'' + \beta f''',\ h = -nf'',\ \theta' = -\delta(1 + \theta)\ \text{at}\ \eta = 0, \\
f' \to 0,\ h \to 0,\ \theta \to 0\ \text{as}\ \eta \to \infty,
\end{array}\right\} \tag{3.9}
$$

where prime$(')$ represents the derivative with respect to the η. The non-dimensional physical parameters are defined in the form of the buoyancy parameter $\lambda = Gr_x/Re_x$ for the local Grashof number $Gr_x = \text{g}\beta_T T_\infty x/a\nu$ and the local Reynolds number $Re_x = ax^2/\nu$, heat generation (> 0) or absorption (< 0) parameter $Q = Q_o/a\rho c_p$ and Prandtl number $Pr = \mu c_p/k$ in Equations (3.6)–(3.8). In

Equation (3.9), $f_w = -(a\nu)^{-\frac{1}{2}}v_o$ is the suction (> 0) or injection (< 0) parameter, $\alpha = A\sqrt{a/\nu} > 0$ and $\beta = Ba/\nu < 0$ are the first and second order slip flow parameters and $\delta = \frac{h_s}{k}\sqrt{\nu/a}$ is the Newtonian heating parameter. Moreover, the physical quantities such as local skin friction co-efficients (C_{f_x}), local wall couple stress (M_x) and the local Nusselt number (Nu_x) are expressed as

$$
\begin{aligned}
C_{f_x} &= \frac{-\tau_{w_x}}{\rho(u_w(x))^2} \text{ for } \tau_{w_x} = (\mu + \chi)\frac{\partial u}{\partial y} + \chi\omega \bigg|_{y=0}, \\
M_x &= \frac{-m_w}{\rho x(u_w(x))^2} \text{ for } m_w = \left(\mu + \frac{\chi}{2}\right)j\frac{\partial\omega}{\partial y}\bigg|_{y=0}, \\
Nu_x &= \frac{-xq_w}{k_f(T - T_\infty)} \text{ for } q_w = k_f\frac{\partial T}{\partial y}\bigg|_{y=0},
\end{aligned}
$$

and the similarity transformation yields them

$$
\left.
\begin{aligned}
C_{f_x}Re_x^{\frac{1}{2}} &= -(1 + K - nK)\,f''(\eta)|_{\eta=0}, \\
M_x Re_x &= -\left(1 + \frac{K}{2}\right)h'(\eta)\bigg|_{\eta=0}, \\
Nu_x Re_x^{-\frac{1}{2}} &= \delta\left(1 + \frac{1}{\theta(\eta)}\right)\bigg|_{\eta=0}.
\end{aligned}
\right\}
\tag{3.10}
$$

3.2 Series Solution

A semi-analytical technique named Homotopy Analysis Method (HAM), introduced by Liao [96], is applied to solve the set of transformed nonlinear Equations (3.6)–(3.8) along with the boundary conditions Equation (3.9). HAM has a great advantage to control the convergence of the obtained series solutions and preferable to apply on the nonlinear ordinary differential equations as compared to the perturbation and non-perturbation, Adomian decomposition method, artificial small parameter method and δ-expansion method (see reference in [96]). The basic features of the HAM solution in accordance with the nonlinear system of Equations (3.6)–(3.8) with corresponding boundary conditions Equation (3.9) are treated here. The homotopy series solution for the $f(\eta), h(\eta)$ and $\theta(\eta)$ are expressed by a set of base functions

$$
\left\{\eta^p e^{-q\eta} | p \geq 0, q \geq 0\right\},
\tag{3.11}
$$

in the form of

$$f(\eta) = \sum_{p=0}^{\infty}\sum_{q=0}^{\infty} a_{p,q}\eta^p e^{-q\eta}, \tag{3.12}$$

$$h(\eta) = \sum_{p=0}^{\infty}\sum_{q=0}^{\infty} b_{p,q}\eta^p e^{-q\eta}, \tag{3.13}$$

$$\theta(\eta) = \sum_{p=0}^{\infty}\sum_{q=0}^{\infty} c_{p,q}\eta^p e^{-q\eta}, \tag{3.14}$$

where $a_{p,q}, b_{p,q}$ and $c_{p,q}$ are constants. The first rule of solution expressions and boundary conditions yield the initial approximation for Equations (3.12)–(3.14) as

$$f_0(\eta) = f_w + \frac{s(1 - e^{-\eta})}{1 + \alpha - \beta}, \tag{3.15}$$

$$h_0(\eta) = \frac{sne^{-\eta}}{1 + \alpha - \beta}, \tag{3.16}$$

$$\theta_0(\eta) = \frac{\delta e^{-\eta}}{1 - \delta} \quad ; \delta \neq 1, \tag{3.17}$$

with corresponding linear operators

$$\mathcal{L}_f = \frac{d^3}{d\eta^3} - \frac{d}{d\eta}, \ \mathcal{L}_h = \frac{d^2}{d\eta^2} + \frac{d}{d\eta} \ \text{and} \ \mathcal{L}_\theta = \frac{d^2}{d\eta^2} + \frac{d}{d\eta}, \tag{3.18}$$

satisfying the following properties (as reported in [96, 107])

$$\left.\begin{array}{r}\mathcal{L}_f\left[F_1 + F_2 e^{\eta} + F_3 e^{-\eta}\right] = 0,\\ \mathcal{L}_h\left[F_4 + F_5 e^{-\eta}\right] = 0,\\ \mathcal{L}_\theta\left[F_6 + F_7 e^{-\eta}\right] = 0,\end{array}\right\} \tag{3.19}$$

in which $F_i(i$ varies from 1 to 7) are arbitrary constants. Moreover, auxiliary functions are defined as $H_f(\eta) = H_h(\eta) = H_\theta(\eta) = 1$ in combination with the auxiliary parameters $\hbar_f = \hbar_h = \hbar_\theta = \hbar$ during the computation. MATHEMATICA computation software is then used to solve the given system.

3.2.1 Convergence Control Region

The convergence of the Homotopy series solutions can be controlled by the non-zero auxiliary parameter $(\hbar)$ which is evident in Figure 3.2. For the sake of the validation of the current results and analysing the influence of the governing parameters on the prescribed velocities and temperature distributions, the appropriate values of $\hbar$ are chosen from the common tolerable range $-0.55 \leq \hbar < 0$ which is obtained at the 20th–order of approximation of the HAM solution for $n = 0.5, \ Pr = 5, \ K =$

$\lambda = Q = \delta = f_w = 0.1$, $\alpha = 1$ and $\beta = -1$. Here, it is noticeable that when the sheet stretches $(s = 1)$, $\hbar$ curves are plotted at $\eta = 0$ and when it shrinks $(s = -1)$, curves are sketched at $\eta = 50$ to get the smooth horizontal lines.
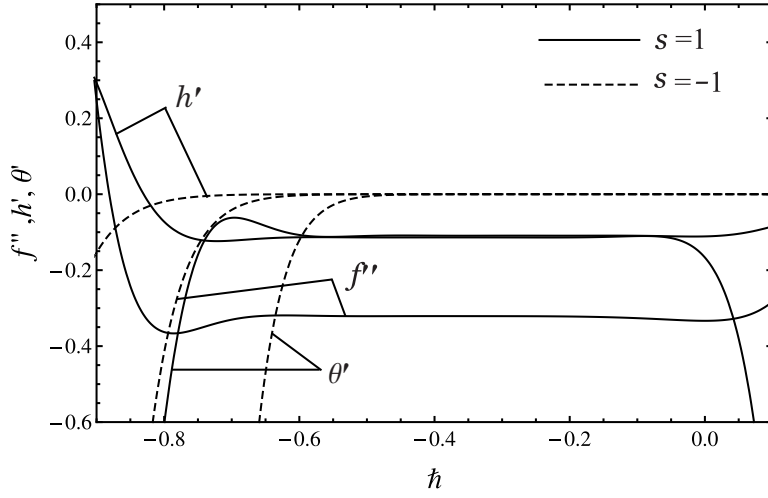
Figure 3.2: $\hbar$ curves

3.2.2 Study Validation

The present study is validated in three different ways. Firstly, the case of forced convective micropolar fluid flow over a porous shrinking sheet with the slip flow model as presented by Rosca and Pop [84] is considered. The obtained HAM solutions are in excellent agreement, as depicted in Figure 3.3 for the stable and physically reliable solutions as reported in [84] at $K = \alpha = 1$, $\lambda = 0$, $f_w = 3$, $s = \beta = -1$, and $n = 0.2$. In Figure 3.3, the lower curve is sketched for velocity component (f') at $\hbar = -0.095$ and an upper curve is plotted for micro-rotational velocity (h) at $\hbar = -0.13$.
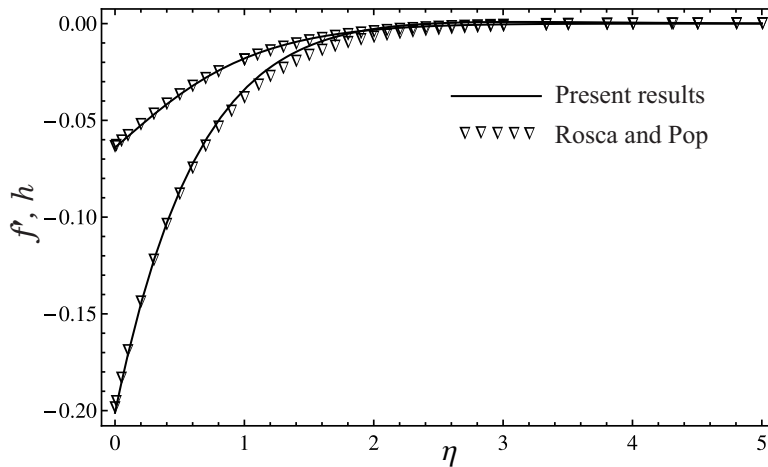
Figure 3.3: Result validation with [84]

24

Secondly, the forced convective micropolar fluid flow over a permeable shrinking sheet [33] is validated with the current HAM results in a special case at $K = 0.1$, $\lambda = \alpha = \beta = 0$, $f_w = 2.1$, $s = -1$, and $n = 0.5$, as depicted in Figure 3.4, which is again in good correspondence. In Figure 3.4, it is to be noted that the lower and upper curves are for f' and h, respectively, which are computed at $\hbar = -0.5$. Lastly, the present results are also in a very good compatibility with the analytical results reported by Turkyilmazoglu [34] for the stretching sheet case at $K = 1$, $\lambda = \alpha = \beta = 0$, $f_w = 1$, $s = 1$, and $n = 0.5$ as shown in Figure 3.5. The upper and lower curves are plotted for f' and h at $\hbar = -0.25$ and -0.1, respectively.
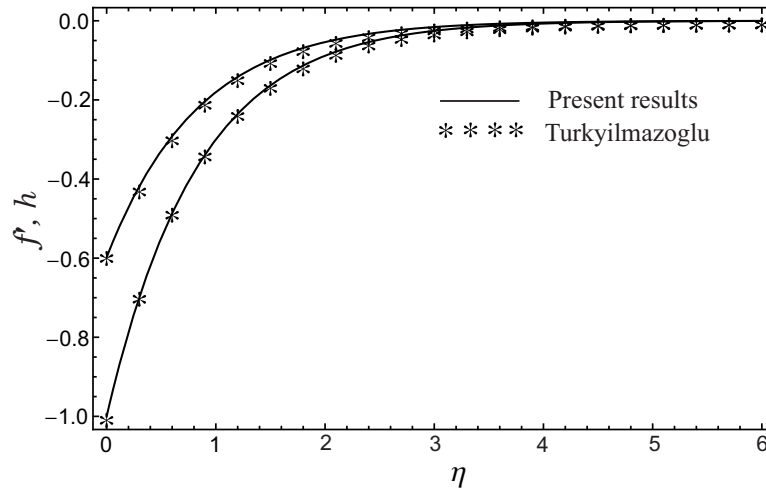
Figure 3.4: Result validation with [33]
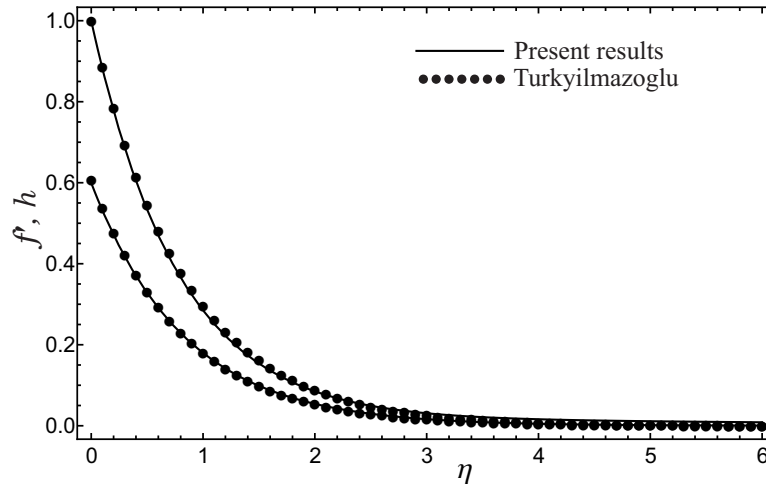
Figure 3.5: Result validation with [34]

3.3 Results and Discussion

In this section, obtained HAM results are discussed at the fixed values of the prescribed parameters $K = f_w = Q = \delta = 0.5$, $\lambda = \alpha = 1$, $\beta = -1$, $Pr = 5$, and $n = 0.5$ for stretching $(s = 1)$/shrinking $(s = -1)$ sheet or otherwise specified. Figures 3.6–3.7 illustrate the effect of the material parameter K on the velocity component (f') and the microrotational velocity (h) with the increasing value of the η, respectively. It is observed that when the sheet stretches, with the increase of the concentration of microelements in the fluid flow, the prescribed velocities increase and generally, the Newtonian fluid $(K = 0)$ has the lowest velocity as compared to the non-Newtonian, i.e. micropolar $(K > 0)$ fluid flow. Moreover, when the sheet shrinks; the increasing concentration of microelements cause to slow down the velocity component (f') and oppositely, enhance the microrotational velocity of the fluid flow. Note that the Figure 3.6 is computed at $\hbar = -0.01$ and in Figure 3.7; $\hbar = -0.05$ is used for stretching the sheet and $\hbar = -0.015, -0.004, -0.001, -0.0001$ are set for shrinking case along with the increasing value of K, respectively. In Table 3.1, it is evident that when sheet stretches, the local skin friction, local wall couple stress and heat transfer rate increase with the increasing concentration of micro-elements in the fluid flow while all of these physical quantities show the reverse impact when the sheet shrinks as tabulated in Table 3.2.
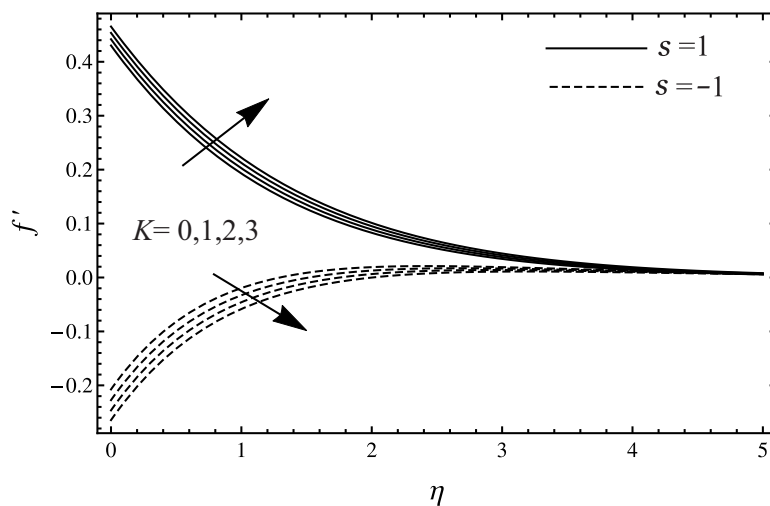
Figure 3.6: Influence of K on f'.

The influence of the buoyancy parameter (λ) is depicted in Figures 3.8–3.9. It is observed that mixed convective micropolar fluid flow has higher velocity component as compared to the forced convective flow for both cases of the stretching and shrinking of the sheet. However, the velocity component is increasing with the increasing value of the buoyancy parameter when the sheet stretches or shrinks.

26
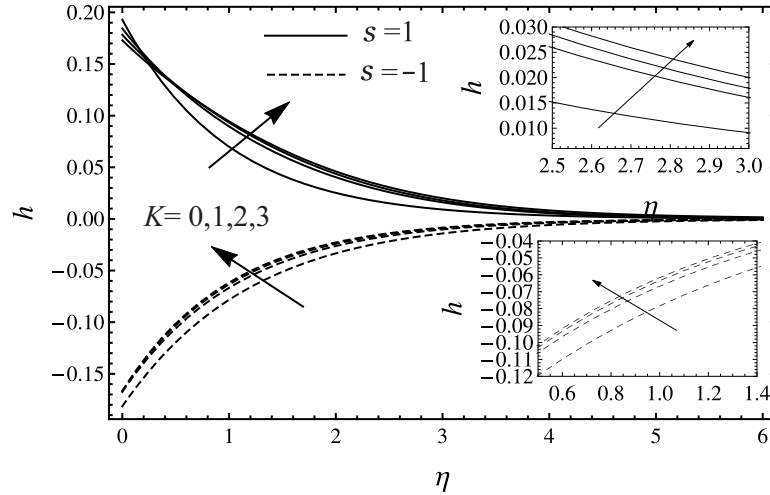
Figure 3.7: Influence of K on h.

While an increase in the buoyancy parameter causes to reduce the thermal boundary layer thickness in Figure 3.9. Moreover, shrinking sheet has higher thermal boundary layer thickness as compared to the stretching sheet. Figure 3.8 is plotted at $\hbar = -0.01$ for $s = 1$ and $\hbar = -0.005$ for $s = -1$, Figure 3.9 is sketched at $\hbar = -0.01$. When the sheet stretches, an increase in the buoyancy parameter yields higher local skin friction and heat transfer rate in the micropolar fluid flow while it reduces the local wall couple stress as shown in Table 3.1. However, local skin friction and wall couple stress decrease and the local Nusselt number increases with the increasing value of the λ for $s = -1$ as shown in Table 3.2.
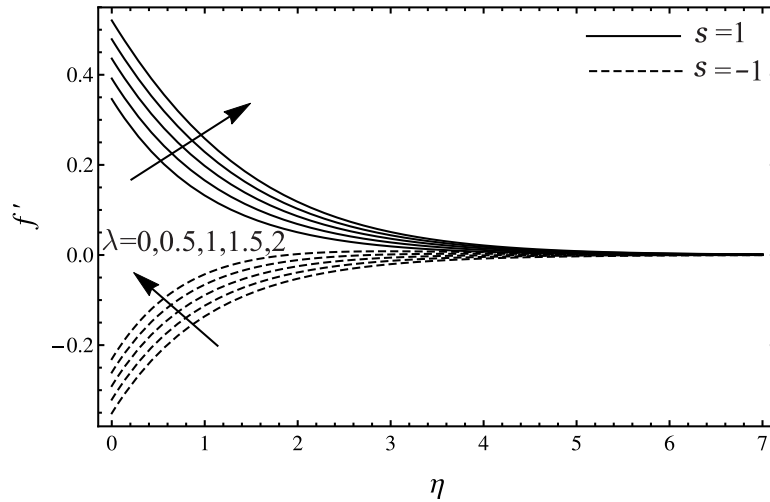
Figure 3.8: Influence of λ on f'.

Figure 3.10 displays the impact of various values of the Prandtl number with the increasing value of the similarity variable η. It shows that either the sheet stretches or shrinks, a decrease in the thermal diffusivity or an increase in the momentum diffusivity, in other words, an increase in the Prandtl number causes to reduce the
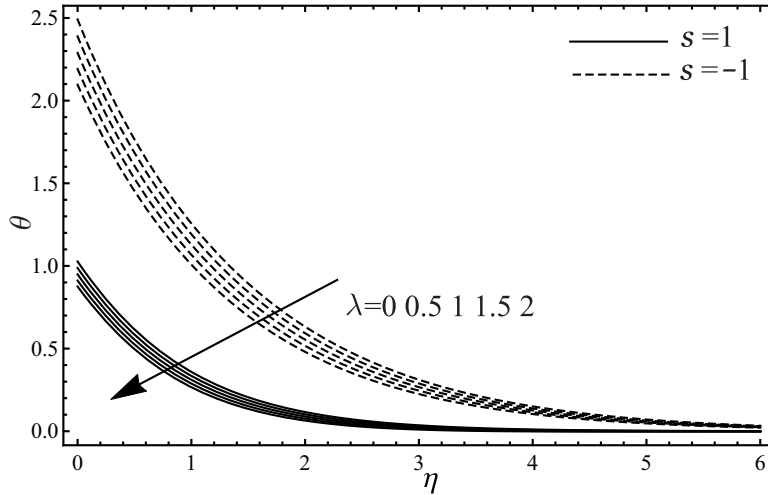
Figure 3.9: Influence of λ on θ.

temperature of the micropolar fluid flow. It is also noted that at the constant concentration of micro-elements at $\eta = 0$, stretching sheet causes to reduce the $\approx 25\%$ more temperature as compared to the shrinking of the sheet. However, the thickness of the thermal boundary layer is shorter in the shrinking case. Moreover, $\hbar = -0.01, -0.007, -0.006, -0.003, -0.0015, -0.0009, -0.0005, -0.0004, -0.0001$ and $\hbar = -0.01, -0.007, -0.006, -0.003, -0.0015, -0.0007, -0.0002, -0.00006, -0.000001$ are used for $s = 1$ and $s = -1$ with the increasing value of the Pr, respectively. When the momentum diffusivity is dominant on the thermal diffusivity, it is interesting to note that the heat transfer rate increases along with the local skin friction in both cases of the stretching and shrinking of the sheet as displayed in Tables 3.1–3.2. Furthermore, local wall couple stress increases for $s = 1$, and it decreases for $s = -1$.
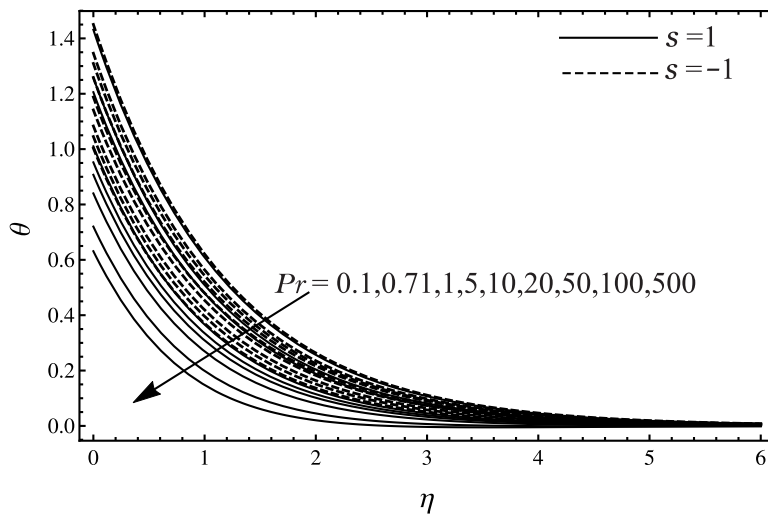
Figure 3.10: Influence of Pr on θ.

Figures 3.11–3.12 show the influence of the heat generation (> 0) / absorption

28
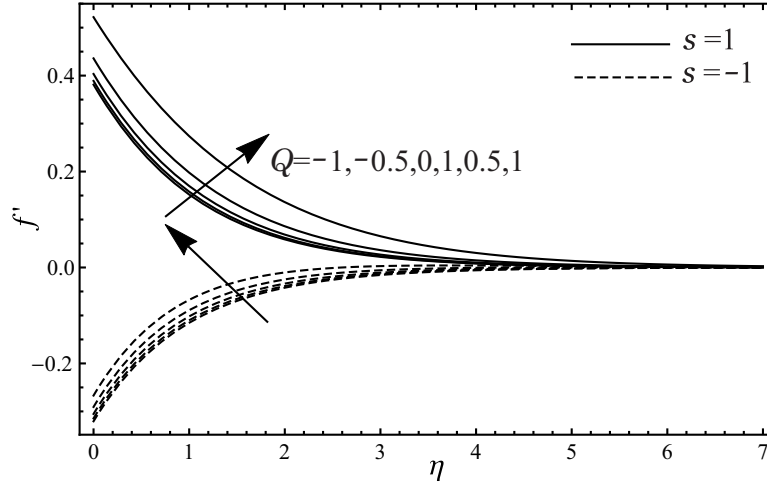
Figure 3.11: Influence of Q on f'.

Table 3.1: Influences of K, λ, Pr, Q on physical quantities for $s = 1$.

K	λ	Pr	Q	$C_{f_x}Re_x^{\frac{1}{2}}$	$-\hbar$	M_xRe_x	$-\hbar$	$Nu_xRe_x^{-\frac{1}{2}}$	$-\hbar$
0.0	1	5	0.5	0.33418	0.01	0.16433	0.01	1.02377	0.01
1.0				0.49927	0.01	0.21698	0.01	1.03024	0.01
2.0				0.66322	0.01	0.26029	0.01	1.03686	0.01
3.0				0.82599	0.01	0.29695	0.01	1.04360	0.01
0.5	0			0.41662	0.01	0.19407	0.01	0.98694	0.01
	0.5			0.41676	0.014	0.19298	0.01	1.00647	0.01
	1			0.41686	0.01	0.19208	0.01	1.02699	0.01
	1.5			0.41750	0.01	0.19136	0.01	1.04855	0.01
	2			0.41847	0.01	0.19083	0.01	1.07124	0.01
	1	0.1		0.41139	0.01	0.18903	0.01	0.84932	0.01
		0.71		0.41440	0.007	0.19539	0.007	0.89744	0.007
		1		0.41510	0.006	0.19739	0.006	0.91473	0.006
		5		0.41661	0.003	0.203165	0.003	0.99506	0.003
		10		0.41670	0.001	0.20579	0.0015	1.02511	0.0015
		20		0.41680	0.001	0.20683	0.0009	1.05115	0.0009
		50		0.41707	0.001	0.20752	0.0005	1.09526	0.0005
		100		0.41750	0.001	0.20771	0.0004	1.27744	0.0005
		500		0.41848	0.0014	0.20818	0.0001	1.29224	0.0001
		5	1.0	0.39950	0.01	0.18222	0.01	0.94863	0.001
			0.5	0.41686	0.01	0.19208	0.01	0.99723	0.001
			0.0	0.42251	0.01	0.19548	0.01	1.04874	0.001
			−0.5	0.42447	0.01	0.19678	0.01	1.10293	0.001
			−1.0	0.42519	0.01	0.19734	0.01	1.1595	0.001

(< 0) parameter on the velocity component and the temperature profile at $\hbar = -0.01$ and $\hbar = -0.001$, respectively. It is observed that an increase in the heat generation parameter results in an increase in the velocity component and the thermal boundary layer thickness which shows a rise in the temperature of the micropolar fluid flow and on the other hand, velocity component and the temperature of the fluid reduce when the heat absorption parameter increases.

This flow behaviour is noticed when the sheet stretches or shrinks. An increase in the heat generation parameter yields a decrease in the local skin friction and contrastively, reduces the heat transfer rate. In addition, the local wall couple stress decreases. Furthermore, increasing value of the heat absorption parameter produces an increase in the local skin friction, and local wall couple stress and adversely, rising the heat transfer rate. This flow behaviour is numerically reported in the Tables 3.1–3.2.
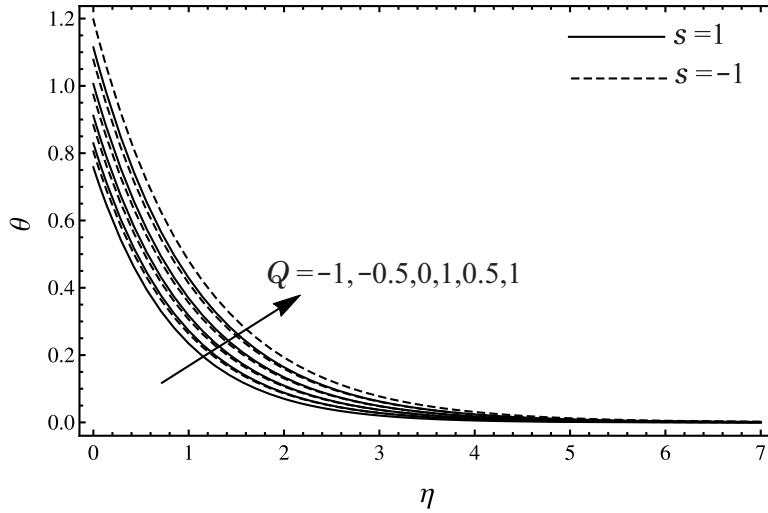
Figure 3.12: Influence of Q on θ.

The suction/injection effect on the velocity component, microrotational velocity and the temperature profiles is illustrated in Figures 3.13–3.15 at $\hbar = -0.005, -0.01$ and -0.001, respectively. Obtained results show that when the sheet stretches or shrinks, higher the suction parameter lower the velocity component and higher the injection parameter, higher the velocity component of the micropolar fluid flow as depicted in Figure 3.13. When sheet stretches, microrotational velocity decreases with an increase in the suction parameter and it increases with an increase in the injection parameter as shown in the Figure 3.14.

Furthermore, an increase in the suction parameter yields an increase in the microrotational velocity and it reduces with the higher values of the injection parameter. The temperature of the micropolar fluid flow decreases with an increase in the suction parameter and it increases with the increasing value of the injection parameter for $s = 1, -1$ as in Figure 3.15. It is seen from the Tables 3.3–3.4, local skin friction, local wall couple stress and local Nusselt number increase as the suction parameter increases, on the other hand, these physical quantities decrease with the increasing value of the injection parameter. An increase in the stretching parameter leads to an increase in the velocity component and microrotational velocity, and oppositely, thermal boundary layer thickness decreases. On the other hand, increasing value of the shrinking parameter
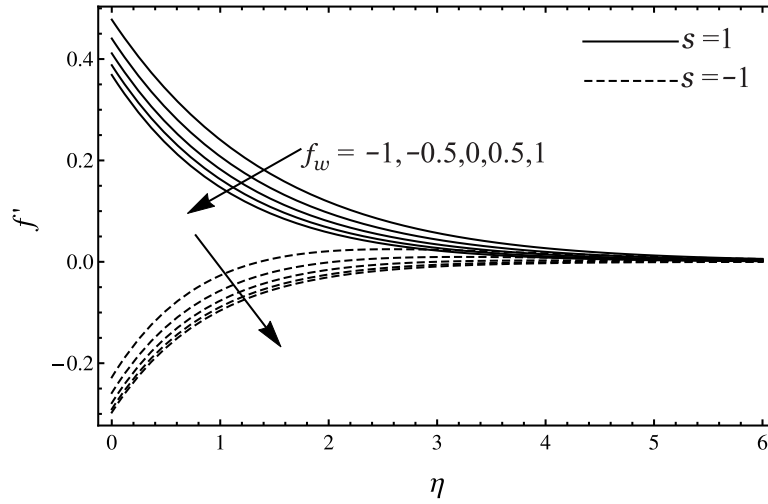
Figure 3.13: Influence of f_w on f'.
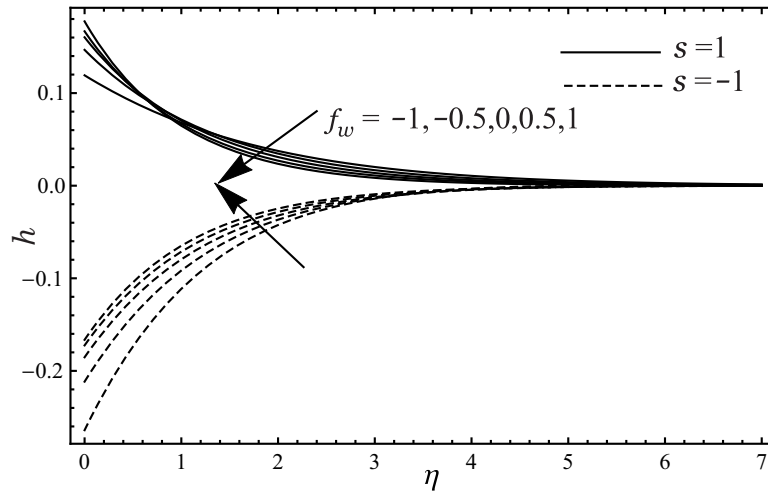
Figure 3.14: Influence of f_w on h.
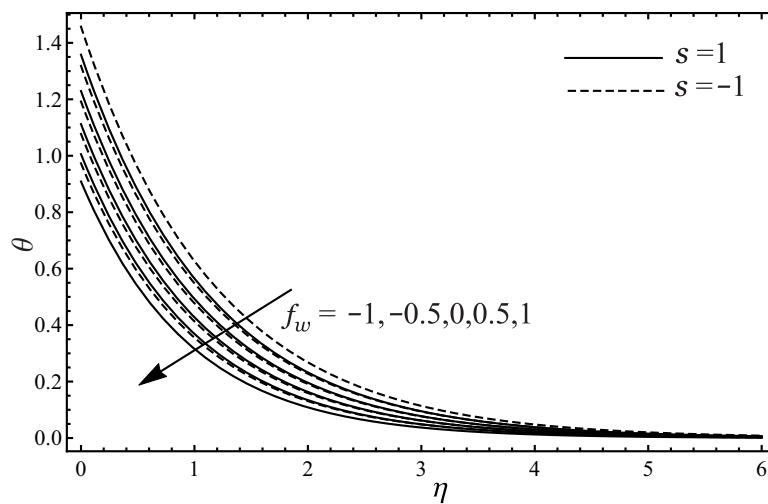
Figure 3.15: Influence of f_w on θ.

results in a lower velocity component, microrotational velocity, and reversely, thermal boundary layer thickness increases as sketched in Figures 3.16–3.18 at

Table 3.2: Influences of K, λ, Pr, Q on physical quantities for $s = -1$.

K	λ	Pr	Q	$-C_{f_x}Re_x^{\frac{1}{2}}$	$-\hbar$	$-M_xRe_x$	$-\hbar$	$Nu_xRe_x^{-\frac{1}{2}}$	$-\hbar$
0.0	1	5	0.5	0.34418	0.01	0.14871	0.01	0.71982	0.01
1.0				0.51838	0.01	0.22160	0.01	0.71717	0.01
2.0				0.6933	0.01	0.28934	0.01	0.71460	0.01
3.0				0.86848	0.01	0.35129	0.01	0.71210	0.01
0.5	0			0.41606	0.01	0.16804	0.01	0.70070	0.01
	0.5			0.42398	0.01	0.17710	0.01	0.70933	0.01
	1			0.43116	0.01	0.18571	0.01	0.71848	0.01
	1.5			0.43762	0.01	0.19387	0.01	0.72820	0.01
	2			0.44340	0.01	0.20159	0.01	0.73852	0.01
	1	0.1		0.42309	0.01	0.18024	0.01	0.84471	0.01
		0.71		0.42010	0.007	0.18539	0.007	0.87136	0.007
		1		0.41928	0.006	0.18769	0.006	0.88186	0.006
		5		0.41769	0.003	0.19663	0.003	0.89723	0.003
		10		0.41703	0.0015	0.20208	0.0015	0.92089	0.0015
		20		0.41679	0.0007	0.20531	0.0007	0.93803	0.0007
		50		0.41669	0.0002	0.20745	0.0002	0.96146	0.0002
		100		0.41667	0.00007	0.20807	0.00006	0.97830	0.00006
		500		0.41667	0.000001	0.20833	0.000001	0.99831	0.000001
		5	1.0	0.47430	0.01	0.21416	0.01	0.91759	0.001
			0.5	0.43116	0.01	0.18571	0.01	0.96410	0.001
			0.0	0.41672	0.01	0.17527	0.01	1.01365	0.001
			−0.5	0.41156	0.01	0.17102	0.01	1.06605	0.001
			−1.0	0.40951	0.01	0.16904	0.01	1.12102	0.001

$\hbar = -0.01, -0.01$ and -0.005, respectively.
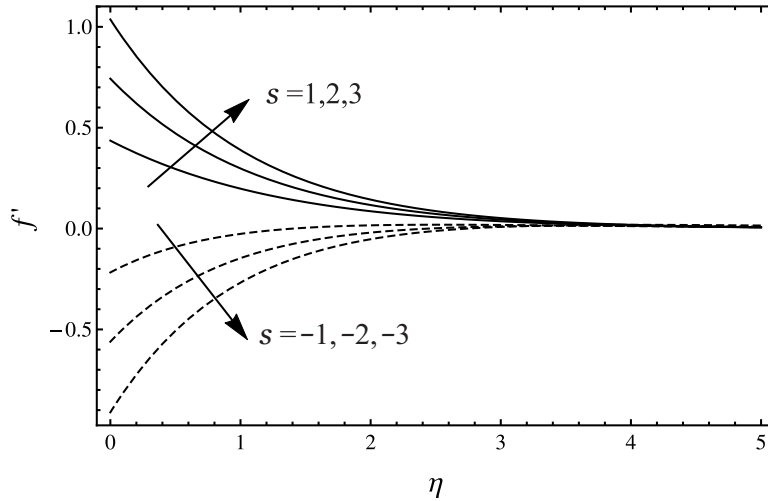
Figure 3.16: Influence of s on f'.

The impacts of the first order (α) and second order (β) slip flow parameters on the velocity component, microrotational velocity and temperature profiles are plotted in the Figures 3.19–3.24. It can be seen that increasing value of the slip flow parameters reduces the velocity component and the microrotational velocity profile, while it enhances the temperature of the micropolar fluid flow
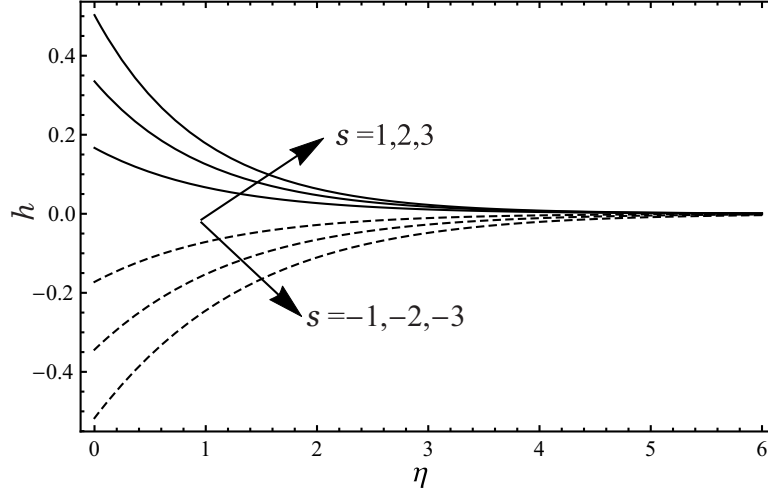
Figure 3.17: Influence of s on h.

Table 3.3: Influences of $f_w, \alpha, \beta, \delta$ on physical quantities for $s = 1$.

f_w	α	β	δ	$C_{f_x}Re_x^{\frac{1}{2}}$	$-\hbar$	M_xRe_x	$-\hbar$	$Nu_xRe_x^{-\frac{1}{2}}$	$-\hbar$
1.0	1	−1	0.5	0.42399	0.01	0.21345	0.01	1.05015	0.001
0.5				0.41686	0.01	0.19208	0.01	0.99723	0.001
0.0				0.40070	0.01	0.16624	0.01	0.94963	0.001
−0.5				0.36670	0.01	0.13169	0.01	0.90679	0.001
−1.0				0.29799	0.01	0.08030	0.01	0.86822	0.001
0.5	1			0.41686	0.01	0.19208	0.01	1.0270	0.01
	2			0.31164	0.01	0.14005	0.01	0.97627	0.01
	3			0.24880	0.01	0.10964	0.01	0.94758	0.01
	1	−1		0.41686	0.01	0.19208	0.01	1.02699	0.01
		−2		0.34460	0.01	0.15627	0.01	0.98342	0.01
		−3		0.30201	0.01	0.13562	0.01	0.95826	0.01
		−1	0.1	0.41667	0.001	0.19382	0.01	0.98934	0.005
			0.2	0.416664	0.001	0.19351	0.01	0.99062	0.005
			0.3	0.416663	0.001	0.19313	0.01	0.99227	0.005
			0.4	0.416661	0.001	0.19266	0.01	0.99447	0.005
			0.5	0.416659	0.001	0.19208	0.01	0.99756	0.005

for stretching sheet case. However, a reverse trend is noted for the shrinking sheet. In Figures 3.19–3.24, all curves are plotted at $\hbar = -0.01$ and $\hbar = -0.005$ is used for all values of β for $s = 1$. From the Tables 3.3–3.4, it is depicted that the increasing value of both slip flow parameters causes to reduce the local skin friction, local wall couple stress and local Nusselt number for $s = 1$, a reverse phenomenon is observed for $s = -1$.

An increase in the Newtonian heating parameter produces a higher velocity component and the thermal boundary layer thickness which results in a higher temperature of the micropolar fluid flow with the stretching or shrinking the sheet. $\hbar = -0.01$ and -0.005 are used for Figures 3.25–3.26, respectively. It is observed from the sketch; shrinking sheet rises the $\approx 165\%$ more temperature

Figure 3.18: Influence of s on θ.
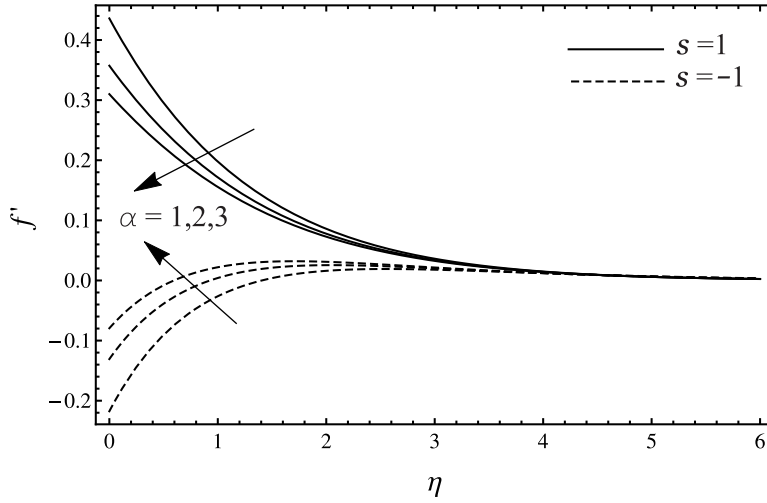
Figure 3.19: Influence of α on f'.
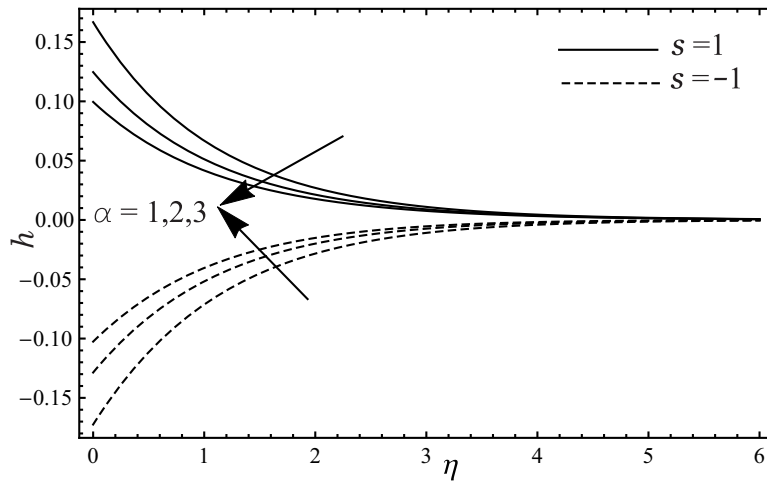
Figure 3.20: Influence of α on h.

of the micropolar fluid flow as compared to the stretching of the sheet at $\eta = 0$. This increase in temperature reinforces the heat transfer rate from the bonding
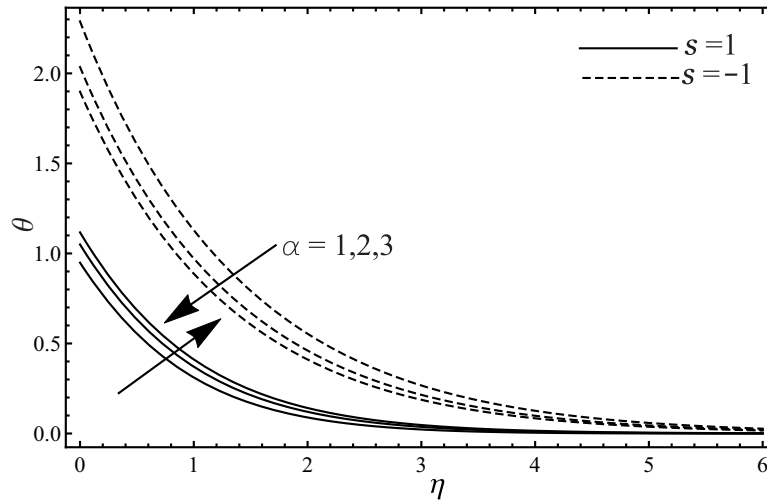
Figure 3.21: Influence of α on θ.
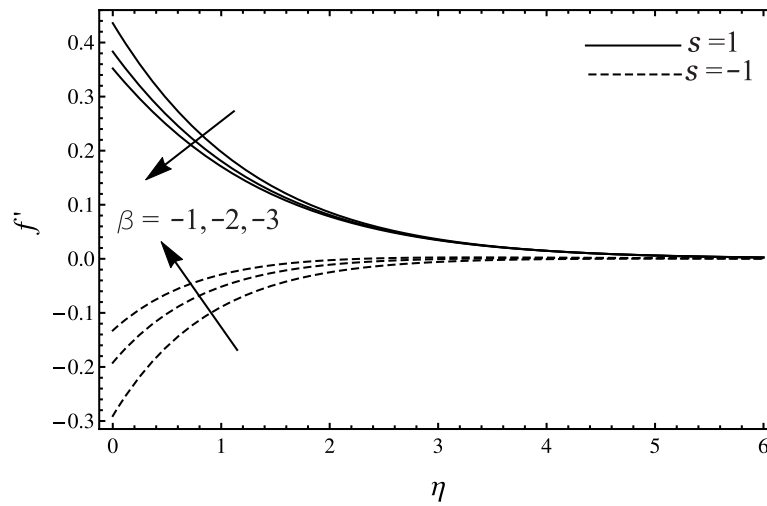
Figure 3.22: Influence of β on f'.
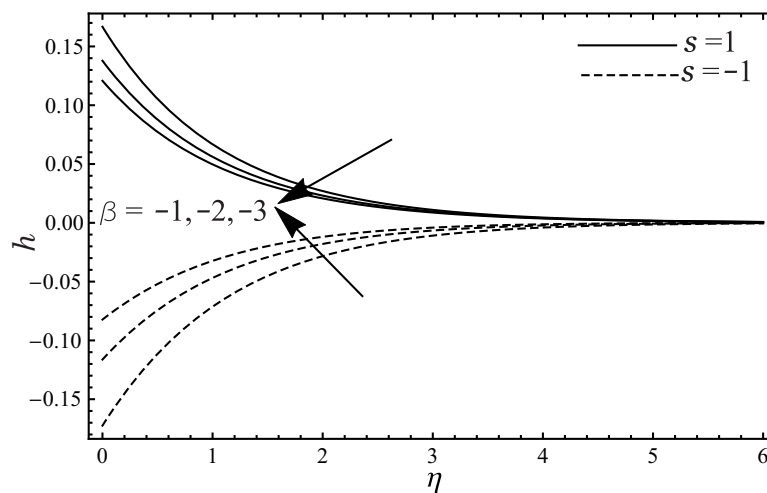
Figure 3.23: Influence of β on h.

surface of the micropolar fluid flow. However, local skin friction and local wall couple stress increase with stretching the sheet and decrease with shrinking the

35
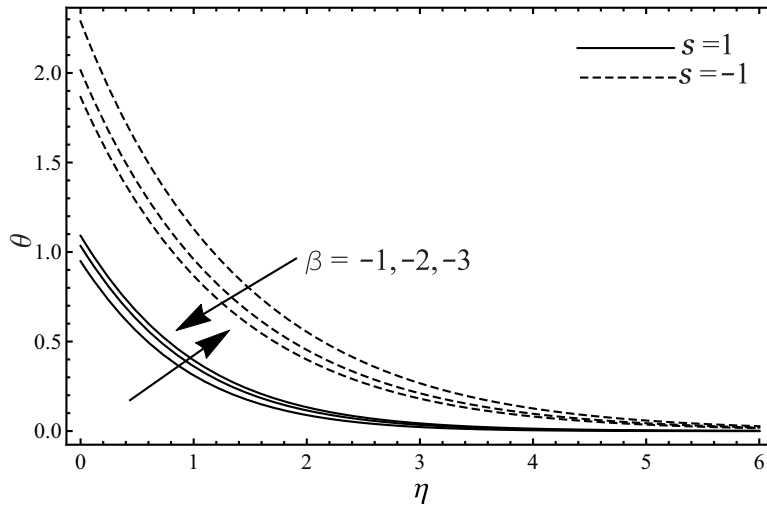
Figure 3.24: Influence of β on θ.

sheet as shown in Tables 3.3–3.4.
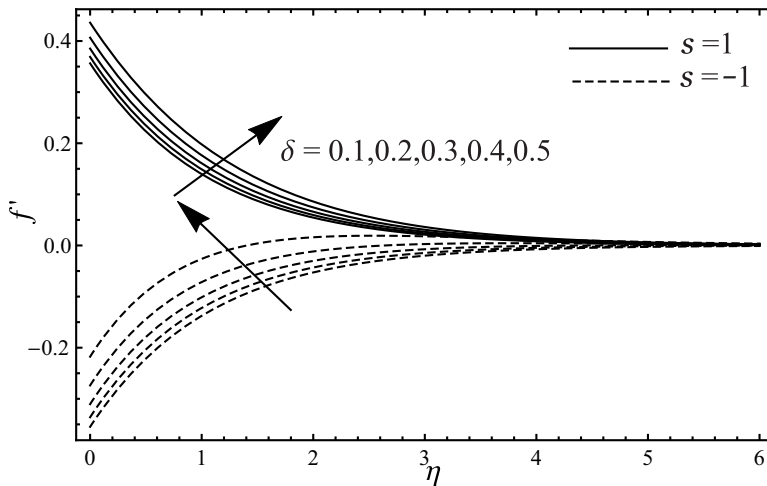
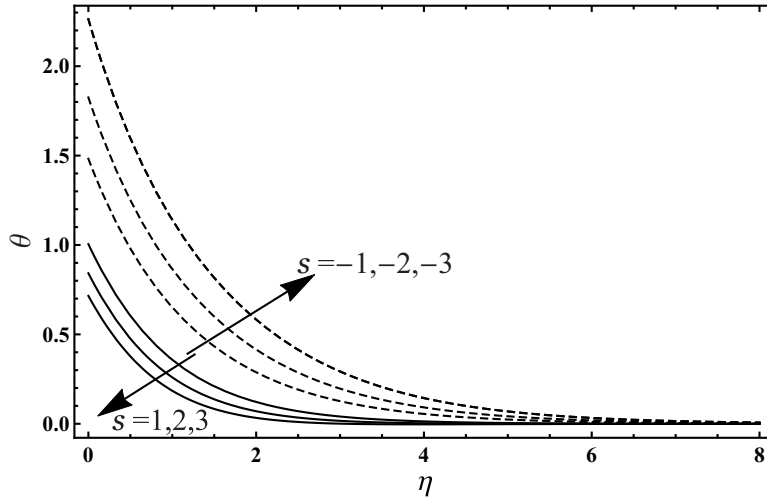**Figure 3.25:** Influence of δ on f'.
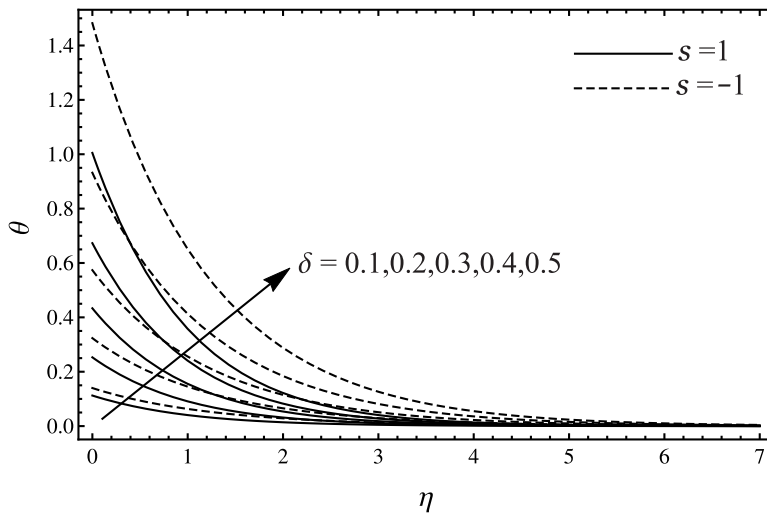
Figure 3.26: Influence of δ on θ.

Table 3.4: Influences of $f_w, \alpha, \beta, \delta$ on physical quantities for $s = -1$.

f_w	α	β	δ	$-C_{f_x}Re_x^{\frac{1}{2}}$	$-\hbar$	$-M_xRe_x$	$-\hbar$	$Nu_xRe_x^{-\frac{1}{2}}$	$-\hbar$
1.0	1	−1	0.5	0.416111	0.01	0.18238	0.01	1.01385	0.001
0.5				0.431161	0.01	0.18571	0.01	0.96410	0.001
0.0				0.463233	0.01	0.18838	0.03	0.91942	0.001
−0.5				0.529064	0.01	0.21052	0.01	0.87925	0.001
−1.0				0.660126	0.01	0.26914	0.01	0.84312	0.001
0.5	1			0.431161	0.01	0.18571	0.01	0.71848	0.01
	2			0.321567	0.01	0.14226	0.01	0.74568	0.01
	3			0.256442	0.01	0.11568	0.01	0.76341	0.01
	1	−1		0.431161	0.01	0.18571	0.01	0.71848	0.01
		−2		0.290721	0.01	0.12828	0.01	0.74815	0.01
		−3		0.205674	0.01	0.09250	0.01	0.76802	0.01
		−1	0.1	0.417693	0.01	0.16986	0.01	0.81408	0.005
			0.2	0.419752	0.01	0.17220	0.01	0.81807	0.005
			0.3	0.422429	0.01	0.17527	0.01	0.82299	0.005
			0.4	0.426042	0.01	0.17952	0.01	0.82921	0.005
			0.5	0.431161	0.01	0.18571	0.01	0.83733	0.005

3.4   Chapter Summary

In this chapter the influence of the heat source/sink parameter on the mixed convective micropolar fluid flow is investigated by using a semi-analytical technique named Homotopy Analysis Method. The fluid is moving over a stretching/shrinking sheet under the impact of the second order slip boundary condition. It can be concluded that increasing value of the heat source (generation) parameter enhances the velocity component and the temperature of the micropolar fluid flow passing over the stretching/shrinking sheet. The heat sink (absorption) parameter has an opposite effect on the flow.

Chapter 4

Radiative MHD Micropolar Fluid Flow[1]

In this chapter,the work reported in [79, 86] is extended to study the MHD micropolar fluid flow behaviour on the stretching/shrinking sheet in the presence of the thermal radiation parameter. Fang *et al.* [79] examined the boundary layer flow of a viscous fluid flowing over a stretching sheet with a second order slip at the boundary and furthermore, Ibrahim [86] analyzed the heat transfer MHD micropolar fluid flow over a stretching sheet by using the same slip boundary condition as reported in [79]. However, in this investigation, we study the heat transfer MHD micropolar fluid flow over a stretching/shrinking sheet with second order slip and the Newtonian heating conditions at the boundary. In industry, the impact of MHD fluid flow is of great importance in bearings with liquid-metal lubrications. Being a lubricant, it controls the lubricant viscosity with varying temperature under certain extreme operating conditions [108].

4.1   Problem Formulation

It is assumed that a steady state, two dimensional mixed convective, laminar, incompressible micropolar fluid flow over a vertical permeable stretching/shrinking sheet with velocity $u_w(x) = sax$ for a positive dimensional constant $(a > 0)$. A transverse uniform magnetic field is applied along the y–axis, i.e. $(0, B_o)$, as shown in Figure 4.1. The velocity boundary layer equation is formulated by a second order slip flow model [11], and the thermal boundary layer equation represents the Newtonian heating [89, 90] effect in it. For radiative magneto-micropolar fluid

---

[1]Copyright permission: please see in Appendix B.

flow, the system of equations $(1.4)_1 - (1.4)_2$, $(1.4)_4 - (1.4)_5$ and Equation (1.5) can be simplified by substituting $\mathfrak{A} = \mathfrak{C} = \mathfrak{D} = 0$ and $\mathfrak{B} = \mathfrak{E} = 1$ without considering the Hall effect and the mass transfer. The system reads as [84, 86]
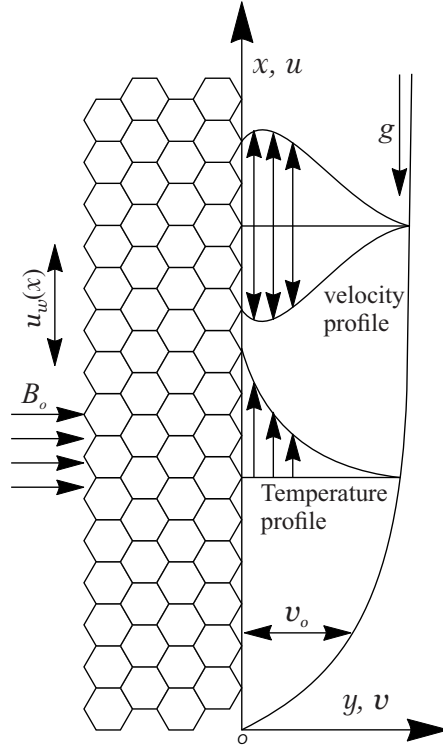
Figure 4.1: Flow model.

$$\frac{\partial u}{\partial x} + \frac{\partial v}{\partial y} = 0, \tag{4.1}$$

$$u\frac{\partial u}{\partial x} + v\frac{\partial u}{\partial y} = \frac{\mu + \chi}{\rho}\left(\frac{\partial^2 u}{\partial y^2}\right) + g\beta_T\left(T - T_\infty\right) + \frac{\chi}{\rho}\left(\frac{\partial \omega}{\partial y}\right) - \frac{\sigma B_o^2}{\rho}u, \tag{4.2}$$

$$u\frac{\partial \omega}{\partial x} + v\frac{\partial \omega}{\partial y} = \frac{\gamma}{\rho j}\left(\frac{\partial^2 \omega}{\partial y^2}\right) - \frac{\chi}{\rho j}\left(2\omega + \frac{\partial u}{\partial y}\right), \tag{4.3}$$

$$u\frac{\partial T}{\partial x} + v\frac{\partial T}{\partial y} = \frac{k}{\rho c_p}\left(\frac{\partial^2 T}{\partial y^2}\right) - \frac{1}{\rho c_p}\frac{\partial q_r}{\partial y}, \tag{4.4}$$

with boundary conditions,

$$\left.\begin{array}{c} u = su_w(x) + u_{\text{slip}}, \ v = v_o, \ \omega = -n\dfrac{\partial u}{\partial y}, \ k\dfrac{\partial T}{\partial y} = -h_sT \text{ at } y = 0, \\ u \to 0, \ \omega \to 0, \ T \to T_\infty \text{ as } y \to \infty. \end{array}\right\} \tag{4.5}$$

The equations $(4.5)_1$ and $(4.5)_4$ are for second order slip flow and the Newtonian heating conditions at the boundary, respectively. The second term of $(4.5)_1$ is defined in Equations (1.6)–(1.7).

40

The following similarity variables with velocity components $u = axf'(\eta)$ and $v = -(a\nu)^{1/2} f(\eta)$ along with

$$\eta = \sqrt{a/\nu} y, \ \omega = \sqrt{a/\nu} axh(\eta) \ \text{and} \ \theta(\eta) = \frac{T - T_\infty}{T_\infty}, \qquad (4.6)$$

are defined to nondimensionalized the system of Equations (4.1)–(4.5) which reduces it into the following nonlinear set of coupled equations (see in Section A.2 of appendix):

$$(1 + K)f''' - (f')^2 + ff'' + Kh' + \lambda\theta - Mf' = 0, \qquad (4.7)$$

$$(1 + K/2)h'' - f'h + fh' - K(2h + f'') = 0, \qquad (4.8)$$

$$(1 + R)\theta'' + Prf\theta' = 0, \qquad (4.9)$$

with the boundary conditions

$$\left.\begin{array}{l} f = f_w, f' = s + \alpha f'' + \beta f''', \ h = -nf'', \theta' = -\delta(1 + \theta) \ \text{at} \ \eta = 0, \\ f' \to 0, \ h \to 0, \ \theta \to 0 \ \text{as} \ \eta \to \infty, \end{array}\right\} \qquad (4.10)$$

where $(')$ denotes the derivative with respect to the similarity variable (η). In the system of Equations (4.7)–(4.9), the non-dimensional physical parameters are defined as buoyancy parameter $\lambda = Gr_x/Re_x$ for local Grashof number $Gr_x = g\beta_T T_\infty x/a\nu$ and local Reynolds number $Re_x = ax^2/\nu$, magnetic field parameter $M = \sigma B_o^2/a\rho$, thermal radiation parameter $R = (16\sigma^* T_\infty^3)(3k^* k)^{-1}$ and Prandtl number $Pr = \mu c_p/k$. In Equation (4.10), the suction/injection parameter is $f_w = -(a\nu)^{-\frac{1}{2}} v_o$, the first and second order slip flow parameters are $\alpha = A\sqrt{a/\nu} > 0$ and $\beta = Ba/\nu < 0$, and the Newtonian heating parameter is $\delta = h_s k^{-1}(\nu/a)^{1/2}$. Moreover, the physical quantities such as local skin friction co-efficient (C_{f_x}), local wall couple stress (M_x) and the local Nusselt number (Nu_x) are defined in Equation (3.10).

4.2 Homotopy Analysis Method

Liao [96] introduced a semi-analytical method named Homotopy Analysis Method (HAM) which is quite useful to solve the system of coupled linear and nonlinear ordinary differential equations even with mixed derivative boundary conditions. Using the standard basic features of the HAM with a set of base functions $\{\eta^r e^{-i\eta} | r \geq 0, i \geq 0\}$ and the initial set of solutions in the following form:

$$
\left.
\begin{aligned}
f_0(\eta) &= f_w + \frac{s(1 - e^{-\eta})}{1 + \alpha - \beta}, \\
h_0(\eta) &= \frac{s n e^{-\eta}}{1 + \alpha - \beta}, \\
\theta_0(\eta) &= \frac{\delta e^{-\eta}}{1 - \delta} \quad ; \delta \neq 1,
\end{aligned}
\right\}
\tag{4.11}
$$

the linear operators $\mathcal{L}_f = \frac{d^3}{d\eta^3} - \frac{d}{d\eta}$ for the velocity equation, $\mathcal{L}_h = \frac{d^2}{d\eta^2} + \frac{d}{d\eta}$ for the microrotational velocity equation and $\mathcal{L}_\theta = \frac{d^2}{d\eta^2} + \frac{d}{d\eta}$ for the temperature equation satisfy the properties $\mathcal{L}_f\left[F_1 + F_2 e^\eta + F_3 e^{-\eta}\right] = 0$, $\mathcal{L}_h\left[F_4 + F_5 e^{-\eta}\right] = 0$ and $\mathcal{L}_\theta\left[F_6 + F_7 e^{-\eta}\right] = 0$, respectively for arbitrary constants $F_1, F_2, F_3, \ldots$ and F_7. Moreover, auxiliary functions corresponding to velocity, microrotational velocity and temperature equations are defined as $H_f(\eta) = H_h(\eta) = H_\theta(\eta) = 1$ and corresponding auxiliary parameters (convergence control parameters) are set to be the same, $\hbar_f = \hbar_h = \hbar_\theta = \hbar$, during the entire computation.

4.2.1 Convergence Control Region

In HAM, a non–zero auxiliary parameter ($\hbar$) has a great influence on the convergence of the series solution. Its value is selected from the horizontal line segment of the so-called $\hbar$–curves as shown in Figure 4.2. At 20th–order of approximation of the HAM, the admissible range for the auxiliary parameter is defined as $-0.3 \leq \hbar_f < 0$, $-0.3 \leq \hbar_h < 0$, $-0.28 \leq \hbar_\theta < 0$ at $K = \lambda = f_w = n = \delta = 0.5$, $\alpha = M = R = 1$, $\beta = -1$, $Pr = 5$. Here, in this sketch it is worthy to mention that $\eta = 0$ is used for $s = 1$ and $\eta = 10$ for $s = -1$. Moreover, the validation and the analysis of the current results is carried out within these ranges.
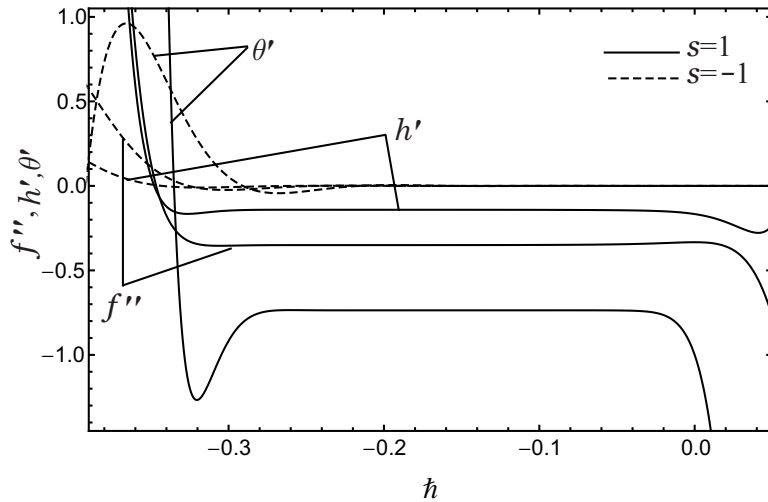
Figure 4.2: $\hbar$ curves

4.3 Validation of the Results

The current HAM results are validated by comparing with exact and numerical results. Firstly, the obtained results are equated with the exact solutions reported by Fang *et al.* [79] in a special case. In this comparison, forced convective boundary layer flow over a porous sheet $(s = -1)$ is taken into account with slip model at $K = M = n = R = 0$. There is an excellent agreement between the Fang *et al.* [79] and the current results for $f_w = 2$ and $\alpha = 1$ as shown in Table 4.1.

Table 4.1: Result validation for $s = -1$.

	[79]	Present	
β	$f''(0)$	$f''(0)$	$-\hbar$
0 .01	0.6360698	0.63606984	0.171916
0.1	0.5780061	0.57800608	0.141216
0.5	0.4043172	0.40431709	0.2579
1.0	0.2905478	0.29054709	0.20675
2.0	0.1846568	0.18465658	0.16638

Secondly, we focus on the flow problem over an impermeable stretching sheet $(s = 1)$ taking into account the effect of forced convective magneto-micropolar fluid flow in the absence of thermal radiation effect using $\alpha = M = 1, \beta = -1$ and $n = 0.5$. To investigate the impact of the concentration of microelements (K), two values of K are chosen to be 0 and 2 along with the $\hbar = -0.015$ and -0.1, respectively. The current results (solid lines) in Figure 4.3 are compared with those (dotted lines) obtained by Ibrahim [86].
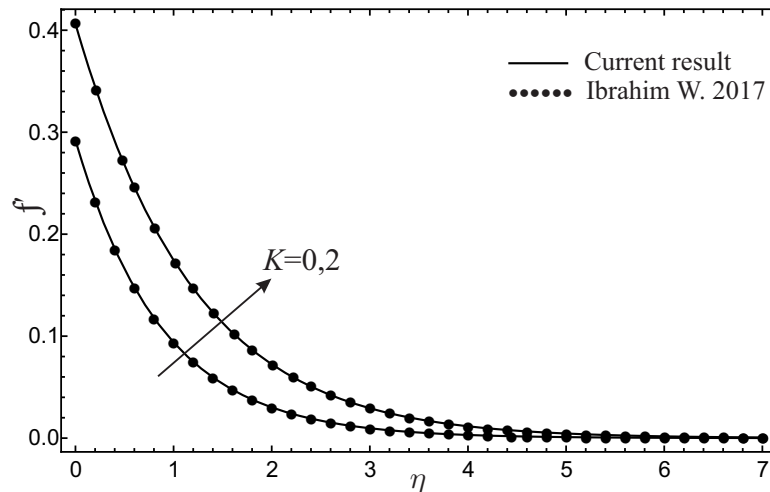
Figure 4.3: Result validation with [86]

4.4 Results and Discussion

The current HAM results are presented graphically for the fixed values of the physical parameters, i.e. $Pr = 5, K = \lambda = n = \delta = f_w = 0.5, M = R = \alpha = 1$ and $\beta = -1$ for both stretching and shrinking sheets or otherwise reported in the illustration. the influence of the concentration of the microelements is displayed in Figures 4.4–4.6. It can be seen that an increase in the concentration of the microelements raises the velocity component (f') and the microrotational velocity (h), and reduces the thermal boundary layer thickness for stretching sheet $(s = 1)$. It decreases the prescribed velocities and enhances the temperature of the fluid flow for shrinking sheet $(s = -1)$. In Figure 4.4, from the increasing values of the K, it can also be noted that the boundary layer thickness increases 78% for stretching sheet and decreases 46% for shrinking sheet at $\eta = 0$. It is noted that
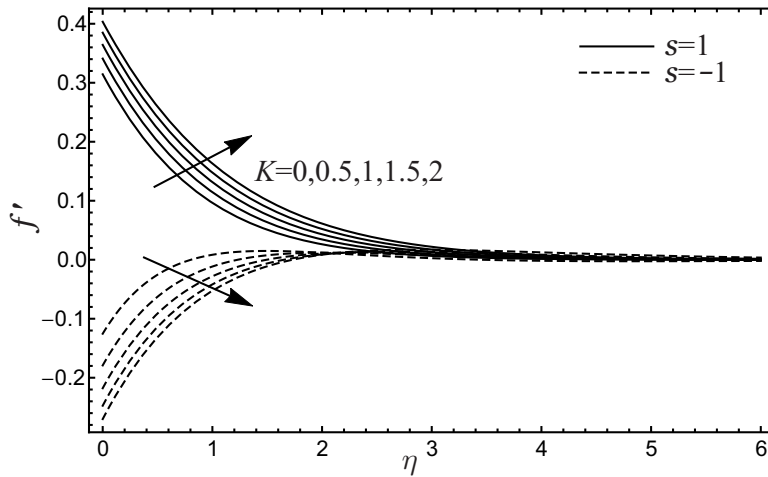
Figure 4.4: Impact of K on f'

$\hbar = -0.1$ is used in Figure 4.4, $\hbar = -0.01$ is used in Figure 4.5 and $\hbar = -0.01$ and -0.02 are used in Figure 4.6 for $s = 1$ and $s = -1$, respectively.

With constant concentration of microelements, Figures 4.7–4.8 show that an increase in the buoyancy parameter causes to increase the velocity component and reduces the temperature profile of the micropolar fluid flow for stretching and shrinking of the sheet at $\hbar = -0.01$. It is also noted that shrinking sheet produces higher thermal boundary layer as compared to the stretching sheet. Local skin friction co-efficient, wall couple stress and Nusselt number are increasing with the increasing values of the K and λ for $s = 1$, while a reverse impact is observed for $s = -1$ as depicted in Tables 4.2–4.3.

Effect of Prandtl number (Pr) with the increasing similarity variable η on the temperature distribution is investigated by using the $\hbar$ values from $\{-0.01, -0.01, -0.01, -0.001, -0.001, -0.001, -0.0006, -0.0004, -0.0001\}$ and $\{-0.009, -0.007, -0.005, -0.005, -0.001, -0.001, -0.0006, -0.0004, -0.0001\}$ for
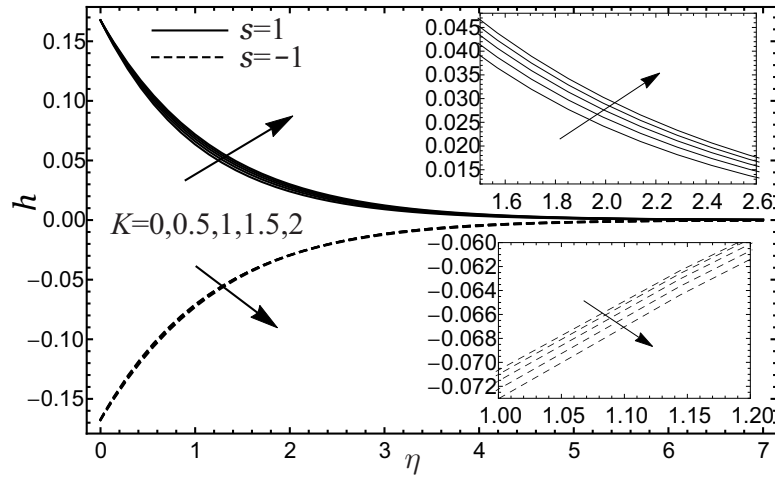
Figure 4.5: Impact of K on h
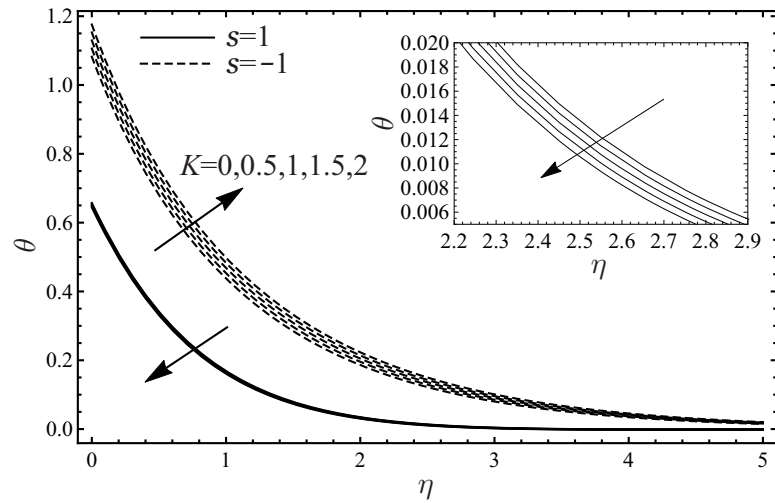
Figure 4.6: Impact of K on θ

$s = 1$ and $s = -1$, respectively. The results as shown in Figure 4.9 indicate that an increase in the Pr values reduces the micropolar fluid temperature and the thickness of the thermal boundary layer. It is also noted that thermal boundary thickness of the stretching sheet decreases faster than that of the shrinking sheet. An increase in the Pr causes to increase the local skin friction coefficient and Nusselt number for stretching and shrinking of the sheet. However, Tables 4.2–4.3 show that the local wall couple stress increases for stretching of the sheet and it decreases for shrinking of the sheet with the increasing value of the Prandtl number.

Figures 4.10–4.13 show the impacts of the magnetic field parameter (M) on the velocity component and the thermal boundary layer thickness for two values of the thermal radiation parameter R, i.e. $R = 1$ and 7. It is observed that an increase in the magnetic field parameter yields a decrease in the velocity component at the lower value of the thermal radiation parameter for $s = 1$. At the same time

Table 4.2: Influences of K, λ, M, Pr, R on physical quantities for $s = 1$.

K	λ	M	Pr	R	$C_{f_x}Re_x^{\frac{1}{2}}$	$-\hbar$	M_xRe_x	$-\hbar$	$Nu_xRe_x^{-\frac{1}{2}}$	$-\hbar$
0.0	1	1	5	1	0.34844	0.1	0.16290	0.01	1.26081	0.01
0.5					0.43684	0.1	0.19513	0.01	1.26446	0.01
1.0					0.52364	0.1	0.22517	0.01	1.26812	0.01
1.5					0.60838	0.1	0.25333	0.01	1.27179	0.01
2.0					0.69094	0.1	0.27979	0.01	1.27548	0.01
0.5	0.0				0.41667	0.01	0.19378	0.011	1.24695	0.01
	0.5				0.41906	0.01	0.19513	0.01	1.26446	0.01
	1.0				0.42161	0.01	0.19556	0.01	1.28227	0.01
	1.5				0.42434	0.01	0.19609	0.01	1.30038	0.01
	2.0				0.42724	0.01	0.19672	0.01	1.31878	0.01
	1.0	0			0.43118	0.1	0.17926	0.03	2.05398	0.001
		1			0.42709	0.03	0.17733	0.1	2.05373	0.001
		3			0.40593	0.1	0.17030	0.1	2.05324	0.001
		5			0.37405	0.1	0.16094	0.1	2.05276	0.001
		7			0.34809	0.1	0.15278	0.1	2.05228	0.001
			0.1		0.41286	0.01	0.19155	0.01	0.75968	0.01
			0.71		0.41402	0.01	0.19221	0.01	0.79998	0.01
			1		0.41452	0.01	0.19249	0.01	0.82105	0.01
			5		0.41670	0.001	0.20665	0.001	1.02687	0.001
			10		0.41676	0.001	0.20668	0.001	1.10009	0.001
			20		0.41687	0.001	0.20673	0.001	1.27657	0.001
			50		0.41708	0.001	0.20739	0.0006	1.53909	0.0006
			100		0.41867	0.01	0.20772	0.0004	1.86271	0.0004
			500		0.42182	0.0031	0.20818	0.0001	2.30174	0.0001
			5	0	0.42003	0.01	0.19572	0.01	3.23277	0.01
				1	0.41906	0.01	0.19513	0.01	2.52891	0.01
				3	0.41646	0.01	0.19358	0.01	1.84439	0.01
				5	0.41285	0.01	0.19149	0.01	1.51957	0.01
				7	0.40800	0.01	0.18872	0.01	1.33776	0.01
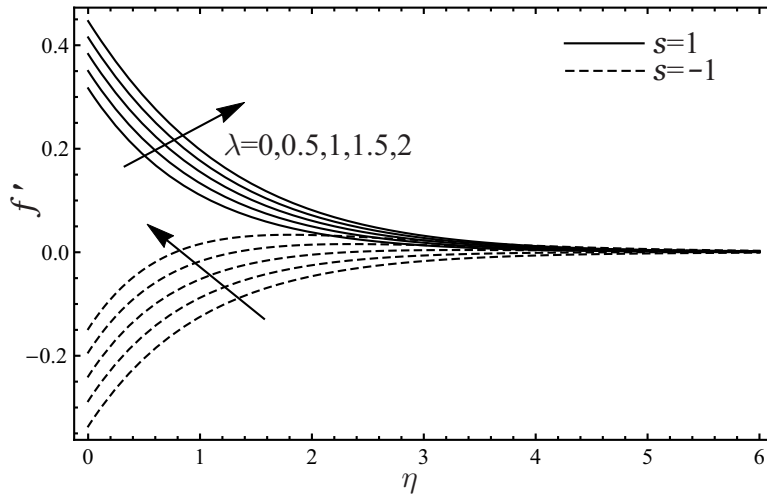
Figure 4.7: Impact of λ on f'

when sheet shrinks, the increasing value of the magnetic field parameter produces a higher velocity component of the fluid flow at $R = 7$ in comparison to the
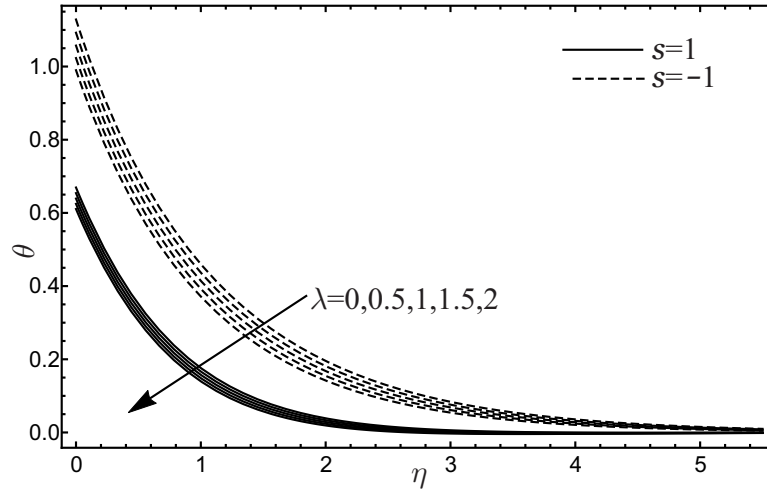
Figure 4.8: Impact of λ on θ
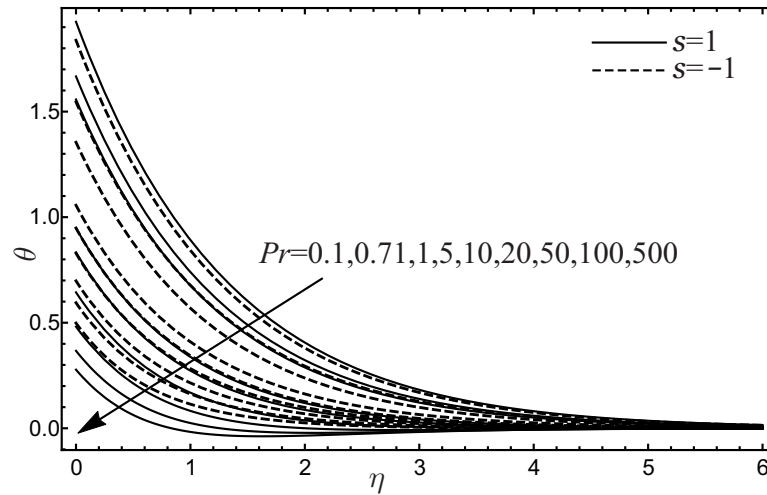
Figure 4.9: Impact of Pr on θ

velocity component at $R = 1$. When the sheet stretches, in Figure 4.12, the temperature of the micropolar fluid flow dramatically increases with the higher values of the magnetic field parameter at $R = 7$. This is maybe because the Lorentz force is reinforced by radiative heat flux which increases the thermal boundary thickness. However, Figure 4.13 shows a reverse behavior for shrinking of the sheet. Tables 4.2–4.3 show that local skin friction coefficient, wall couple stress and Nusselt number decrease with the higher values of the magnetic field parameter for stretching sheet case and when the sheet shrinks, local skin friction coefficient and Nusselt number increase, and the local wall couple stress decreases.

Increasing value of the thermal radiation parameter produces a higher impact on the velocity component and reduces the thermal boundary layer thickness at the lower value of the magnetic field parameter for stretching sheet as shown in Figure 4.14 and Figure 4.16. In the presence of the higher magnetic field parameter ($M = 7$), an increase in the thermal radiation parameter produces a

47

Table 4.3: Influences of K, λ, M, Pr, R on physical quantities for $s = -1$.

K	λ	M	Pr	R	$-C_{f_x}Re_x^{\frac{1}{2}}$	$-\hbar$	$-M_xRe_x$	$-\hbar$	$Nu_xRe_x^{-\frac{1}{2}}$	$-\hbar$
0.0	1	1	5		0.31028	0.1	0.14256	0.01	0.96032	0.01
0.5					0.41515	0.1	0.17542	0.01	0.95774	0.01
1.0					0.517328	0.1	0.20685	0.01	0.95520	0.01
1.5					0.617723	0.1	0.23678	0.01	0.95270	0.01
2.0					0.717034	0.1	0.26523	0.01	0.95024	0.01
0.5	0.0				0.41694	0.01	0.10951	0.05	0.94308	0.01
	0.5				0.41817	0.01	0.15779	0.05	0.95774	0.01
	1.0				0.41905	0.01	0.17959	0.05	0.97295	0.01
	1.5				0.41959	0.01	0.18768	0.05	0.98874	0.01
	2.0				0.41980	0.01	0.19038	0.05	1.00513	0.01
	1.0	0			0.45177	0.1	0.14878	0.1	1.98701	0.001
		1			0.41515	0.1	0.15072	0.1	1.98724	0.001
		3			0.37078	0.1	0.15306	0.1	1.98770	0.001
		5			0.33760	0.1	0.15949	0.03	1.98814	0.001
		7			0.31362	0.1	0.16224	0.02	1.98858	0.001
			0.1		0.42163	0.01	0.179814	0.009	0.756548	0.01
			0.71		0.42111	0.01	0.189479	0.005	0.77556	0.01
			1		0.420875	0.01	0.199905	0.002	0.785104	0.01
			5		0.416685	0.001	0.203958	0.001	0.99362	0.001
			10		0.416658	0.001	0.204372	0.0009	1.02737	0.001
			20		0.416607	0.001	0.204785	0.0008	1.10309	0.001
			50		0.416481	0.001	0.205634	0.0006	1.21621	0.0006
			100		0.416335	0.001	0.206514	0.0004	1.34088	0.0004
			500		0.416243	0.001	0.207872	0.0001	1.50349	0.0001
			5	0	0.41645	0.01	0.17409	0.01	2.32120	0.01
				1	0.41817	0.01	0.17542	0.01	1.91547	0.01
				3	0.42259	0.01	0.17873	0.01	1.50540	0.01
				5	0.42859	0.01	0.18305	0.01	1.30761	0.01
				7	0.43660	0.01	0.18863	0.01	1.19732	0.01
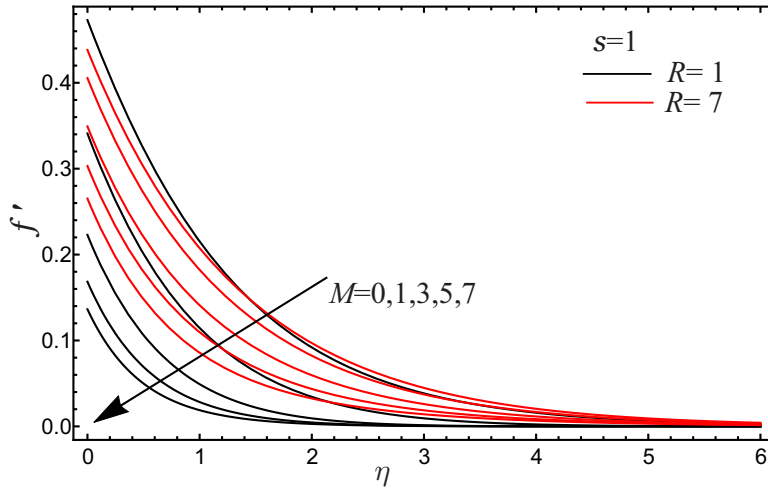
Figure 4.10: Impact of M on f' for $s = 1$

higher velocity component as compared to that obtained from a lower value of the magnetic field parameter ($M = 1$) as depicted in the Figure 4.15. On the
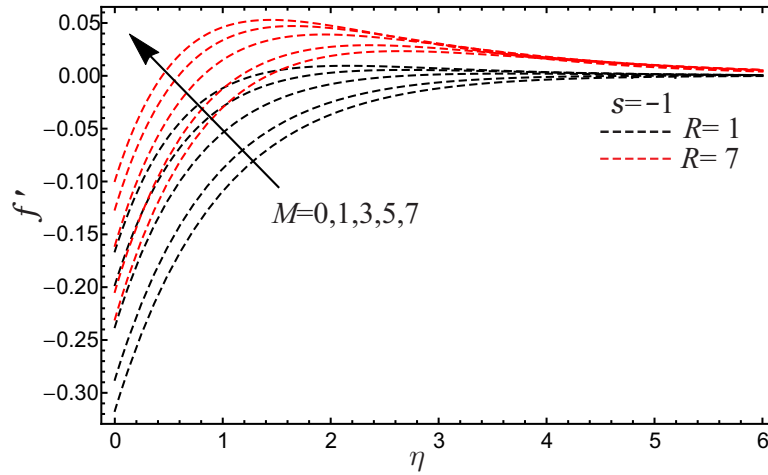
Figure 4.11: Impact of M on f' for $s = -1$
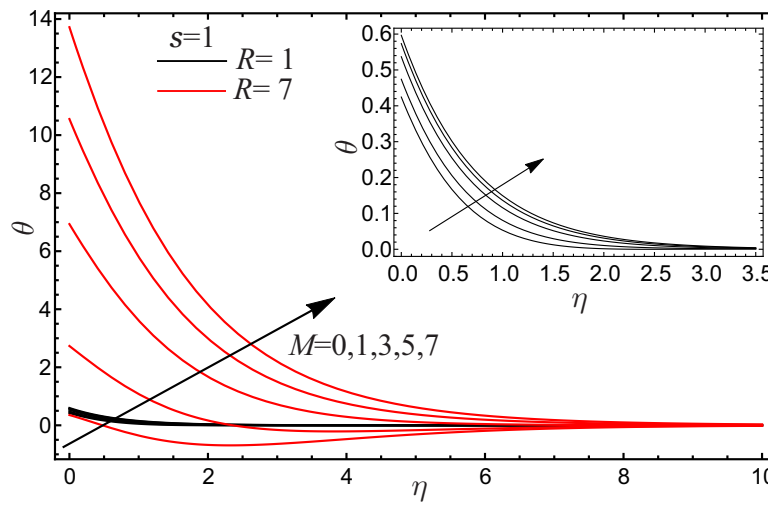

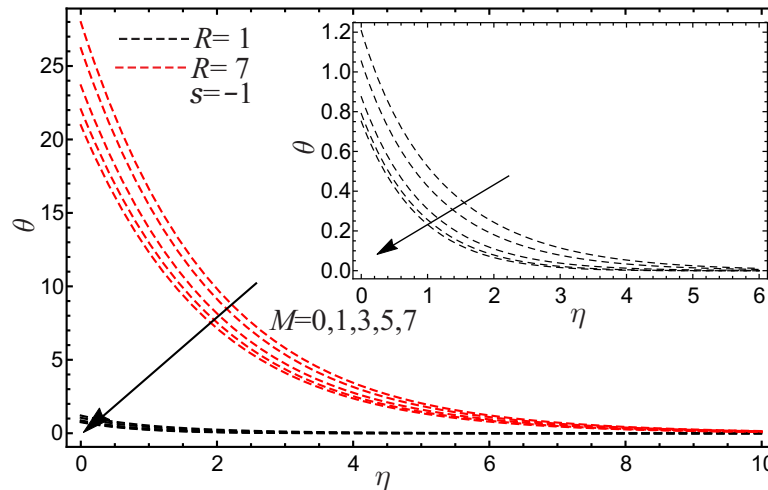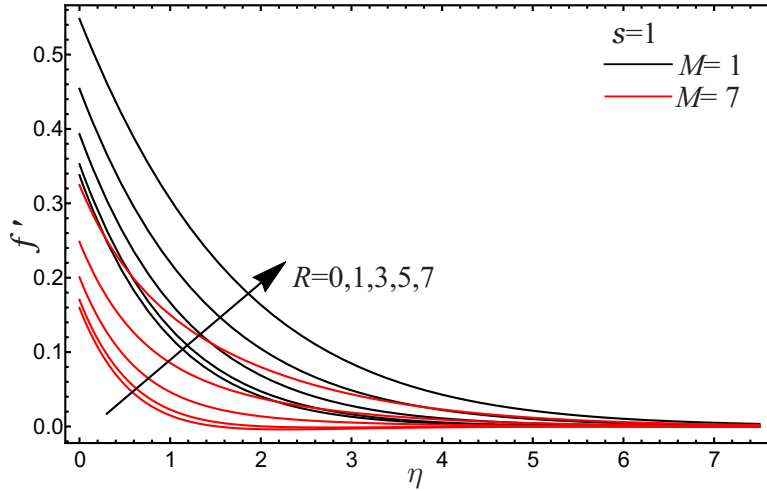**Figure 4.12:** Impact of M on θ for $s = 1$

Figure 4.13: Impact of M on θ for $s = -1$

other hand, a reverse behaviour is noted for the temperature profile at $s = -1$ as illustrated in Figure 4.17. An increase in the thermal radiation parameter causes
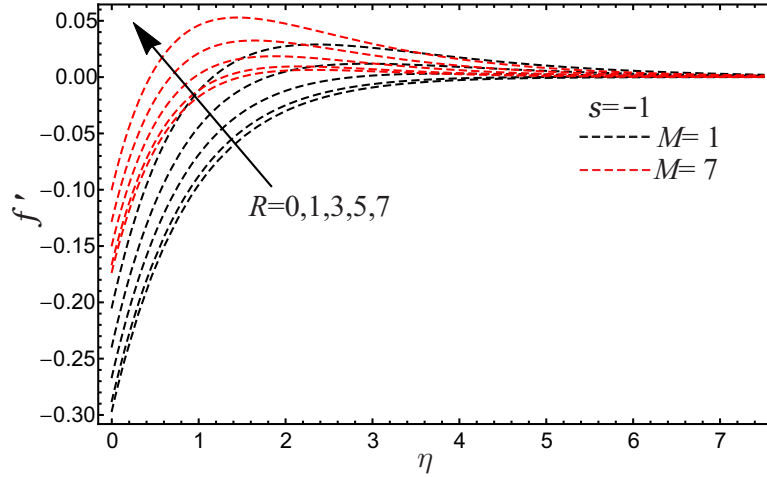
Figure 4.14: Impact of R on f' for $s = 1$

to reduce the influence of local physical quantities for stretching and shrinking of the sheet as reported in Tables 4.2–4.3.

Table 4.4: Influences of $f_w, \alpha, \beta, \delta$ on physical quantities for $s = 1$.

f_w	α	β	δ	$C_{f_x}Re_x^{\frac{1}{2}}$	$-\hbar$	M_xRe_x	$-\hbar$	$Nu_xRe_x^{-\frac{1}{2}}$	$-\hbar$
1.0	1	-1	0.5	0.42045	0.01	0.21318	0.01	1.48065	0.005
0.5				0.41906	0.01	0.19513	0.01	1.13591	0.005
0.0				0.41527	0.01	0.17597	0.01	0.90848	0.005
-0.5				0.40715	0.01	0.15479	0.01	0.76132	0.005
-1.0				0.39099	0.01	0.12986	0.01	0.66716	0.005
0.5	1			0.436835	0.1	0.17733	0.1	1.26446	0.01
	2			0.327954	0.1	0.12443	0.1	1.22474	0.01
	3			0.26229	0.1	0.09390	0.1	1.20088	0.01
	1	-1		0.41906	0.01	0.19513	0.01	1.26446	0.01
		-2		0.32264	0.01	0.14784	0.01	1.22703	0.01
		-3		0.26655	0.01	0.12092	0.01	1.20490	0.01
		-1	0.1	0.41967	0.1	0.17274	0.1	1.23034	0.01
			0.2	0.42287	0.1	0.17351	0.1	1.23533	0.01
			0.3	0.42669	0.1	0.17449	0.1	1.24193	0.01
			0.4	0.43128	0.1	0.17573	0.1	1.25104	0.01
			0.5	0.43684	0.1	0.17733	0.1	1.26446	0.01

Figures 4.18–4.19 display the effect of the suction and the injection parameters on stretching/shrinking sheet, respectively. It can be seen that increasing values of the suction parameter reduces the prescribed velocities and raises the micropolar fluid temperature for stretching and shrinking of the sheet, however, for shrinking sheet case it increases the microrotational velocity for shrinking sheet. On the other hand, increasing value of the injection parameter increases the prescribed velocities and temperature profile, however, for shrinking sheet case it decreases the microrotational velocity of the micropolar fluid flow. Figures 4.18–4.19 are computed at $\hbar = -0.01$, except $\hbar = -0.008$ is used in Figure 4.19 for $s = -1$.

Furthermore, $\hbar = -0.001$ is used Figure 4.20. Tables 4.4–4.5 show that higher the suction parameter higher will be the physical quantities for stretching sheet case, on the other hand, local skin friction coefficient decreases, and local wall couple stress and Nusselt number increase for shrinking sheet case. However, an increase in the injection parameter shows the reverse effect.

Figure 4.15: Impact of R on f' for $s = -1$
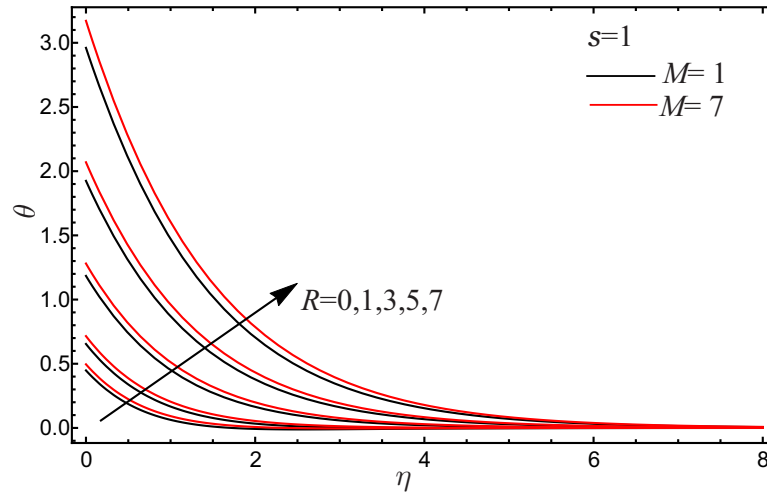
Figure 4.16: Impact of R on θ for $s = 1$

Figures 4.21–4.26 present the influences of the slip flow parameters on the prescribed velocities and the temperature profiles. It is observed that an increase in the first and second order slip flow parameters yields a decrease in the velocity component and microrotational velocity, and it enhances the temperature profile for stretching sheet. Alternatively, a reverse trend is observed for shrinking sheet case. $\hbar = -0.01$ and $\hbar = -0.1$ are used for Figures 4.21–4.22 and Figures 4.23–4.26, respectively. Local skin friction and wall couple stress decrease with the increasing value of the first and second order slip flow parameters for $s = 1$ and
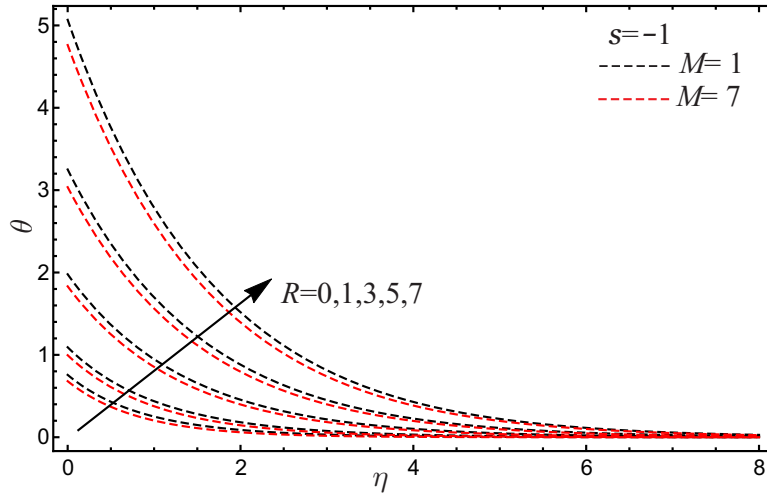
Figure 4.17: Impact of R on θ for $s = -1$
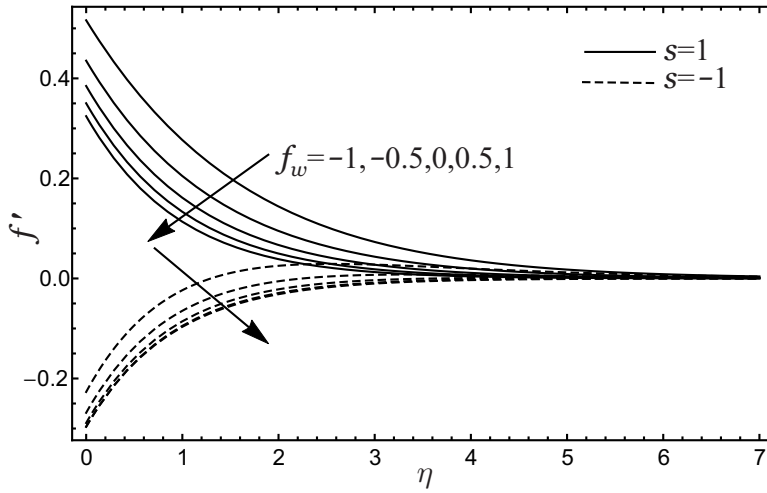
Figure 4.18: Impact of f_w on f'
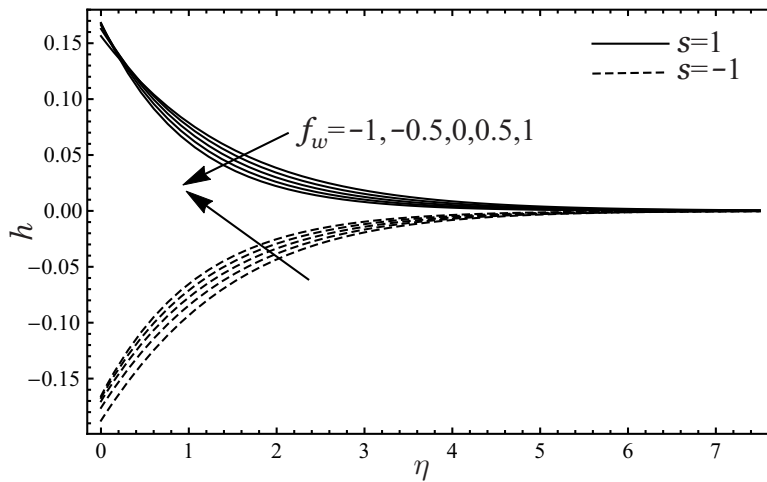
Figure 4.19: Impact of f_w on h

-1, and the local Nusselt number decreases for $s = 1$ and it increases for $s = -1$ as shown in the Tables 4.4–4.5.

Figure 4.20: Impact of f_w on θ

Table 4.5: Influences of $f_w, \alpha, \beta, \delta$ on physical quantities for $s = -1$.

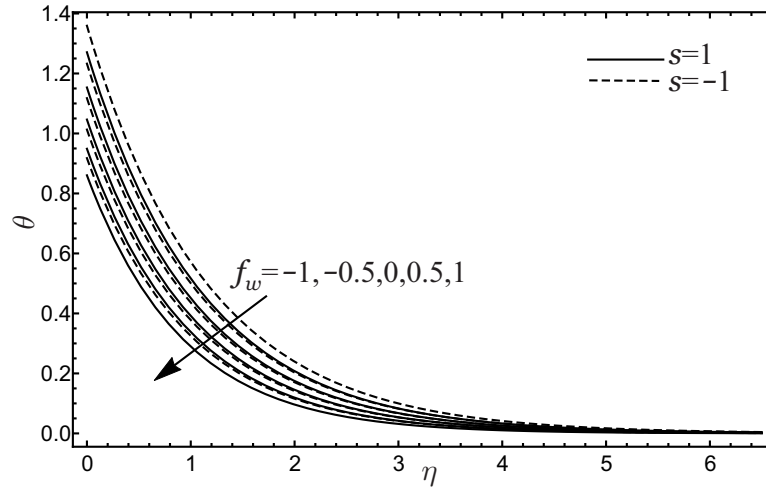| f_w	α	β	δ	$-C_{f_x}Re_x^{\frac{1}{2}}$	$-\hbar$	$-M_xRe_x$	$-\hbar$	$Nu_xRe_x^{-\frac{1}{2}}$	$-\hbar$
1.0	1	−1	0.5	0.41421	0.01	0.20809	0.0001	1.25380	0.005
0.5				0.41817	0.01	0.20788	0.0001	0.97330	0.005
0.0				0.42573	0.01	0.20768	0.0001	0.79706	0.005
−0.5				0.44045	0.01	0.20747	0.0001	0.68703	0.005
−1.0				0.46904	0.01	0.20726	0.0001	0.61840	0.005
0.5	1			0.41515	0.1	0.15072	0.1	0.95774	0.01
	2			0.30820	0.1	0.12191	0.1	0.99337	0.01
	3			0.24490	0.1	0.10281	0.1	1.01530	0.01
	1	−1		0.41817	0.01	0.17542	0.01	0.95774	0.01
		−2		0.29912	0.01	0.12795	0.01	0.99590	0.01
		−3		0.22778	0.01	0.09864	0.01	1.01959	0.01
		−1	0.1	0.43027	0.2	0.10744	0.1	0.943269	0.01
			0.2	0.43026	0.2	0.12111	0.1	0.945593	0.01
			0.3	0.42867	0.2	0.13416	0.1	0.948541	0.01
			0.4	0.42823	0.2	0.14455	0.1	0.952410	0.01
			0.5	0.39395	0.2	0.15072	0.1	0.957735	0.01

In comparison with the higher value of the magnetic field parameter $M = 7$, the result obtained from the stretching sheet at the lower value of the magnetic field parameter $M = 1$ indicate that an increase in the Newtonian heating parameter causes to produce the higher velocity component in Figure 4.27 at $\hbar = -0.1$. On the other hand, a reverse phenomenon occurs for the shrinking sheet case in Figure 4.28 at $\hbar = -0.1$. Furthermore, stretching sheet at the higher value of the magnetic field parameter reveals that an increase in the Newtonian heating parameter raises the micropolar fluid temperature. However, when sheet shrinks at $M = 1$, higher values of the Newtonian heating parameter enhances the temperature profile as illustrated in Figures 4.29–4.30 at $\hbar = -0.01$. It can be observed that increasing value of the Newtonian heating parameter yields an
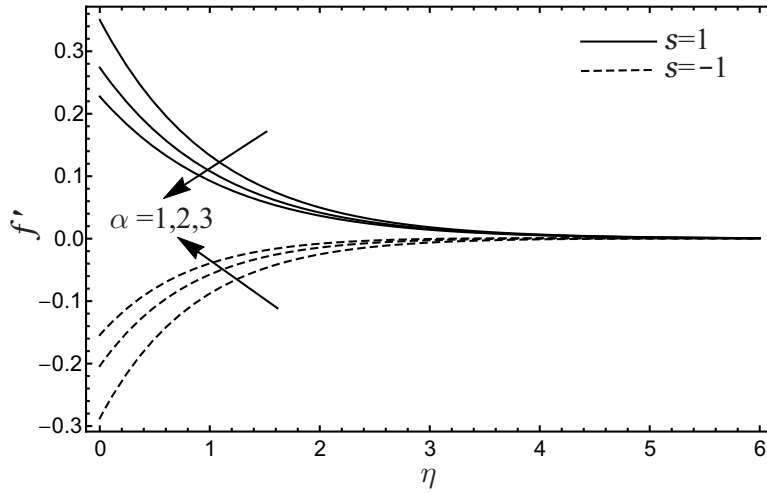
Figure 4.21: Impact of α on f'
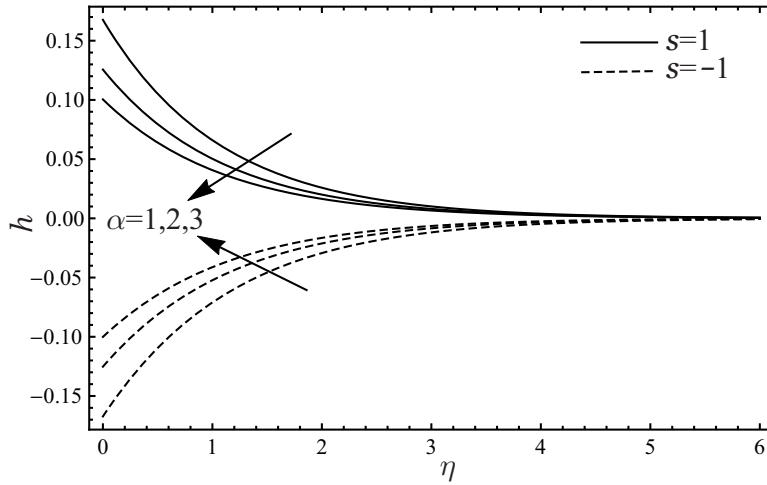
Figure 4.22: Impact of α on h
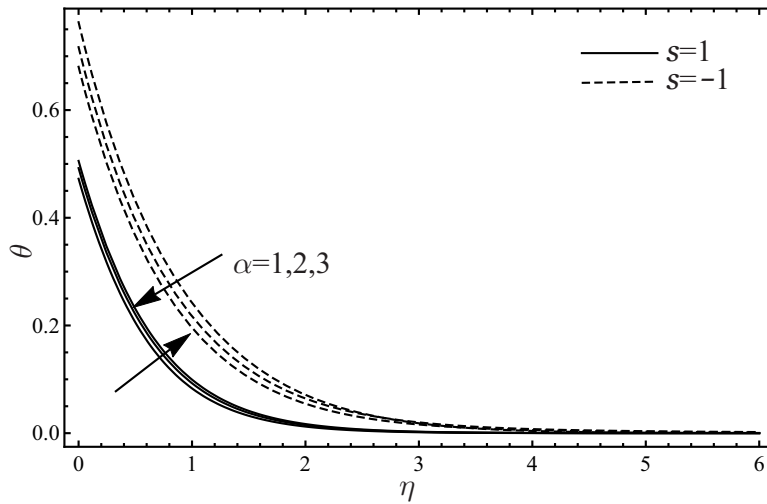
Figure 4.23: Impact of α on θ

increase in the local wall couple stress and the local Nusselt number for stretching and shrinking of the sheet, while it causes an increase in the local skin friction
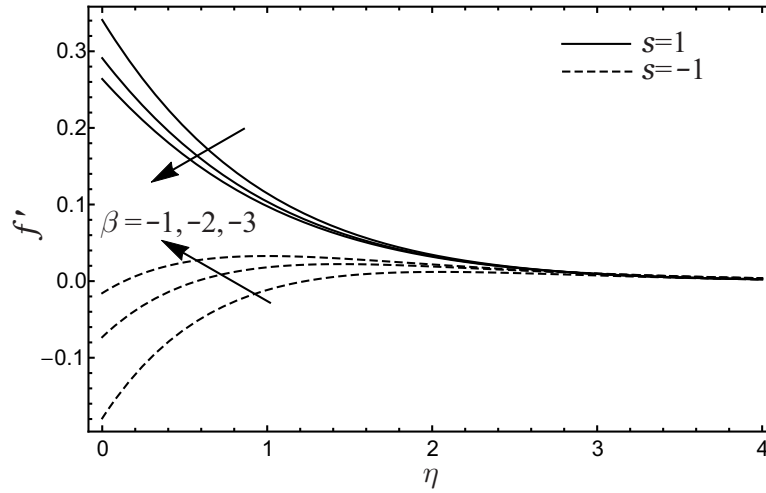
Figure 4.24: Impact of β on f'
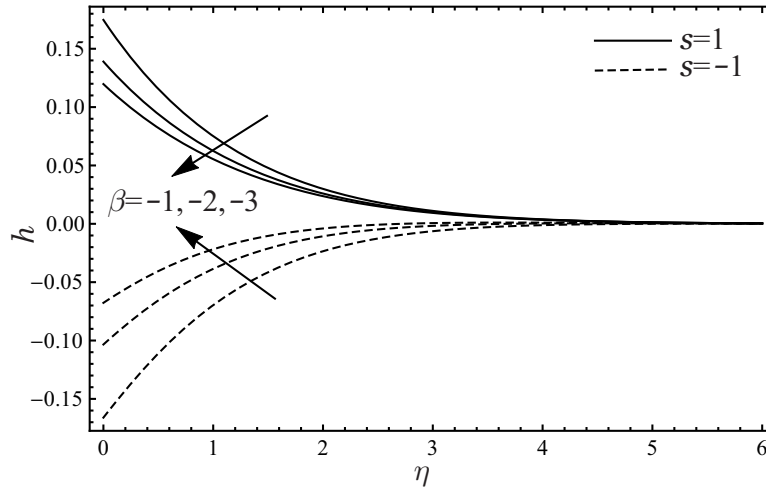
Figure 4.25: Impact of β on h
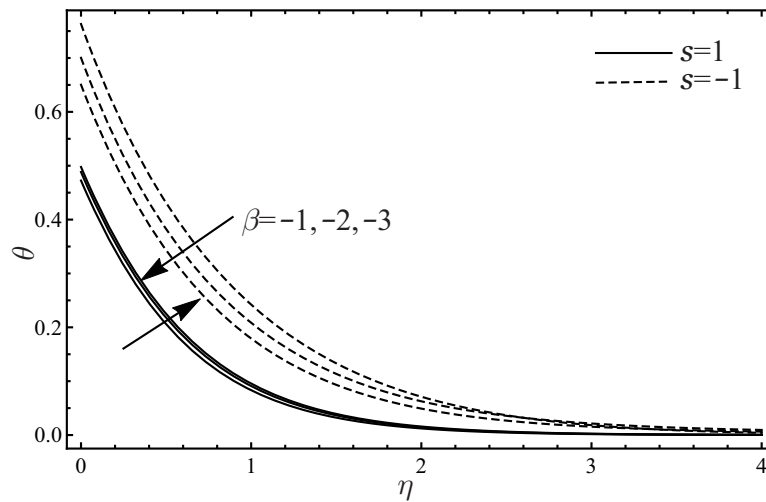
Figure 4.26: Impact of β on θ

coefficient for the stretching sheet case and reduces the local skin friction coefficient for the shrinking sheet case which is tabulated in Tables 4.4–4.5.
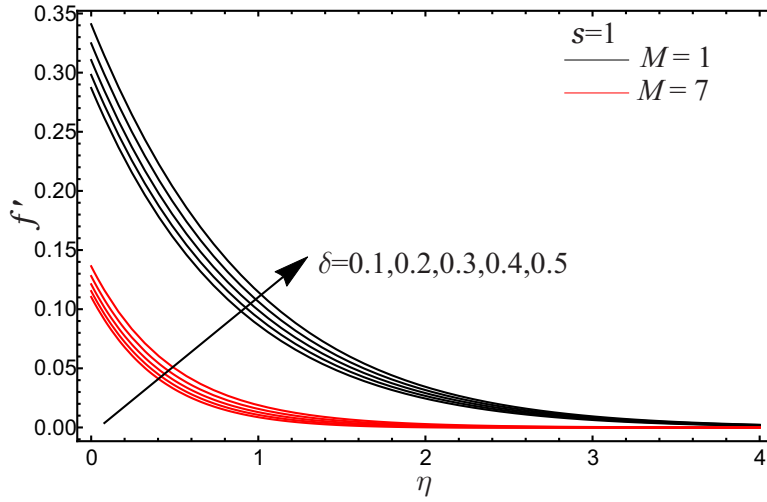
Figure 4.27: Impact of δ on f' for $s = 1$
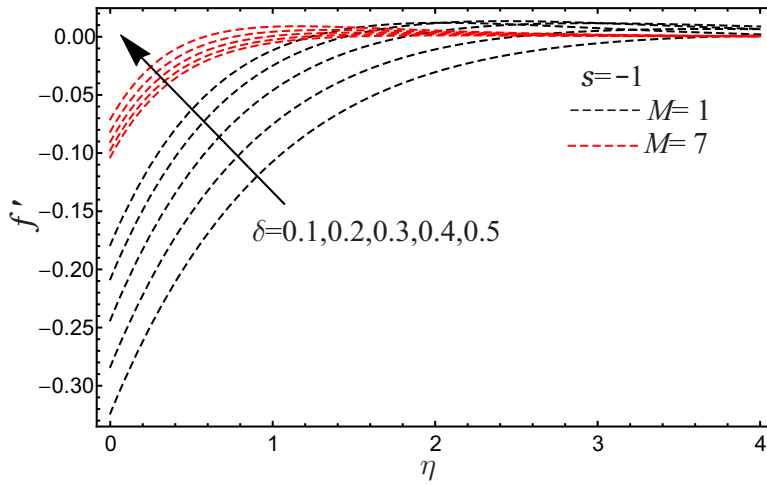
Figure 4.28: Impact of δ on f' for $s = -1$
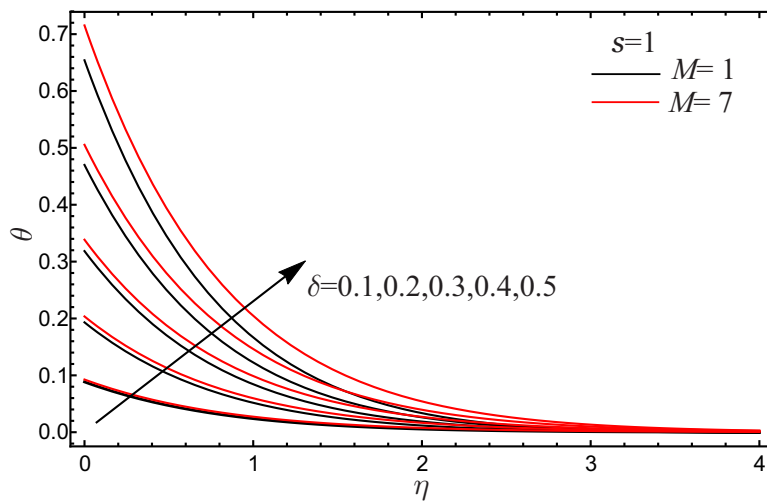
Figure 4.29: Impact of δ on θ for $s = 1$
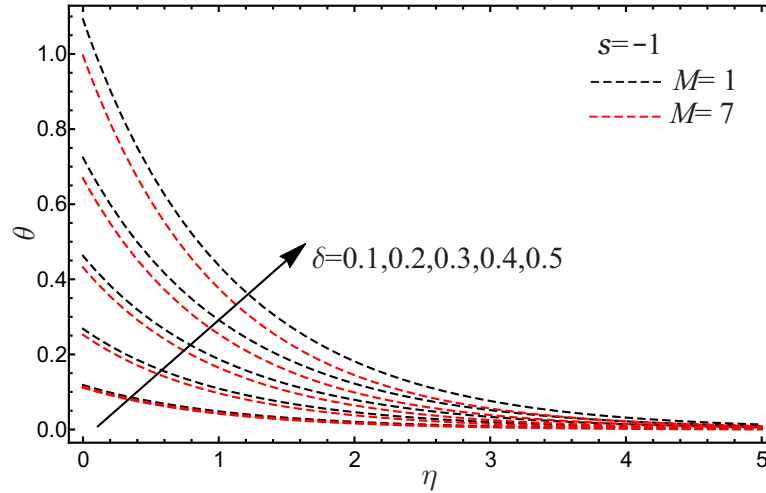
Figure 4.30: Impact of δ on θ for $s = -1$

4.5 Chapter Summary

This chapter presents an investigation of a mixed convective incompressible magneto-micropolar fluid flow over a permeable stretching/shrinking sheet under the influence of the thermal radiation parameter. The Newtonian heating effect was considered with the slip flow regime. Transformed nonlinear fluid flow model revealed that when the sheet stretched; higher the magnetic field parameter, lower the velocity and thermal boundary layer thicknesses at $R = 1$. On the other hand, velocity component and the thermal boundary layer thickness increased at higher values of the thermal radiation parameter for $M = 1$. Furthermore, when sheet stretched, the temperature of the micropolar fluid flow raised significantly with the increased value of the magnetic field parameter at $R = 7$ and when the sheet shrunk, the temperature of the fluid reduced, but it was noticeably higher than that at $R = 1$.

Chapter 5

Impact of Hall Current on MHD Micropolar Fluid Flow[1]

The work of Pop and Watanabe [110] was concerned with the Hall effect on MHD natural convection fluid flow over a semi-infinite vertical plate and Pal *et al.* [58] were studied the Hall effect on heat and mass transfer mixed convection radiative magneto-micropolar fluid flow in the rotating system. The published work, as mentioned above, governs to investigate the influence of the Hall current on the mixed convective magneto-micropolar fluid flow over a stretching/shrinking porous sheet with the second order slip and the Newtonian heating conditions at the boundary. The Hall effect plays an important role in electro-magnetic appliances such as in Hall accelerators, flight magnetohydrodynamics and the MHD Hall generators [58].

5.1 Governing Equations

As in previous chapter, it is considered a steady state mixed convective flow of an incompressible magneto-micropolar fluid passing over a permeable stretching/shrinking surface with second order slip velocity. Stretching/shrinking behavior is described by the velocity $u = sax$. This MHD fluid flow, new to this chapter, is taken along the x-axis and the uniform magnetic field (B_o) is supplied in a direction normal to the flow field, as shown in Figure 5.1, neglecting the induced magnetic field [111]. It is also assumed that the Newtonian heating causes a natural convection flow, i.e., the heat transfer rate on the stretching/shrinking sheet is taken to be proportional to the surface temperature [89,90]. In this MHD

---

[1]Copyright permission: please see in Appendix B.

flow, the Hall effect induces a Hall current which causes a force in the direction (along with z-axis) normal to the steady flow of the electrically conducting fluid and magnetic force. Therefore, the prescribed mathematical model becomes three dimensional. For simplicity, no changes are considered in the fluid flow and heat transfer quantities along the z-axis, so the fluid model reduces to two-dimensional flow. In the absence of the ion-slip and pressure diffusion effects, the generalized Ohm's law with Maxwell's equations [110–112] can be written as

$$\mathbf{J} = \sigma \left(\mathbf{E} + \mathbf{V} \times \mathbf{B} - \frac{1}{en_e} \mathbf{J} \times \mathbf{B} \right), \tag{5.1}$$

$$\bigtriangledown \times \mathbf{B} = \mu_o \mathbf{J}, \tag{5.2}$$

$$\bigtriangledown \cdot \mathbf{B} = 0, \tag{5.3}$$

$$\bigtriangledown \times \mathbf{E} = 0, \tag{5.4}$$

$$\bigtriangledown \cdot \mathbf{J} = 0, \tag{5.5}$$

where $\mathbf{J}$ is an electric current density vector with cartesian components (J_x, J_y, J_z),
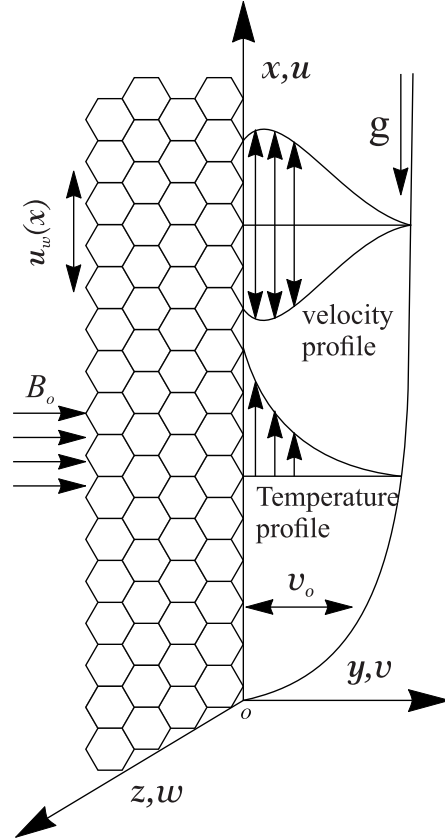
Figure 5.1: Flow model.

μ_o is the permeability of free space , $\sigma = n_e e^2 \tau / m_e$ is the electrical conductivity in which n_e is the number of charge on the electron density; e is the electron charge; τ is the electron collision time; m_e is the electron mass; $\mathbf{E} = (E_x, E_y, E_z), \mathbf{V} =$

(u, v, w), and $\mathbf{B} = (0, B_o, 0)$ are vectors of the electric field, velocity, and magnetic induction, respectively. It is considered that the stretching/shrinking sheet is electrically non-conducting material which gives $J_y = 0$ everywhere in the flow regime. Moreover, flow field is assumed without any applied voltage which results in $\mathbf{E} = 0$ from Equation (5.4). Hence the Equation (5.1) yields (see in Section A.3 of appendix),

$$J_x = \frac{\sigma B_o}{1 + m^2}(mu - w), \tag{5.6}$$

$$J_z = \frac{\sigma B_o}{1 + m^2}(u + mw), \tag{5.7}$$

where $m = \sigma B_o/en_e$ is the Hall parameter. Furthermore, in the absence of mass transfer, viscous dissipation and Ohmic heating by taking $\mathfrak{A} = \mathfrak{D} = \mathfrak{E} = 0$ and $\mathfrak{B} = \mathfrak{C} = 1$ the system of Equations (1.4)–(1.5) reduces to obtained the mathematical form of governing equations [110] as

$$\frac{\partial u}{\partial x} + \frac{\partial v}{\partial y} = 0, \tag{5.8}$$

$$u\frac{\partial u}{\partial x} + v\frac{\partial u}{\partial y} = \frac{\mu + \chi}{\rho}\left(\frac{\partial^2 u}{\partial y^2}\right) + g\beta_T(T - T_\infty) + \frac{\chi}{\rho}\left(\frac{\partial \omega}{\partial y}\right) - \frac{B_o}{\rho}J_z, \tag{5.9}$$

$$u\frac{\partial w}{\partial x} + v\frac{\partial w}{\partial y} = \frac{\mu + \chi}{\rho}\left(\frac{\partial^2 w}{\partial y^2}\right) + \frac{B_o}{\rho}J_x, \tag{5.10}$$

$$u\frac{\partial \omega}{\partial x} + v\frac{\partial \omega}{\partial y} = \frac{\gamma}{\rho j}\left(\frac{\partial^2 \omega}{\partial y^2}\right) - \frac{\chi}{\rho j}\left(2\omega + \frac{\partial u}{\partial y}\right), \tag{5.11}$$

$$u\frac{\partial T}{\partial x} + v\frac{\partial T}{\partial y} = \frac{k}{\rho c_p}\left(\frac{\partial^2 T}{\partial y^2}\right), \tag{5.12}$$

with pertaining boundary conditions

$$\left.\begin{array}{l} u = su_w(x) + u_{\text{slip}}; v = v_o; w = 0; \omega = -n\dfrac{\partial u}{\partial y}; k\dfrac{\partial T}{\partial y} = -h_s T \text{ at } y = 0, \\[2mm] u \to 0; \ w \to 0; \ \omega \to 0; \ T \to T_\infty \text{ as } y \to \infty. \end{array}\right\} \tag{5.13}$$

The equations $(5.13)_1$ and $(5.13)_5$ are for second order slip flow and the Newtonian heating conditions at the boundary, respectively. The second term of $(5.13)_1$ is defined in Equations (1.6)–(1.7). By introducing the non-dimensional similarity variables,

$$\eta = \sqrt{a/\nu}\,y, \ \psi = \sqrt{a\nu}xf(\eta), \ w = axg(\eta), \ \omega = \sqrt{a/\nu}ah(\eta) \text{ and } \theta(\eta) = \frac{T - T_\infty}{T_\infty},$$

with velocity components $u = \partial\psi/\partial y$ and $v = -\partial\psi/\partial x$ in which the stream function (ψ) usually satisfies the equation of the conservation of mass Equation (5.8). The governing equations (Equations (5.9)–(5.12)) are transformed (see in Section A.3 of appendix) into a set of non-linear ordinary differential equations as follows:

$$(1 + K)f''' - (f')^2 + ff'' + \lambda\theta + Kh' - \frac{M}{1 + m^2}(f' + mg) = 0, \qquad (5.14)$$

$$(1 + K)g'' + fg' - f'g + \frac{M}{1 + m^2}(mf' - g) = 0, \qquad (5.15)$$

$$(1 + K/2)h'' - f'h + fh' - K(2h + f'') = 0, \qquad (5.16)$$

$$\theta'' + Prf\theta' = 0. \qquad (5.17)$$

The boundary conditions Equation (5.13) become

$$\left.\begin{array}{r} f = f_w; \ f' = s + \alpha f'' + \beta f'''; \ g = 0; \ h = -nf''; \ \theta' = -\delta(1 + \theta) \text{ at } \eta = 0, \\ f' \to 0; \ g \to 0; \ h \to 0; \ \theta \to 0 \text{ as } \eta \to \infty, \end{array}\right\}$$

$$(5.18)$$

where prime$(')$ is used for the derivative with respect to η. $\lambda = Gr_x/Re_x$ is the buoyancy parameter for $Gr_x = \text{g}\beta_T T_\infty x/a\nu$ (local Grashof number) and $Re_x = ax^2/\nu$ (local Reynolds number), $M = \sigma B_o^2/a\rho$ is the Magnetic field parameter, $Pr = \mu c_p/k$ represents the Prandtl number. Equation (5.18) contains suction (> 0) or injection (< 0) parameter $f_w = -(a\nu)^{-\frac{1}{2}}v_o$, first order slip flow parameter $\alpha = A\sqrt{a/\nu} > 0$, second order slip flow parameter $\beta = Ba/\nu < 0$, and Newtonian heating parameter $\delta = (h_s/k)\sqrt{\nu/a}$. Moreover, the physical quantities including local skin friction coefficients (C_{f_x} and C_{f_z}), local wall couple stress (M_x) and the local Nusselt number (Nu_x) are determined as follows:

$$C_{f_x} = \frac{-\tau_{w_x}}{\rho(u_w(x))^2} \text{ for } \tau_{w_x} = (\mu + \chi)\frac{\partial u}{\partial y} + \chi\omega\bigg|_{y=0},$$

$$C_{f_z} = \frac{\tau_{w_z}}{\rho(u_w(x))^2} \text{ for } \tau_{w_z} = (\mu + \chi)\frac{\partial w}{\partial y}\bigg|_{y=0},$$

$$M_x = \frac{-m_w}{\rho x(u_w(x))^2} \text{ for } m_w = \left(\mu + \frac{\chi}{2}\right)j\frac{\partial\omega}{\partial y}\bigg|_{y=0},$$

$$Nu_x = \frac{-xq_w}{(T - T_\infty)} \text{ for } q_w = \frac{\partial T}{\partial y}\bigg|_{y=0}.$$

Using the similarity transformation to make the above physical quantities dimensionless, we have

62

$$C_{f_x} Re_x^{\frac{1}{2}} = -\left(1 + K - nK\right) f''(\eta)\big|_{\eta=0},$$

$$C_{f_z} Re_x^{\frac{1}{2}} = \left(1 + K\right) g'(\eta)\big|_{\eta=0},$$

$$M_x Re_x = -\left(1 + \frac{K}{2}\right) h'(\eta)\bigg|_{\eta=0},$$

$$Nu_x Re_x^{-\frac{1}{2}} = \delta\left(1 + \frac{1}{\theta(\eta)}\right)\bigg|_{\eta=0}.$$

5.2 OHAM Solution

An efficient approximate analytical technique, named Optimal Homotopy Analysis Method (OHAM), is used to solve the coupled nonlinear system of equations (Equations (5.14)–(5.17)) with boundary conditions in (Equation (5.18)). This semi-analytical approach, proposed and developed by Liao [95–97], has an advantage on the perturbation and non-perturbation methods and has a great freedom to get the convergent series solution.

The homotopy series solutions corresponding to a set of the base function $\{\eta^r e^{-i\eta} | r \geq 0, i \geq 0\}$ can be expressed in the following form:

$$\left.\begin{aligned}
f(\eta) &= \sum_{r=0}^{\infty}\sum_{i=0}^{\infty} a_{r,i}\eta^r e^{-i\eta}, \\
g(\eta) &= \sum_{r=0}^{\infty}\sum_{i=0}^{\infty} b_{r,i}\eta^r e^{-i\eta}, \\
h(\eta) &= \sum_{r=0}^{\infty}\sum_{i=0}^{\infty} c_{r,i}\eta^r e^{-i\eta}, \\
\theta(\eta) &= \sum_{r=0}^{\infty}\sum_{i=0}^{\infty} d_{r,i}\eta^r e^{-i\eta},
\end{aligned}\right\} \tag{5.19}$$

with the constant coefficients $a_{r,i}, b_{r,i}\, c_{r,i}$ and $d_{r,i}$. The set of initial solutions is chosen to be

$$\left.\begin{aligned}
f_0(\eta) &= f_w + \frac{s(1 - e^{-\eta})}{1 + \alpha - \beta}, \\
g_0(\eta) &= 0, \\
h_0(\eta) &= \frac{sne^{-\eta}}{1 + \alpha - \beta}, \\
\theta_0(\eta) &= \frac{\delta e^{-\eta}}{1 - \delta} \quad ; \delta \neq 1,
\end{aligned}\right\} \tag{5.20}$$

with the corresponding linear operators

$$\mathcal{L}_f = \frac{d^3}{d\eta^3} - \frac{d}{d\eta}, \ \mathcal{L}_g = \frac{d^2}{d\eta^2} + \frac{d}{d\eta}, \ \mathcal{L}_h = \frac{d^2}{d\eta^2} + \frac{d}{d\eta} \text{ and } \mathcal{L}_\theta = \frac{d^2}{d\eta^2} + \frac{d}{d\eta}, \quad (5.21)$$

satisfying the following properties

$$\left.\begin{aligned} \mathcal{L}_f \left[F_1 + F_2 e^\eta + F_3 e^{-\eta} \right] = 0, \\ \mathcal{L}_g \left[F_4 + F_5 e^{-\eta} \right] = 0, \\ \mathcal{L}_h \left[F_6 + F_7 e^{-\eta} \right] = 0, \\ \mathcal{L}_\theta \left[F_8 + F_9 e^{-\eta} \right] = 0, \end{aligned}\right\} \quad (5.22)$$

for arbitrary constants $F_i(i$ varies from 1 to 9). Let $\phi(\eta, q), \varphi(\eta, q), \Phi(\eta, q)$ and $\Psi(\eta, q)$ be the unknown functions of η and q, and $q(\in [0, 1])$ be the embedding parameter, $\hbar$ denote the non–zero auxiliary parameter and $H(\eta)$ be a non–zero auxiliary function. The zero–order deformation equations with corresponding non–linear functions $(\mathcal{N}_f, \mathcal{N}_g, \mathcal{N}_h, \mathcal{N}_\theta)$ can be written as

$$\left.\begin{aligned} (1-q)\mathcal{L}_f \left[\phi(\eta, q) - f_0(\eta) \right] = q\hbar_f H_f(\eta)\mathcal{N}_f \left[\phi(\eta, q), \varphi(\eta, q), \Phi(\eta, q), \Psi(\eta, q) \right], \\ (1-q)\mathcal{L}_g \left[\varphi(\eta, q) - g_0(\eta) \right] = q\hbar_g H_g(\eta)\mathcal{N}_g \left[\phi(\eta, q), \varphi(\eta, q), \Phi(\eta, q), \Psi(\eta, q) \right], \\ (1-q)\mathcal{L}_h \left[\Phi(\eta, q) - h_0(\eta) \right] = q\hbar_h H_h(\eta)\mathcal{N}_h \left[\phi(\eta, q), \varphi(\eta, q), \Phi(\eta, q), \Psi(\eta, q) \right], \\ (1-q)\mathcal{L}_\theta \left[\Psi(\eta, q) - \theta_0(\eta) \right] = q\hbar_\theta H_\theta(\eta)\mathcal{N}_\theta \left[\phi(\eta, q), \varphi(\eta, q), \Phi(\eta, q), \Psi(\eta, q) \right], \end{aligned}\right\}$$
$$(5.23)$$

with the following associated boundary conditions at $\eta = 0$ and $\eta \to \infty$, i.e.

$$\left.\begin{aligned} \phi(0, q) = f_w; \ \left.\frac{\partial \phi(\eta, q)}{\partial \eta}\right|_{\eta=0} = s + \alpha \left.\frac{\partial^2 \phi(\eta, q)}{\partial \eta^2}\right|_{\eta=0} + \beta \left.\frac{\partial^3 \phi(\eta, q)}{\partial \eta^3}\right|_{\eta=0}; \\ \left.\frac{\partial \phi(\eta, q)}{\partial \eta}\right|_{\eta\to\infty} \to 0; \ \varphi(0, q) \to 0; \ \varphi(\infty, q) \to 0; \ \Phi(0, q) = -n \left.\frac{\partial^2 \phi(\eta, q)}{\partial \eta^2}\right|_{\eta=0}; \\ \Phi(\infty, q) \to 0; \ \left.\frac{\partial \Psi(\eta, q)}{\partial \eta}\right|_{\eta=0} = -\delta(1 + \Psi(0, q)); \ \Psi(\infty, q) \to 0, \end{aligned}\right\}$$
$$(5.24)$$

where $\hbar$ and $H(\eta)$ are chosen in a way that the series solutions converge at $q = 1$. Therefore,

$$\left.\begin{aligned} f(\eta) = f_0(\eta) + \sum_{p=1}^{\infty} f_p(\eta)q^p, \\ g(\eta) = g_0(\eta) + \sum_{p=1}^{\infty} g_p(\eta)q^p, \end{aligned}\right]$$

$$h(\eta) = h_0(\eta) + \sum_{p=1}^{\infty} h_p(\eta)q^p, \Bigg]$$
$$\theta(\eta) = \theta_0(\eta) + \sum_{p=1}^{\infty} \theta_p(\eta)q^p, \Bigg]$$

$$(5.25)$$

in which

$$f_p(\eta) = \frac{1}{p!} \frac{\partial^p \phi(\eta, q)}{\partial q^p}\Bigg|_{q=0}, \quad g_p(\eta) = \frac{1}{p!} \frac{\partial^p \varphi(\eta, q)}{\partial q^p}\Bigg|_{q=0}, \quad h_p(\eta) = \frac{1}{p!} \frac{\partial^p \Phi(\eta, q)}{\partial q^p}\Bigg|_{q=0},$$

$$\theta_p(\eta) = \frac{1}{p!} \frac{\partial^p \Psi(\eta, q)}{\partial q^p}\Bigg|_{q=0}.$$

Differentiating the zero-order deformation equations Equation (5.23) p-times with respect to q and dividing by $p!$ yield the pth–order deformation equations in the following form when $q = 0$:

$$\mathcal{L}_f \left[f_p(\eta) - \mathcal{X}_p f_{p-1}(\eta)\right] = \hbar_f H_f(\eta) \mathfrak{R}_p^f(f_{p-1}(\eta), g_{p-1}(\eta), h_{p-1}(\eta), \theta_{p-1}(\eta)), \Bigg\}$$
$$\mathcal{L}_g \left[g_p(\eta) - \mathcal{X}_p g_{p-1}(\eta)\right] = \hbar_g H_g(\eta) \mathfrak{R}_p^g(f_{p-1}(\eta), g_{p-1}(\eta), h_{p-1}(\eta), \theta_{p-1}(\eta)), \Bigg\}$$
$$\mathcal{L}_h \left[h_p(\eta) - \mathcal{X}_p h_{p-1}(\eta)\right] = \hbar_h H_h(\eta) \mathfrak{R}_p^h(f_{p-1}(\eta), g_{p-1}(\eta), h_{p-1}(\eta), \theta_{p-1}(\eta)), \Bigg\}$$
$$\mathcal{L}_\theta \left[\theta_p(\eta) - \mathcal{X}_p \theta_{p-1}(\eta)\right] = \hbar_\theta H_\theta(\eta) \mathfrak{R}_p^\theta(f_{p-1}(\eta), g_{p-1}(\eta), h_{p-1}(\eta), \theta_{p-1}(\eta)), \Bigg\}$$

$$(5.26)$$

with the associated boundary conditions at $\eta = 0$ and $\eta \to \infty$ as follows:

$$f_p(0) = f_w, \ f_p'(0) = s + \alpha f_p''(0) + \beta f_p'''(0), \ g_p(0) = 0, \ h_p(0) = -n f_p''(0), \Bigg\}$$
$$\theta_p'(0) = -\delta(1 + \theta_p(0)), \ f_p'(\infty) \to 0, \ g_p(\infty) \to 0, \ h_p(\infty) \to 0, \ \theta_p(\infty) \to 0. \Bigg\}$$

$$(5.27)$$

In Equation (5.26),

$$\mathcal{X}_p = \begin{cases} 0 \text{ for } p \leq 1, \\ 1 \text{ for } p > 1, \end{cases}$$

$$\mathfrak{R}_p^f(f_{p-1}(\eta), g_{p-1}(\eta), h_{p-1}(\eta), \theta_{p-1}(\eta)) = (1 + K)f_{p-1}'''(\eta) + \sum_{i=0}^{p-1} f_i(\eta)f_{p-1-i}''(\eta) -$$

$$\sum_{i=0}^{p-1} f_i'(\eta)f_{p-1-i}'(\eta) + \lambda\theta_{p-1}(\eta) + Kh_{p-1}'(\eta) - \frac{M}{1+m^2}(f_{p-1}(\eta) + mg_{p-1}(\eta)),$$

$$\mathfrak{R}_p^g(f_{p-1}(\eta), g_{p-1}(\eta), h_{p-1}(\eta), \theta_{p-1}(\eta)) = (1 + K)g_{p-1}''(\eta) + \sum_{i=0}^{p-1} f_i(\eta)g_{p-1-i}'(\eta) -$$

$$\sum_{i=0}^{p-1} f_i'(\eta)g_{p-1-i}(\eta) + \frac{M}{1+m^2}(mf_{p-1}'(\eta) - g_{p-1}(\eta)),$$

$$\mathfrak{R}_p^h(f_{p-1}(\eta), g_{p-1}(\eta), h_{p-1}(\eta), \theta_{p-1}(\eta)) = (1 + K/2)h''_{p-1}(\eta) + \sum_{i=0}^{p-1} f_i(\eta)h'_{p-1-i}(\eta) -$$

$$\sum_{i=0}^{p-1} f'_i(\eta)h_{p-1-i}(\eta) - K\left(2h_{p-1}(\eta) + f''_{p-1}(\eta)\right) \text{ and}$$

$$\mathfrak{R}_p^\theta(f_{p-1}(\eta), g_{p-1}(\eta), h_{p-1}(\eta), \theta_{p-1}(\eta)) = \theta''_{p-1}(\eta) + Pr\sum_{i=0}^{p-1} f_i(\eta)\theta'_{p-1-i}(\eta).$$

For the sack of simplicity, values of all auxiliary functions are set as

$$H_f(\eta) = H_g(\eta) = H_h(\eta) = H_\theta(\eta) = 1.$$

From Equation (5.26), we then obtain the general solutions in the following form:

$$\left.\begin{aligned}
f_p(\eta) &= f_p^*(\eta) + F_1 + F_2 e^\eta + F_3 e^{-\eta}, \\
g_p(\eta) &= g_p^*(\eta) + F_4 + F_5 e^{-\eta}, \\
h_p(\eta) &= h_p^*(\eta) + F_6 + F_7 e^{-\eta}, \\
\theta_p(\eta) &= \theta_p^*(\eta) + F_8 + F_9 e^{-\eta},
\end{aligned}\right\} \quad (5.28)$$

where $f_p^*(\eta)$, $g_p^*(\eta)$, $h_p^*(\eta)$ and $\theta_p^*(\eta)$ are particular solutions extracted by Equation (5.26), and $F_i(i = 1, \cdots, 9)$ are determined by using Equation (5.27).

It is noted that the particular solutions in Equation (5.28) contain the four unknown convergence control parameters $\hbar_f, \hbar_g, \hbar_h$ and $\hbar_\theta$ which determine the convergence region for the Homotopy series solutions as derived in Equation (5.28). Obviously, if values of the convergence control parameters are properly chosen, solutions in Equation (5.28) may converges fast. So, we should determine the good enough values of these parameters so that the solutions in Equation (5.28) converge fast enough. For brevity, the optimal values of the convergence control parameters can be determined with the help of average squared residual errors

$$\left.\begin{aligned}
E_p^f &= \frac{1}{r}\sum_{j=0}^{r}\left[\mathcal{N}\left(\sum_{r=0}^{p} f_r(j\Delta\eta)\right)\right]^2, \\
E_p^g &= \frac{1}{r}\sum_{j=0}^{r}\left[\mathcal{N}\left(\sum_{r=0}^{p} g_r(j\Delta\eta)\right)\right]^2, \\
E_p^h &= \frac{1}{r}\sum_{j=0}^{r}\left[\mathcal{N}\left(\sum_{r=0}^{p} h_r(j\Delta\eta)\right)\right]^2, \\
E_p^\theta &= \frac{1}{r}\sum_{j=0}^{r}\left[\mathcal{N}\left(\sum_{r=0}^{p} \theta_r(j\Delta\eta)\right)\right]^2,
\end{aligned}\right\} \quad (5.29)$$

in which $\Delta\eta = 10/r$ and $r = 20$ and the total squared residual error is $E_p^t = E_p^f + E_p^g + E_p^h + E_p^\theta$. Furthermore, computation software MATHEMATICA is used to solve the system of ODEs in Equations (5.14)–(5.17) with boundary conditions in Equation (5.18).

5.2.1 Optimal Convergence Control Parameters

Homotopy analysis method has a freedom to control the convergence of the series solution by fixing the value of the non-zero convergence control parameter (auxiliary parameter). The values of the optimal convergence control parameters against sixth order of Homotopy approximations are presented in Table 5.1. It is found that as the order of the Homotopy approximation increases, the optimal convergence control parameters give the minimum of the total average squared residual error. Table 5.1 is computed for $K = \lambda = \alpha = s = 1$, $m = M = f_w = \delta = 0.1$, $\beta = -1$, $Pr = 2$, $n = 0.5$.

Table 5.1: Values of convergence control parameters.

p	$-\hbar_f$	$-\hbar_g$	$-\hbar_h$	$-\hbar_\theta$	E_p^t	CPU Time(s)
1	0.893200	0.557970	0.418652	0.087445	0.0006333	0.59
2	0.717632	0.347083	0.520176	0.578200	0.0000850	2.56
3	0.580908	0.254204	0.386921	0.442041	0.0000342	13.60
4	0.912440	0.431717	0.635011	0.447151	0.0000223	32.66
5	0.809656	0.106664	0.323863	0.404719	0.0000101	90.74
6	0.676212	0.312604	0.355828	0.425257	0.0000033	315.59

Table 5.2: Individual average squared residual error.

p	E_p^f	E_p^g	E_p^h	E_p^θ	CPU Time(s)
2	0.00713945	2.2622×10^{-7}	3.9966×10^{-4}	1.503×10^{-4}	0.55
4	0.00504071	1.0345×10^{-7}	9.3490×10^{-5}	9.683×10^{-5}	1.51
6	0.00339773	5.6185×10^{-8}	1.9300×10^{-5}	6.281×10^{-5}	3.37
8	0.00219339	3.6338×10^{-8}	5.2798×10^{-6}	4.167×10^{-5}	6.46
10	0.00135467	2.6144×10^{-8}	4.4309×10^{-6}	2.853×10^{-5}	11.09
12	0.00079764	1.9415×10^{-8}	4.8582×10^{-6}	2.013×10^{-5}	18.04
14	0.00044514	1.4220×10^{-8}	4.4657×10^{-6}	1.449×10^{-5}	28.16
16	0.00023340	1.0058×10^{-8}	3.4876×10^{-6}	1.052×10^{-5}	43.00
18	0.00011349	6.8116×10^{-9}	2.4045×10^{-6}	7.626×10^{-6}	64.66
20	0.00005016	4.4072×10^{-9}	1.4975×10^{-6}	5.493×10^{-6}	95.17

Moreover, using the same parametric values (as used for Table 5.1), the average squared residual error is tabulated in Table 5.2 along with the computation time. A machine of 8 GB RAM and Intel(R) Core i7-4790 CPU with 3.60GHz processor

is used. Furthermore, for the flexibility of results we fixed $\hbar_f = \hbar_g = \hbar_h = \hbar_\theta = \hbar$ and the curves of convergence control parameter $(\hbar)$ are plotted and displayed in Figures 5.2–5.3. The parametric values of Table 5.1 (or otherwise mentioned in the graph) are assigned to generate these graphs at 20th-order of iterations of OHAM. In Figure 5.2, it is to be noted that for stretching case $(s = 1)$, curves are plotted at $\eta = 0$ while for shrinking case $(s = -1)$ at $\eta = 30$ is used. It is observed that the $\hbar$-values can be chosen within the common admissible range of $-0.35 \leq \hbar < 0$ to analyse the effects of the prescribed parameters on the micropolar fluid flow. Moreover, the $(\hbar)$ curve in Figure 5.3 is used to validate the exact analytical results.
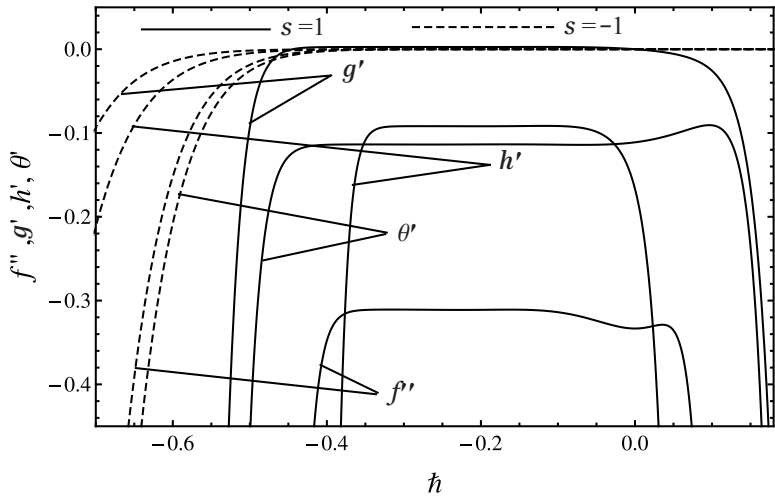
Figure 5.2: $\hbar$ curves
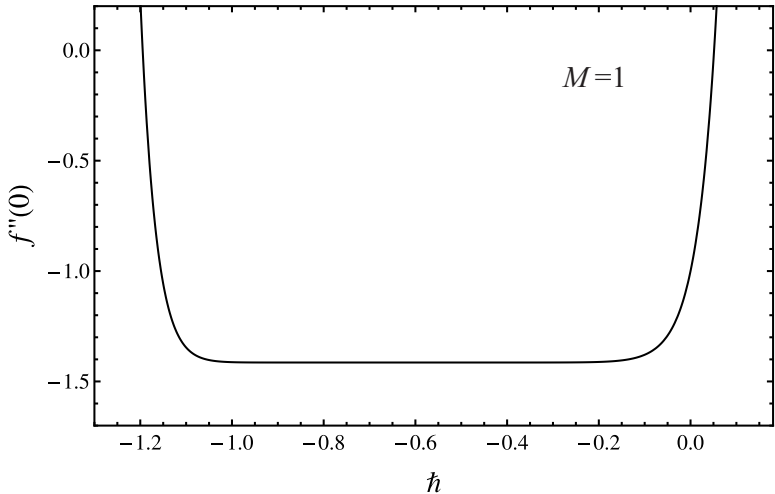
Figure 5.3: $\hbar$ curves

5.3   Study Validation

In this section, the present study is validated with the exact solution of Equation (5.14) and the already published numerical results of the Rosca and Pop [84]. Firstly, the special case arising from the Equation (5.14) in which the forced convective ($\lambda = 0$) Newtonian ($K = 0$) fluid flow passing over an impermeable ($f_w = 0$) stretching sheet ($s = 1$) is considered in the absence of the slip flow condition ($\alpha = \beta = 0$) and the Hall effect ($m = 0$). This case yields the Equation (5.14) as

$$f''' - (f')^2 + ff'' - Mf' = 0 \tag{5.30}$$

with boundary conditions $f(0) = 0, f'(0) = 1,$ and $f'(\infty) = 0$ and it's exact solution, for $\Lambda = 2\sqrt{1 + M}$, has the form

$$f(\eta) = \frac{1}{\Lambda}(2 - 2e^{-\Lambda\eta/2}) \tag{5.31}$$
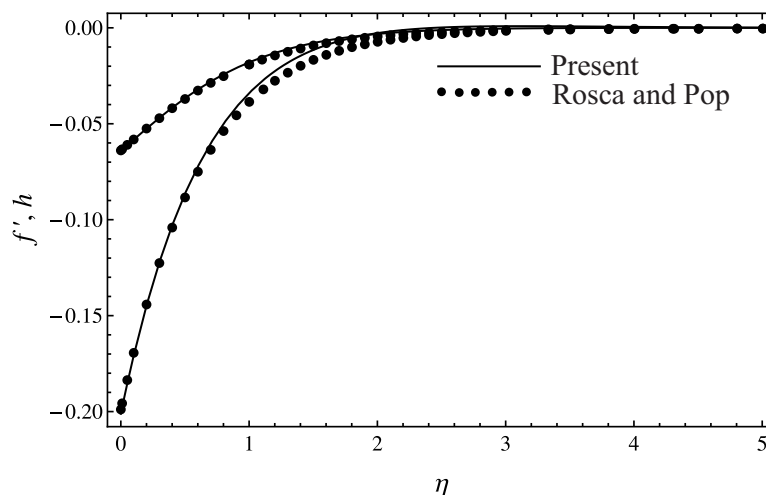
Figure 5.4: validation with Rosca and Pop [84]

which satisfies the boundary conditions. From Figure 5.3 the auxiliary parameter $\hbar$ is chosen within the range of $-1 \leq \hbar \leq -0.1$. The solution in Equation (5.31) is compared with the obtained OHAM solution at the 20th-order of approximation in Table 5.3 for different values of the M which is found to be in excellent agreement.

Secondly, the accuracy of the OHAM results also assessed with the help of the numerical results presented by the Rosca and Pop [84]. In this comparison, magnetic field and Hall effects are not taken into account for shrinking case and again it is found to be in an excellent correspondence at $K = \alpha = 1$, $\lambda = m = M = 0$, $f_w = 3$, $s = \beta = -1$ and $n = 0.2$, in Figure 5.4. In this comparison, the lower curve is sketched for f' at $\hbar = -0.095$ and upper curve is plotted for h at

$\hbar = -0.13$.

Table 5.3: Comparison with the exact solution for numerous values of M

|	Equation (5.31)	Present			
M	$-f_e''(0)$	$-f''(0)$	$-\hbar$	E_f	CPU Time(s)
0.0	1	1	0.6	——	——
0.5	1.224744871391589	1.22474487139158	0.71	9.05×10^{-25}	25.15
1.0	1.414213562373095	1.41421356237061	0.7101	6.06×10^{-21}	25.36
3.0	2	1.99999554494570	0.43	2.64×10^{-10}	25.64

5.4 Results and Discussion

The current results are calculated at $K = m = n = f_w = \delta = 0.5$, $M = \alpha = \lambda = 1$, $Pr = 5$, $\beta = -1$ or otherwise specified in the graph. In Figures 5.5–5.8, the influence of the material parameter (K) is sketched for the horizontal velocity component (f'), transverse velocity (g), micro-rotational velocity (h) and the temperature profiles with the increasing value of the similarity variable (η), respectively. When the sheet stretches, prescribed velocities and the temperature profiles increase with an increase in the concentration of the microparticles in the fluid flow, however, transverse and micro rotational velocities have a reverse impact near the stretching sheet. On the other hand, in case of the shrinking sheet, horizontal velocity component, transverse velocity and the temperature profiles decrease while the micro-rotational velocity increases by increasing the material parameter. Moreover, physical quantities of interest such as local skin frictions, local wall couple stress and heat transfer rate increase in Table 5.4 and decrease in Table 5.5 by enhancing the material parameter. Furthermore, Figures 5.5–5.6 and Figure 5.8 are plotted at $\hbar = -0.1$ and in Figure 5.7, when sheet stretches, $\hbar = -0.05$ is used and when sheet shrinks $\hbar = -0.015, -0.01, -0.004, -0.002, -0.001$ are set along with the increasing value of the K.

The influence of the buoyancy parameter (λ) is illustrated in Figures 5.9–5.12. It is observed that when either the sheet stretches or shrinks, an increase in the buoyancy parameter causes to enhance the prescribed velocities as shown in Figures 5.9–5.11 at $\hbar = -0.1$. Moreover, the temperature of the micropolar fluid flow decreases with the increasing values of the λ as depicted in Figure 5.12 at $\hbar = -0.1$. Furthermore, as the buoyancy parameter increases, local skin frictions, local wall couple stress and local Nusselt number increase as shown in Tables 5.6–5.7 for stretching and shrinking cases, but local wall couple stress decreases in Table 5.7. It is to be noted that $\hbar = -0.1$ is used to plot Figure 5.8.
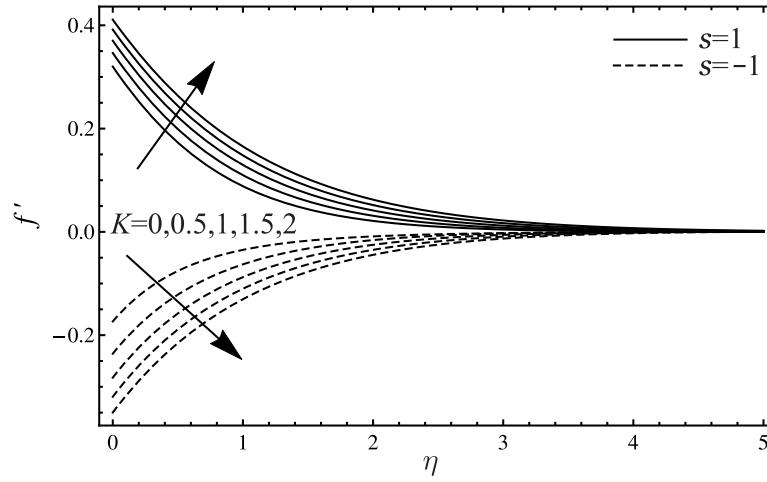
Figure 5.5: Impact of K on f'
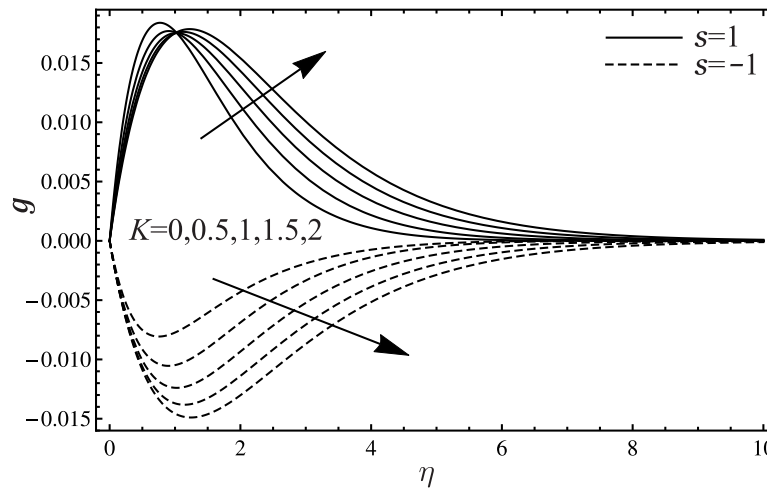
Figure 5.6: Impact of K on g
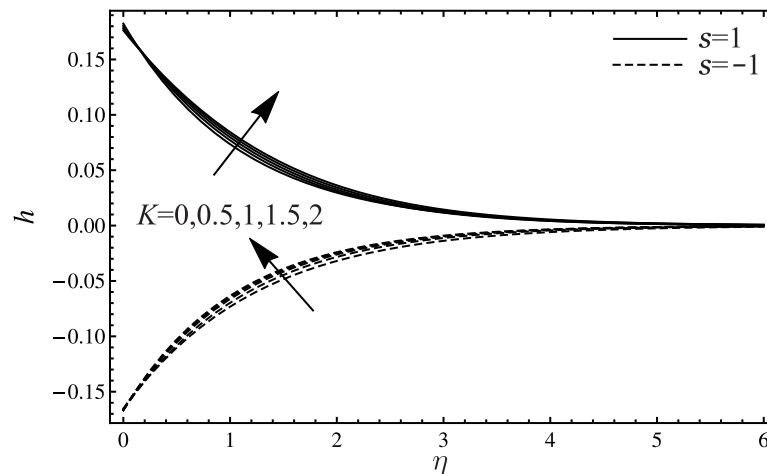
Figure 5.7: Impact of K on h

Figures 5.13–5.16 display the effect of the transverse magnetic field parameter on the f', g, h and θ at $\hbar = -0.1$. A variation in the magnetic field parameter with the fixed viscosity of the microparticles, i.e., at $K = 0.5$, results in a decrease

Figure 5.8: Impact of K on θ

in the prescribed velocities with the stretching sheet and when the sheet shrinks, a reverse trend is observed. However, temperature of the micropolar fluid flow increases for $s = 1$ and it decreases for $s = -1$ in Figure 5.16.

Table 5.4: Influences of K, M, m, f_w on physical quantities for $s = 1$

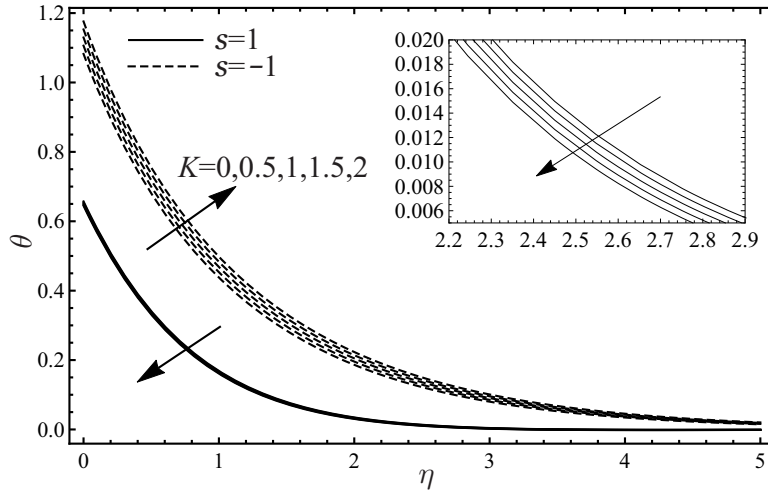| K	M	m	f_w	$C_{f_x}Re_x^{\frac{1}{2}}$	$-\hbar$	$C_{f_z}Re_x^{\frac{1}{2}}$	$-\hbar$	M_xRe_x	$-\hbar$	$Nu_xRe_x^{-\frac{1}{2}}$	$-\hbar$
0.0	1	0.5	0.5	0.36962	0.1	0.06329	0.1	0.15731	0.1	2.85013	0.1
0.5				0.45563	0.1	0.07818	0.1	0.18582	0.1	2.89193	0.1
1.0				0.54035	0.1	0.09145	0.1	0.20634	0.1	2.92713	0.1
1.5				0.62315	0.1	0.10434	0.1	0.22399	0.1	2.95723	0.1
2.0				0.70379	0.1	0.11704	0.1	0.23975	0.1	2.98316	0.1
0.5	0			0.44696	0.1	0.00000	0.1	0.17915	0.1	2.09748	0.001
	1			0.44292	0.03	0.07818	0.1	0.18582	0.1	2.09726	0.001
	3			0.43390	0.1	0.10340	0.1	0.18636	0.06	2.09684	0.001
	5			0.40540	0.1	0.10544	0.1	0.18933	0.03	2.09642	0.001
	7			0.38062	0.1	0.10896	0.118	0.19052	0.02	2.09601	0.001
	1	0.0		0.45107	0.1	0.00000	0.1	0.18467	0.1	2.86930	0.1
		0.5		0.45563	0.1	0.07818	0.1	0.18582	0.1	2.89193	0.1
		1.0		0.46002	0.1	0.12025	0.1	0.18645	0.1	2.93337	0.1
		1.5		0.46067	0.1	0.13160	0.1	0.18842	0.03	2.96714	0.1
		2.0		0.46585	0.1	0.16962	0.245	0.19590	0.01	2.99001	0.1
		0.5	1.0	0.42602	0.01	0.03326	0.01	0.21544	0.01	1.73923	0.005
			0.5	0.42361	0.01	0.03645	0.01	0.19663	0.01	1.28265	0.005
			0.0	0.41747	0.01	0.04079	0.01	0.17604	0.01	0.99238	0.005
			-0.5	0.40432	0.01	0.04706	0.01	0.15211	0.01	0.80987	0.005
			-1.0	0.37798	0.01	0.05656	0.01	0.12194	0.01	0.69565	0.005

From Figures 5.17–5.18, it is observed that the increasing value of the magnetic field parameter exerts a normal force on the moving microparticles and that force causes to reduce the horizontal velocity component, even with the increasing value of the Hall parameter (as depicted in Figure 5.17) and consequently, that normal force reinforces the increasing value of the Hall parameter (in Figure 5.18)

and thus, it causes an increase in the transverse velocity of the micropolar fluid flow as shown in Figure 5.18, in the case of the stretching sheet. It is also noted that at the higher value of the magnetic field ($M = 7$), velocity boundary layer thickness is greater than that of the lower magnetic field ($M = 1$) in Figure 5.18, which supports the assumptions. However, when the sheet shrinks, an increase in the Hall parameter yields a decrease in the horizontal velocity component and transverse velocity. It is worth mentioning that at $M = 0$ in Figure 5.14 and at $m = 0$ in Figure 5.18 the transverse velocity component is zero for both cases of the sheet which reveals the correctness of our obtained results. Tables 5.6–5.7 show that as sheet stretches, increasing value of the transverse magnetic field parameter causes to decrease the local skin friction ($C_{f_x}Re_x^{1/2}$) and heat transfer rate while it increases the local skin friction ($C_{f_z}Re_x^{1/2}$) and local wall couple stress. In addition a reverse trend has been observed in case of the shrinking sheet. Similarly, all physical quantities increase as the Hall parameter increases for $s = 1$ as illustrated in Table 5.4. Local skin frictions and local Nusselt number decrease and the local wall couple stress increases at $s = -1$ as tabulated in Table 5.5.

Table 5.5: Influences of K, M, m, f_w on physical quantities for $s = -1$

K	M	m	f_w	$-C_{f_x}Re_x^{\frac{1}{2}}$	$-\hbar$	$-C_{f_z}Re_x^{\frac{1}{2}}$	$-\hbar$	$-M_xRe_x$	$-\hbar$	$Nu_xRe_x^{-\frac{1}{2}}$	$-\hbar$
0.0	1	0.5	0.5	0.29531	0.1	0.02974	0.1	0.05843	0.1	2.33375	0.1
0.5				0.39622	0.1	0.04813	0.1	0.12623	0.1	2.15285	0.1
1.0				0.49219	0.1	0.06565	0.1	0.15471	0.1	2.00842	0.1
1.5				0.58388	0.1	0.08213	0.1	0.17427	0.1	1.88315	0.1
2.0				0.67189	0.1	0.09742	0.1	0.18991	0.1	1.7715	0.1
0.5	0			0.40051	0.1	0.00000	0.1	0.10169	0.1	2.02731	0.001
	1			0.39622	0.1	0.04813	0.1	0.12623	0.1	2.0275	0.001
	3			0.36959	0.1	0.05950	0.1	0.14054	0.1	2.02789	0.001
	5			0.34454	0.1	0.07122	0.01	0.15773	0.03	2.02827	0.001
	7			0.32389	0.1	0.10701	0.135	0.16435	0.02	2.02865	0.001
	1	0.0		0.39172	0.1	0.00000	0.1	0.12879	0.1	2.19489	0.1
		0.5		0.39624	0.1	0.04813	0.1	0.12623	0.1	2.15285	0.1
		1.0		0.40187	0.1	0.07672	0.1	0.12061	0.1	2.0675	0.1
		1.5		0.40393	0.1	0.08605	0.1	0.11530	0.1	1.99456	0.1
		2.0		0.40406	0.1	0.09966	0.16	0.11146	0.1	1.94567	0.1
		0.5	1.0	0.41013	0.01	0.02652	0.01	0.20599	0.01	1.44516	0.005
			0.5	0.41613	0.01	0.02509	0.01	0.17677	0.01	1.07763	0.005
			0.0	0.42829	0.01	0.02179	0.01	0.16727	0.001	0.85520	0.005
			−0.5	0.45264	0.01	0.01533	0.01	0.16508	0.01	0.72016	0.005
			−1.0	0.50051	0.01	0.00352	0.01	0.16387	0.008	0.63768	0.005

Figure 5.19 shows the effect of Prandtl number (Pr) on the thermal boundary layer thickness of the micropolar fluid flow. It displays that an increase in the Pr, i.e. an increase in the momentum diffusivity, causes a decrease in the thermal boundary layer thickness. This results in the reducing tem-
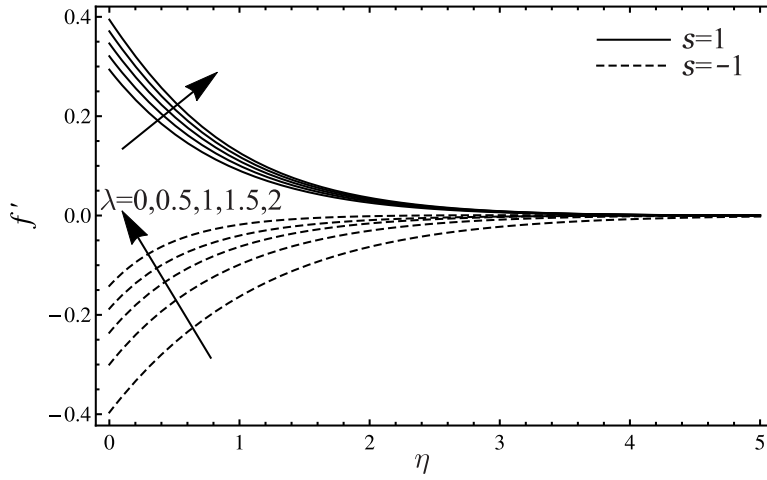
Figure 5.9: Impact of λ on f'
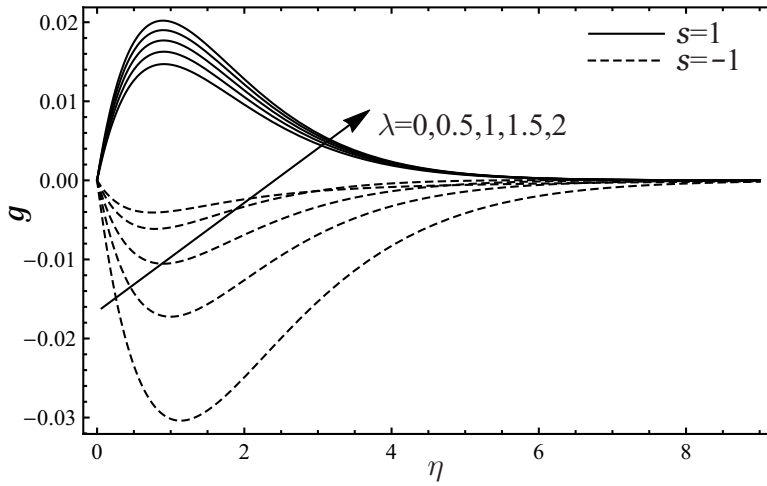
Figure 5.10: Impact of λ on g
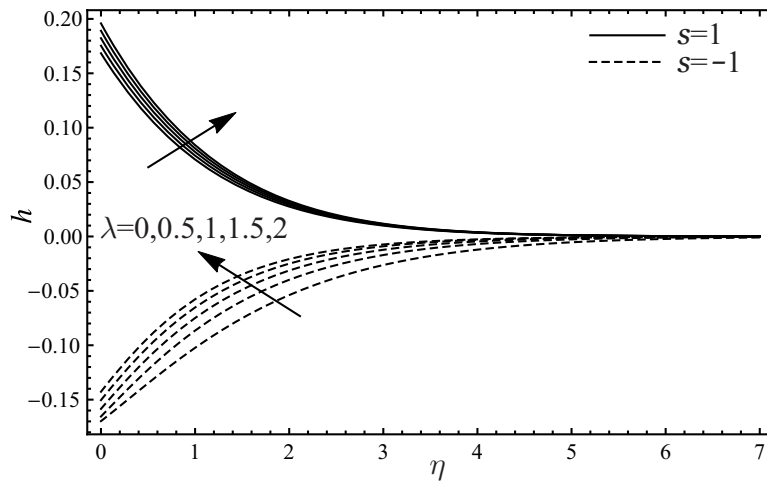
Figure 5.11: Impact of λ on h

perature of the micropolar fluid flow. This impact is observed at various values of $Pr = 0.1, 0.71, 1, 5, 10, 20, 50, 100, 500$ corresponding to various values of $\hbar = -0.01, -0.01, -0.01, -0.001, -0.001, -0.001, -0.0006, -0.0004, -0.0001$, re-
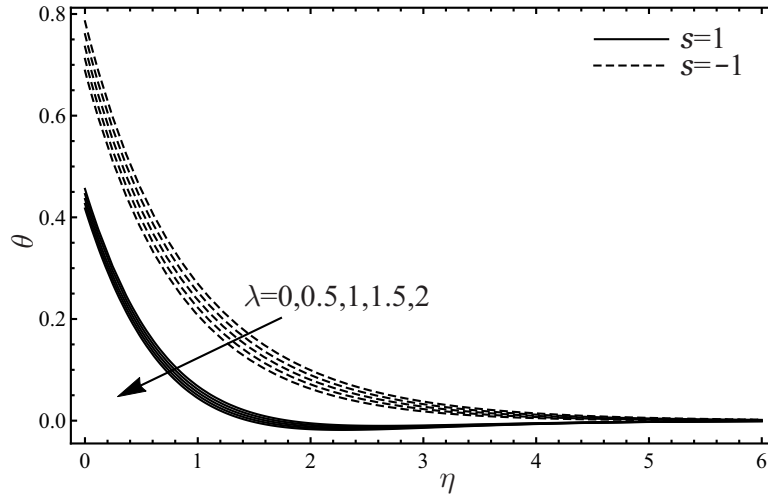
Figure 5.12: Impact of λ on θ
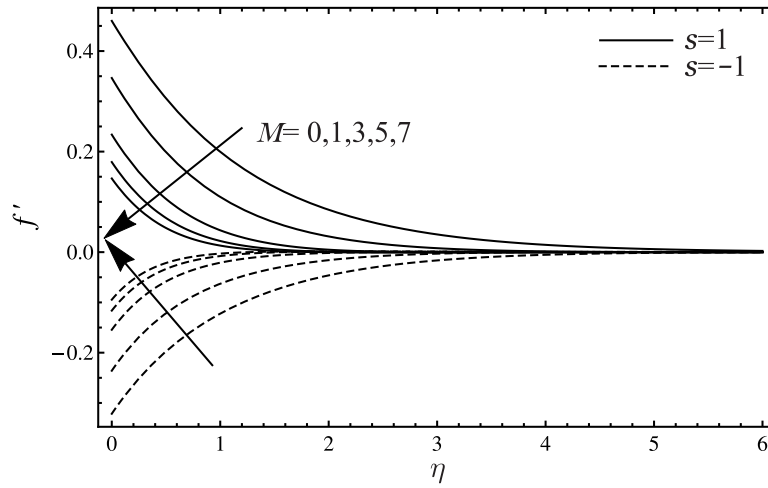
Figure 5.13: Impact of M on f'
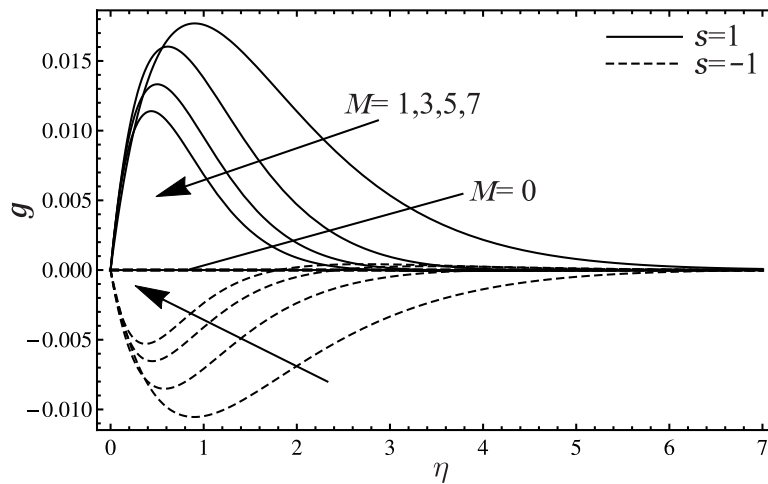
Figure 5.14: Impact of M on g

spectively. However, $Pr = 5$ and $\hbar = -0.0001$ are chosen for $s = -1$ (dashed line) in Figure 5.19. It is noted that the local skin friction ($C_{f_x} Re_x^{1/2}$), local wall

Figure 5.15: Impact of M on h
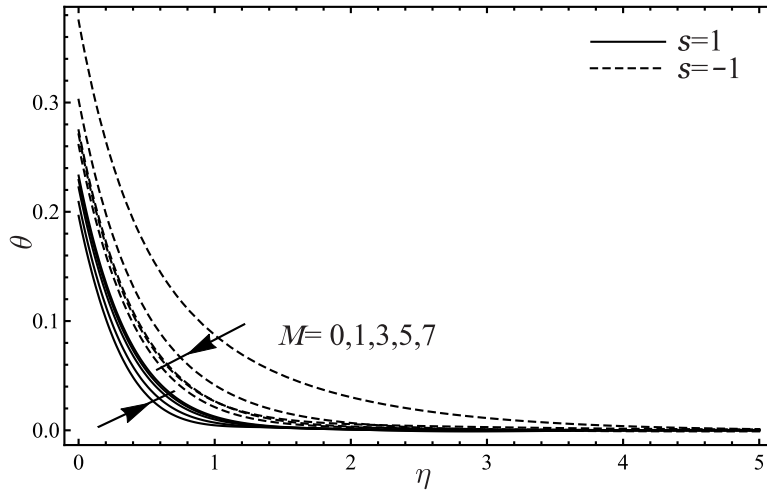
Figure 5.16: Impact of M on θ

couple stress and local Nusselt number increase with an increase in the Pr while a decrease is observed in the local skin friction $(C_{f_z}Re_x^{1/2})$ as the sheet stretches in Table 5.6. Furthermore, when the sheet shrinks (in Table 5.7), local skin frictions and heat transfer rate increase and local wall couple stress decreases as the Prandtl number increases.

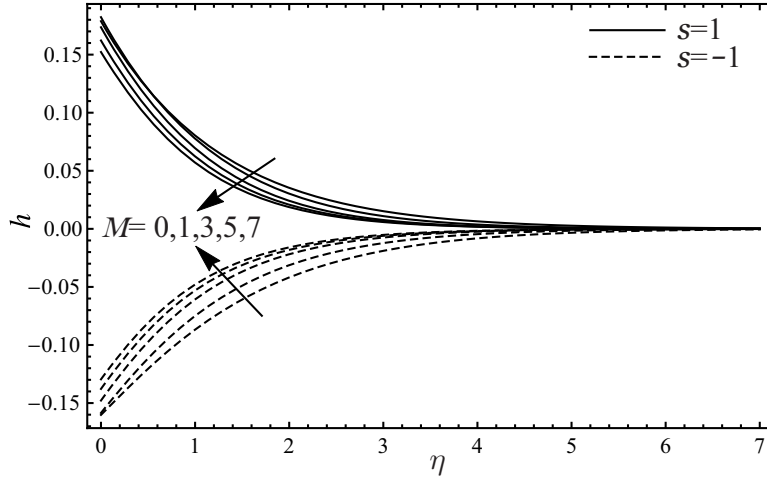To investigate the impact of suction $(f_w > 0)$/injection $(f_w < 0)$ parameter, Figures 5.20–5.23 are plotted with the increasing value of the similarity variable (η). As predicted, at the constant magnetic field $(M = 1)$, Hall current $(m = 0.5)$ and viscosity of the micro-particles $(K = 0.5)$, the increasing value of the suction parameter causes to reduce the prescribed velocities and the temperature profiles for stretching and shrinking of the sheet. However, micro-rotational velocity increases with an increase in the suction parameter for shrinking sheet. On the other hand, a reverse trend yields by higher values of the injection parameter. An increasing value of the suction parameter gives an increase in the local skin friction

Table 5.6: Influences of $\delta, \lambda, Pr, \alpha, \beta$ on physical quantities for $s = 1$

δ	λ	Pr	α	β	$C_{f_x}Re_x^{\frac{1}{2}}$	$-\hbar$	$C_{f_z}Re_x^{\frac{1}{2}}$	$-\hbar$	M_xRe_x	$-\hbar$	$Nu_xRe_x^{-\frac{1}{2}}$	$-\hbar$
0.1	1	5	1	−1	0.426964	0.1	0.067429	0.1	0.175053	0.1	2.8382	0.1
0.2					0.433355	0.1	0.069948	0.1	0.177378	0.1	2.85109	0.1
0.3					0.440234	0.1	0.072575	0.1	0.17993	0.1	2.86429	0.1
0.4					0.447643	0.1	0.075317	0.1	0.182735	0.1	2.87789	0.1
0.5					0.455632	0.1	0.078183	0.1	0.18582	0.1	2.89193	0.1
0.5	0.0				0.421024	0.1	0.065009	0.1	0.172935	0.1	1.59661	0.01
	0.5				0.438395	0.1	0.071845	0.1	0.179244	0.1	1.62144	0.01
	1.0				0.455632	0.1	0.078183	0.1	0.18582	0.1	1.6466	0.01
	1.5				0.472738	0.1	0.084101	0.1	0.192628	0.1	1.67208	0.01
	2.0				0.489718	0.1	0.089662	0.1	0.199639	0.1	1.69787	0.01
	0.5	0.1			0.41359	0.01	0.040961	0.01	0.190776	0.01	0.85618	0.01
		0.71			0.415514	0.01	0.040201	0.01	0.191875	0.01	0.91627	0.01
		1			0.416342	0.01	0.037906	0.0095	0.19235	0.01	0.94797	0.01
		5			0.416771	0.001	0.036445	0.01	0.206665	0.001	1.04863	0.001
		10			0.416895	0.001	0.034203	0.01	0.206728	0.001	1.12598	0.001
		20			0.417106	0.001	0.031209	0.0095	0.206836	0.001	1.31313	0.001
		50			0.417516	0.001	0.026413	0.008	0.207484	0.0006	1.57138	0.0006
		100			0.420545	0.01	0.017674	0.005	0.207793	0.0004	1.8937	0.0004
		500			0.422557	0.0031	0.011111	0.003	0.208203	0.0001	2.31303	0.0001
		5	1		0.455632	0.1	0.07818	0.1	0.18582	0.1	2.89193	0.1
			2		0.341856	0.1	0.064748	0.1	0.130589	0.1	2.82473	0.1
			3		0.273342	0.1	0.056193	0.1	0.099005	0.1	2.7812	0.1
			1	−1	0.455632	0.1	0.07818	0.1	0.18582	0.1	2.89193	0.1
				−2	0.370753	0.1	0.068315	0.1	0.144306	0.1	2.84114	0.1
				−3	0.323899	0.1	0.062649	0.1	0.122204	0.1	2.81168	0.1
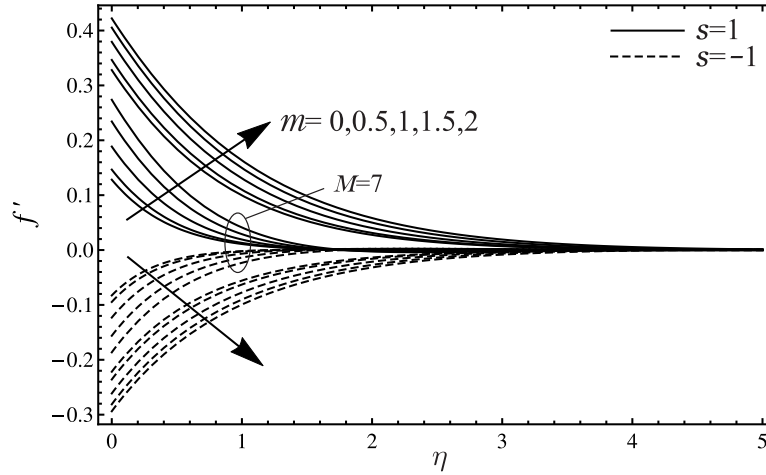
Figure 5.17: Impact of m on f'

$(C_{f_x}Re_x^{1/2})$, local wall couple stress and local Nusselt number while it causes a decrease in the local skin friction $(C_{f_z}Re_x^{1/2})$, as the sheet stretches. An opposite trend is noted in the case of an increasing value of the injection parameter in Table 5.4. However, on the other hand, local skin friction $(C_{f_x}Re_x^{1/2})$ and heat transfer rate increase, and local skin friction $(C_{f_z}Re_x^{1/2})$ and local wall couple
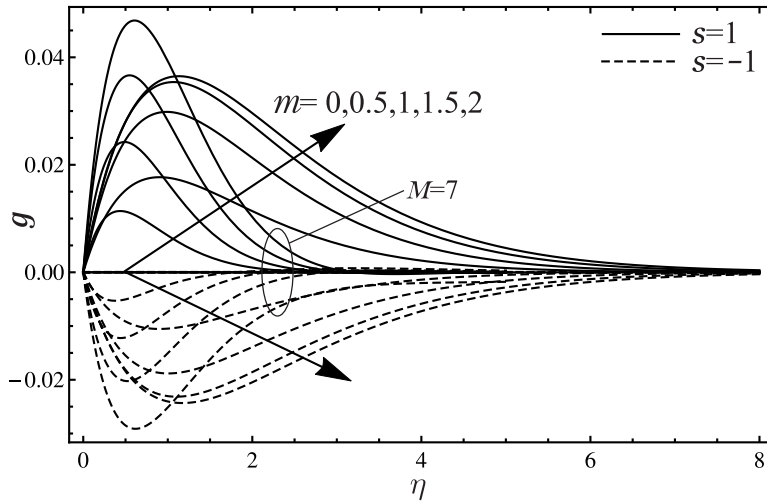
Figure 5.18: Impact of m on g
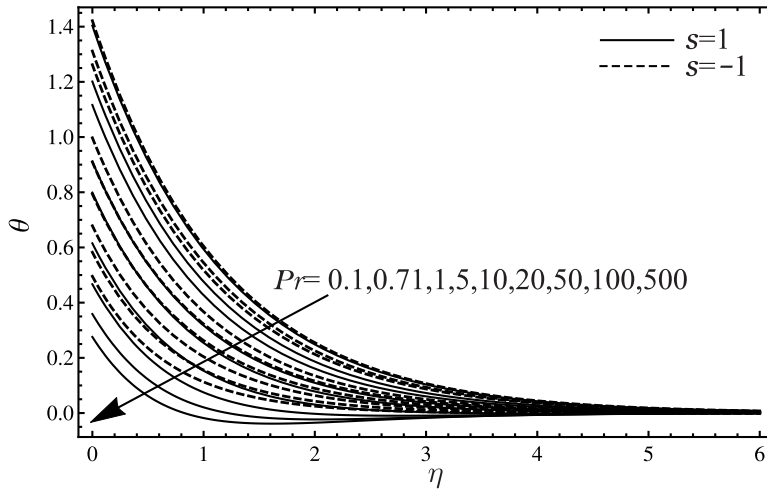
Figure 5.19: Impact of Pr on θ

stress decrease as the suction parameter increases by shrinking the sheet, and a reverse effect is observed by increasing the injection parameter in Table 5.5.
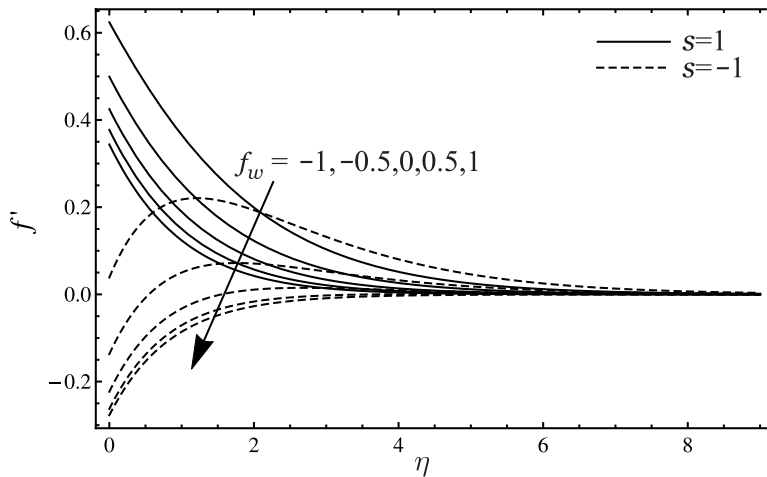
Figure 5.20: Impact of f_w on f'
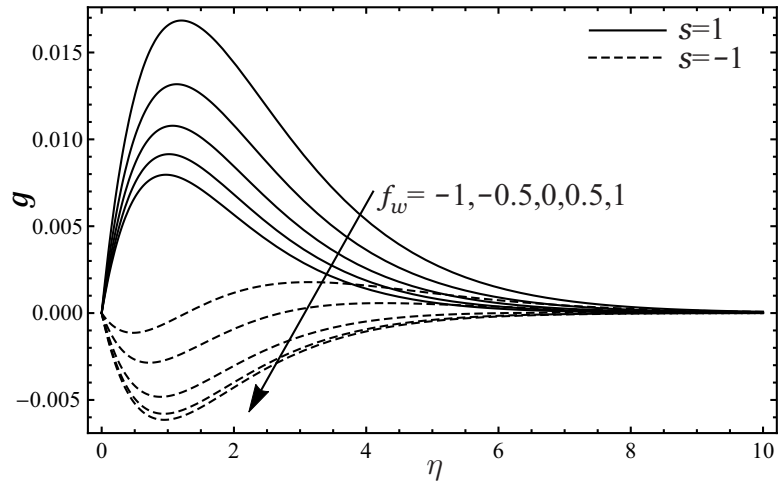
Figure 5.21: Impact of f_w on g
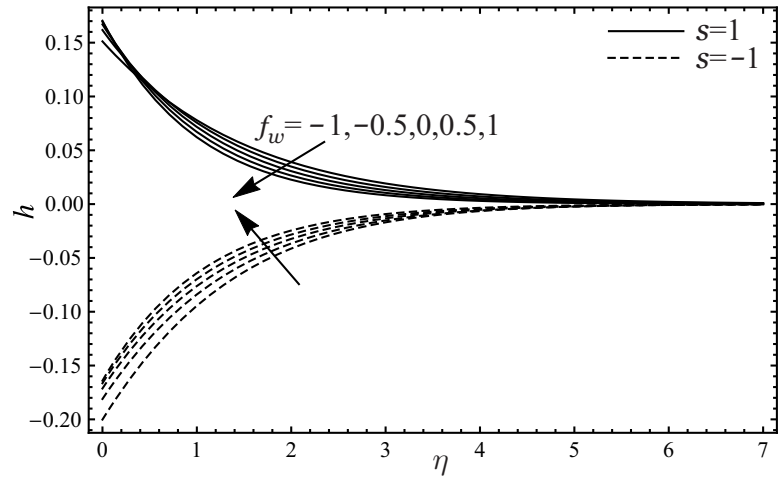
Figure 5.22: Impact of f_w on h
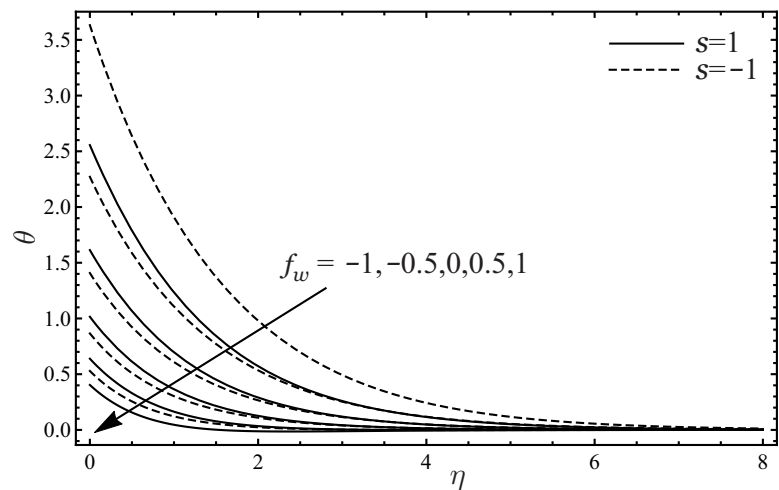
Figure 5.23: Impact of f_w on θ

Figures 5.24–5.31 depict the effects of the first and second order slip flow parameters on the horizontal velocity component, transverse velocity, microrotation

79
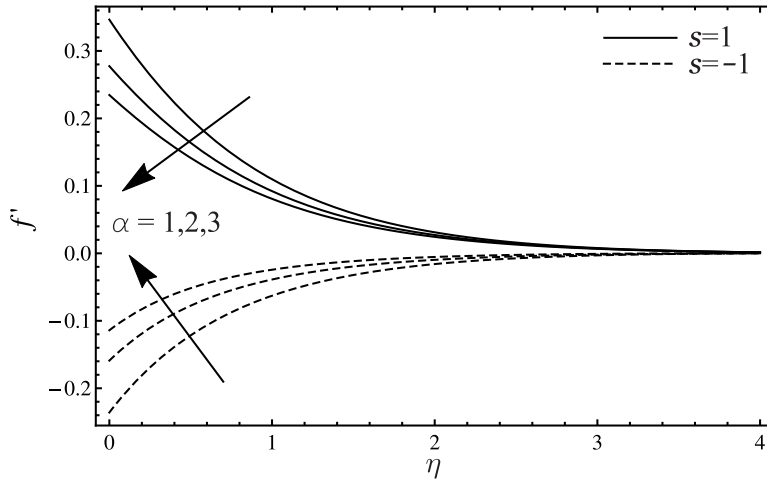
Figure 5.24: Impact of α on f'
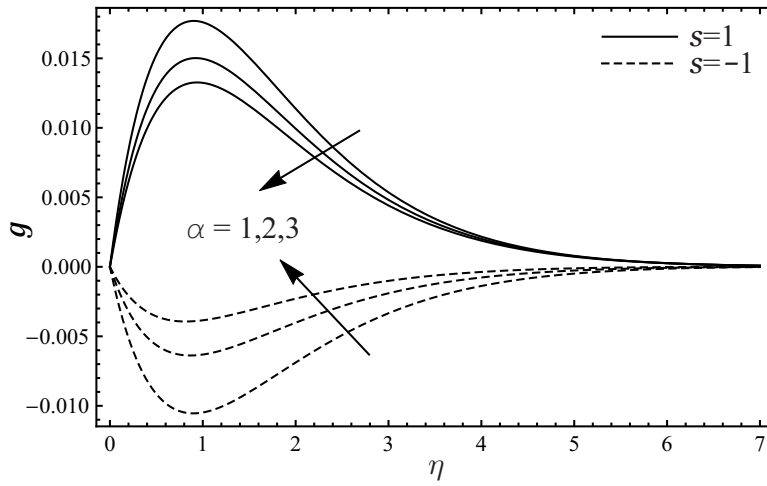
Figure 5.25: Impact of α on g
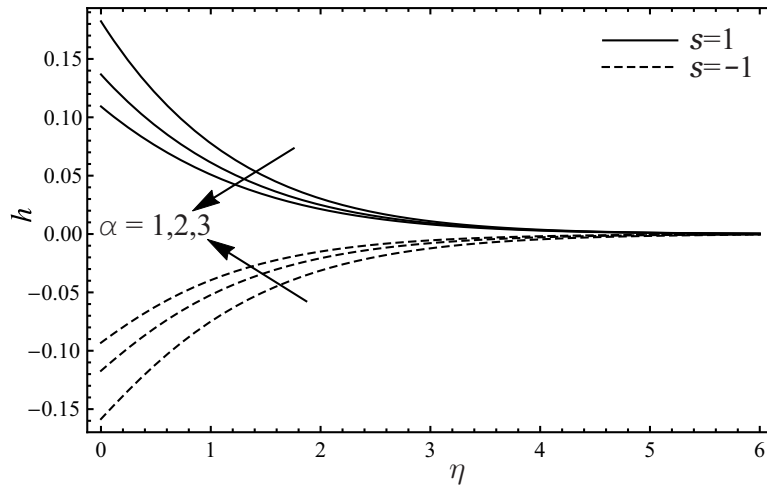
Figure 5.26: Impact of α on h

velcoity and the temperature profiles for the stretching/shrinking sheet at $\hbar = -0.1$. These figures illustrate that an increase in the first or second order slip flow
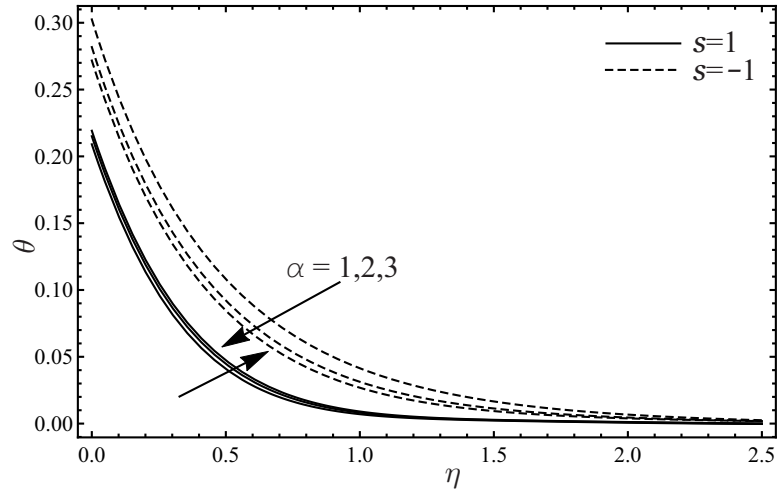
Figure 5.27: Impact of α on θ

parameters reduces the prescribed velocities and enhances the temperature of the micropolar fluid flow for the stretching sheet while an opposite behaviour is noted for the shrinking sheet. From Tables 5.6–5.7, it is clear that all of the physical quantities increase when the sheet shrinks and decrease when it stretches.

Table 5.7: Influences of $\delta, \lambda, Pr, \alpha, \beta$ on physical quantities for $s = -1$

δ	λ	Pr	α	β	$-C_{f_x}Re_x^{\frac{1}{2}}$	$-\hbar$	$-C_{f_z}Re_x^{\frac{1}{2}}$	$-\hbar$	$-M_xRe_x$	$-\hbar$	$Nu_xRe_x^{-\frac{1}{2}}$	$-\hbar$
0.1	1	5	1	−1	0.42330	0.1	0.09374	0.1	0.09519	0.1	1.70189	0.1
0.2					0.41932	0.1	0.08031	0.1	0.10488	0.1	1.85421	0.1
0.3					0.41292	0.1	0.06910	0.1	0.11280	0.1	1.95752	0.1
0.4					0.40515	0.1	0.05891	0.1	0.11968	0.1	2.02653	0.1
0.5					0.39624	0.1	0.04813	0.1	0.12623	0.1	2.15285	0.1
0.5	0.0				0.42437	0.1	0.10937	0.1	0.08375	0.1	1.13641	0.01
	0.5				0.41370	0.1	0.07057	0.1	0.11190	0.1	1.15766	0.01
	1.0				0.39624	0.1	0.04813	0.1	0.12623	0.1	1.1797	0.01
	1.5				0.37608	0.1	0.03212	0.1	0.13429	0.1	1.20255	0.01
	2.0				0.35684	0.1	0.02296	0.1	0.13843	0.1	1.22625	0.01
	0.5	0.1			0.42190	0.01	0.01926	0.007	0.18255	0.009	0.85173	0.01
		0.71			0.42103	0.01	0.01763	0.006	0.19036	0.005	0.88123	0.01
		1			0.42063	0.01	0.01557	0.005	0.20006	0.002	0.89616	0.01
		5			0.41667	0.001	0.01329	0.004	0.20399	0.001	1.01375	0.001
		10			0.41661	0.001	0.01051	0.003	0.20438	0.0009	1.04955	0.001
		20			0.41651	0.001	0.00736	0.002	0.20478	0.0008	1.1301	0.001
		50			0.41627	0.001	0.00384	0.001	0.20560	0.0006	1.23687	0.0006
		100			0.41598	0.001	0.00349	0.0009	0.20648	0.0004	1.35825	0.0004
		500			0.41582	0.001	0.00314	0.0008	0.20786	0.0001	1.50909	0.0001
		5	1		0.39624	0.1	0.04813	0.1	0.12623	0.1	2.15285	0.1
			2		0.29299	0.1	0.03044	0.1	0.10251	0.1	2.27437	0.1
			3		0.23287	0.1	0.02006	0.1	0.08686	0.1	2.34015	0.1
			1	−1	0.39624	0.1	0.04813	0.1	0.12623	0.1	2.15285	0.1
				−2	0.24781	0.1	0.02258	0.1	0.09082	0.1	2.32714	0.1
				−3	0.16029	0.1	0.00777	0.1	0.06587	0.1	2.41082	0.1

81

Figure 5.28: Impact of β on f'

Figure 5.29: Impact of β on g
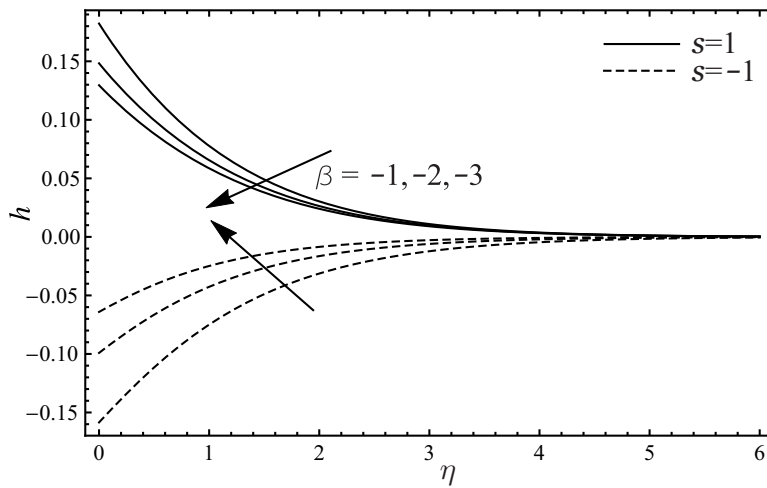
Figure 5.30: Impact of β on h

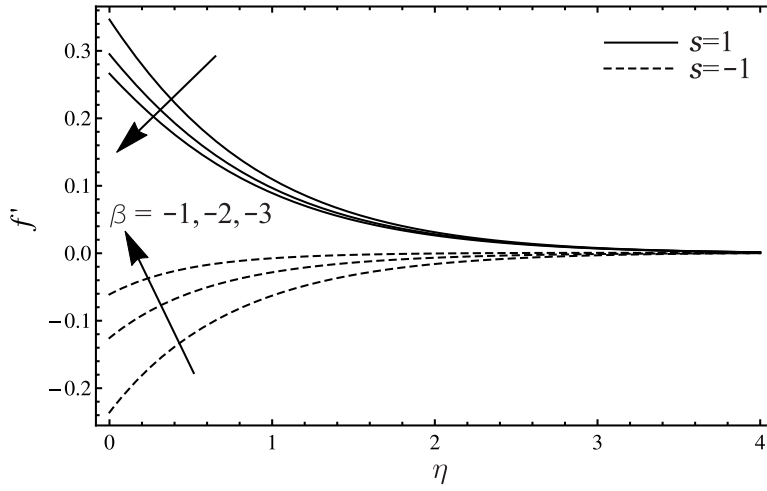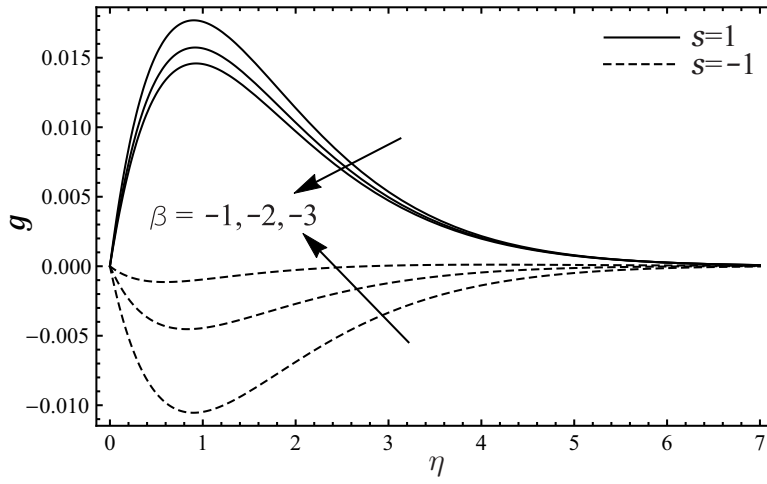When sheet stretches or shrinks in Figures 5.32–5.34, the increasing value of the Newtonian heating parameter results in a higher prescribed velocity profiles.

However, horizontal velocity component starts decreasing at $\delta = 2$.
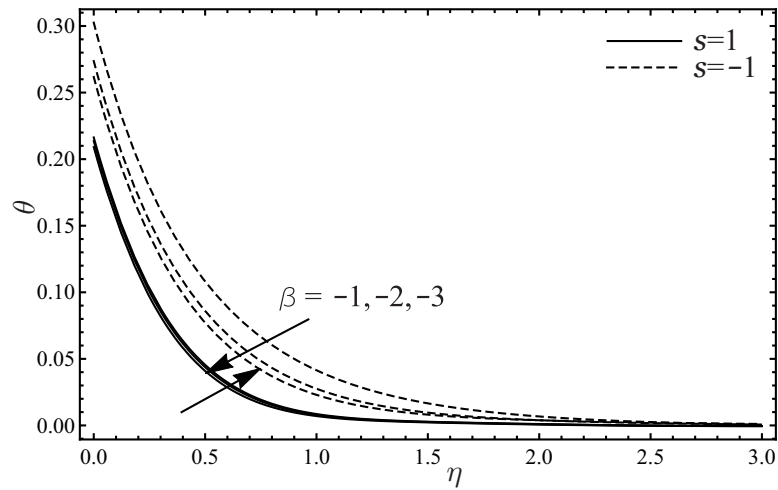
Figure 5.31: Impact of β on θ
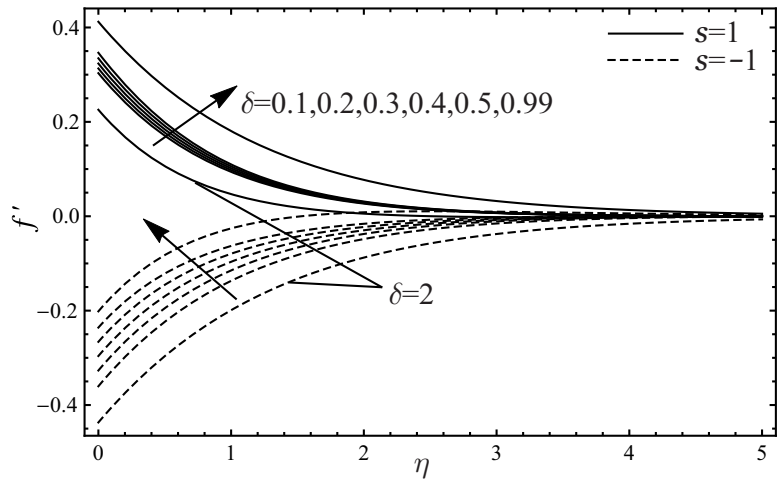
Figure 5.32: Impact of δ on f'
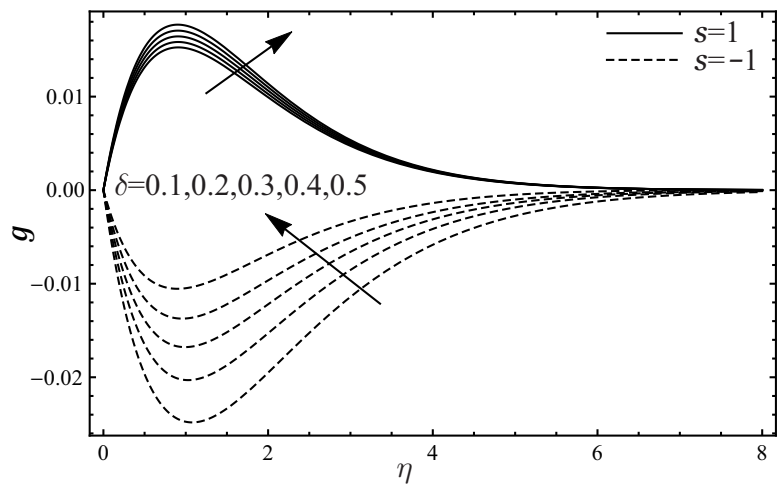
Figure 5.33: Impact of δ on g

It is to be noted that $\hbar = -0.0001$ and -0.005 are used for $\delta = 0.99$ and 2 at $s = 1$, and $\hbar = -0.00015$ and -0.005 are used for $\delta = 0.99$ and 2 at $s = -1$ in Figure 5.32 and rest of the curves are plotted at $\hbar = -0.1$ in Figures 5.32–5.34. Furthermore, the influence of the Newtonian heating parameter is sketched in Figure 5.35 by fixing $\hbar = -0.1$ except for $\delta = 0.99$ and $\delta = 2$, $\hbar = -0.0048$ and $\hbar = -0.02$ for the stretching sheet and $\hbar = -0.0059$ and $\hbar = -0.005$ for the shrinking sheet, respectively.
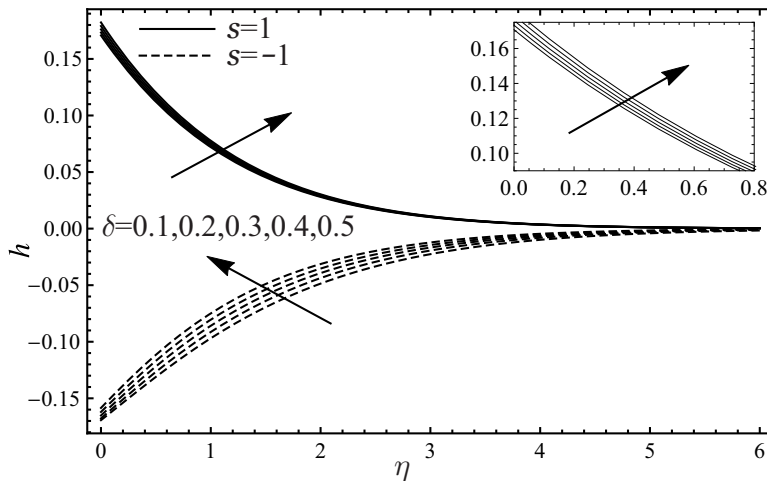
Figure 5.34: Impact of δ on h
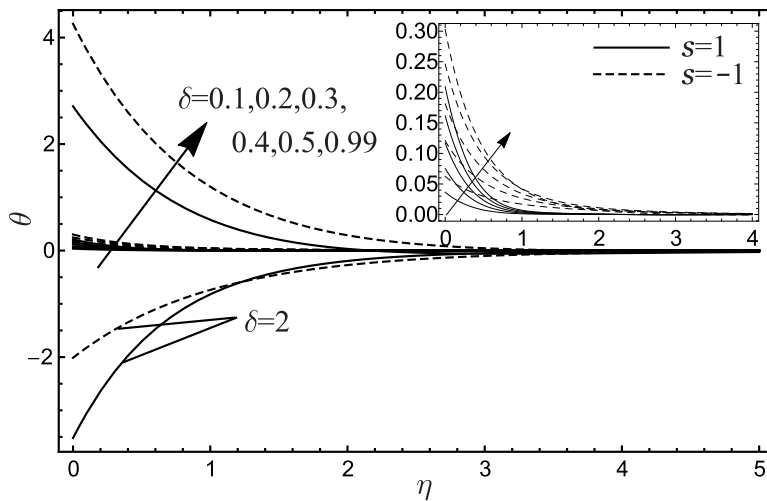
Figure 5.35: Impact of δ on θ

It displays that a small increment in the Newtonian heating parameter significantly enhances the thermal boundary layer thickness which leads to a raise in the temperature of the micopolar fluid flow. A shrinking sheet produces a higher thermal boundary layer thickness as compared to a stretching sheet as depicted in Figure 5.35. On the other hand, when Newtonian heating parameter δ gets a value greater than 1 then the temperature of the micropolar fluid flow decreases

which is a significant representation of the initial solution. Moreover, all physical quantities increase with an increase in the Newtonian heating parameter, except the local wall couple stress, which decreases when the sheet shrinks as shown in Tables 5.6–5.7.

5.5   Chapter Summary

In this chapter, the Hall current effect on the mixed convective magneto-micropolar fluid flow passing over a stretching/shrinking porous sheet is studied and analysed under the influence of the Newtonian heating. Slip flow condition is also considered in this study. From the present results, the following key points can be summarized:

- When the sheet stretches with the constant concentration of the micro-elements, increasing value of the magnetic field parameter slows down the horizontal velocity component and the transverse velocity of the micropolar fluid flow, oppositely, an increase in the Hall current parameter not only yields a raise in the horizontal velocity component but also leads to an increase in the transverse velocity. Reverse and similar patterns are observed for the magnetic field and Hall parameters as in the case of the shrinking sheet, respectively.

- An increasing value of the Newtonian heating parameter increases the fluid temperature and heat transfer rate.

- Furthermore, higher value of the first order or the second order slip flow parameters, horizontal velocity component decreases as the sheet stretches and it increases as the sheet shrinks.

- However, in comparison with the stretching sheet, an increasing magnitude of the Prandtl number rapidly decreases the fluid temperature of the porous sheet. It is noted that it reduces more temperature with heat transfer rate of 93% in contrast to the shrinking sheet.

Chapter 6

Micropolar Fluid Flow with Chemical Reaction[1]

This chapter deals with the influence of the homogeneous first order chemical reaction on the mixed convective micropolar fluid flow over a stretching/shrinking sheet in the slip flow regime. A Newtonian heating condition is assumed at the thermal boundary layer. The present chapter extends the work of Rosca and Pop [84] which was based on an analytical study of the viscous boundary layer flow of a quiescent fluid with the second order slip flow model [79]. Rosca and Pop [84] prolonged the boundary layer flow over a porous shrinking sheet in the micropolar fluid flow with the second order slip boundary condition. Chemical reaction with slip condition is considered as an important application in refrigerating coils, polishing artificial heart valves and internal cavities.

6.1 Governing Equations

Considered a steady state mixed convective incompressible micropolar fluid flow past over a porous surface which stretches and shrinks with the velocity $u = sax$. The flow is taken along the $x-$axis and $y-$axis normal to it. Wu's [11] second order slip flow model (u_{slip}) and the Newtonian heating [89] are assumed in the boundary conditions. In the absence of the Hall effect and by substituting $\mathfrak{B} = \mathfrak{C} = \mathfrak{D} = \mathfrak{E} = 0$, and $\mathfrak{A} = 1$ in the system of Equations (1.4)–(1.5), the mathematical form of the governing flow equations influencing with the first order homogeneous chemical reaction can be written as [67, 84]:

$$\frac{\partial u}{\partial x} + \frac{\partial v}{\partial y} = 0, \tag{6.1}$$

$$u\frac{\partial u}{\partial x} + v\frac{\partial u}{\partial y} = \frac{\mu + \chi}{\rho}\left(\frac{\partial^2 u}{\partial y^2}\right) + \frac{\chi}{\rho}\left(\frac{\partial \omega}{\partial y}\right) + \mathrm{g}\beta_T\left(T - T_\infty\right) + \mathrm{g}\beta_C\left(C - C_\infty\right),$$
$$\tag{6.2}$$

$$u\frac{\partial \omega}{\partial x} + v\frac{\partial \omega}{\partial y} = \frac{\gamma}{\rho j}\left(\frac{\partial^2 \omega}{\partial y^2}\right) - \frac{\chi}{\rho j}\left(2\omega + \frac{\partial u}{\partial y}\right), \tag{6.3}$$

$$u\frac{\partial T}{\partial x} + v\frac{\partial T}{\partial y} = \frac{k}{\rho c_p}\left(\frac{\partial^2 T}{\partial y^2}\right), \tag{6.4}$$

$$u\frac{\partial C}{\partial x} + v\frac{\partial C}{\partial y} = D_m\left(\frac{\partial^2 C}{\partial y^2}\right) - \xi\left(C - C_\infty\right), \tag{6.5}$$

with boundary conditions

$$\left.\begin{array}{l} u = su_w(x) + u_{\text{slip}};\ v = v_o;\ \omega = -n\dfrac{\partial u}{\partial y};\ k\dfrac{\partial T}{\partial y} = -h_s T;\ C = C_w \text{ at } y = 0, \\[2mm] u \to 0;\ \omega \to 0;\ T \to T_\infty;\ C \to C_\infty \text{ as } y \to \infty. \end{array}\right\}$$
$$\tag{6.6}$$
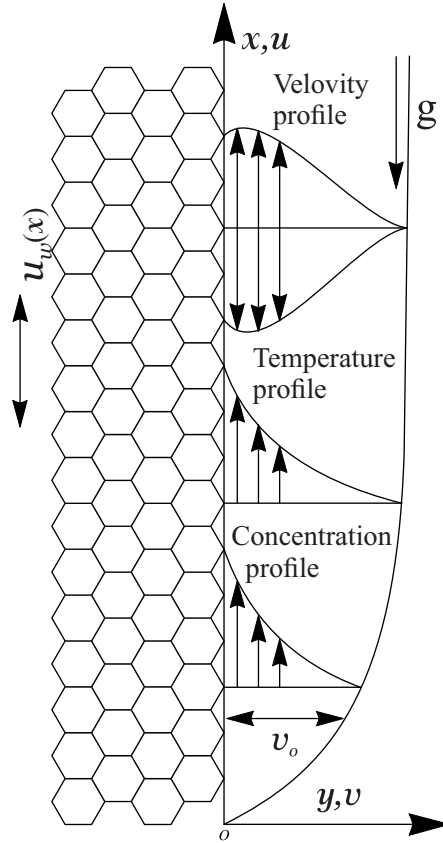
Figure 6.1: Flow model.

The equations $(6.6)_1$ and $(6.6)_4$ are for second order slip flow and the Newtonian heating conditions at the boundary, respectively. The second term of $(6.6)_1$ is defined in Equations (1.6)–(1.7).

By introducing the non-dimensional similarity variables with velocity components $u = axf'(\eta)$ and $v = -(a\nu)^{1/2}f(\eta)$ as follows:

$$\eta = \sqrt{a/\nu}y, \ \omega = \sqrt{a/\nu}axh(\eta), \ \theta(\eta) = \frac{T - T_\infty}{T_\infty}, \ \phi = \frac{C - C_\infty}{C_w - C_\infty},$$

and the governing equations (Equations (6.2)–(6.6)) are transformed (see in Section A.4 of appendix) into a set of non-linear ordinary differential equations as follows:

$$(1 + K)f''' - (f')^2 + ff'' + Kh' + \lambda\theta + \lambda\Lambda\phi = 0, \tag{6.7}$$

$$(1 + K/2)h'' - f'h + fh' - K(2h + f'') = 0, \tag{6.8}$$

$$\theta'' + Prf\theta' = 0, \tag{6.9}$$

$$\phi'' + Scf\phi' - C_mSc\phi = 0, \tag{6.10}$$

with the boundary conditions,

$$\left.\begin{array}{l} f = f_w; \ f' = s + \alpha f'' + \beta f'''; \ h = -nf''; \ \theta' = -\delta(1 + \theta); \ \phi = 1 \text{ at } \eta = 0, \\ f' \to 0; \ h \to 0; \ \theta \to 0; \ \phi \to 0 \text{ as } \eta \to \infty, \end{array}\right\} \tag{6.11}$$

where prime($'$) represents the derivative with respect to the η. The non-dimensional physical parameters used in Equations (6.7)–(6.10) are buoyancy parameter $\lambda = Gr_x/Re_x$ for the local Grashof number $Gr_x = \mathrm{g}\beta_T T_\infty x/a\nu$ and the local Reynolds number $Re_x = ax^2/\nu$, concentration to thermal buoyancy ratio parameter $\Lambda = \beta_c(C_w - C_\infty)/\beta_T T_\infty$, Prandtl number $Pr = \mu c_p/k$, Schmidt number $Sc = \nu/D_m$ and chemical reaction parameter $C_m = \xi/a$. In Equation (6.11), suction or injection parameter $f_w = -(a\nu)^{-\frac{1}{2}}v_o$, first order slip flow parameter $\alpha = A\sqrt{a/\nu} > 0$, second order slip flow parameter $\beta = Ba/\nu < 0$, Newtonian heating parameter $\delta = \frac{h_s}{k}\sqrt{\nu/a}$ are defined.

The physical quantities including local skin friction (C_{f_x}), local wall couple stress (M_x), the local Nusselt number (Nu_x) and the local Sherwood number (Sh_x) are determined as follows:

$$C_{f_x} = \frac{-\tau_w}{\rho(ax)^2} \text{ for } \tau_{w_x} = (\mu + \chi)\frac{\partial u}{\partial y} + \chi\omega\bigg|_{y=0},$$

$$M_x = \frac{-m_w}{\rho x (ax)^2} \text{ for } m_w = \left(\mu + \frac{\chi}{2}\right) j \frac{\partial \omega}{\partial y}\bigg|_{y=0},$$

$$Nu_x = \frac{-x q_w}{(T - T_\infty)} \text{ for } q_w = \frac{\partial T}{\partial y}\bigg|_{y=0},$$

$$Sh_x = \frac{-x S_m}{(C - C_w)} \text{ for } S_m = \frac{\partial C}{\partial y}\bigg|_{y=0}.$$

Similarity transformation yields

$$C_{f_x} Re_x^{\frac{1}{2}} = -(1 + K - nK) f''(\eta)|_{\eta=0}, \tag{6.12}$$

$$M_x Re_x = -\left(1 + \frac{K}{2}\right) h'(\eta)\bigg|_{\eta=0}, \tag{6.13}$$

$$Nu_x Re_x^{-\frac{1}{2}} = \delta \left(1 + \frac{1}{\theta(\eta)}\right)\bigg|_{\eta=0}, \tag{6.14}$$

$$Sh_x Re_x^{-\frac{1}{2}} = -\phi'(\eta)|_{\eta=0}. \tag{6.15}$$

6.2 Solution by Homotopy Analysis Method

Homotopy Analysis Method (HAM) developed by Liao [95–97] producing approximately analytical series solution of the nonlinear ordinary differential equations has an advantage on the perturbation and non-perturbation methods and has a great freedom to adjust the convergence of the series solution. Here, HAM is applied to solve the system of coupled nonlinear ODEs (Equations (6.7)–(6.10)) with its pertaining boundary conditions (Equation (6.11)). The homotopy series solutions of the $f(\eta), h(\eta), \theta(\eta)$ and the $\phi(\eta)$ with the help of a set of the base functions $\{\eta^r exp(-i\eta)|r \geq 0, i \geq 0\}$ can be written as

$$\left.\begin{aligned}
f(\eta) &= \sum_{r=0}^{\infty} \sum_{i=0}^{\infty} a_{r,i} \eta^r exp(-i\eta), \\
h(\eta) &= \sum_{r=0}^{\infty} \sum_{i=0}^{\infty} b_{r,i} \eta^r exp(-i\eta), \\
\theta(\eta) &= \sum_{r=0}^{\infty} \sum_{i=0}^{\infty} c_{r,i} \eta^r exp(-i\eta), \\
\phi(\eta) &= \sum_{r=0}^{\infty} \sum_{i=0}^{\infty} d_{r,i} \eta^r exp(-i\eta),
\end{aligned}\right\} \tag{6.16}$$

where $a_{r,i}, b_{r,i} \, c_{r,i}$ and $d_{r,i}$ are constants.

6.2.1 Zero-order Deformation Equation

The first rule of the solution expressions represented by Equation (6.16) and the boundary conditions (in Equation (6.11)) play an important role to choose the initial solutions as

$$
\left.\begin{aligned}
f_0(\eta) &= f_w + \frac{s(1 - e^{-\eta})}{1 + \alpha - \beta}, \\
h_0(\eta) &= \frac{sne^{-\eta}}{1 + \alpha - \beta}, \\
\theta_0(\eta) &= \frac{\delta e^{-\eta}}{1 - \delta} \quad ; \delta \neq 1, \\
\phi_0(\eta) &= e^{-\eta},
\end{aligned}\right\} \tag{6.17}
$$

with the corresponding linear operators

$$
\mathcal{L}_f = \frac{\partial^3}{\partial \eta^3} - \frac{\partial}{\partial \eta}, \ \mathcal{L}_h = \frac{\partial^2}{\partial \eta^2} + \frac{\partial}{\partial \eta}, \ \mathcal{L}_\theta = \frac{\partial^2}{\partial \eta^2} + \frac{\partial}{\partial \eta}, \text{ and } \mathcal{L}_\phi = \frac{\partial^2}{\partial \eta^2} + \frac{\partial}{\partial \eta}, \tag{6.18}
$$

which satisfy the following properties

$$
\left.\begin{aligned}
\mathcal{L}_f \left[X_1 + X_2 e^\eta + X_3 e^{-\eta}\right] &= 0, \\
\mathcal{L}_h \left[X_4 + X_5 e^{-\eta}\right] &= 0, \\
\mathcal{L}_\theta \left[X_6 + X_7 e^{-\eta}\right] &= 0, \\
\mathcal{L}_\phi \left[X_8 + X_9 e^{-\eta}\right] &= 0,
\end{aligned}\right\} \tag{6.19}
$$

in which X_i (i varies from 1 to 9) are arbitrary constants. If $q (\in [0, 1])$ represents the embedding parameter, $\hbar$ denotes the non–zero auxiliary parameter and $H(\eta)$ is taken as a non–zero auxiliary function then, in Homotopy Analysis Method, continuous mappings are defined as $f(\eta) \rightarrow \psi(\eta; q)$, $h(\eta) \rightarrow \varphi(\eta; q)$, $\theta(\eta) \rightarrow \Phi(\eta; q)$, $\phi(\eta) \rightarrow \Psi(\eta; q)$ such that, when embedding parameter (q) changes from 0 to 1 then $\{\psi(\eta; q), \varphi(\eta; q), \Phi(\eta; q), \Psi(\eta; q)\}$ vary from initial solutions $\{f_0(\eta), h_0(\eta), \theta_0(\eta), \phi_0(\eta)\}$ to the exact solutions $\{f(\eta), h(\eta), \theta(\eta), \phi(\eta)\}$. In order to ensure it, the nonlinear operators with their corresponding unknown functions, respectively, are defined as

$$
\begin{aligned}
\mathcal{N}_f \left[\psi(\eta; q)\right] &= (1 + K)\psi(\eta; q)''' - \left(\psi(\eta; q)'\right)^2 + \psi(\eta; q)\psi(\eta; q)'' + K\varphi(\eta; q)' + \\
&\qquad \lambda \Phi(\eta; q) + \lambda \Lambda \Psi(\eta; q), \\
\mathcal{N}_h \left[\varphi(\eta; q)\right] &= (1 + K/2)\varphi(\eta; q)'' - \psi(\eta; q)'\varphi(\eta; q) + \psi(\eta; q)\varphi(\eta; q)' - K(2\varphi \\
&\qquad (\eta; q) + \psi(\eta; q)''),
\end{aligned}
$$

$$\mathcal{N}_\theta \left[\Phi(\eta; q)\right] = \Phi(\eta; q)'' + Pr\psi(\eta; q)\Phi(\eta; q)',$$

$$\mathcal{N}_\phi \left[\Psi(\eta; q)\right] = \Psi(\eta; q)'' + Sc\psi(\eta; q)\Psi(\eta; q)' - C_m Sc\Psi(\eta; q),$$

then the zero–order deformation equations can be written as

$$\left.\begin{aligned}
(1-q)\mathcal{L}_f \left[\psi(\eta; q) - f_0(\eta)\right] &= q\hbar_f H_f(\eta)\mathcal{N}_f \left[\psi(\eta; q), \varphi(\eta; q), \Phi(\eta; q), \Psi(\eta; q)\right], \\
(1-q)\mathcal{L}_h \left[\varphi(\eta; q) - h_0(\eta)\right] &= q\hbar_h H_h(\eta)\mathcal{N}_h \left[\psi(\eta; q), \varphi(\eta; q), \Phi(\eta; q), \Psi(\eta; q)\right], \\
(1-q)\mathcal{L}_\theta \left[\Phi(\eta; q) - \theta_0(\eta)\right] &= q\hbar_\theta H_\theta(\eta)\mathcal{N}_\theta \left[\psi(\eta; q), \varphi(\eta; q), \Phi(\eta; q), \Psi(\eta; q)\right], \\
(1-q)\mathcal{L}_\phi \left[\Psi(\eta; q) - \phi_0(\eta)\right] &= q\hbar_\phi H_\phi(\eta)\mathcal{N}_\phi \left[\psi(\eta; q), \varphi(\eta; q), \Phi(\eta; q), \Psi(\eta; q)\right],
\end{aligned}\right\} \tag{6.20}$$

with the following associated boundary conditions at $\eta = 0$ and $\eta \to \infty$ as, i.e.

$$\left.\begin{aligned}
\psi(0; q) &= f_w, \quad \left.\frac{\partial\psi(\eta; q)}{\partial\eta}\right|_{\eta=0} = s + \alpha \left.\frac{\partial^2\psi(\eta; q)}{\partial\eta^2}\right|_{\eta=0} + \beta \left.\frac{\partial^3\psi(\eta; q)}{\partial\eta^3}\right|_{\eta=0}, \\
& \left.\frac{\partial\psi(\eta; q)}{\partial\eta}\right|_{\eta\to\infty} \to 0, \quad \varphi(\infty; q) \to 0, \\
\varphi(0; q) &= -n \left.\frac{\partial^2\psi(\eta; q)}{\partial\eta^2}\right|_{\eta=0}, \quad \left.\frac{\partial\Phi(\eta; q)}{\partial\eta}\right|_{\eta=0} = -\delta(1 + \Phi(0; q)), \\
& \Phi(\infty; q) \to 0, \quad \Psi(0; q) = 1, \quad \Psi(\infty; q) \to 0.
\end{aligned}\right\} \tag{6.21}$$

It is obvious to show that the solutions of Equation (6.20) subject to Equation (6.21) when $q = 0$ are

$$\left.\begin{aligned}
\psi(\eta; 0) &= f_0(\eta), \\
\varphi(\eta; 0) &= h_0(\eta), \\
\Phi(\eta; 0) &= \theta_0(\eta), \\
\Psi(\eta; 0) &= \phi_0(\eta).
\end{aligned}\right\} \tag{6.22}$$

Since $\hbar \neq 0$ and $H(\eta) \neq 0$, Equation (6.20) and Equation (6.21) are then equivalent to the Equations (6.7)–(6.10) with boundary conditions in Equation (6.11) at $q = 1$. We obtain

$$\left.\begin{aligned}
\psi(\eta; 1) &= f(\eta), \\
\varphi(\eta; 1) &= h(\eta), \\
\Phi(\eta; 1) &= \theta(\eta), \\
\Psi(\eta; 1) &= \phi(\eta).
\end{aligned}\right\} \tag{6.23}$$

By Taylor's theorem, $\psi(\eta; q)$, $\varphi(\eta; q)$, $\Phi(\eta; q)$ and $\Psi(\eta; q)$ can be expressed in the power series of q as follows:

$$\left.\begin{aligned}
\psi(\eta;q) &= f_0(\eta) + \sum_{p=1}^{\infty} f_p(\eta)q^p, \\
\varphi(\eta;q) &= h_0(\eta) + \sum_{p=1}^{\infty} h_p(\eta)q^p, \\
\Phi(\eta;q) &= \theta_0(\eta) + \sum_{p=1}^{\infty} \theta_p(\eta)q^p, \\
\Psi(\eta;q) &= \phi_0(\eta) + \sum_{p=1}^{\infty} \phi_p(\eta)q^p,
\end{aligned}\right\} \tag{6.24}$$

in which

$$\left.\begin{aligned}
f_p(\eta) &= \frac{1}{p!}\frac{\partial^p \psi(\eta,q)}{\partial q^p}\bigg|_{q=0}, \quad h_p(\eta) = \frac{1}{p!}\frac{\partial^p \varphi(\eta,q)}{\partial q^p}\bigg|_{q=0}, \\
\theta_p(\eta) &= \frac{1}{p!}\frac{\partial^p \Phi(\eta,q)}{\partial q^p}\bigg|_{q=0}, \quad \phi_p(\eta) = \frac{1}{p!}\frac{\partial^p \Psi(\eta,q)}{\partial q^p}\bigg|_{q=0}.
\end{aligned}\right\}$$

Here, it is assumed that $\hbar$ and $H(\eta)$ are properly chosen in a way that the series solutions converge at $q = 1$. Therefore,

$$\left.\begin{aligned}
f(\eta) &= f_0(\eta) + \sum_{p=1}^{\infty} f_p(\eta), \\
h(\eta) &= h_0(\eta) + \sum_{p=1}^{\infty} h_p(\eta), \\
\theta(\eta) &= \theta_0(\eta) + \sum_{p=1}^{\infty} \theta_p(\eta), \\
\phi(\eta) &= \phi_0(\eta) + \sum_{p=1}^{\infty} \phi_p(\eta).
\end{aligned}\right\} \tag{6.25}$$

6.2.2 High-order Deformation Equation

In regard to get the higher order deformation equations, the set of solutions is defined by

$$\left.\begin{aligned}
f_n &= \{f_0(\eta), f_1(\eta), f_2(\eta), \cdots, f_n(\eta)\}, \\
h_n &= \{h_0(\eta), h_1(\eta), h_2(\eta), \cdots, h_n(\eta)\}, \\
\theta_n &= \{\theta_0(\eta), \theta_1(\eta), \theta_2(\eta), \cdots, \theta_n(\eta)\}, \\
\phi_n &= \{\phi_0(\eta), \phi_1(\eta), \phi_2(\eta), \cdots, \phi_n(\eta)\}.
\end{aligned}\right\} \tag{6.26}$$

Differentiating the zero-order deformation equations Equation (6.20) p-times with respect to q, for $q = 0$, and dividing by $p!$, yield the pth–order deformation equations in the following form:

$$\left.\begin{array}{l}\mathcal{L}_f\left[f_p(\eta) - \mathcal{X}_p f_{p-1}(\eta)\right] = \hbar_f H_f(\eta)\mathfrak{R}_p^f(f_{p-1}(\eta), h_{p-1}(\eta), \theta_{p-1}(\eta), \phi_{p-1}(\eta)), \\ \mathcal{L}_h\left[h_p(\eta) - \mathcal{X}_p h_{p-1}(\eta)\right] = \hbar_h H_h(\eta)\mathfrak{R}_p^h(f_{p-1}(\eta), h_{p-1}(\eta), \theta_{p-1}(\eta), \phi_{p-1}(\eta)), \\ \mathcal{L}_\theta\left[\theta_p(\eta) - \mathcal{X}_p \theta_{p-1}(\eta)\right] = \hbar_\theta H_\theta(\eta)\mathfrak{R}_p^\theta(f_{p-1}(\eta), h_{p-1}(\eta), \theta_{p-1}(\eta), \phi_{p-1}(\eta)), \\ \mathcal{L}_\phi\left[\phi_p(\eta) - \mathcal{X}_p \phi_{p-1}(\eta)\right] = \hbar_\phi H_\phi(\eta)\mathfrak{R}_p^\phi(f_{p-1}(\eta), h_{p-1}(\eta), \theta_{p-1}(\eta), \phi_{p-1}(\eta))\end{array}\right\} \tag{6.27}$$

with the associated boundary conditions at $\eta = 0$ and $\eta \to \infty$ as follows:

$$\left.\begin{array}{l}f_p(0) = f_w; \ f_p'(0) = s + \alpha f_p''(0) + \beta f_p'''(0); \ h_p(0) = -n f_p''(0); \\ \theta_p'(0) = -\delta(1 + \theta_p(0)); \ \phi_p(0) = 1, \\ f_p'(\infty) \to 0; \ h_p(\infty) \to 0; \ \theta_p(\infty) \to 0; \ \phi_p(\infty) \to 0,\end{array}\right\} \tag{6.28}$$

where

$$\mathcal{X}_p = \begin{cases} 0 \text{ for } p \leq 1, \\ 1 \text{ for } p > 1, \end{cases}$$

$$\mathfrak{R}_p^f(f_{p-1}(\eta), h_{p-1}(\eta), \theta_{p-1}(\eta), \phi_{p-1}(\eta)) = (1 + K)f_{p-1}'''(\eta) + \sum_{i=0}^{p-1} f_i(\eta)f_{p-1-i}''(\eta)$$

$$- \sum_{i=0}^{p-1} f_i'(\eta)f_{p-1-i}'(\eta) + K h_{p-1}'(\eta) + \lambda\theta_{p-1}(\eta) + \lambda\Lambda\phi_{p-1}(\eta),$$

$$\mathfrak{R}_p^h(f_{p-1}(\eta), h_{p-1}(\eta), \theta_{p-1}(\eta), \phi_{p-1}(\eta)) = (1 + K/2)h_{p-1}''(\eta) + \sum_{i=0}^{p-1} f_i(\eta)h_{p-1-i}'(\eta)$$

$$- \sum_{i=0}^{p-1} f_i'(\eta)h_{p-1-i}(\eta) - K\left(2h_{p-1}(\eta) + f_{p-1}''(\eta)\right),$$

$$\mathfrak{R}_p^\theta(f_{p-1}(\eta), h_{p-1}(\eta), \theta_{p-1}(\eta), \phi_{p-1}(\eta)) = \theta_{p-1}''(\eta) + Pr\sum_{i=0}^{p-1} f_i(\eta)\theta_{p-1-i}'(\eta) \text{ and}$$

$$\mathfrak{R}_p^\phi(f_{p-1}(\eta), h_{p-1}(\eta), \theta_{p-1}(\eta), \phi_{p-1}(\eta)) = \phi_{p-1}''(\eta) + Sc\sum_{i=0}^{p-1} f_i(\eta)\phi_{p-1-i}'(\eta) -$$

$$Sc\, C_m\phi_{p-1}(\eta).$$

For the sack of simplicity, auxiliary parameters and auxiliary functions are chosen as $\hbar_f = \hbar_g = \hbar_h = \hbar_\theta = \hbar$ and $H_f(\eta) = H_g(\eta) = H_h(\eta) = H_\theta(\eta) = 1$. Then, from Equation (6.27), the general solutions are

$$
\left.\begin{array}{l}
f_p(\eta) = f_p^*(\eta) + X_1 + X_2 e^{\eta} + X_3 e^{-\eta}, \\[4pt]
h_p(\eta) = h_p^*(\eta) + X_4 + X_5 e^{-\eta}, \\[4pt]
\theta_p(\eta) = \theta_p^*(\eta) + X_6 + X_7 e^{-\eta}, \\[4pt]
\phi_p(\eta) = \phi_p^*(\eta) + X_8 + X_9 e^{-\eta},
\end{array}\right\} \tag{6.29}
$$

where $f_p^*(\eta), h_p^*(\eta),\ \theta_p^*(\eta),$ and $\phi_p^*(\eta)$ are particular solutions, and $X_i (i = 1 - 9)$ are constants which can be evaluated by using Equation (6.28).

6.2.3 Region of Convergence

In Homotopy analysis method, the value of the convergence control parameter $(\hbar)$ has an important role on the convergence and the rate of the approximation of the series solution.
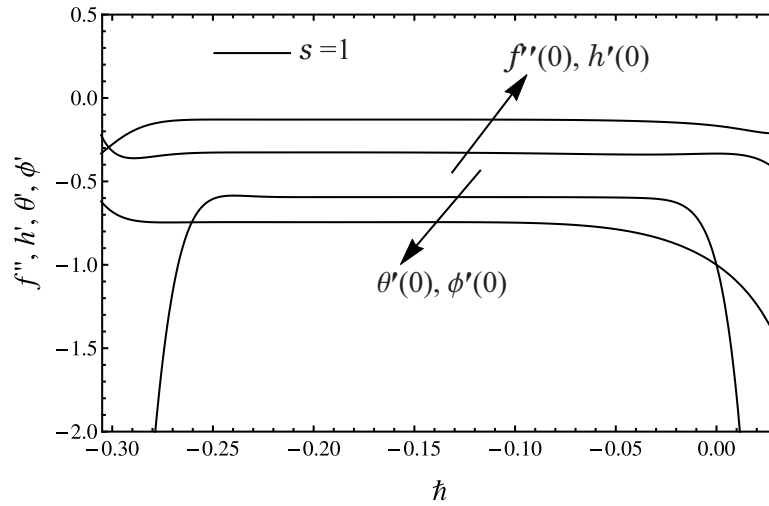
Figure 6.2: $\hbar$ curves for $s = 1$

This value is chosen from the so-called $\hbar-$curves which are normally considered parallel to the horizontal axis. Figures 6.2–6.3 are computed at $20^{th}-$order of iterations HAM series solution by using $K = \lambda = \Lambda = Sc = C_m = f_w = n = \delta = 0.5,\ \alpha = 1,\ \beta = -1,\ Pr = 5$ for stretching $(s = 1)$ and shrinking $(s = -1)$ sheets respectively. The admissible ranges of $\hbar-$values for stretching sheet are $-0.3 \leq \hbar_f, \hbar_h, \hbar_\phi < 0$ and $-0.25 \leq \hbar_\theta < 0$. When sheet shrinks, the ranges are considered as $-0.42 \leq \hbar_f < 0$ and $-0.3 \leq \hbar_h, \hbar_\theta, \hbar_\phi < 0$. These values of $\hbar-$ are chosen to validate the HAM series solutions and to analyse impacts of the pertinent parameters on the fluid flow in sections 6.4.
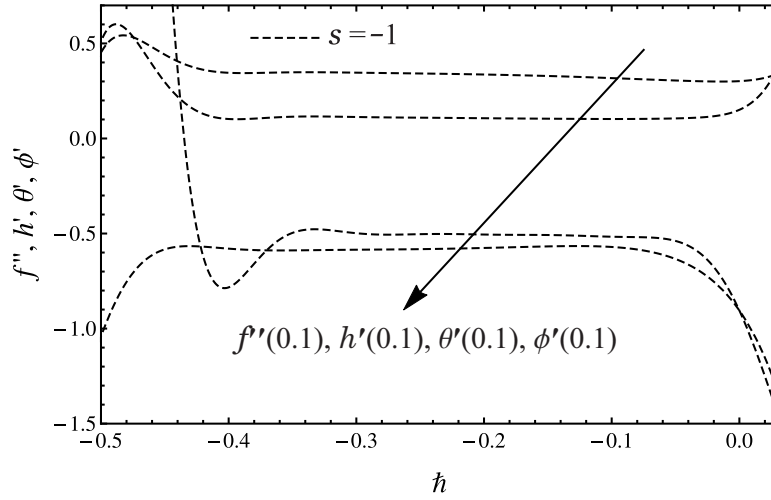
Figure 6.3: $\hbar$ curves for $s = -1$

6.3 Study Validation

The accuracy of the presented study is validated with the following two ways.

6.3.1 Approximation Analysis

To check the accuracy of the proposed solution in the form of the combination of polynomial and exponential functions, we generate the results and compared with those obtained by using the solution set of the exponential functions which is defined as follows:

$$
\left.
\begin{aligned}
f(\eta) &= \sum_{r=0}^{\infty} \sum_{i=0}^{\infty} a_{r,i} e^{-i\eta}, \\
h(\eta) &= \sum_{r=0}^{\infty} \sum_{i=0}^{\infty} b_{r,i} e^{-i\eta}, \\
\theta(\eta) &= \sum_{r=0}^{\infty} \sum_{i=0}^{\infty} c_{r,i} e^{-i\eta}, \\
\phi(\eta) &= \sum_{r=0}^{\infty} \sum_{i=0}^{\infty} d_{r,i} e^{-i\eta},
\end{aligned}
\right\}
\tag{6.30}
$$

with the properly chosen so-called auxiliary function as $H_f(\eta) = H_g(\eta) = H_h(\eta) = H_\theta(\eta) = H(\eta) = e^{-\eta}$. Using the same parametric values as used in the Figure 6.24 for $\alpha = s = 1$, Figure 6.4 compared the squared residual error of the obtained solutions in the form of the exponential function (Equation (6.30)) and the combination of polynomial and exponential functions (Equation (6.16)). This analysis yields that the solution expression consists on a combination of the

polynomial and exponential expression, i.e. $H(\eta) = 1$ for Equation (6.16), produces a lower squared residual error as compared to the merely exponential expression, i.e. $H(\eta) = e^{-\eta}$ for Equation (6.30). It is also noted that our proposed solution in the form of the combination of polynomial and exponential functions give lower squared residual error and takes less computation time and converges quickly as compared to the merely exponential function. Hence in the following section 6.5, the presented results are based on the $H(\eta) = 1$.
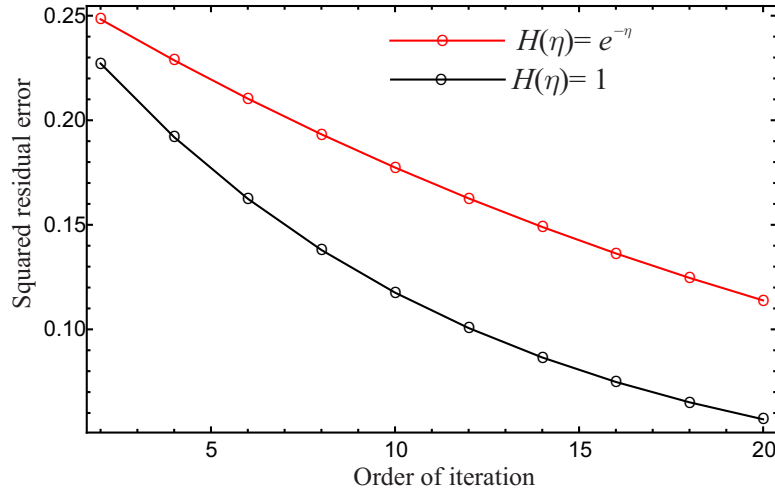
Figure 6.4: Choice of auxiliary function $H(\eta)$

6.3.2   Model Validation

The validation of the current model is carried out in two special ways. Firstly, the present HAM results are compared with exact analytical results of Fang *et al.*'s work [79] and numerical results presented by Rosca and Pop [84] for the micropolar fluid flow over a permeable shrinking sheet with the second order slip flow model. It is observed that our results have an excellent agreement with already published results as tabulated in Table 6.1.

Table 6.1: Current study validation with exact and numerical results.

			[79]	[84]	Present	
f_w	α	$-\beta$	$-f''(0)$	$-f''(0)$	$-f''(0)$	$-\hbar$
2.0	0.5	1	0.341213	0.3412	0.341214	0.20629
2.0	0.5	2	0.203824	0.2038	0.203825	0.3074
2.0	1.0	1	0.290548	0.2905	0.29054	0.2068
2.0	1.0	2	0.184657	0.1846	0.184657	0.31136
3.0	0.5	1	0.262681	0.2627	0.262681	0.209816
3.0	0.5	2	0.147012	0.1470	0.147012	0.273175
3.0	1.0	1	0.232017	0.2320	0.232014	0.2132
3.0	1.0	2	0.136905	0.1369	0.136905	0.27912

Secondly, the accuracy of the HAM results is also assessed numerically with the help of the three-stage Lobatto IIIA method (please see [84] and references therein). This numerical technique is considered to be very good in the higher order of accuracy for the boundary value problems. For this purpose, the MATLAB generated code bvp4c is used which is based on the three-stage collocation at Lobatto points. Furthermore, solved examples and helping material related to bvp4c can be found in the book of the Shampine *et al.* [113] and online tutorials by Shampine *et al.* [114]. For this validation, we choose the maximum value of η to be 10 and the same parametric values are used as for Figures 6.2–6.3 and $\hbar = -0.12, -0.1, -0.1, -0.05$, and $\hbar = -0.402, -0.08, -0.075, -0.07$ are adjusted for velocity component (f'), micro-rotational velocity (h), temperature (θ) and concentration (ϕ) profiles in Figure 6.5 and Figure 6.6, respectively.
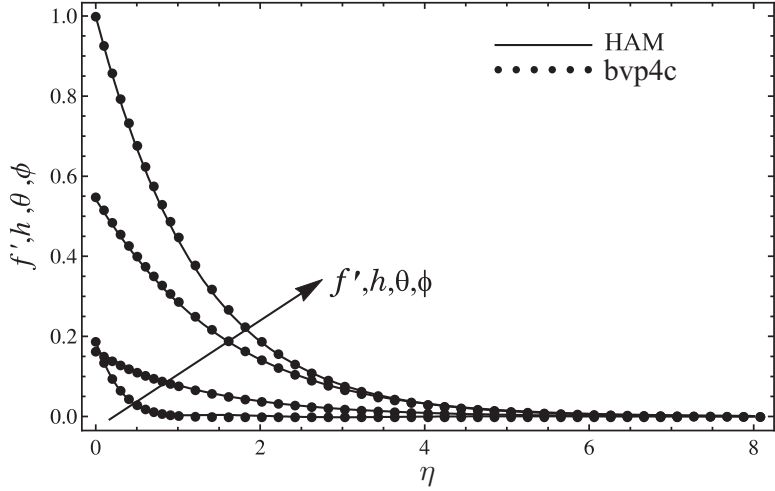

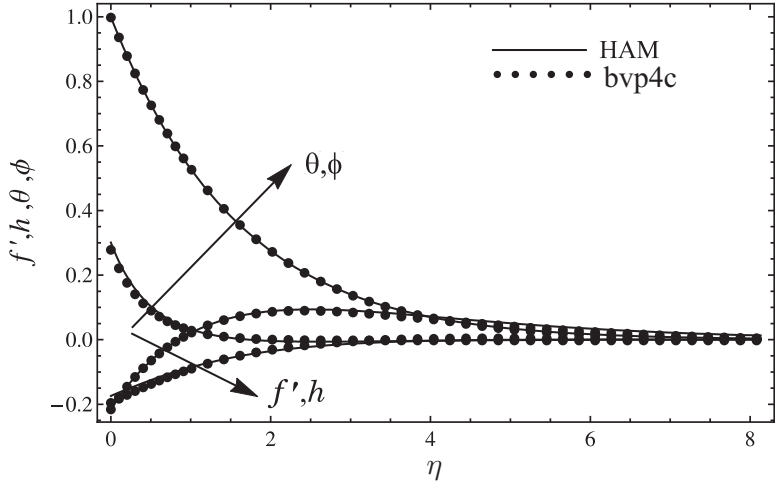**Figure 6.5:** comparison with bvp4c for $s = 1$

Figure 6.6: comparison with bvp4c for $s = -1$

6.4 Results and Discussion

A mathematical model of the heat and mass transfer micropolar fluid flow over a stretching/shrinking sheet with slip flow model has been formulated, solved and validated in the preceding sections. Now, in this section, the asymptomatic analysis is carried out from the obtained results. The influences of the governing parameters such as material parameter (K), buoyancy parameter (λ), concentration to thermal buoyancy ratio parameter (Λ), Prandtl number (Pr), Schmidt number (Sc), chemical reaction parameter (C_m), suction/injection parameter (f_w), first and second order slip flow parameters (α, β), and the Newtonian heating parameters (δ) along with the physical quantities, i.e., local skin friction coefficient, local wall couple stress, local Nusselt number and the local Sherwood number are reported with the help of graphical and tabular illustrations. It is to be noted that all of the presented results are computed at fixed values of the pertaining parameters which are used to calculate the $\hbar-$curves otherwise stated with description.
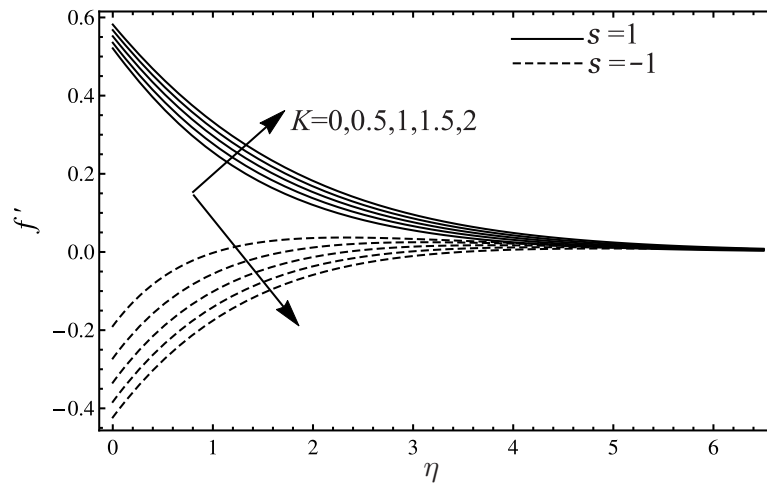
Figure 6.7: Impact of K on f'

Figures 6.7–6.10 depict the influence of the material parameter on the velocity component, the microrotation velocity, temperature and concentration profiles with the increasing values of the η for $\hbar = -0.1, -0.01, -0.01$ and -0.2, respectively. It is observed that when the concentration of micro-particles increases, the corresponding velocities increase and temperature and concentration profiles decrease for $s = 1$ and and a reverse trend is observed for $s = -1$. In Figure 6.7 as the material parameter increases from 0 to 2, it is observed that the boundary layer thickness increases the 0.06 unit for the stretching case and it decreases 0.23 unit for the shrinking case at $\eta = 0$. However, there is a small change in Figure 6.8 as the similarity variable η moves away from the stretching/shrinking permeable sheet. All the physical quantities increase with the increasing values of the K as tabulated in Table 6.2, while a reverse pattern is observed in Table 6.3.
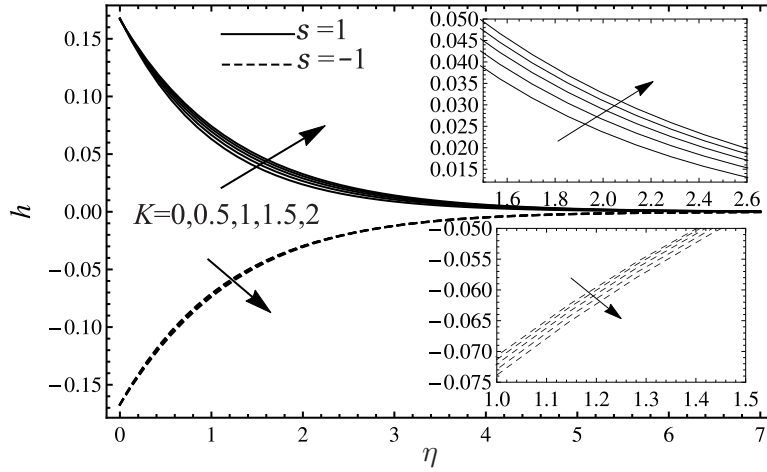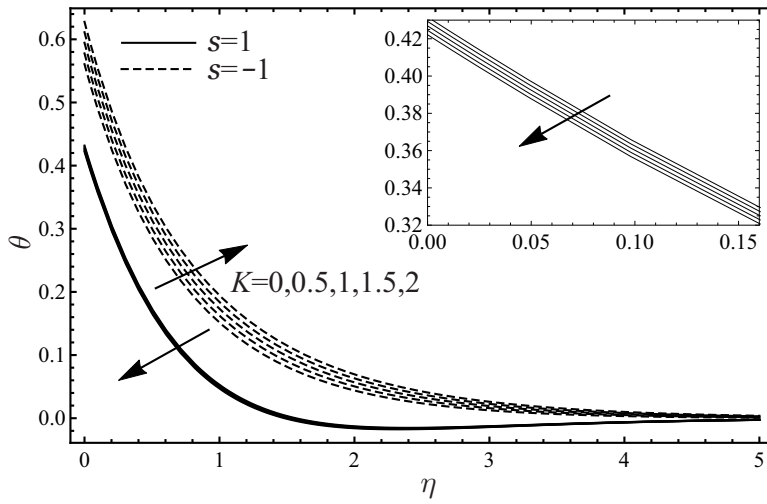
Figure 6.8: Impact of K on h

Figure 6.9: Impact of K on θ

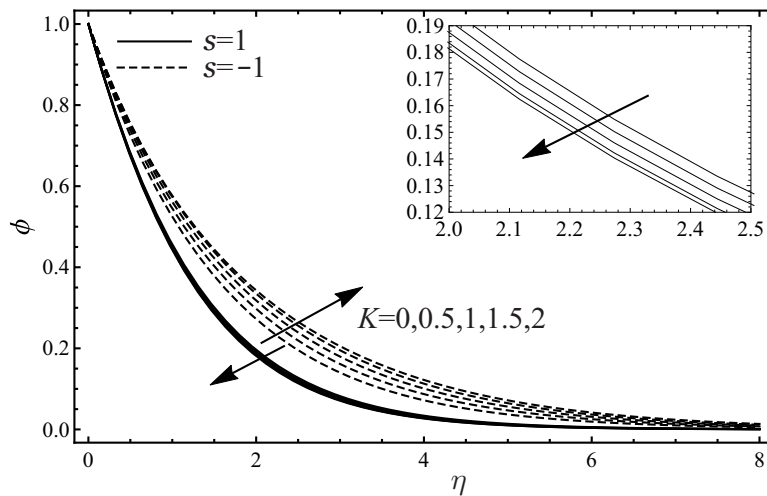**Figure 6.10:** Impact of K on ϕ

Table 6.2: Influences of K, Λ, Sc, C_m, f_w on physical quantities for $s = 1$.

K	Λ	Sc	C_m	f_w	$C_{f_x}Re_x^{\frac{1}{2}}$	$-\hbar$	M_xRe_x	$-\hbar$	$Nu_xRe_x^{-\frac{1}{2}}$	$-\hbar$	$Sh_xRe_x^{-\frac{1}{2}}$	$-\hbar$
0.0	1	0.5	0.5	0.5	0.34372	0.1	0.16424	0.01	1.65823	0.01	0.74187	0.1
0.5					0.41359	0.1	0.19393	0.01	1.66467	0.01	0.74720	0.1
1.0					0.48229	0.1	0.22104	0.01	1.67119	0.01	0.75252	0.1
1.5					0.54884	0.1	0.24601	0.01	1.67776	0.01	0.75755	0.1
2.0					0.61307	0.1	0.26913	0.01	1.68437	0.01	0.76223	0.1
0.5	0.5				0.41893	0.01	0.19393	0.01	1.66467	0.01	0.92833	0.01
	1.0				0.41839	0.01	0.19313	0.01	1.68613	0.01	0.92911	0.01
	1.5				0.41786	0.01	0.19234	0.01	1.70818	0.01	0.92990	0.01
	2.0				0.41735	0.01	0.19156	0.01	1.73086	0.01	0.93068	0.01
		0.5	0.5		0.41359	0.1	0.16243	0.1	1.66467	0.01	0.74720	0.1
		1.0			0.43197	0.1	0.16996	0.1	1.66426	0.01	1.14879	0.1
		1.5			0.44311	0.1	0.17491	0.1	1.66387	0.01	1.48886	0.1
		2.0			0.45072	0.1	0.17851	0.1	1.66351	0.01	1.80004	0.1
			0.5	0.0	0.40141	0.1	0.15757	0.1	1.66510	0.01	0.12158	0.1
				0.5	0.41359	0.1	0.16243	0.1	1.66467	0.01	0.74720	0.1
				1.0	0.42165	0.1	0.16570	0.1	1.66426	0.01	1.14879	0.1
				1.5	0.42749	0.1	0.16813	0.1	1.66387	0.01	1.48886	0.1
				2.0	0.43199	0.1	0.17005	0.1	1.66351	0.01	1.80004	0.1
			0.5	1.0	0.42098	0.01	0.21229	0.01	1.74435	0.005	0.79984	0.01
				0.5	0.41893	0.01	0.19393	0.01	1.28438	0.005	0.84223	0.01
				0.0	0.41474	0.01	0.17462	0.01	0.99266	0.005	0.88512	0.01
				−0.5	0.40670	0.01	0.15356	0.01	0.80963	0.005	0.92833	0.01
				−1.0	0.39155	0.01	0.12924	0.01	0.69529	0.005	0.97176	0.01

**Table 6.3:** Influences of K, Λ, Sc, C_m, f_w on physical quantities for $s = -1$.

K	Λ	Sc	C_m	f_w	$-C_{f_x}Re_x^{\frac{1}{2}}$	$-\hbar$	$-M_xRe_x$	$-\hbar$	$Nu_xRe_x^{-\frac{1}{2}}$	$-\hbar$	$Sh_xRe_x^{-\frac{1}{2}}$	$-\hbar$
0.0	1	0.5	0.5	0.5	0.34555	0.1	0.14216	0.01	1.16213	0.01	0.62335	0.1
0.5					0.44139	0.1	0.17418	0.01	1.15765	0.01	0.60786	0.1
1.0					0.52961	0.1	0.20460	0.01	1.15325	0.01	0.59459	0.1
1.5					0.61123	0.1	0.23340	0.01	1.14894	0.01	0.58271	0.1
2.0					0.68733	0.1	0.26061	0.01	1.14471	0.01	0.57201	0.1
0.5	0.5				0.41762	0.01	0.13602	0.05	1.15765	0.01	0.89720	0.01
	1.0				0.41868	0.01	0.16634	0.05	1.17042	0.01	0.89805	0.01
	1.5				0.41973	0.01	0.19554	0.05	1.18359	0.01	0.89889	0.01
	2.0				0.42076	0.01	0.22362	0.05	1.19716	0.01	0.89973	0.01
		0.5	0.5		0.44139	0.1	0.12969	0.1	1.15765	0.01	0.60786	0.1
		1.0			0.42396	0.1	0.12033	0.1	1.15751	0.01	0.93273	0.1
		1.5			0.41219	0.1	0.11377	0.1	1.15738	0.01	1.20634	0.1
		2.0			0.40347	0.1	0.10875	0.1	1.15726	0.01	1.45798	0.1
			0.5	0.0	0.46038	0.1	0.13961	0.1	1.15779	0.01	0.12158	0.1
				0.5	0.44139	0.1	0.12969	0.1	1.15765	0.01	0.60786	0.1
				1.0	0.42943	0.1	0.12334	0.1	1.15751	0.01	0.93273	0.1
				1.5	0.42108	0.1	0.11881	0.1	1.15738	0.01	1.20634	0.1
				2.0	0.41480	0.1	0.11534	0.1	1.15726	0.01	1.45798	0.1
			0.5	1.0	0.41430	0.01	0.20809	0.0001	1.43749	0.005	0.76556	0.01
				0.5	0.41762	0.01	0.20788	0.0001	1.07259	0.005	0.80881	0.01
				0.0	0.42409	0.01	0.20768	0.0001	0.85196	0.005	0.85279	0.01
				−0.5	0.43690	0.01	0.20747	0.0001	0.71811	0.005	0.89720	0.01
				−1.0	0.46203	0.01	0.20726	0.0001	0.63638	0.005	0.94189	0.01

The impact of the buoyancy parameter (λ) on the prescribed velocities (f' and h), temperature and concentration profiles in plotted in . The increasing behaviour of λ leads to enhance the prescribed velocities and reduces the thermal and concentration boundary layer thicknesses for $s = 1$ and -1. Fig-

ures 6.11–6.14 are computed at $\{\hbar = -0.01,\ \hbar = -0.01\}$; $\{\hbar = -0.1,\ \hbar = -0.03\}$; $\{\hbar = -0.01,\ \hbar = -0.01\}$ and $\{\hbar = -0.2$ and $\lambda = 2$ at $\hbar = -0.198,\ \hbar = -0.1\}$ for $\{s = 1,\ s = -1\}$, respectively. Table 6.4 shows that an increase in the buoyancy parameter (λ) for stretching sheet leads an increase in all of the physical quantities. On the other hand in Table 6.5 for shrinking sheet, it reduces the local skin friction and local wall couple stress and raises the local Nusselt and Sherwood number.

The effect of the concentration to thermal buoyancy ratio (Λ) parameter is illustrated in Figures 6.15–6.18. When the sheet stretches or shrinks, the increase in the Λ causes to exert a force to raise the velocity component and microrotational velocity of the micropolar fluid flow. On the other hand, temperature and concentration profiles decrease with the increasing value of the Λ. Moreover, Figure 6.17 shows that shrinking sheet has higher thermal boundary layer thickness as compared to the stretching sheet. It is to be noted that Figures 6.15–6.18 are computed at $\{\hbar = -0.01,\ \hbar = -0.01\}$; $\{\hbar = -0.1,\ \hbar = -0.03\}$; $\{\hbar = -0.1,\ \hbar = -0.1\}$ and $\{\hbar = -0.01,\ \hbar = -0.01\}$ for $\{s = 1,\ s = -1\}$, respectively. When sheet stretches or shrinks, increasing values of concentration to thermal buoyancy ratio (Λ) causes to decrease the local skin friction and the local wall couple stress while it raises the heat and mass transfer rate as shown in the Tables 6.2–6.3.
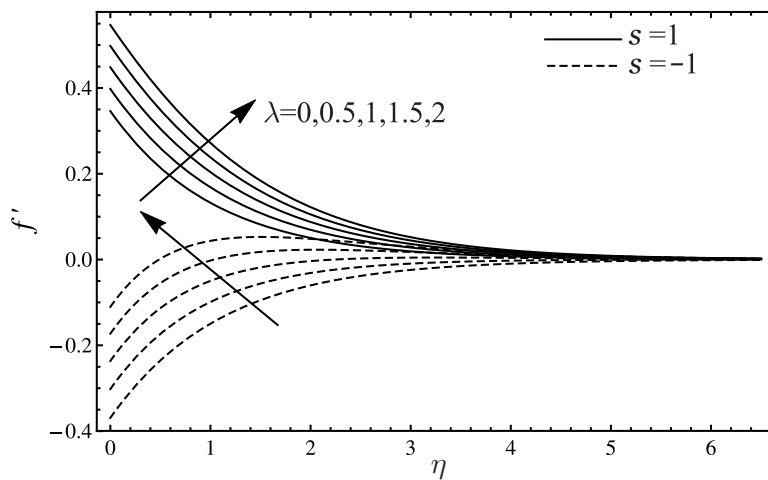

Figure 6.11: Impact of λ on f'

Various values of Pr are chosen to investigate it's influence on the thermal boundary layer thickness. The results as shown in Figure 6.19 using $\hbar = -0.01, -0.01, -0.01, -0.001, -0.001, -0.001, -0.0006, -0.0004, -0.0001$ are used for stretching case and $\hbar = -0.009, -0.007 - 0.005, -0.0001, -0.001, -0.001, -0.00 06, -0.0004, -0.0001$ corresponding to the increasing values of the Pr indicate that increasing values of the Pr, an increase in the momentum diffusivity, causes to reduce the fluid temperature for $s = 1, -1$. It is also observed that stretching sheet yields a wider thickness of the thermal boundary as compared to the shrinking of the sheet. All the physical quantities increase with the increasing values of
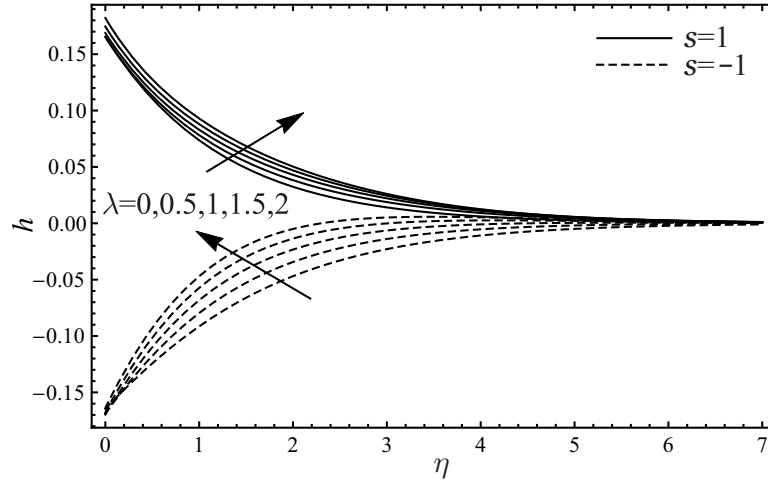
Figure 6.12: Impact of λ on h
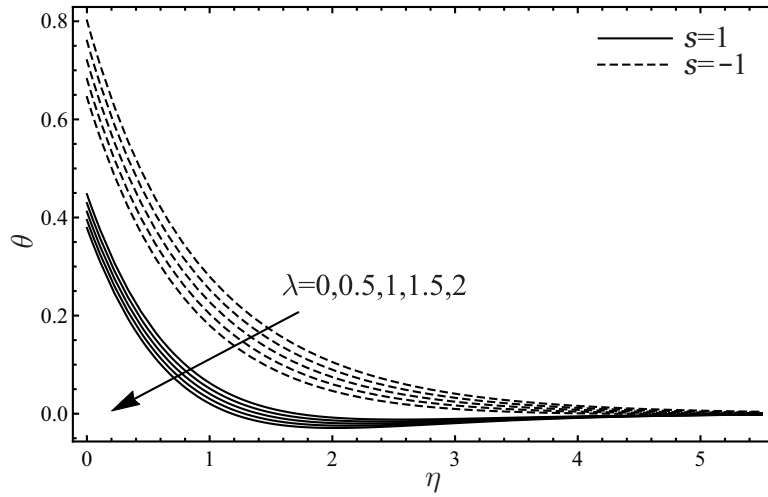
Figure 6.13: Impact of λ on θ
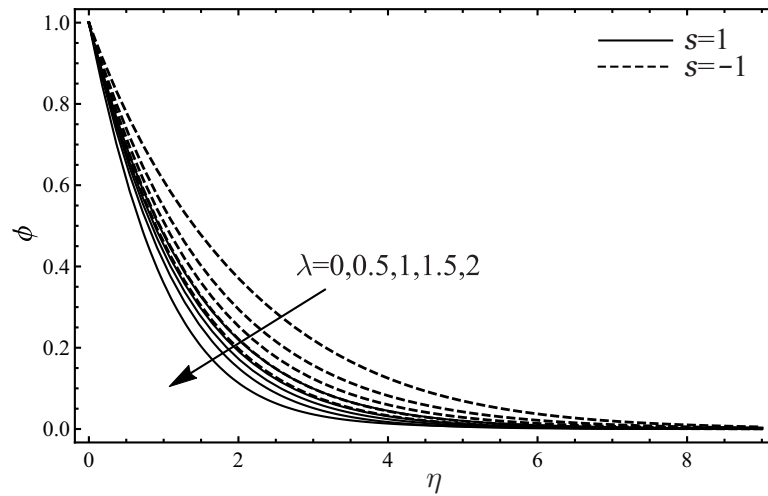
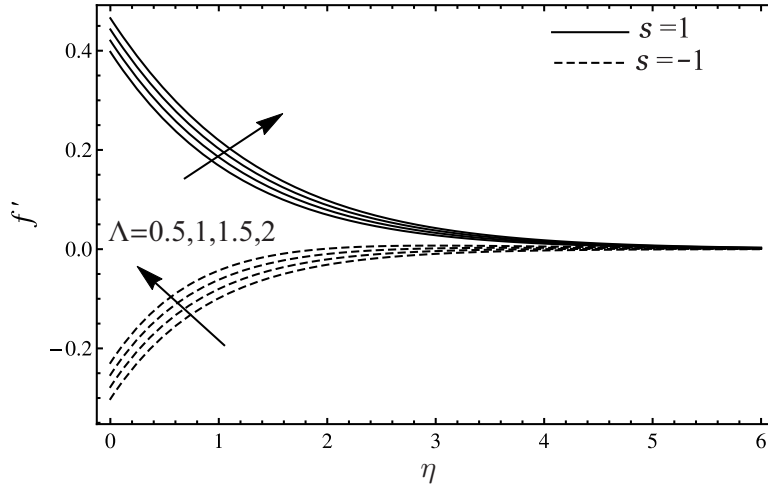**Figure 6.14:** Impact of λ on ϕ
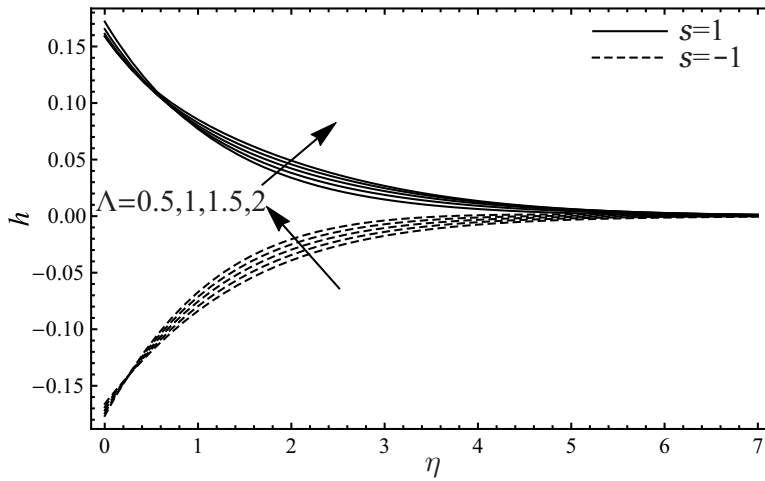
Figure 6.15: Impact of Λ on f'

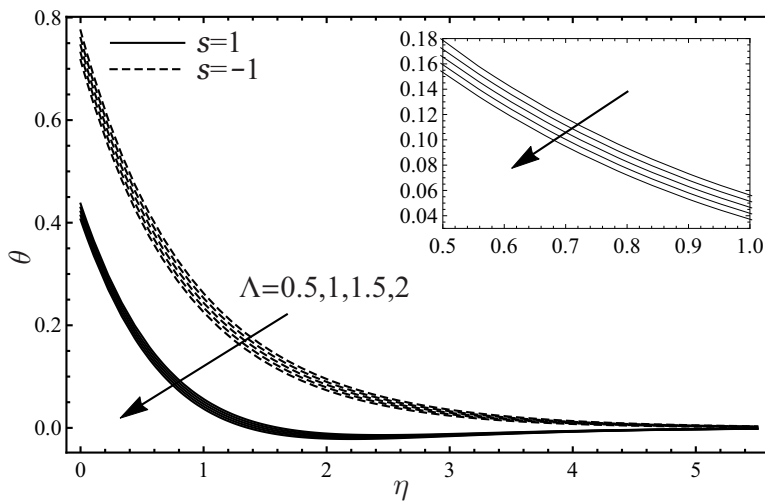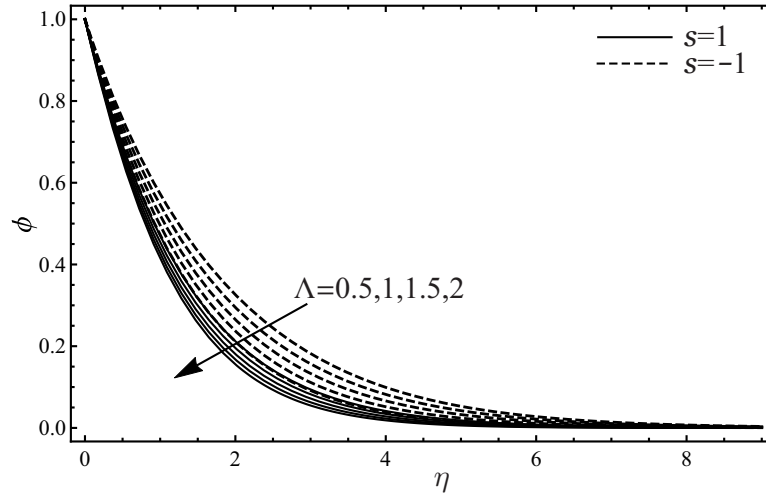

Figure 6.16: Impact of Λ on h

Figure 6.17: Impact of Λ on θ

Figure 6.18: Impact of Λ on ϕ

the Pr in Tables 6.4–6.5 , expect for shrinking case, only local wall couple stress decreases.

Table 6.4: Influences of $\delta, \Lambda, Pr, \alpha, \beta$ on physical quantities for $s = 1$.

δ	λ	Pr	α	β	$C_{f_x}Re_x^{\frac{1}{2}}$	$-\hbar$	M_xRe_x	$-\hbar$	$Nu_xRe_x^{-\frac{1}{2}}$	$-\hbar$	$Sh_xRe_x^{-\frac{1}{2}}$	$-\hbar$
0.1	1	5	1	−1	0.39841	0.1	0.15604	0.1	1.53027	0.01	0.74318	0.1
0.2					0.40183	0.1	0.15745	0.1	1.54900	0.01	0.74412	0.1
0.3					0.40548	0.1	0.15898	0.1	1.57427	0.01	0.74510	0.1
0.4					0.40939	0.1	0.16063	0.1	1.61012	0.01	0.74612	0.1
0.5					0.41359	0.1	0.16243	0.1	1.66467	0.01	0.74720	0.1
0.5	0.0				0.41662	0.01	0.19294	0.011	1.61716	0.01	0.92643	0.01
	0.5				0.41893	0.01	0.19393	0.01	1.66467	0.01	0.92833	0.01
	1.0				0.42153	0.01	0.19395	0.01	1.71431	0.01	0.93021	0.01
	1.5				0.42439	0.01	0.19412	0.01	1.76615	0.01	0.93206	0.01
	2.0				0.42752	0.01	0.19444	0.01	1.82027	0.01	0.93389	0.01
	0.5	0.1			0.41351	0.01	0.19079	0.01	0.85617	0.01	0.92901	0.01
		0.71			0.41454	0.01	0.19137	0.01	0.91631	0.01	0.99180	0.001
		1			0.41498	0.01	0.19162	0.01	0.94812	0.01	0.99834	0.0002
		5			0.41670	0.001	0.20663	0.001	1.04865	0.001	0.99917	0.0001
		10			0.41677	0.001	0.20666	0.001	1.12604	0.001	0.99992	0.00001
		20			0.41687	0.001	0.20672	0.001	1.31341	0.001	0.99993	0.000008
		50			0.41707	0.001	0.20739	0.0006	1.57190	0.0006	0.99995	0.000006
		100			0.41780	0.01	0.20772	0.0004	1.89454	0.0004	0.99997	0.000004
		500			0.42185	0.0031	0.20818	0.0001	2.31347	0.0001	0.99999	0.000001
		5	1		0.41359	0.1	0.16243	0.1	1.66467	0.1	0.74720	0.1
			2		0.30744	0.1	0.10655	0.1	1.59889	0.1	0.73576	0.1
			3		0.24458	0.1	0.07517	0.1	1.55928	0.1	0.72839	0.1
			1	−1	0.41893	0.01	0.19393	0.01	1.66467	0.01	0.92833	0.01
				−2	0.33515	0.01	0.15273	0.01	1.60962	0.01	0.92503	0.01
				−3	0.28467	0.01	0.12846	0.01	1.57586	0.01	0.92303	0.01

Figures 6.20–6.23 display the impact of the Schmidt number (Sc) on the velocity component, microrotational velocity, temperature profile and concentration of species. It is well known that dimensionless parameter Sc is a ratio of viscous diffusion rate to molecular diffusion rate. A decrease in the mass diffusion rate, i.e., an increase in the Sc leads to decrease the velocity component and the concentration profiles, and increase in the microrotational velocity and the

temperature profile. The plot (Figure 6.23) also shows that the stretching sheet reduces more concentration of the micropolar fluid flow in comparison with the shrinking sheet. These plots (Figures 6.20–6.23) are plotted at $\{\hbar = -0.05, \ \hbar = -0.05\}$; $\{\hbar = -0.1, \ \hbar = -0.1\}$; $\{\hbar = -0.01, \ \hbar = -0.01\}$ and $\{\hbar = -0.05, \ \hbar = -0.04\}$ for $\{s = 1, \ s = -1\}$, respectively. However, an increase in the Schmidt number yields a decrease in the heat transfer rate and an increase in all other physical quantities as shown in the Tables 6.2–6.3.
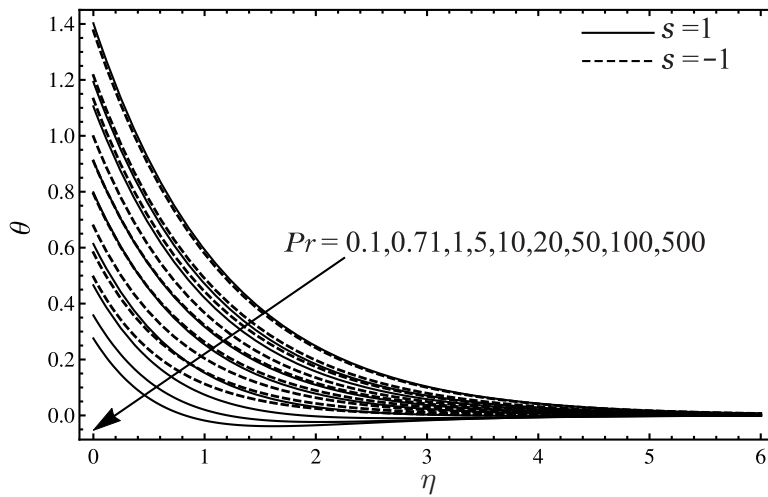

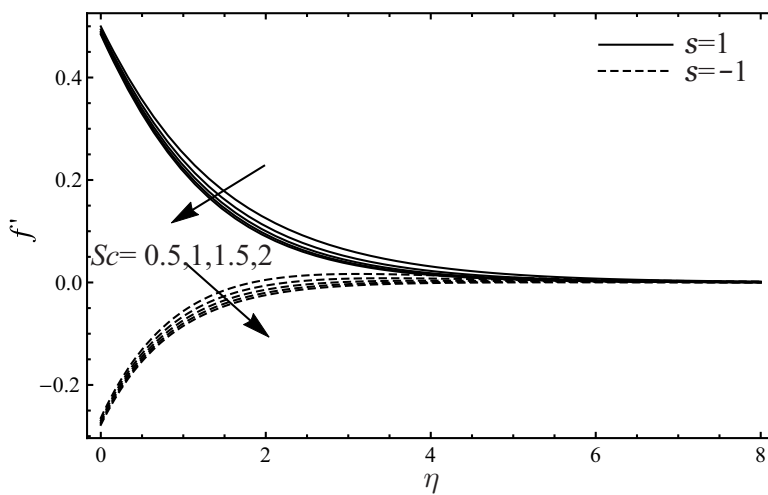**Figure 6.19:** Impact of Pr on θ

Figure 6.20: Impact of Sc on f'

The effects of first and second order slip flow parameters is illustrated in Figures 6.24–6.31 on the prescribed velocities, temperature and concentration profiles. When sheet stretches, an increase in the α and β cause to decrease in the prescribed velocities, and increase in the thermal boundary thickness and concentration spices. While in case of the shrinking sheet, a reverse trend is observed. An increase in the slip flow parameters enhances the tendency of the
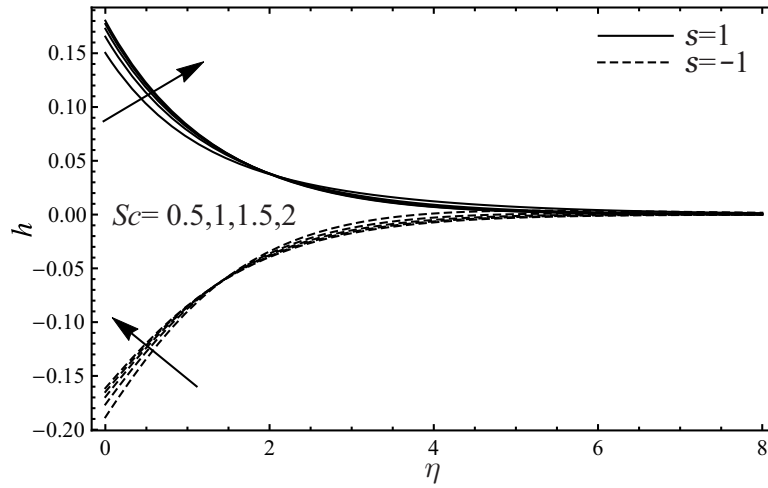
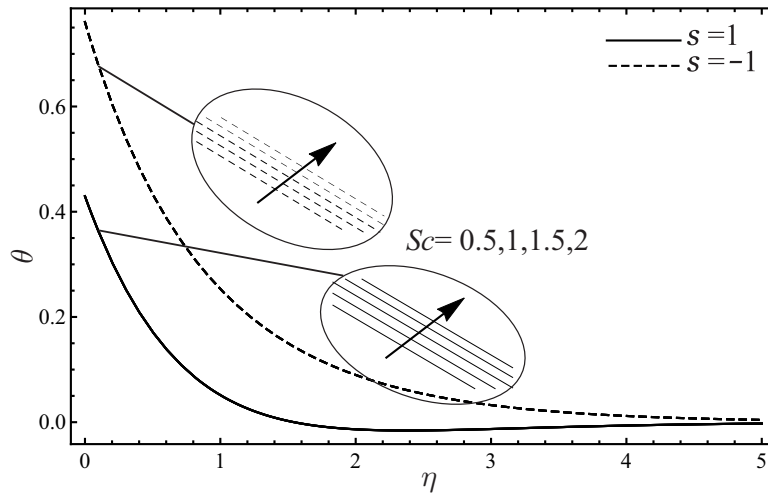**Figure 6.21:** Impact of Sc on h

Figure 6.22: Impact of Sc on θ

Figure 6.23: Impact of Sc on ϕ

Figure 6.24: Impact of α on f'

Figure 6.25: Impact of α on h
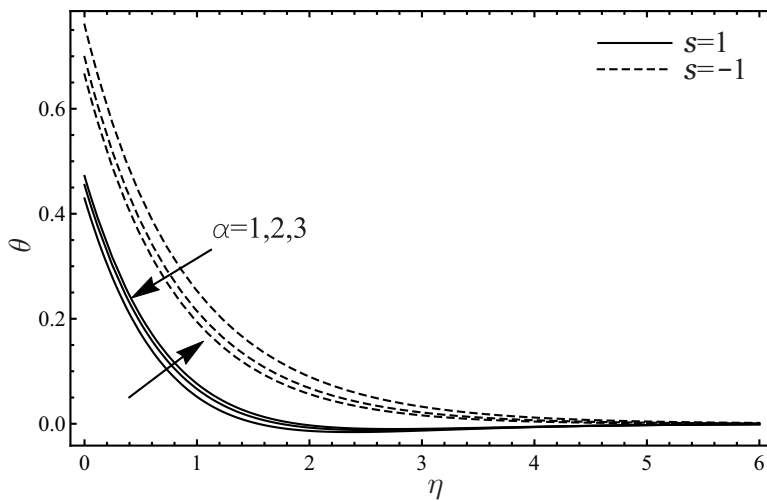
Figure 6.26: Impact of α on θ
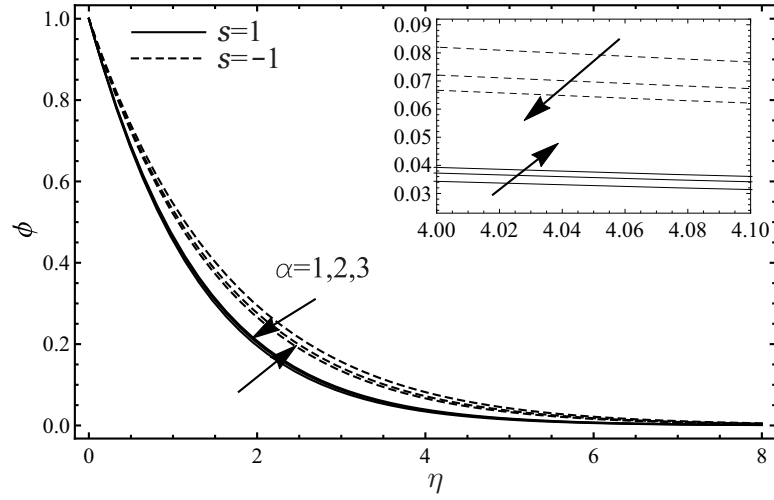
Figure 6.27: Impact of α on ϕ
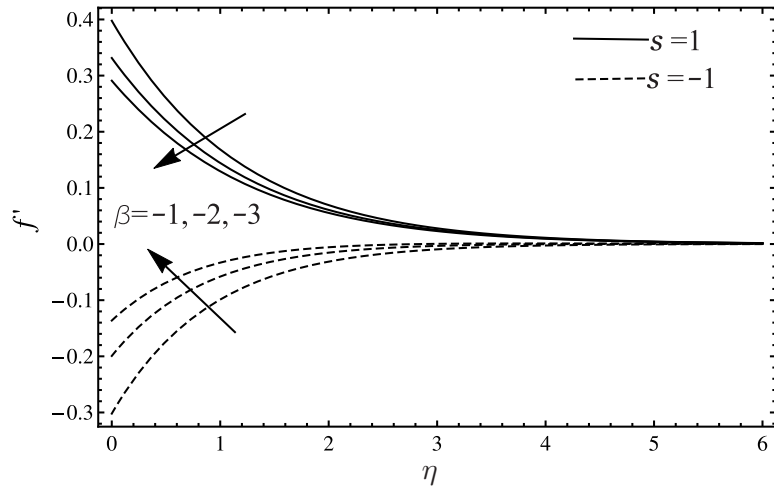
Figure 6.28: Impact of β on f'
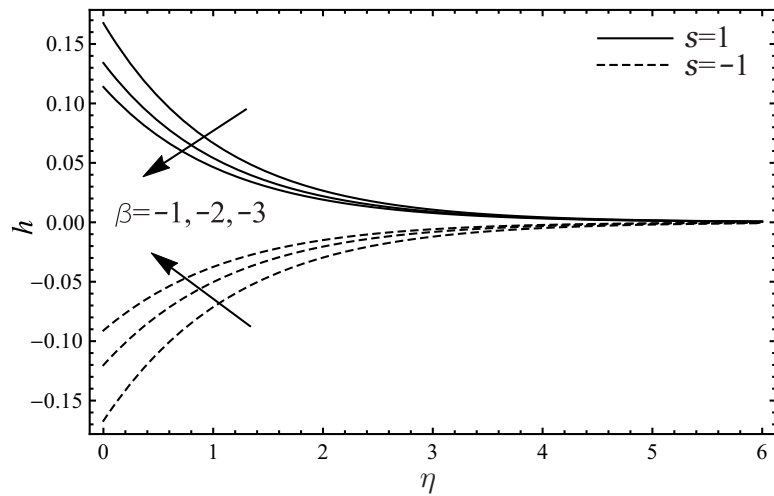
Figure 6.29: Impact of β on h

109

Figure 6.30: Impact of β on θ
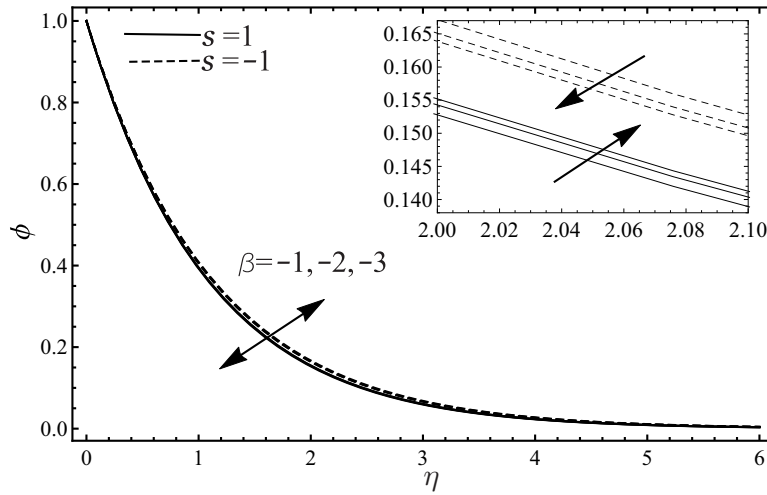
Figure 6.31: Impact of β on ϕ
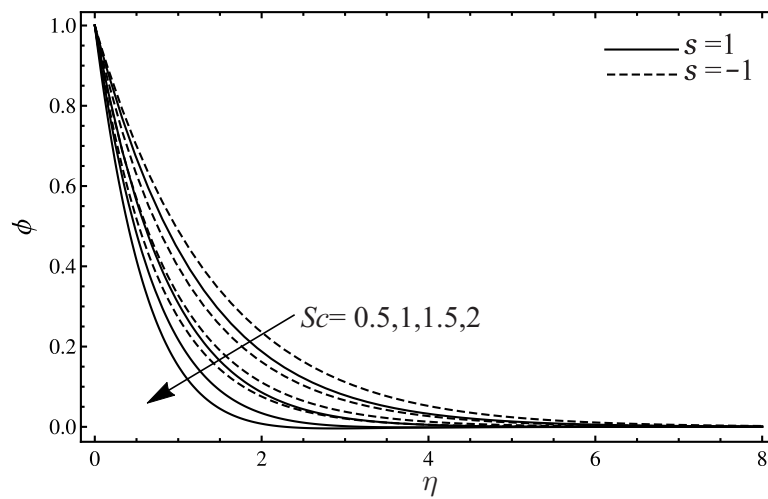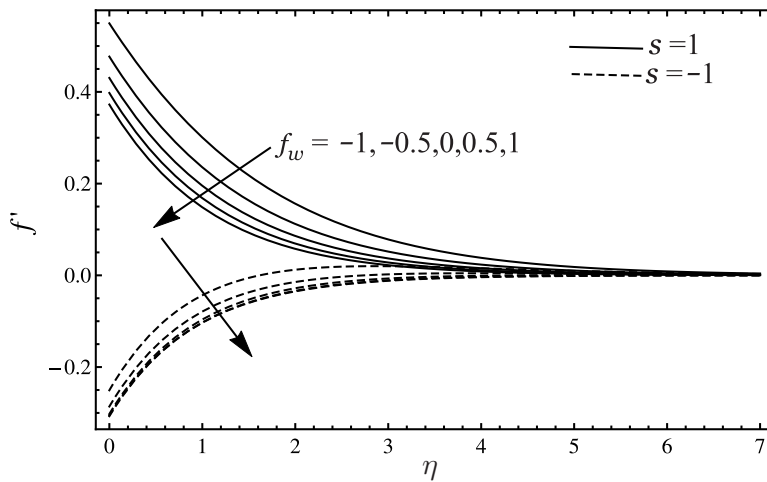

Figure 6.32: Impact of f_w on f'

110
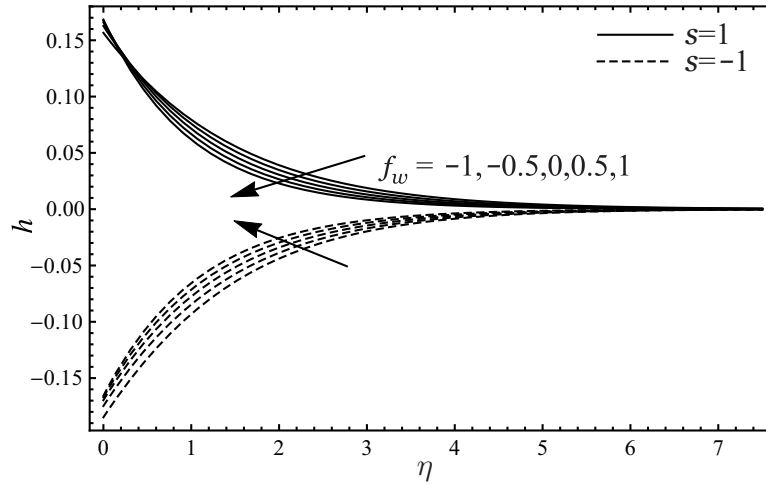
Figure 6.33: Impact of f_w on h
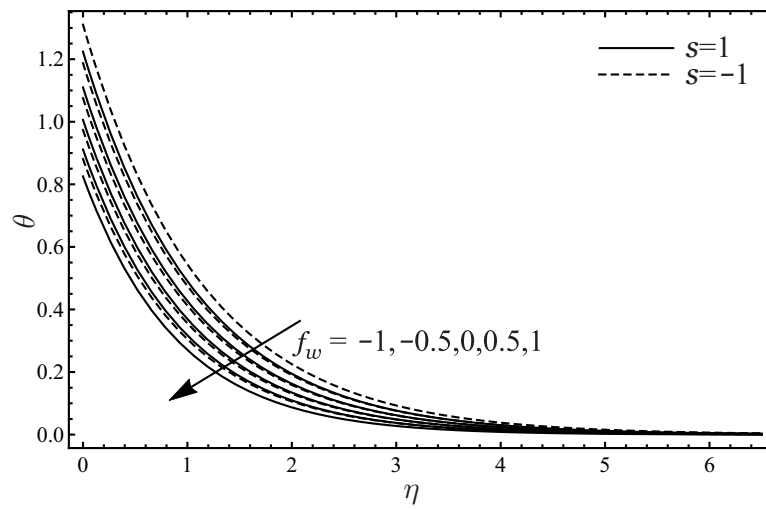
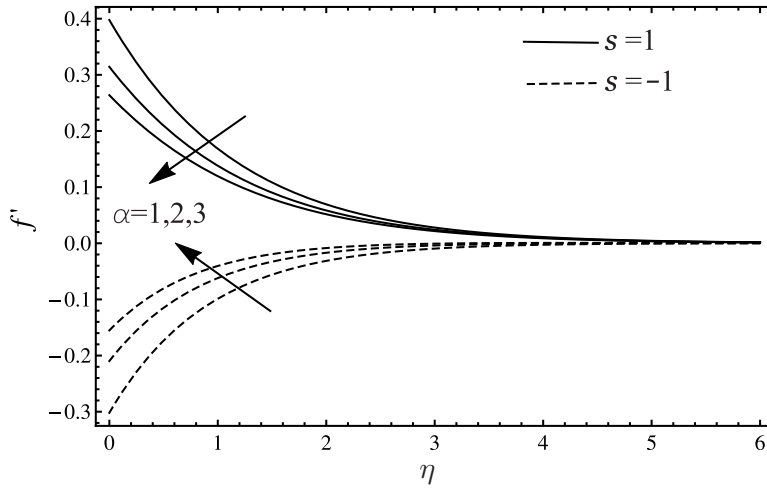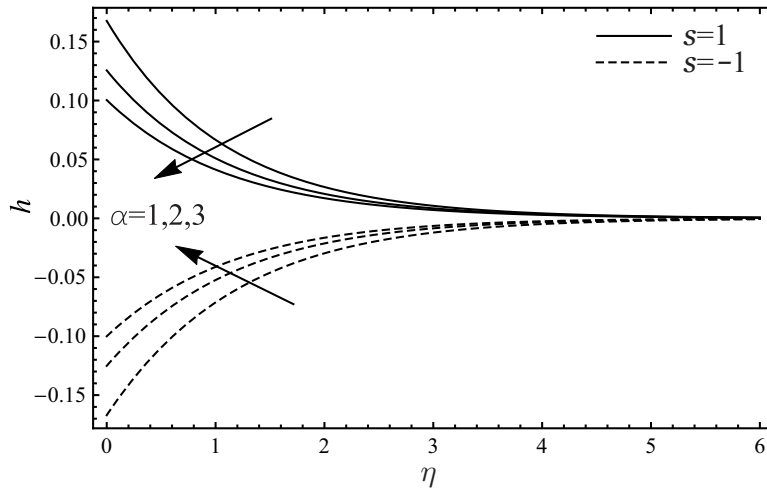**Figure 6.34:** Impact of f_w on θ
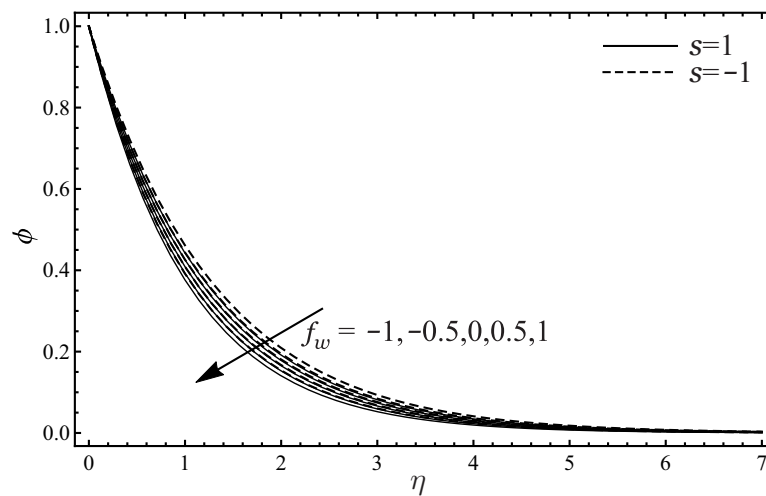
Figure 6.35: Impact of f_w on ϕ
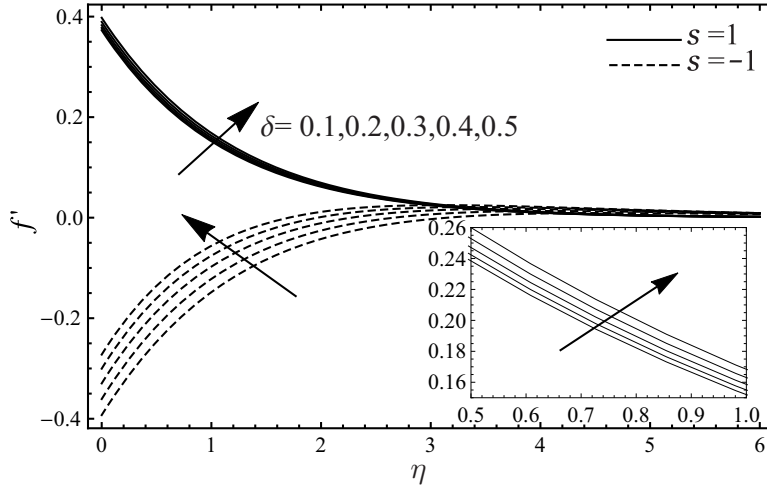
Figure 6.36: Impact of δ on f'
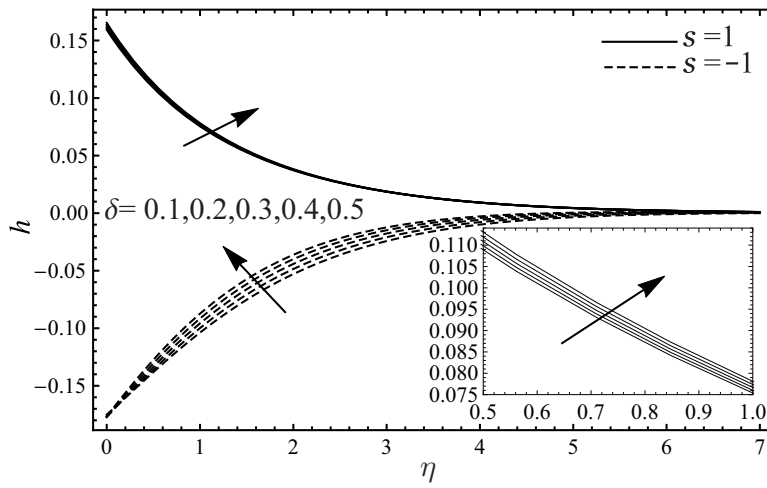
Figure 6.37: Impact of δ on h

Figure 6.38: Impact of δ on θ

Figure 6.39: Impact of δ on ϕ

Figure 6.40: Impact of C_m on ϕ for $s = 1$
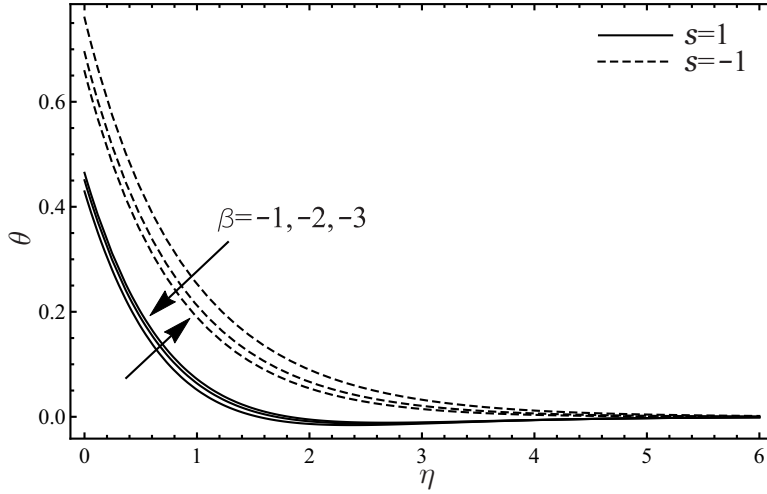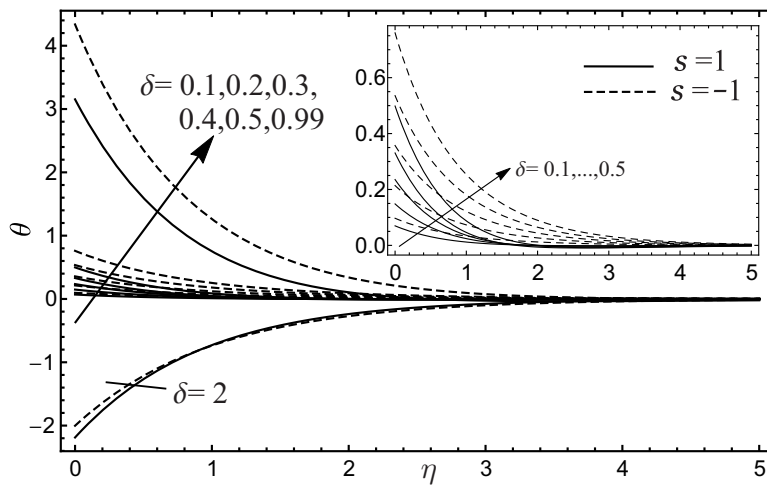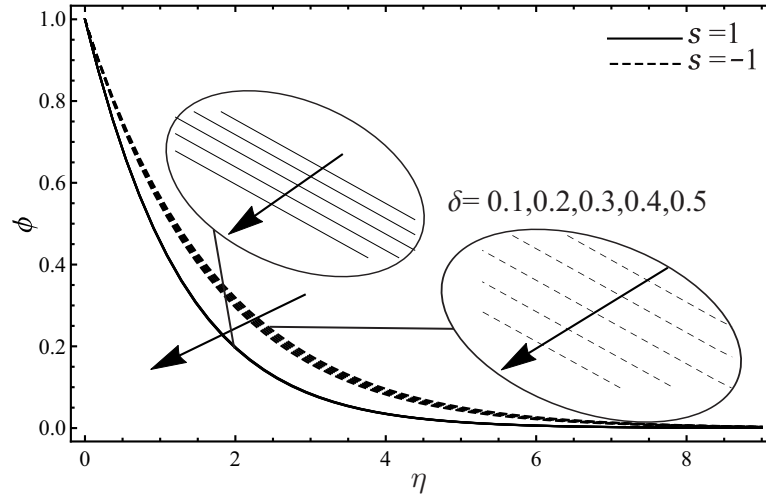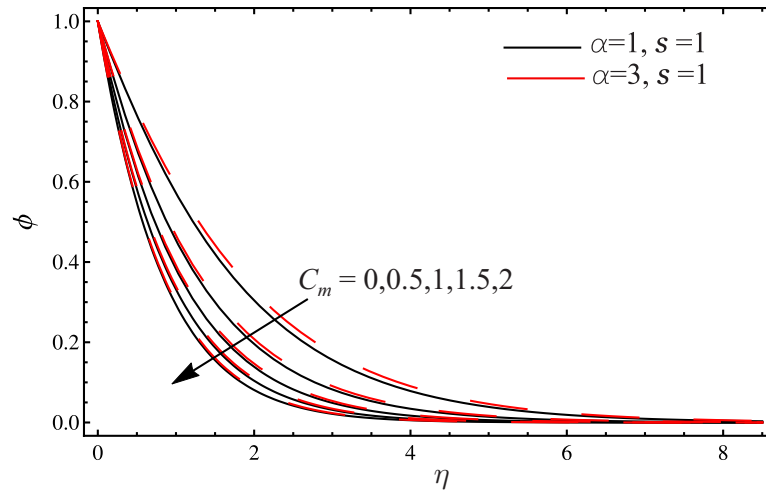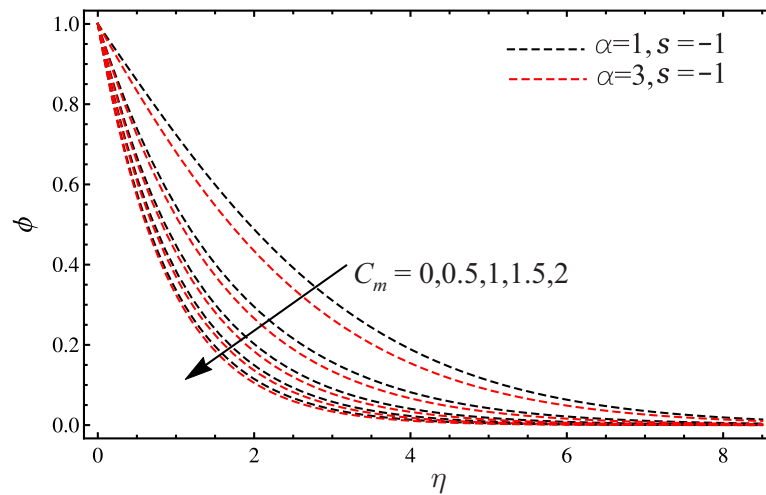

Figure 6.41: Impact of C_m on ϕ for $s = -1$

micro-particles to stick to the wall and causes to reduce the prescribed velocities. Figures 6.24–6.31 are sketched at $\hbar = -0.01$ except Figure 6.27 at $\hbar = -0.1$.

All physical quantities decrease when the sheet stretches and increase with the shrinking of the sheet in the presence of the higher values of the first and second order slip flow parameters in Tables 6.4–6.5.

Table 6.5: Influences of $\delta, \Lambda, Pr, \alpha, \beta$ on physical quantities for $s = -1$.

δ	λ	Pr	α	β	$-C_{f_x}Re_x^{\frac{1}{2}}$	$-\hbar$	$-M_xRe_x$	$-\hbar$	$Nu_xRe_x^{-\frac{1}{2}}$	$-\hbar$	$Sh_xRe_x^{-\frac{1}{2}}$	$-\hbar$
0.1	1	5	1	−1	0.42592	0.05	0.08983	0.1	1.13073	0.01	0.57792	0.1
0.2					0.42709	0.05	0.10106	0.1	1.13459	0.01	0.58561	0.1
0.3					0.42795	0.05	0.11169	0.1	1.13972	0.01	0.59338	0.1
0.4					0.42817	0.05	0.12124	0.1	1.14690	0.01	0.60089	0.1
0.5					0.42990	0.06	0.12969	0.1	1.15765	0.01	0.60786	0.1
0.5	0.0				0.41606	0.01	0.06392	0.05	1.12377	0.01	0.89483	0.01
	0.5				0.41762	0.01	0.13602	0.05	1.15765	0.01	0.89720	0.01
	1.0				0.41868	0.01	0.18076	0.05	1.19396	0.01	0.89954	0.01
	1.5				0.41926	0.01	0.21136	0.05	1.23291	0.01	0.90185	0.01
	2.0				0.41936	0.01	0.23538	0.05	1.27475	0.01	0.90412	0.01
	0.5	0.1			0.42061	0.01	0.17859	0.009	0.85149	0.01	0.89760	0.01
		0.71			0.42017	0.01	0.18916	0.005	0.87941	0.01	0.98848	0.001
		1			0.41996	0.01	0.19986	0.002	0.89350	0.01	0.99767	0.0002
		5			0.41668	0.001	0.20395	0.001	1.01356	0.001	0.99884	0.0001
		10			0.41665	0.001	0.20436	0.0009	1.04915	0.001	0.99988	0.00001
		20			0.41660	0.001	0.20478	0.0008	1.12918	0.001	0.99991	0.000008
		50			0.41648	0.001	0.20563	0.0006	1.23589	0.0006	0.99993	0.000006
		100			0.41634	0.001	0.20651	0.0004	1.35722	0.0004	0.99995	0.000004
		500			0.41625	0.001	0.20787	0.0001	1.50871	0.0001	0.99999	0.000001
		5	1		0.44139	0.1	0.12969	0.1	1.15765	0.1	0.60786	0.1
			2		0.32971	0.1	0.11933	0.1	1.21561	0.1	0.63240	0.1
			3		0.26341	0.1	0.10825	0.1	1.25154	0.1	0.64640	0.1
			1	−1	0.41762	0.01	0.17418	0.01	1.15765	0.01	0.89720	0.01
				−2	0.30047	0.01	0.12830	0.01	1.21981	0.01	0.90155	0.01
				−3	0.22759	0.01	0.09867	0.01	1.25955	0.01	0.90417	0.01
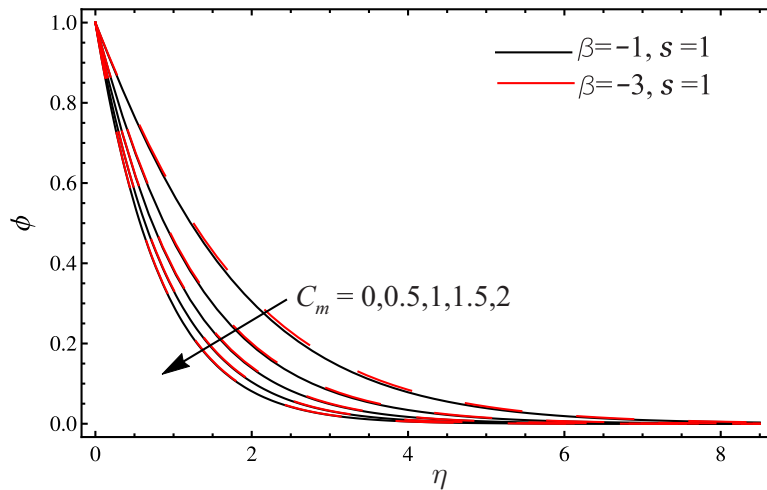
Figure 6.42: Impact of C_m on ϕ for $s = 1$

When sheet stretches or shrinks, an increase in the suction velocity yields a decrease in the prescribed velocities, temperature and concentration profiles. However, microrotational velocity increases for shrinking case. This behaviour has a good agreement with the theoretical concept. On the other hand, an increase in the injection parameter results in an increase in the prescribed velocities,

temperature and concentration profiles. Moreover, microrotational velocity decreases for shrinking case. The influence of f_w in plotted in Figures 6.32–6.35 at $\{\hbar = -0.01, \ \hbar = -0.008\}$; $\{\hbar = -0.01, \ \hbar = -0.01\}$; $\{\hbar = -0.001, \ \hbar = -0.001\}$ and $\{\hbar = -0.01, \ \hbar = -0.01\}$ for $\{s = 1, \ s = -1\}$, respectively. Table 6.2 displays a decrease in the mass transfer rate and an increase in the local skin friction, wall couple stress and heat transfer rate with the increasing values of the suction parameter and on the other hand in Table 6.3, local skin friction and heat transfer rate increase, and local wall couple stress and mass transfer rate decrease. An opposite behaviour is noted with the increasing values of the injection parameter.
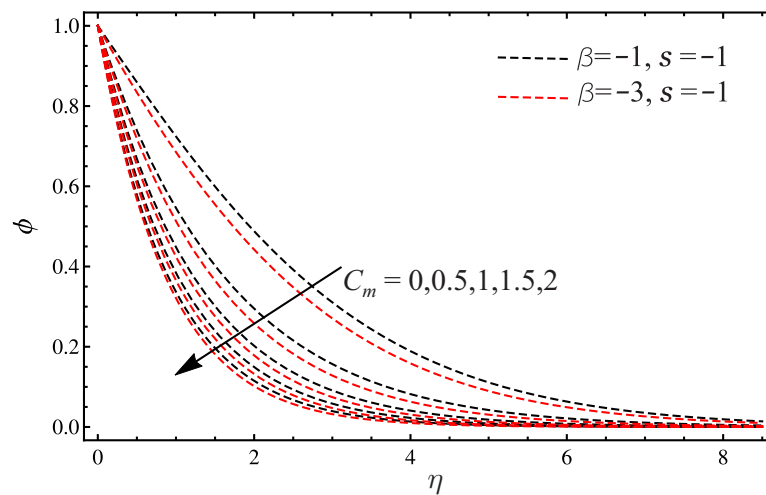
Figure 6.43: Impact of C_m on ϕ for $s = -1$
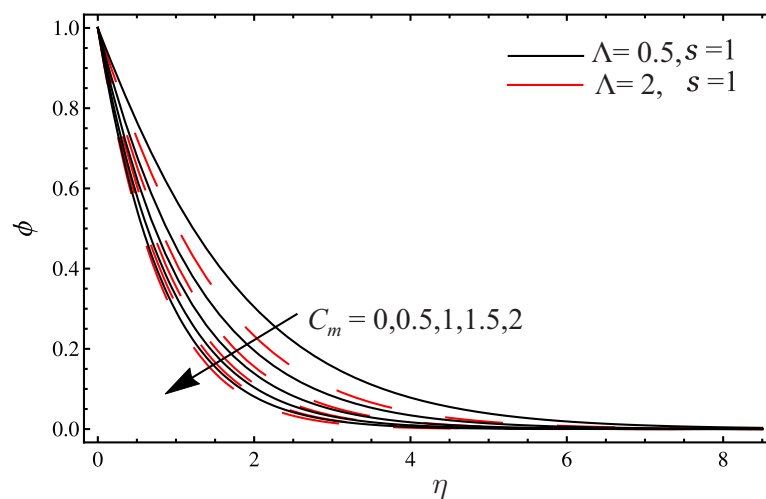
Figure 6.44: Impact of C_m on ϕ for $s = 1$

For different values of the Newtonian heating parameter (δ), f', h, θ and ϕ profiles are plotted in Figures 6.36–6.39. It is reveal that the increasing values of the Newtonian heating parameter causes to raise the fluid temperature which leads to enhances the prescribed velocities. It is noted that the shrinking sheet produces

a higher thermal boundary layer thickness as compared to the stretching sheet, and with a 31.6% difference at $\eta = 0$ for $\delta = 0.99$. On the other hand, for $\delta = 2$ the temperature of the micropolar fluid flow starts decreasing which is in a good agreement with Equation (6.17). The auxiliary parameter ($\hbar$) for stretching sheet is chosen to be $-0.008, -0.00055$ and -0.002 for $\delta = 0.5, 0.99$ and 2, respectively. And for shrinking sheet $\hbar = -0.0008$ and -0.0001 for $\delta = 0.99$ and 2, respectively. Moreover, rest of the curves generated from other values of the δ are displayed at $\hbar = -0.01$ in Figure 6.36 and Figure 6.38. However, Figure 6.37 and Figure 6.39 are plotted at $\hbar = -0.1$. When sheet stretches, higher values of the Newtonian heating parameter produce an increase in all of the physical quantities as tabulated in Table 6.4 and when sheet shrinks, local skin friction and wall couple stress decrease, and heat and mass transfer rate increase as depicted in Table 6.5.

Figures 6.40–6.47 are plotted to analyse the impact of the first order chemical reaction parameter on the concentration profile of the micropolar fluid flow at $\hbar = -0.1$ with the asymptotically increasing curves. All these results show that the concentration profile decreases by increasing the chemical reaction parameter. More importantly, in contrast to the stretching sheet, when sheet shrinks the thickness of the concentration boundary layer at the lower values of α, β, Λ and δ is wider than that at their higher values. For stretching sheet, there is a small difference in the concentration boundary layer thicknesses for different values values of α, β, Λ and δ. An increase in the chemical reaction parameter causes to raise the local skin friction, wall couple stress and mass transfer rate, and reduce the heat transfer rate as shown in Tables 6.2–6.3. It is interesting to observe that the mass transfer rate for the stretched sheet was 281.35% more than that of the shrunk sheet.
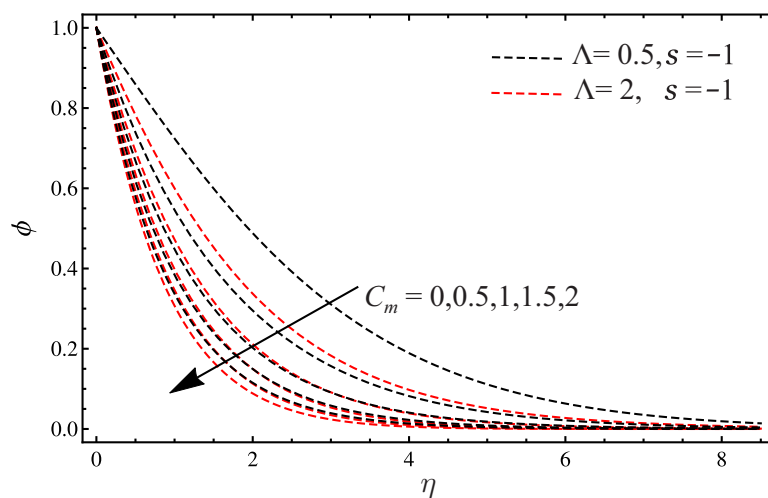
Figure 6.45: Impact of C_m on ϕ for $s = -1$

Figure 6.46: Impact of C_m on ϕ for $s = 1$
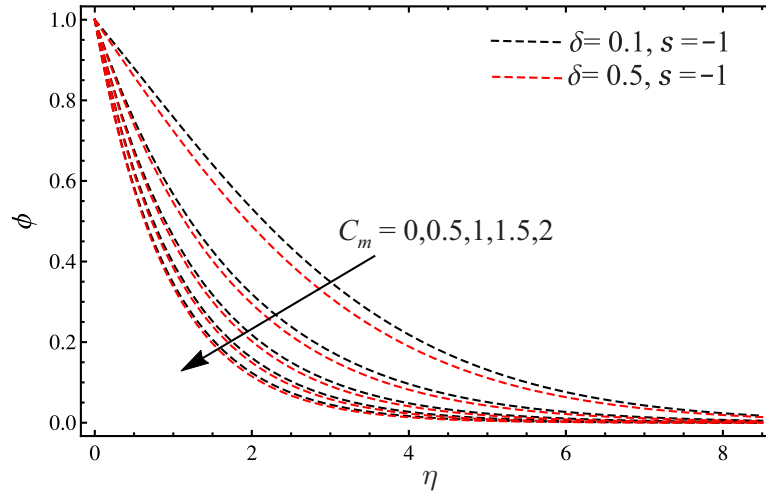
Figure 6.47: Impact of C_m on ϕ for $s = -1$

6.5 Chapter Summary

In this chapter, we reported the asymptomatic study of the chemical reaction and the Newtonian heating parameters on an incompressible mixed convective micropolar fluid flow. A second-order slip flow model was considered in the presence of the dilute concentration of microparticles. S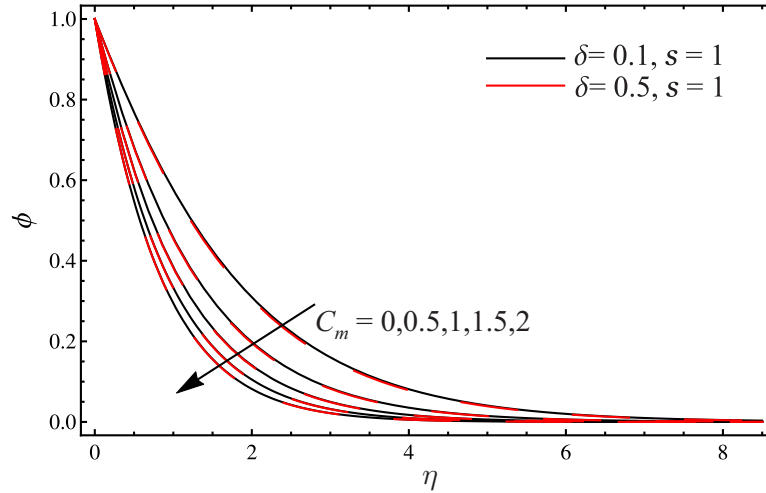emi-analytical results obtained from the Homotopy Analysis Method were, in all cases, found to give an excellent comparison with the already published analytical and numerical results. It was found that when sheet stretched, the thickness of the concentration boundary layer became shorter with a small change in the chemical reaction parameter. On the other hand with the shrunk sheet, an increase in the values of the chemical reaction parameter produced a wider concentration boundary layer thickness at the lower values of the pertaining parameters. It was interesting to observe that the mass transfer rate for the stretched sheet was very high in

comparison to the shrunk sheet. As expected, the first and second order slip flow parameters reduced the velocity component for the stretched sheet, and an opposite trend was noted with the shrunk sheet. Furthermore, in case of the Newtonian heating parameter, shrunk sheet produced higher thermal boundary layer thickness, and the stretched sheet had 6.4% higher heat transfer rate than that of shrunk sheet.

Chapter 7

Conclusion and Future Work

This thesis focuses on the development of the mathematical models of the Navier–Stokes equations based on a theory of the micropolar fluids for the study of the various impacts, such as, heat generation/absorption, magnetohydrodynamics, thermal radiation, the Hall current and the homogeneous first order chemical reaction on the flow behaviour of an incompressible fluid over a stretching/shrinking sheet. For this study, second order slip and the Newtonian heating conditions are imposed at the boundary. In this chapter, the conclusions obtained from the presented results are summarised in the following categories.

1. A mathematical model of the micropolar fluid flow influenced by heat source/sink (generation/absorption) parameter has been formulated and solved by using an analytical technique. An analytical study of the heat transfer micropolar fluid flow has led to the following conclusions.

    (i) The impact of heat source/sink parameter has a direct influence on the velocity component and the temperature profiles. It is observed that with the stretching/shrinking sheet, an increase in the heat source parameter results in an increase in the velocity component profile and the temperature of the micropolar fluid flow. On the other hand, the heat sink parameter has a reverse impact on fluid flow behaviour.

    (ii) The effect of the first order slip flow parameter (α) on the velocity component (f') reveals that when α increases from 1 to 3 then f' achieves the -28.90% change near the stretching sheet and 63.46% change near the shrinking sheet.

    (iii) When the second order slip flow parameter (β) changes from -1 to -3 then the velocity component gets a -19.25% change near the stretching sheet and 54.40% change near shrinking sheet.

(iv) The shrinking sheet produces a higher (958.42%) change in the thermal boundary layer thickness as compared to the stretching sheet which enhances up to 793.71% when the Newtonian heating parameter increases.

Hence, in this study of heat source/sink, the first order slip flow parameter is more capable of producing the slip effect in contrast to the second order slip flow parameter at the constant values of the other governing flow parameters.

2. A magneto-micropolar fluid flow model under the influence of the thermal radiation effect has been derived by considering the second order slip and the Newtonian heating conditions at the boundary. We transformed the governing flow model into a dimensionless nonlinear system of equations and then the analytical solution has revealed the following conclusions.

(i) At the higher value of the thermal radiation parameter $(R = 7)$, the influence of the magnetic field parameter has a dramatic impact on the thermal boundary layer thickness. Thermal boundary layer produces 3769.68% change in at $R = 7$ and 40.56% change at $R = 1$ when M moves from 0 to 7 near the stretching sheet. This is because the temperature profile is much wider at $R = 7$ than the temperature profile at $R = 1$. In case of shrinking sheet, on the other hand, the thermal boundary layer thickness is higher and slightly wider at $R = 7$ in contrast to the thermal boundary layer thickness at $R = 1$.

(ii) Width of the temperature profile is strongly governed by the thermal radiation parameter. Under the influence of the higher magnetic field parameter $(M = 7)$, an increase in the thermal radiation parameter yields a higher temperature profile for stretching of the sheet. While, in the case of the shrinking sheet, thermal boundary thickness is slightly higher at the lower value of the magnetic field parameter $M = 1$ when thermal radiation parameter changes from 0 to 7.

(iii) The first order slip flow parameter has a significant influence on the velocity component. Velocity component decreases with -35% change when first order slip flow parameter changes from 1 to 3 near the stretching sheet. Alternatively, an increase in the first order slip flow parameter yields 46.37% change in the velocity component near the shrinking sheet.

(iv) Near the stretching sheet, velocity component is about -22.62% change when the second order slip flow parameter varies from -1 to -3. On

the other hand, near the shrinking sheet, it enhances 91.231% change in. It is observed that the second order slip flow parameter produces more slip effect near the shrinking sheet in comparison with the stretching sheet.

(v) Under the influence of the varying magnetic field parameter, i.e. M from 1 to 7, when the Newtonian heating parameter changes from 0.1 to 0.5 then the thermal boundary thickness increases from about 639% to 672% near the stretching sheet and reversely it reduces from about 821% to 787% near the shrinking sheet.

In this investigation of MHD micropolar fluid flow over a stretching/shrinking sheet, the second order slip flow parameter effectively enhances the slip effect for shrinking sheet.

3. A mixed convective magneto-micropolar fluid flow model has been designed to investigate the influence of the Hall current on the stretching/shrinking sheet with second order slip and the Newtonian heating conditions at the boundary. Series solutions obtained by Optimal Homotopy Analysis Method have been validated in an excellent agreement with the analytical and numerical solutions for different values of the pertaining parameters under individual cases. Result analysis of the Hall current in the slip flow regime has demonstrated the following conclusions.

(i) The velocity component profile is about 28.71% to 113.58% change for stretching sheet and 32.4741% to 125.403% change for shrinking sheet when the intensity of the magnetic field enhances from 1 to 7 by increasing values of the Hall current parameter, respectively. It is also observed that the boundary layer of the velocity component is higher for stretching sheet and lower for shrinking sheet at the constant value of the magnetic field parameter, i.e., $M = 1$.

(ii) When the first order slip flow parameter increases from 1 to 3, the boundary layer thickness reduces to -32.25% near the stretching sheet and enhances to 51.65% near the shrinking sheet. It is found that the first order slip flow parameter produces more slip effect near the shrinking sheet in comparison with the stretching sheet.

(iii) In the presence of the dilute concentration of the micro-elements, the second order slip flow parameter varying from -1 to -3 gives the change in the boundary layer thickness about -23.16% and 74.15% for stretching and shrinking of the sheet, respectively.

(iv) In Hall current investigation, an increase of the Newtonian heating

parameter from 0.1 to 0.99 results in a dramatic enhancement in the thermal boundary layer thickness of the micropolar fluid flow. It produces 7320.41% and 6721.52% changes in the thicknesses for stretching and shrinking of the sheet, respectively.

The work presented in Chapter 5 concludes that the first and second order slip flow parameters produce significant slip effects near the stretching and shrinking sheet, respectively.

4. A steady state two-dimensional model for the heat and mass transfer micropolar fluid flow over a stretching/shrinking sheet has been derived. In this model, second order slip and the Newtonian heating conditions are imposed at the boundary. The influences of the non-dimensional physical parameters have been investigated by using a semi-analytical technique named Homotopy Analysis Method. The study of heat and mass transfer flow behaviour in the presence of the homogeneous chemical reaction effect has led to the following conclusions.

   (i) At higher values of the first and second order slip flow parameters, an increase in the chemical reaction parameter leads to an increase in the concentration profile when sheet stretches. Alternatively, a reverse trend is observed when sheet shrinks.

   (ii) In the heat and mass transfer flow of the chemical reaction, stretching sheet produces -33.67% change in the boundary layer thickness of the velocity component when first order slip flow parameter enhances from 1 to 3. However, shrinking sheet results in about 48.61% change in the thickness of the boundary layer. Furthermore, when the second order slip flow parameter alters from -1 to -3 then the boundary layer thickness for the velocity component decreases about -26.85% and increases about 54.88% for stretching and shrinking of the sheet, respectively.

   (iii) It is also observed that under the influence of the first order homogeneous chemical reaction, the thermal boundary layer thickness for shrinking sheet enhances about 39.94% than the one for the stretching sheet.

7.1   Future Work

The presented work in this thesis can be extended to numerous studies such as the free/forced/mixed convective heat and mass transfer micropolar fluid flow over

a permeable/impermeable horizontal/vertical cylinders and wedges or any other different geometry in the presence of the second order slip and the Newtonian heating conditions at the boundary.

Appendix A

Transformation

In this part of appendix, we will derive the dimensionless nonlinear system of ordinary differential equations by applying a suitable similarity transformation on the governing flow mathematical models for chapters 3 to 6. A comprehensive working for each model is demonstrated in the following sections.

A.1 Nondimensionalization of Heat Source/Sink Model

The set of Equations (3.1)-(3.5) in chapter 3 can be rewritten as follows:

$$\frac{\partial u}{\partial x} + \frac{\partial v}{\partial y} = 0, \tag{A.1}$$

$$u\frac{\partial u}{\partial x} + v\frac{\partial u}{\partial y} = \frac{\mu + \chi}{\rho}\left(\frac{\partial^2 u}{\partial y^2}\right) + g\beta_T\left(T - T_\infty\right) + \frac{\chi}{\rho}\left(\frac{\partial \omega}{\partial y}\right), \tag{A.2}$$

$$u\frac{\partial \omega}{\partial x} + v\frac{\partial \omega}{\partial y} = \frac{\gamma}{\rho j}\left(\frac{\partial^2 \omega}{\partial y^2}\right) - \frac{\chi}{\rho j}\left(2\omega + \frac{\partial u}{\partial y}\right), \tag{A.3}$$

$$u\frac{\partial T}{\partial x} + v\frac{\partial T}{\partial y} = \frac{k}{\rho c_p}\left(\frac{\partial^2 T}{\partial y^2}\right) + \frac{Q_o}{\rho c_p}\left(T - T_\infty\right), \tag{A.4}$$

with boundary conditions,

$$\left.\begin{array}{l} u = su_w(x) + u_{\text{slip}}, v = v_o, \omega = -n\dfrac{\partial u}{\partial y}, k\dfrac{\partial T}{\partial y} = -h_s T \text{ at } y = 0, \\[2mm] u \to 0,\ \omega \to 0,\ T \to T_\infty \text{ as } y \to \infty. \end{array}\right\} \tag{A.5}$$

with u_{slip} as

$$u_{\text{slip}} = \frac{2}{3}\left(\frac{3 - \epsilon l^3}{\epsilon} - \frac{3}{2}\frac{1 - l^2}{k_n}\right)d\frac{\partial u}{\partial y} - \frac{1}{4}\left(l^4 + \frac{2}{k_n^2}(1 - l^2)\right)d^2\frac{\partial^2 u}{\partial y^2},$$

here we rewrite the u_{slip} as below,

$$u_{\text{slip}} = A\frac{\partial u}{\partial y} + B\frac{\partial^2 u}{\partial y^2},$$

where, A and B are defined in Chapter 1. The similarity transform,

$$\left.\begin{array}{c} u_w(x) = ax, \ u = \partial\psi/\partial y, \ v = -\partial\psi/\partial x, \ \eta = \sqrt{u_w(x)}(\nu x)^{-\frac{1}{2}}y, \\[2mm] \psi = \sqrt{x\nu u_w(x)}f(\eta), \ \omega = \sqrt{xu_w(x)}(\nu)^{-\frac{1}{2}}ah(\eta) \text{ and } \theta(\eta) = \dfrac{T-T_\infty}{T_\infty}, \end{array}\right\} \quad \text{(A.6)}$$

satisfies the continuity Equation (A.1) automatically and Equation (A.2) can be written as

$$\frac{\partial\psi}{\partial y}\cdot\frac{\partial}{\partial x}\left(\frac{\partial\psi}{\partial y}\right) - \frac{\partial\psi}{\partial x}\frac{\partial}{\partial y}\left(\frac{\partial\psi}{\partial y}\right) = \frac{\mu+\chi}{\rho}\frac{\partial^2}{\partial y^2}\left(\frac{\partial\psi}{\partial y}\right) + \text{g}\beta_T\left(T-T_\infty\right) + \frac{\chi}{\rho}\left(\frac{\partial\omega}{\partial y}\right),$$

$$\frac{\partial \sqrt{x\nu u_w(x)}f(\eta)}{\partial \ \eta\sqrt{\nu/a}}\frac{\partial}{\partial x}\left(\frac{\partial\sqrt{x\nu u_w(x)}f(\eta)}{\partial \ \eta\sqrt{\nu/a}}\right) - \frac{\partial \sqrt{x\nu u_w(x)}f(\eta)}{\partial x}\frac{\partial}{\partial \ \eta\sqrt{\nu/a}}$$
$$\left(\frac{\partial \sqrt{x\nu u_w(x)}f(\eta)}{\partial \ \eta\sqrt{\nu/a}}\right) = \frac{\mu+\chi}{\rho}\frac{\partial^2}{\partial(\eta^2\nu/a)}\left(\frac{\partial \sqrt{x\nu u_w(x)}f(\eta)}{\partial \ \eta\sqrt{\nu/a}}\right) + \text{g}\beta_T\theta T_\infty +$$
$$\frac{\chi}{\rho}\left(\frac{\partial \sqrt{xu_w(x)}(\nu)^{-\frac{1}{2}}ah(\eta)}{\partial\eta\sqrt{\nu/a}}\right),$$

$$axf'af' - \sqrt{a\nu}f\sqrt{a/\nu}axf'' = \frac{\mu}{\rho}(1+K)a/\nu axf''' + \text{g}\beta_T\theta T_\infty + \frac{\chi}{\rho}ax\frac{a}{\nu}h',$$

$$a^2x(f')^2 - a^2xff'' = (1+K)a^2xf''' + \text{g}\beta_T\theta T_\infty + a^2xKh'$$
$$(f')^2 - ff'' = (1+K)f''' + \frac{\text{g}\beta_T T_\infty}{a^2x}\theta + Kh'$$
$$(f')^2 - ff'' = (1+K)f''' + \lambda\theta + Kh'$$

$$(1+K)f''' - (f')^2 + ff'' + \lambda\theta + Kh' = 0 \quad \text{(A.7)}$$

Now Equation (A.3) can be written as

$$\frac{\partial\psi}{\partial y}\frac{\partial\omega}{\partial x} - \frac{\partial\psi}{\partial x}\frac{\partial\omega}{\partial y} = \frac{\gamma}{\rho j}\left(\frac{\partial^2\omega}{\partial y^2}\right) - \frac{\chi}{\rho j}\left(2\omega + \frac{\partial}{\partial y}\frac{\partial\psi}{\partial y}\right)$$

$$\frac{\partial \sqrt{x\nu u_w(x)}f(\eta)}{\partial \eta \sqrt{\nu/a}}\frac{\partial \sqrt{xu_w(x)}(\nu)^{-\frac{1}{2}}ah(\eta)}{\partial x} - \frac{\partial \sqrt{x\nu u_w(x)}f(\eta)}{\partial x}\frac{\partial \sqrt{xu_w(x)}(\nu)^{-\frac{1}{2}}ah(\eta)}{\partial \eta \sqrt{\nu/a}}$$

$$= \frac{\gamma}{\rho j}\left(\frac{\partial^2 \sqrt{xu_w(x)}(\nu)^{-\frac{1}{2}}ah(\eta)}{\partial \eta^2 \nu/a}\right) - \frac{\chi}{\rho j}\left(2\sqrt{xu_w(x)}(\nu)^{-\frac{1}{2}}ah(\eta) + \frac{\partial}{\partial \eta \sqrt{\nu/a}}\right.$$

$$\left.\frac{\partial \sqrt{x\nu u_w(x)}f(\eta)}{\partial \eta \sqrt{\nu/a}}\right)$$

$$axf'\sqrt{a/\nu}ah - \sqrt{a\nu}f\frac{a}{\nu}axh' = \frac{\gamma}{\rho j}\sqrt{a/\nu}\frac{a^2 x}{\nu}h'' - \frac{\chi}{\rho j}\left(2\sqrt{a/\nu}axh + \sqrt{a/\nu}axf''\right)$$

$$a^2 x\sqrt{a/\nu}f'h - a^2 x\sqrt{a/\nu}fh' = \frac{\gamma}{\rho\nu j}a^2 x\sqrt{a/\nu}h'' - \frac{\chi}{\rho j}ax\sqrt{a/\nu}(2h + f'')$$

$$f'h - fh' = (1 + K/2)h'' - K(2h + f'')$$

$$(1 + K/2)h'' - f'h + fh' - K(2h + f'') = 0 \tag{A.8}$$

Moreover, Equation (A.4) can be nondimensionalize as

$$\frac{\partial \psi}{\partial y}\frac{\partial T}{\partial x} - \frac{\partial \psi}{\partial x}\frac{\partial T}{\partial y} = \frac{k}{\rho c_p}\frac{\partial^2 T}{\partial y^2} + \frac{Q_o}{\rho c_p}(T - T_\infty)$$

$$\frac{\partial \sqrt{x\nu u_w(x)}f(\eta)}{\partial \eta \sqrt{\nu/a}}\frac{\partial(\theta T_\infty + T_\infty)}{\partial x} - \frac{\partial \sqrt{x\nu u_w(x)}f(\eta)}{\partial x}\frac{\partial(\theta T_\infty + T_\infty)}{\partial \eta \sqrt{\nu/a}} =$$

$$\frac{k}{\rho c_p}\frac{\partial^2(\theta T_\infty + T_\infty)}{\partial \eta^2 \nu/a} + \frac{Q_o}{\rho c_p}(\theta T_\infty + T_\infty)$$

$$0 - \sqrt{a\nu}f\sqrt{a/\nu}T_\infty\theta' = \frac{k}{\rho c_p}T_\infty\theta''a/\nu + \frac{Q_o}{\rho c_p}T_\infty\theta$$

$$-aT_\infty f\theta' = \frac{1}{Pr}aT_\infty\theta'' + \frac{Q_o}{\rho c_p}\theta T_\infty$$

$$-f\theta' = \frac{1}{Pr}\theta'' + \frac{Q_o}{a\rho c_p}\theta$$

$$\theta'' + Prf\theta' + QPr\theta = 0 \tag{A.9}$$

Furthermore, dimensionless boundary conditions from Equation (A.5) can be

obtained as

$$u = su_w + \left(A\frac{\partial u}{\partial y} + B\frac{\partial^2 u}{\partial y^2} \right), v = v_o, \omega = -n\frac{\partial u}{\partial y}, k\frac{\partial T}{\partial y} = -h_s T \text{ at } y = 0,$$

$$u \to 0, \ \omega \to 0, \ T \to T_\infty \text{ as } y \to \infty,$$

$$\frac{\partial \psi}{\partial y} = sax + \left(A\frac{\partial}{\partial y}\frac{\partial \psi}{\partial y} + B\frac{\partial^2}{\partial y^2}\frac{\partial \psi}{\partial y} \right), -\frac{\partial \psi}{\partial x} = v_o, \omega = -n\frac{\partial}{\partial y}\frac{\partial \psi}{\partial y},$$

$$k\frac{\partial T}{\partial y} = -h_s T \text{ at } y = 0,$$

$$\frac{\partial \psi}{\partial y} \to 0, \ \omega \to 0, \ T \to T_\infty \text{ as } y \to \infty,$$

$$\frac{\partial \sqrt{x\nu u_w(x)}f(\eta)}{\partial \eta \sqrt{\nu/a}} = sax + \left(A\frac{\partial}{\partial \eta \sqrt{\nu/a}}\frac{\partial \sqrt{x\nu u_w(x)}f(\eta)}{\partial \eta \sqrt{\nu/a}} + B\frac{\partial^2}{\partial \eta^2 \nu/a}\frac{\partial \sqrt{x\nu u_w(x)}f(\eta)}{\partial \eta \sqrt{\nu/a}} \right),$$

$$-\frac{\partial \sqrt{x\nu u_w(x)}f(\eta)}{\partial x} = v_o, \ \sqrt{x u_w(x)}(\nu)^{-\frac{1}{2}}ah(\eta) = -n\frac{\partial}{\partial \eta \sqrt{\nu/a}}\frac{\partial \sqrt{x\nu u_w(x)}f(\eta)}{\partial \eta \sqrt{\nu/a}},$$

$$k\frac{\partial(\theta T_\infty + T_\infty)}{\partial \eta \sqrt{\nu/a}} = -h_s(\theta T_\infty + T_\infty) \text{ at } \eta\sqrt{\nu/a} = 0,$$

$$\frac{\partial \sqrt{x\nu u_w(x)}f(\eta)}{\partial \eta \sqrt{\nu/a}} \to 0, \ \sqrt{x u_w(x)}(\nu)^{-\frac{1}{2}}ah(\eta) \to 0, \ \theta \to 0 \text{ as } y \to \infty,$$

$$axf' = sax + \left(Aax\sqrt{a/\nu}f'' + Baxa/\nu f''' \right), \ f = -v_o/\sqrt{a\nu}, \ axh\sqrt{a/\nu} = -naxf''\sqrt{a/\nu},$$

$$kT_\infty \theta' \sqrt{a/\nu} = -h_s T_\infty(\theta + 1) \text{ at } \eta = 0$$

$$f' \to 0, \ h \to 0, \ \theta \to 0 \text{ as } y \to \infty,$$

$$f = -v_o/\sqrt{a\nu}, \ f' = s + \left(A\sqrt{a/\nu}f'' + Ba/\nu f''' \right), \ h = -nf'',$$

$$\theta' = -(\theta + 1)(h_s/k\sqrt{a/\nu}) \text{ at } \eta = 0$$

$$f' \to 0, \ h \to 0, \ \theta \to 0 \text{ as } y \to \infty,$$

$$\left. \begin{aligned} f = f_w, f' = s + \alpha f'' + \beta f''', \ h = -nf'', \theta' = -\delta(1+\theta) \text{ at } \eta = 0, \\ f' \to 0, \ h \to 0, \ \theta \to 0 \text{ as } \eta \to \infty. \end{aligned} \right\} \quad \text{(A.10)}$$

Hence, the dimensionless system of nonlinear ordinary differential Equations (A.7)–

128

is

$$(1+K)f''' - (f')^2 + ff'' + \lambda\theta + Kh' = 0,$$
$$(1+K/2)h'' - f'h + fh' - K(2h + f'') = 0,$$
$$\theta'' + Prf\theta' + QPr\theta = 0,$$

with the boundary conditions,

$$\left. \begin{array}{r} f = f_w, f' = s + \alpha f'' + \beta f''', h = -nf'', \theta' = -\delta(1+\theta) \text{ at } \eta = 0, \\ f' \to 0, \ h \to 0, \ \theta \to 0 \text{ as } \eta \to \infty. \end{array} \right\}$$

Here in the above system, the dimensionless parameters can be defined as

$$\left. \begin{array}{l} \lambda = Gr_x/Re_x \text{ for } Gr_x = \mathrm{g}\beta_T T_\infty x/a\nu \text{ and } Re_x = ax^2/\nu, \\ Q = Q_o/a\rho c_p, \gamma = (\mu + \chi/2)j, \ Pr = \mu c_p/k, \ f_w = -(a\nu)^{-\frac{1}{2}}v_o, \\ \alpha = A\sqrt{a/\nu}, \ \beta = Ba/\nu, \ \delta = \dfrac{h_s}{k}\sqrt{\nu/a}, \ j = \nu/a, \ K = \chi/\mu. \end{array} \right\} \quad \text{(A.11)}$$

In a similar fashion, we can nondimensionalized the physical quantities such as local skin friction co-efficients (C_{f_x}), local wall couple stress (M_x) and the local Nusselt number (Nu_x) for this and coming governing flow models.

A.2 Nondimensionalization of Radiative MHD Model

In this section, we presents the nondimensionalization of radiative magneto-micropolar fluid flow model which is presented in Chapter 4.
The governing system of equations for the fluid flow,

$$\frac{\partial u}{\partial x} + \frac{\partial v}{\partial y} = 0, \tag{A.12}$$

$$u\frac{\partial u}{\partial x} + v\frac{\partial u}{\partial y} = \frac{\mu + \chi}{\rho}\left(\frac{\partial^2 u}{\partial y^2}\right) + \mathrm{g}\beta_T(T - T_\infty) + \frac{\chi}{\rho}\left(\frac{\partial \omega}{\partial y}\right) - \frac{\sigma B_o^2}{\rho}u, \tag{A.13}$$

$$u\frac{\partial \omega}{\partial x} + v\frac{\partial \omega}{\partial y} = \frac{\gamma}{\rho j}\left(\frac{\partial^2 \omega}{\partial y^2}\right) - \frac{\chi}{\rho j}\left(2\omega + \frac{\partial u}{\partial y}\right), \tag{A.14}$$

$$u\frac{\partial T}{\partial x} + v\frac{\partial T}{\partial y} = \frac{k}{\rho c_p}\left(\frac{\partial^2 T}{\partial y^2}\right) - \frac{1}{\rho c_p}\frac{\partial q_r}{\partial y}, \tag{A.15}$$

with boundary conditions,

$$u = s u_w(x) + u_{\text{slip}}, \ v = v_o, \ \omega = -n\frac{\partial u}{\partial y}, \ k\frac{\partial T}{\partial y} = -h_s T \text{ at } y = 0, \bigg\}$$
$$u \to 0, \ \omega \to 0, \ T \to T_\infty \text{ as } y \to \infty, \bigg\} \quad \text{(A.16)}$$

is transformed by using the same similarity variables as defined in Equation (A.6). The Equation (A.13) can be written as follows:

$$\frac{\partial \psi}{\partial y}\frac{\partial}{\partial x}\left(\frac{\partial \psi}{\partial y}\right) - \frac{\partial \psi}{\partial x}\frac{\partial}{\partial y}\left(\frac{\partial \psi}{\partial y}\right) = \frac{\mu + \chi}{\rho}\frac{\partial^2}{\partial y^2}\left(\frac{\partial \psi}{\partial y}\right) + g\beta_T\left(T - T_\infty\right) + \frac{\chi}{\rho}$$
$$\left(\frac{\partial \omega}{\partial y}\right) - \frac{\sigma B_o^2}{\rho}\frac{\partial \psi}{\partial y},$$

$$\frac{\partial \ \sqrt{x\nu u_w(x)}f(\eta)}{\partial \ \eta\sqrt{\nu/a}}\frac{\partial}{\partial x}\left(\frac{\partial\sqrt{x\nu u_w(x)}f(\eta)}{\partial \ \eta\sqrt{\nu/a}}\right) - \frac{\partial \ \sqrt{x\nu u_w(x)}f(\eta)}{\partial x}\frac{\partial}{\partial \ \eta\sqrt{\nu/a}}$$
$$\left(\frac{\partial \ \sqrt{x\nu u_w(x)}f(\eta)}{\partial \ \eta\sqrt{\nu/a}}\right) = \frac{\mu + \chi}{\rho}\frac{\partial^2}{\partial(\eta^2\nu/a)}\left(\frac{\partial \ \sqrt{x\nu u_w(x)}f(\eta)}{\partial \ \eta\sqrt{\nu/a}}\right) + g\beta_T\theta T_\infty +$$
$$\frac{\chi}{\rho}\left(\frac{\partial \ \sqrt{xu_w(x)}(\nu)^{-\frac{1}{2}}ah(\eta)}{\partial\eta\sqrt{\nu/a}}\right) - \frac{\sigma B_o^2}{\rho}\frac{\partial\sqrt{x\nu u_w(x)}f(\eta)}{\partial\eta\sqrt{\nu/a}},$$

$$axf'af' - \sqrt{a\nu}f\sqrt{a/\nu}axf'' = \frac{\mu}{\rho}(1 + K)a/\nu axf''' + g\beta_T\theta T_\infty + \frac{\chi}{\rho}ax\frac{a}{\nu}h' -$$
$$\frac{\sigma B_o^2}{\rho}axf',$$

$$a^2x(f')^2 - a^2xff'' = (1 + K)a^2xf''' + g\beta_T\theta T_\infty + a^2xKh' - \frac{\sigma B_o^2}{\rho}axf',$$
$$(f')^2 - ff'' = (1 + K)f''' + \frac{g\beta_T T_\infty}{a^2x}\theta + Kh' - \frac{\sigma B_o^2}{a\rho}f',$$
$$(f')^2 - ff'' = (1 + K)f''' + \lambda\theta + Kh' - Mf'$$

$$(1 + K)f''' - (f')^2 + ff'' + \lambda\theta + Kh' - Mf' = 0 \quad \text{(A.17)}$$

The Equation (A.14) can be transformed as for Equation (A.8). Moreover, the radiative heat flux has a simplified form with the help of Rosseland approximation [109] as follows:

$$q_r = -\frac{4\sigma^*}{3k^*}\frac{\partial T^4}{\partial y}, \quad \text{(A.18)}$$

where σ^* depicts the Stefan-Boltzmann constant and k^* represents the mean absorption coefficient. In radiative heat flux, to express the T^4 as a linear function of temperature, an expansion by Taylor's series is considered about T_∞ and neglecting higher order terms which yields

$$T^4 \approx 4T_\infty^3 T - 3T_\infty^4.$$

Now, Equation (A.18) can be written as

$$q_r = -\frac{16\sigma^* T_\infty^3}{3k^*}\frac{\partial T}{\partial y}, \tag{A.19}$$

So, with the help of Equation (A.19), Equation (A.15) can be written as follows:

$$\frac{\partial\psi}{\partial y}\frac{\partial T}{\partial x} - \frac{\partial\psi}{\partial x}\frac{\partial T}{\partial y} = \frac{k}{\rho c_p}\frac{\partial^2 T}{\partial y^2} + \frac{16\sigma^* T_\infty^3}{3k^*\rho c_p}\frac{\partial^2 T}{\partial y^2}$$

$$\frac{\partial\sqrt{x\nu u_w(x)}f(\eta)}{\partial\,\eta\sqrt{\nu/a}}\frac{\partial(\theta T_\infty + T_\infty)}{\partial x} - \frac{\partial\sqrt{x\nu u_w(x)}f(\eta)}{\partial x}\frac{\partial(\theta T_\infty + T_\infty)}{\partial\,\eta\sqrt{\nu/a}} = \frac{k}{\rho c_p}$$
$$\frac{\partial^2(\theta T_\infty + T_\infty)}{\partial\,\eta^2\nu/a} + \frac{16\sigma^* T_\infty^3}{3k^*\rho c_p}\frac{\partial^2(\theta T_\infty + T_\infty)}{\partial\eta^2\nu/a},$$

$$0 - \sqrt{a\nu}f.\sqrt{a/\nu}T_\infty\theta' = \frac{k}{\rho c_p}T_\infty\theta'' a/\nu + \frac{16\sigma^* T_\infty^3}{3k^*k}\frac{k}{\rho c_p\nu}aT_\infty\theta'',$$

$$-aT_\infty f\theta' = \frac{1}{Pr}aT_\infty\theta'' + \frac{R}{Pr}\theta'' aT_\infty,$$
$$-fPr\theta' = (1+R)\theta'',$$

$$(1+R)\theta'' + Prf\theta' = 0. \tag{A.20}$$

Furthermore, the boundary conditions are already nondimensionalized as mentioned in Equation (A.10) for this radiative magneto-micropolar fluid flow model. Two new dimensionless physical parameters such as $M = \sigma B_o^2/a\rho$ and $R = (16\sigma^* T_\infty^3)(3k^*k)^{-1}$ are defined in this formulation and the rest of the parameters are described in Equation (A.11).

A.3 Nondimensionalization of Hall Current Model

In this section, we drive the nondimensionalization of the model which is formulated for the influence of the Hall current on a steady state MHD micropolar fluid flow

over a stretching/shrinking sheet with slip and the Newtonian heating conditions at the boundary.

In the absence of the Ion's slip and the pressure diffusion effects, the generalized Ohm's law with Maxwell's equation [110–112] can be written as follows:

$$\mathbf{J} = \sigma \left(\mathbf{E} + \mathbf{V} \times \mathbf{B} - \frac{1}{en_e} \mathbf{J} \times \mathbf{B} \right), \tag{A.21}$$

$$\bigtriangledown \times \mathbf{B} = \mu_o \mathbf{J},$$
$$\bigtriangledown \cdot \mathbf{B} = 0,$$
$$\bigtriangledown \times \mathbf{E} = 0,$$
$$\bigtriangledown \cdot \mathbf{J} = 0.$$

In Equation (A.21), the vectors reads as follows:

$$\mathbf{J} = \begin{pmatrix} J_x \\ 0 \\ J_z \end{pmatrix}, \quad \mathbf{E} = \begin{pmatrix} E_x \\ E_y \\ E_z \end{pmatrix}, \quad \mathbf{V} = \begin{pmatrix} u \\ v \\ w \end{pmatrix}, \quad \mathbf{B} = \begin{pmatrix} 0 \\ B_o \\ 0 \end{pmatrix}.$$

Now,

$$\mathbf{V} \times \mathbf{B} = \begin{vmatrix} \hat{i} & \hat{j} & \hat{k} \\ u & v & w \\ 0 & B_o & 0 \end{vmatrix} = \begin{pmatrix} -wB_o \\ 0 \\ uB_o \end{pmatrix} \quad \text{and} \quad \mathbf{J} \times \mathbf{B} = \begin{vmatrix} \hat{i} & \hat{j} & \hat{k} \\ J_x & 0 & J_z \\ 0 & B_o & 0 \end{vmatrix} = \begin{pmatrix} -J_z B_o \\ 0 \\ J_x B_o \end{pmatrix}.$$

Therefore, Equation (A.21) can be written in its components as

$$J_x = \sigma \left(E_x - wB_o + \frac{B_o J_z}{en_e} \right), \tag{A.22}$$

$$0 = \sigma(E_y + 0 + 0) \Rightarrow E_y = 0, \tag{A.23}$$

$$J_z = \sigma \left(E_z + uB_o - \frac{B_o J_x}{en_e} \right). \tag{A.24}$$

Now, solve Equations (A.22)–(A.24) for J_x and J_z as follows:
applying Equation (A.22)$+\frac{\sigma B_o}{en_e}$ Equation (A.24) yields,

$$J_x \left[1 + \left(\frac{\sigma B_o}{en_e} \right)^2 \right] = \sigma E_x + \frac{\sigma^2 B_o}{en_e} E_z - \sigma wB_o + \frac{\sigma^2 B_o^2}{en_e} u,$$

$$J_x \left(1 + m^2 \right) = \sigma \left[E_x + m(E_z + uB_o) - wB_o \right],$$

$$J_x = \frac{\sigma}{1 + m^2} \left[E_x - wB_o + m(E_z + uB_o) \right], \tag{A.25}$$

and applying Equation (A.24)-$\frac{\sigma B_o}{en_e}$Equation (A.22) reads,

$$J_z \left[1 + \left(\frac{\sigma B_o}{en_e} \right)^2 \right] = \sigma E_z + \sigma u B_o - \frac{\sigma^2 B_o}{en_e} E_x + \frac{\sigma^2 B_o^2}{en_e} w,$$

$$J_z \left(1 + m^2 \right) = \sigma \left[E_z - m(E_x - wB_o) + uB_o \right],$$

$$J_z = \frac{\sigma}{1 + m^2} \left[E_z + uB_o - m(E_x - wB_o) \right], \tag{A.26}$$

where it is assumed that

$$\mathbf{E} = \begin{pmatrix} E_x \\ E_y \\ E_z \end{pmatrix} = \begin{pmatrix} 0 \\ 0 \\ 0 \end{pmatrix},$$

therefore, the Equations (A.25)–(A.26) produces,

$$J_x = \frac{\sigma B_o}{1 + m^2}(mu - w), \tag{A.27}$$

$$J_z = \frac{\sigma B_o}{1 + m^2}(u + mw), \tag{A.28}$$

where $m = \frac{\sigma B_o}{en_e}$.

The governing flow model incorporating with the Hall current can be written as

$$\frac{\partial u}{\partial x} + \frac{\partial v}{\partial y} = 0, \tag{A.29}$$

$$u\frac{\partial u}{\partial x} + v\frac{\partial u}{\partial y} = \frac{\mu + \chi}{\rho} \left(\frac{\partial^2 u}{\partial y^2} \right) + g\beta_T \left(T - T_\infty \right) + \frac{\chi}{\rho} \left(\frac{\partial \omega}{\partial y} \right) - \frac{B_o}{\rho} J_z, \tag{A.30}$$

$$u\frac{\partial w}{\partial x} + v\frac{\partial w}{\partial y} = \frac{\mu + \chi}{\rho} \left(\frac{\partial^2 w}{\partial y^2} \right) + \frac{B_o}{\rho} J_x, \tag{A.31}$$

$$u\frac{\partial \omega}{\partial x} + v\frac{\partial \omega}{\partial y} = \frac{\gamma}{\rho j} \left(\frac{\partial^2 \omega}{\partial y^2} \right) - \frac{\chi}{\rho j} \left(2\omega + \frac{\partial u}{\partial y} \right), \tag{A.32}$$

$$u\frac{\partial T}{\partial x} + v\frac{\partial T}{\partial y} = \frac{k}{\rho c_p} \left(\frac{\partial^2 T}{\partial y^2} \right), \tag{A.33}$$

with pertaining boundary conditions

$$\left. \begin{array}{l} u = su_w(x) + u_{\text{slip}}; v = v_o; w = 0; \omega = -n\frac{\partial u}{\partial y}; k\frac{\partial T}{\partial y} = -h_s T \text{ at } y = 0, \\ u \to 0; \ w \to 0; \ \omega \to 0; \ T \to T_\infty \text{ as } y \to \infty. \end{array} \right\} \tag{A.34}$$

Now transform the system of Equations (A.29)–(A.34) by using the same similarity

variables as defined in Equation (A.6) along with the following additional similarity variable:

$$w = axg(\eta)$$

As usual Equation (A.29) is automatically satisfied by velocity components and Equation (A.30) can be written as

$$\frac{\partial \psi}{\partial y} \frac{\partial}{\partial x} \left(\frac{\partial \psi}{\partial y} \right) - \frac{\partial \psi}{\partial x} \frac{\partial}{\partial y} \left(\frac{\partial \psi}{\partial y} \right) = \frac{\mu + \chi}{\rho} \frac{\partial^2}{\partial y^2} \left(\frac{\partial \psi}{\partial y} \right) + g\beta_T \left(T - T_\infty \right) + \frac{\chi}{\rho}$$
$$\left(\frac{\partial \omega}{\partial y} \right) - \frac{\sigma B_o^2}{\rho(1 + m^2)} \left(\frac{\partial \psi}{\partial y} + m \ axg(\eta) \right),$$

$$\frac{\partial \ \sqrt{x\nu u_w(x)}f(\eta)}{\partial \ \eta\sqrt{\nu/a}} \frac{\partial}{\partial x} \left(\frac{\partial\sqrt{x\nu u_w(x)}f(\eta)}{\partial \ \eta\sqrt{\nu/a}} \right) - \frac{\partial \ \sqrt{x\nu u_w(x)}f(\eta)}{\partial x} \frac{\partial}{\partial \ \eta\sqrt{\nu/a}}$$
$$\left(\frac{\partial \ \sqrt{x\nu u_w(x)}f(\eta)}{\partial \ \eta\sqrt{\nu/a}} \right) = \frac{\mu + \chi}{\rho} \frac{\partial^2}{\partial(\eta^2\nu/a)} \left(\frac{\partial \ \sqrt{x\nu u_w(x)}f(\eta)}{\partial \ \eta\sqrt{\nu/a}} \right) + g\beta_T\theta T_\infty +$$
$$\frac{\chi}{\rho} \left(\frac{\partial \ \sqrt{x u_w(x)}(\nu)^{-\frac{1}{2}}ah(\eta)}{\partial\eta\sqrt{\nu/a}} \right) - \frac{\sigma B_o^2}{\rho(1 + m^2)} \left(\frac{\partial\sqrt{x\nu u_w(x)}f(\eta)}{\partial\eta\sqrt{\nu/a}} + maxg(\eta) \right),$$

$$axf'af' - \sqrt{a\nu}f\sqrt{a/\nu}axf'' = \frac{\mu}{\rho}(1 + K)a/\nu axf''' + g\beta_T\theta T_\infty + \frac{\chi}{\rho}ax\frac{a}{\nu}h' -$$
$$\frac{\sigma B_o^2}{\rho(1 + m^2)}(axf' + maxg),$$

$$a^2x(f')^2 - a^2xff'' = (1 + K)a^2xf''' + g\beta_T\theta T_\infty + a^2xKh' - \frac{\sigma B_o^2 ax}{\rho(1 + m^2)}(f' + mg),$$

$$(f')^2 - ff'' = (1 + K)f''' + \frac{g\beta_T T_\infty}{a^2x}\theta + Kh' - \frac{\sigma B_o^2}{a\rho(1 + m^2)}(f' + mg),$$

$$(f')^2 - ff'' = (1 + K)f''' + \lambda\theta + Kh' - \frac{M}{(1 + m^2)}(f' + mg),$$

$$(1 + K)f''' - (f')^2 + ff'' + \lambda\theta + Kh' - \frac{M}{(1 + m^2)}(f' + mg) = 0. \qquad \text{(A.35)}$$

Now Equation (A.31) can be nondimensionalized as

$$\frac{\partial \psi}{\partial y} \frac{\partial w}{\partial x} - \frac{\partial \psi}{\partial x} \frac{\partial w}{\partial y} = \frac{\mu + \chi}{\rho} \left(\frac{\partial^2 w}{\partial y^2} \right) + \frac{\sigma B_o^2}{\rho(1 + m^2)}(m\frac{\partial \psi}{\partial y} - w),$$

$$\frac{\partial\sqrt{x\nu u_w(x)}f(\eta)}{\partial\eta\sqrt{\nu/a}}\frac{\partial axg(\eta)}{\partial x} - \frac{\partial\sqrt{x\nu u_w(x)}f(\eta)}{\partial x}\frac{\partial axg(\eta)}{\partial\eta\sqrt{\nu/a}} =$$

$$\frac{\mu+\chi}{\rho}\left(\frac{\partial^2 axg(\eta)}{\partial\eta^2\nu/a}\right) + \frac{\sigma B_o^2}{\rho(1+m^2)}(m\frac{\partial\sqrt{x\nu u_w(x)}f(\eta)}{\partial\eta\sqrt{\nu/a}} - axg(\eta)),$$

$$axf' \, ag - \sqrt{a\nu}f \, \sqrt{a/\nu}axg' = (1+K)a^2xg'' + \frac{\sigma B_o^2}{\rho(1+m^2)}ax(mf'-g),$$

$$f'g - fg' = (1+K)g'' + \frac{\sigma B_o^2}{a\rho(1+m^2)}(mf'-g),$$

$$(1+K)g'' - f'g + fg' + \frac{M}{1+m^2}(mf'-g). \quad \text{(A.36)}$$

Moreover, Equations (A.32)–(A.34) are already nondimensionalized as Equations (A.8)–(A.10) along with the transverse velocity boundary conditions $g = 0$ and $g \to 0$ when $\eta = 0$ and $\eta \to 0$, respectively.

A.4 Nondimensionalization of Heat and Mass Transfer Model

This section concerns with the nondimensionalization of the heat and mass transfer micropolar fluid flow over a stretching/shrinking sheet in the presence of first order homogeneous chemical reaction with second order slip and the Newtonian heating at the boundary. The system of Equations $(6.1) - (6.6)$ can be rewritten as below:

$$\frac{\partial u}{\partial x} + \frac{\partial v}{\partial y} = 0, \quad \text{(A.37)}$$

$$u\frac{\partial u}{\partial x} + v\frac{\partial u}{\partial y} = \frac{\mu+\chi}{\rho}\left(\frac{\partial^2 u}{\partial y^2}\right) + \frac{\chi}{\rho}\left(\frac{\partial\omega}{\partial y}\right) + g\beta_T\left(T - T_\infty\right) + g\beta_C\left(C - C_\infty\right),$$

$$\text{(A.38)}$$

$$u\frac{\partial\omega}{\partial x} + v\frac{\partial\omega}{\partial y} = \frac{\gamma}{\rho j}\left(\frac{\partial^2\omega}{\partial y^2}\right) - \frac{\chi}{\rho j}\left(2\omega + \frac{\partial u}{\partial y}\right), \quad \text{(A.39)}$$

$$u\frac{\partial T}{\partial x} + v\frac{\partial T}{\partial y} = \frac{k}{\rho c_p}\left(\frac{\partial^2 T}{\partial y^2}\right), \quad \text{(A.40)}$$

$$u\frac{\partial C}{\partial x} + v\frac{\partial C}{\partial y} = D_m\left(\frac{\partial^2 C}{\partial y^2}\right) - \xi\left(C - C_\infty\right), \quad \text{(A.41)}$$

with boundary conditions

$$u = su_w(x) + u_{\text{slip}}; \; v = v_o; \; \omega = -n\frac{\partial u}{\partial y}; \; k\frac{\partial T}{\partial y} = -h_s T; \; C = C_w \text{ at } y = 0, \left.\right\}$$
$$u \to 0; \; \omega \to 0; \; T \to T_\infty; \; C \to C_\infty \text{ as } y \to \infty. \left.\right\}$$
$$(A.42)$$

The system of Equations (A.37)–(A.42) can be nondimensionalized by using the same similarity variables as defined in Equation (A.6) in addition with the new similarity variable

$$\phi = \frac{C - C_\infty}{C_w - C_\infty}.$$

Now, Equation (A.37) is obvious with the help of similarity variables and Equation (A.38) can be written as

$$\frac{\partial \psi}{\partial y}\frac{\partial}{\partial x}\left(\frac{\partial \psi}{\partial y}\right) - \frac{\partial \psi}{\partial x}\frac{\partial}{\partial y}\left(\frac{\partial \psi}{\partial y}\right) = \frac{\mu + \chi}{\rho}\frac{\partial^2}{\partial y^2}\left(\frac{\partial \psi}{\partial y}\right) + \frac{\chi}{\rho}\left(\frac{\partial \omega}{\partial y}\right) + g\beta_T\left(T - T_\infty\right) +$$
$$g\beta_c\left(C - C_\infty\right),$$
$$\frac{\partial \sqrt{x\nu u_w(x)}f(\eta)}{\partial \eta\sqrt{\nu/a}}\frac{\partial}{\partial x}\left(\frac{\partial\sqrt{x\nu u_w(x)}f(\eta)}{\partial \eta\sqrt{\nu/a}}\right) - \frac{\partial \sqrt{x\nu u_w(x)}f(\eta)}{\partial x}\frac{\partial}{\partial \eta\sqrt{\nu/a}}$$
$$\left(\frac{\partial \sqrt{x\nu u_w(x)}f(\eta)}{\partial \eta\sqrt{\nu/a}}\right) = \frac{\mu + \chi}{\rho}\frac{\partial^2}{\partial(\eta^2\nu/a)}\left(\frac{\partial \sqrt{x\nu u_w(x)}f(\eta)}{\partial \eta\sqrt{\nu/a}}\right) + g\beta_T\theta T_\infty +$$
$$\frac{\chi}{\rho}\left(\frac{\partial \sqrt{xu_w(x)}(\nu)^{-\frac{1}{2}}ah(\eta)}{\partial\eta\sqrt{\nu/a}}\right) + g\beta_c\phi\left(C_w - C_\infty\right),$$

$$a^2x(f')^2 - a^2xff'' = (1+K)a^2xf''' + g\beta_T\theta T_\infty + a^2xKh' + g\beta_c\phi\left(C_w - C_\infty\right),$$
$$(f')^2 - ff'' = (1+K)f''' + Kh' + \frac{g\beta_T T_\infty}{a^2x}\theta + \frac{g\beta_c\phi}{a^2x}\left(C_w - C_\infty\right),$$
$$(f')^2 - ff'' = (1+K)f''' + Kh' + \lambda\theta + \lambda\Lambda\phi,$$
$$(1+K)f''' - (f')^2 + ff'' + Kh' + \lambda\theta + \lambda\Lambda\phi. \qquad (A.43)$$

Moreover, Equations (A.39)–(A.40) can be nondimensionalized as reported in section A.1. However, Equation (A.41) reads as

$$\frac{\partial \psi}{\partial y}\frac{\partial C}{\partial x} - \frac{\partial \psi}{\partial x}\frac{\partial C}{\partial y} = D_m\left(\frac{\partial^2 C}{\partial y^2}\right) - \xi\left(C - C_\infty\right),$$

$$\frac{\partial \sqrt{x\nu u_w(x)}f(\eta)}{\partial \eta \sqrt{\nu/a}}\frac{\partial \left(\phi\left(C_w - C_\infty\right) + C_\infty\right)}{\partial x} - \frac{\partial \sqrt{x\nu u_w(x)}f(\eta)}{\partial x}\frac{\partial \left(\phi\left(C_w - C_\infty\right) + C_\infty\right)}{\partial \eta \sqrt{\nu/a}}$$

$$= D_m \left(\frac{\partial^2 \left(\phi\left(C_w - C_\infty\right) + C_\infty\right)}{\partial \eta^2 \nu/a}\right) - \xi\phi\left(C_w - C_\infty\right),$$

$$0 - af\phi'\left(C_w - C_\infty\right) = \frac{D_m}{\nu}a\phi''\left(C_w - C_\infty\right) - \xi\phi\left(C_w - C_\infty\right),$$

$$-f\phi' = \frac{D_m}{\nu}\phi'' - \frac{\xi}{a}\phi,$$

$$-f\phi' = \frac{1}{Sc}\phi'' - C_m\phi,$$

$$\phi'' + Scf\phi' - C_m Sc\phi = 0, \tag{A.44}$$

where, the new dimensionless parameters are $\Lambda = \beta_c(C_w - C_\infty)/\beta_T T_\infty$, $Sc = \nu/D_m$ and $C_m = \xi/a$. Furthermore, the boundary conditions are same as defined in Equation (A.10) in addition to the $\phi = 1$ and $\phi \to 0$ when $\eta = 0$ and $\eta \to 0$, respectively.

In the results and discussion sections, we used the percentage change and percentage difference formulas which are as below follows:

$$\text{Percentage Change} = \frac{\text{Final value} - \text{Initial value}}{\text{Initial value}} \times 100,$$

$$\text{Percentage Difference} = \frac{2 \times (\text{Final value} - \text{Initial value})}{\text{Final value} + \text{Initial value}} \times 100.$$

Appendix B

Copyright Permission

In this appendix, we presents the proof of copyright permission from those journals who are under creative common attribution or not. In correspondence with chapter 3 to 6, the hierarchical order of permission to re-produce 100% published material of this research into current thesis is demonstrated below.

Copyright Transfer Agreement

Please read the terms of this agreement, and send back a scanned copy of the signed original.

Article entitled:

Heat source/sink and Newtonian heating effects on Convective micropolar fluid flow over a stretching/shrinking sheet with slip flow model

Author/s:

M. Kamran

Corresponding author (if more than one author):

M. Kamran

Journal Name:

International Journal of Heat and Technology

Publisher:

International Information and Engineering Technology Association

1. Copyright Assignment
The author hereby grants the Publisher the exclusive license for commercial use of above article throughout the world, in any form, in any language, for the full term of copyright, effective upon acceptance for publication.

2. Author's Warranties
The author warrants that the article is original, written by stated author/s, has not been published before and it will not be submitted anywhere else for publication prior to acceptance/rejection by the Publisher, contains no unlawful statements, does not infringe the rights of others, is subject to copyright that is vested exclusively in the author and free of any third party rights, and that any necessary written permissions to quote from other sources have been obtained by the author/s.

3. User rights
This article, if accepted, will be an open access article distributed under the terms and conditions of the Creative Commons Attribution License (http://creativecommons.org/licenses/by/3.0/). Publisher will insert the following note at the end of the published text: © 2018 by the authors; licensee IIETA, Edmonton, Canada. This article is an open-access article distributed under the terms and conditions of the Creative Commons Attribution License (http://creativecommons.org/licenses/by/3.0/).

4. Rights of Authors
Authors retain the following rights:
- all proprietary rights relating to the article, other than copyright, such as patent rights,
- the right to use the substance of the article in future own works, including lectures and books,
- the right to reproduce this article for own purposes, provided the copies are not offered for sale.

An author may self-archive an author-created version of his/her article on his/her own website and or in his/her institutional repository. He/she may also deposit this version on his/her funder's or funder's designated repository at the funder's request or as a result of a legal obligation, provided it is not made publicly available until 12 months after official publication. Furthermore, the author may only post his/her version provided acknowledgement is given to the original source of publication and a link is inserted to the published article on http://www.iieta.org. The link must be accompanied by the following text: "The original publication is available also at http://www.iieta.org". He/she may use the Publisher's PDF version, which is posted on http://www.iieta.org, for the purpose of self-archiving or deposit. Any other use of the article requires permission from the Publisher.

5. Co-Authorship
If the article was prepared jointly with other authors, the signatory of this form warrants that he/she has been authorized by all co-authors to sign this agreement on their behalf, and agrees to inform his/her co-authors of the terms of this agreement.

6. Publication Fee

There is no publication fee.

7. Termination

This agreement can be terminated by the author or the Publisher upon two months' notice where the other party has materially breached this agreement and failed to remedy such breach within a month of being given the terminating party's notice requesting such breach to be remedied. No breach or violation of this agreement will cause this agreement or any license granted in it to terminate automatically or affect the definition of the Publisher. After the lapse of forty (40) years of the date of this agreement, this agreement can be terminated without cause by the author or the Publisher upon two years' notice. The author and the Publisher may agree to terminate this agreement at any time. This agreement or any license granted in it cannot be terminated otherwise than in accordance with this section 6.

8. Royalties

This agreement entitles the author to no royalties or other fees. To such extent as legally permissible, the author waives his or her right to collect royalties relative to the article in respect of any use of the article by the Publisher or its sublicense.

9. Miscellaneous

The Publisher will publish the article (or have it published) in the Journal, if the article's editorial process is successfully completed and the Publisher or its sublicense has become obligated to have the article published. The Publisher may conform the article to a style of punctuation, spelling, capitalization and usage that it deems appropriate. The author acknowledges that the article may be published so that it will be publicly accessible and such access will be free of charge for the readers. The Publisher will be allowed to sublicense the rights that are licensed to it under this agreement. This agreement will be governed by the laws of Canada.

10. Scope of the Commercial License

The exclusive right and license granted under this agreement to the Publisher for commercial use is as follows:

a.   to prepare, reproduce, manufacture, publish, distribute, exhibit, advertise, promote, license and sub- license printed and electronic copies of the article, through the Internet and other means of data transmission now known or later to be developed; the foregoing will include abstracts, bibliographic information, illustrations, pictures, indexes and subject headings and other proprietary materials contained in the article,

b.   to exercise, license, and sub-license others to exercise subsidiary and other rights in the article, including the right to photocopy, scan or reproduce copies thereof, to reproduce excerpts from the article in other works, and to reproduce copies of the article as part of compilations with other works, including collections of materials made for use in classes for instructional purposes, customized works, electronic databases, document delivery, and other information services, and publish, distribute, exhibit and license the same.

Where this agreement refers to a license granted to the Publisher in this agreement as exclusive, the author commits not only to refrain from granting such license to a third party but also to refrain from exercising the right that is the subject of such license otherwise than by performing this agreement.

The Publisher will be entitled to enforce in respect of third parties, to such extent as permitted by law, the rights licensed to it under this agreement.

Corresponding author's signature:

M. Kamran

Name printed:

M.kamran

Date:

11/05/2018

RE: Request for permission to 100% re-produce my publication into my thesis

Rights <rights@wspc.com>

Tue 8/21/2018 9:44 AM

To:Muhammad Kamran <muhammad.kamran@curtin.edu.au>;

Dear Muhammad Kamran

You can include the author-final-version (not publisher version) of the article into your thesis, provided that full credit given to the original source in the following format:

Title of the Work, Author (s) and/or Editor(s) Name (s), Title of the Journal, Vol and Issue No., Copyright @ year and name of the publisher

With regards,
Tu Ning

From: Muhammad Kamran <muhammad.kamran@curtin.edu.au>
Sent: Monday, 20 August, 2018 8:31 PM
To: Rights <rights@wspc.com>
Subject: Request for permission to 100% re-produce my publication into my thesis

Dear Officer,

I hope this email finds you well. Recently, my manuscript is accepted for publication in [International Journal of Modern Physics C](https://).

The digital object identifier of my accepted manuscript is https://doi.org/10.1142/S0129183118500900 .

I kindly ask you, under what conditions, will I be able to 100% re-produce (copy the material of this paper and paste it into my thesis) my accepted paper into my thesis?

I am waiting for your nice reply.

Sincerely and Kind Regards!

Muhammad Kamran

First and Corresponding author.

PhD Student (Applied Mathematics)

_____

School of Electrical Engineering, Computing and Mathematical Sciences

Curtin University

Bentley 6102, Perth Western Australia.

Building | 314 Office | 446-7

Tel | +61 8 9266 2942

Email | muhammad.kamran@curtin.edu.au
Web | https:/curtin.edu.au/

Re: [180712-000385]Can I 100% re-produce my published work in my thesis? [180712-000385]

Researcher Support <support@elsevier.com>

Thu 7/12/2018 9:35 AM

To:Muhammad Kamran <muhammad.kamran@curtin.edu.au>;

Dear Dr. Kamran,

Thank you for contacting us via Chat; a copy of our conversation is below for your reference.

Kind regards,

Ma. Fatima Erika N. Dioneda
Researcher Support
ELSEVIER

As a founding and driving partner of Research4Life, we help bridge the digital divide by contributing content, expertise and funds. Find out how we provide access to journals, articles and online databases.

For assistance, please visit our Customer Support site where you can search for solutions on a range of topics and find answers to frequently asked questions.

From: Ma. Fatima Erika Dioneda
Date: 12/07/2018 01.16 AM

Hi, my name is Ma. Fatima Erika Dioneda. How may I help you?
Muhammad Kamran: Hello Fatima.
Ma. Fatima Erika Dioneda: Hello Dr. Kamran
Muhammad Kamran: I am an author of
Muhammad Kamran: https://www.sciencedirect.com/science/article/pii/S0997754618300566
Muhammad Kamran: this published article.
Muhammad Kamran: I want to 100% re-produce this article in my thesis.
Should I require to get permission from Elsevier ?
Ma. Fatima Erika Dioneda: Thank you for your inquiry
Ma. Fatima Erika Dioneda: I would like to inform you that you can use your article for your thesis. But please be advised that you can only use the accepted version and not the final version.
Muhammad Kamran: I am not going to put the .pdf that is generated by Elsevier journal. I will 100 % copy/past the text in my thesis as it is according to thesis format style.
Is that OK ?
Ma. Fatima Erika Dioneda: Yes, but please ensure that the text that you will copy and paste to your thesis is the accepted version of your article and not the final version
Muhammad Kamran: Text in the accepted and final versions is same.
Ma. Fatima Erika Dioneda: Ok. Just use the accepted one.
Muhammad Kamran: Thanks. It means that I do not need to get any kind of permission from European Journal of Mechanics - B/Fluids. Am I right ?
Ma. Fatima Erika Dioneda: Yes
Ma. Fatima Erika Dioneda: As long as you will not publish your published article elsewhere
Muhammad Kamran: Ofcourse.

Muhammad Kamran: Thank you Fatima for your useful information.
Could you please send me this chat on my email address?
Ma. Fatima Erika Dioneda: Yes sure
Muhammad Kamran: Kind Regards !
Ma. Fatima Erika Dioneda: Will send you a follow up e-mail containing this chat transcript
Ma. Fatima Erika Dioneda: Is there anything else I can help you with today?
Muhammad Kamran: No, Thanks. It was the only question that I have in my mind.
Ma. Fatima Erika Dioneda: It was a pleasure assisting you today. If you require any further assistance please contact us again. To close this chat session, please click the Close button in the top corner of this chat window.
Muhammad Kamran: Sure, I am waiting for this chat history.
Have a good time.
'Muhammad Kamran' disconnected ('Concluded by End-user').

October 25, 2018

Assoc. Prof. Benchawan Wiwatanapataphee
b.wiwatanapataphee@curtin.edu.au
Office Phone: +61 8 9266 2405

Faculty of Science and Engineerin, Building 314
Department of Mathematics and Statistics
Curtin University of Technology
GPO Box U1987, Perth
WA 6845 Australia.

To Whom It May Concern

Subject: Percentage of paper contributions
I worked as a co-author for the following three papers:

Paper 1 Muhammad Kamran, Benchawan Wiwatanapataphee, Radiative magneto-micropolar fluid flow over a stretching/shrink sheet with slip flow model, Journal of Physics: Conference series, ESTCON 2018, 13-15 Aug. 2018 Kuala Lumpur Malaysia (accepted/presented): In press.

Paper 2 Muhammad Kamran, Benchawan Wiwatanapataphee and Kuppalapalle Vajravelu, Hall current, Newtonian heating and second order slip effects on convective magneto-micropolar fluid flow over a sheet. International Journal of Modern Physics C, Vol. 29, No. 9 (2018) 1850090 (24 pages).
https://doi.org/10.1142/S0129183118500900

Paper 3 Muhammad Kamran, Benchawan Wiwatanapataphee, Chemical reaction and Newtonian heating effects on steady convection flow of a micropolar fluid with second order slip at the boundary. European Journal of Mechanics-B/Fluids, 71(2018):138-150. https://doi.org/10.1016/j.euromechflu.2018.04.005

The main reason for writing this letter is to address Mr. Kamran's responsible contribution. He developed mathematical models and numerical algorithms, and simulated numerical solutions. He also wrote all manuscripts and contributed to the manuscript revising processes, and the overall quality of the manuscripts. I inform his contribution of 70% of paper 1, 60% of paper 2 and 70% of paper 3.

We are thankful for your consideration.

Sincerely and Kind Regards !

Benchawan Wiwatanapataphee

UNIVERSITY OF CENTRAL FLORIDA

Department of Mathematics

4000 Central Florida Blvd.

P.O. Box 161364

Orlando, FL 32816-1364

October 24, 2018

To whom it may concern,

I am writing to address Mr. Muhammad Kamran's responsible contribution. He developed mathematical model and numerical algorithm, and simulated numerical solutions. He also wrote the first draft of the manuscript and contributed to the manuscript revising processes, and the overall quality of the manuscripts.

I am happy to inform you that his contribution of 60% in the publication "Muhammad Kamran, Benchawan Wiwatanapataphee and Kuppalapalle Vajravelu, Hall current, Newtonian heating and second order slip effects on convective magneto-micropolar fluid flow over a sheet, International Journal of Modern Physics C, Vol. 29, No. 9 (2018) 1850090 (24 pages). https://doi.org/10.1142/S0129183118500900

Sincerely,

Kuppalapalle Vajravelu
Professor of Mathematics
University of Central Florida, Orlando, Florida 32816 - 1364, USA
Ph. # (407) 823 – 5089; Fax # (407) 823 - 6253
Email Address: kuppalapalle.vajravelu@ucf.edu

Bibliography

[1] Eringen A. C., "Simple microfluids ". International Journal of Engineering Science 2, (1964): 205–217.

[2] Eringen A. C., "Theory of micropolar fluids ". Purdue University Lafayette in School of Aeronautics and Astronautics, USA, (1965): Technical Report 27.

[3] Eringen A. C., "Theory of micropolar fluids". Journal of Mathematics and Mechanics, (1966): 1-18.

[4] Eringen A. C., "Theory of thermomicrofluids ". Journal of Mathematical Analysis and Applications 38, (1972): 480–496.

[5] Eringen, A. C., Microcontinuum field theories: I. Foundations and solids. Springer Science & Business Media, 1999.

[6] Eringen A. C., Microcontinuum Field Theories: II Fluent Media, Springer Science & Business Media, New York, 2001.

[7] Grzegorz L., Micropolar Fluids: Theory and Applications (Springer Science & Business Media, New York, 1999).

[8] Latif M. J., Heat convection. Springer-Verlag Berlin Heidelberg, 2009.

[9] Willson A. J., "Boundary layers in micropolar liquids". In Mathematical Proceedings of the Cambridge Philosophical Society: Cambridge University Press 67, no. 2 (1970): 469-476.

[10] Kummerer H., "Similar laminar boundary layers in incompressible micropolar fluids". Rheologica Acta 16, no. 3 (1977): 261-265.

[11] Wu L., "A slip model for rarefied gas flows at arbitrary Knudsen number ". Applied Physics Letters 93, no. 25 (2008): 253103.

[12] Ariman T., and Cakmak A. S., "Some basic viscous flows in micropolar fluids". Rheologica Acta 7, no. 2 (1968): 236-242.

[13] Kazakia Y., and Ariman T., "Heat-conducting micropolar fluids". Rheologica Acta 10, no. 3 (1971): 319-325.

[14] Ariman T., Cakmak A. S., and Hill L. R., "Flow of micropolar fluids between two concentric cylinders". The Physics of Fluids 10, no. 12 (1967): 2545-2550.

[15] Sastry V. U. K., and Maiti G., "Numerical solution of combined convective heat transfer of micropolar fluid in an annulus of two vertical pipes". International Journal of Heat and Mass Transfer 19, no. 2 (1976): 207-211.

[16] Ariman T., Turk M. A., and Sylvester, N. D., "On steady and pulsatile flow of blood". Journal of Applied Mechanics 41, no. 1 (1974): 1-7.

[17] Migun N. P., "Experimental method of determining parameters characterizing the microstructure of micropolar liquids". Journal of Engineering Physics 41, no. 2 (1981): 832-835.

[18] Kolpashchikov V. L., Migun N. P., and Prokhorenko P. P., "Experimental determination of material micropolar fluid constants". International Journal of Engineering Science 21, no. 4 (1983): 405-411.

[19] Bakr A. A., and Chamkha A. J., "Oscillatory Free Convection of a Micropolar Rotating Fluid on a Vertical Plate with Variable Heat Flux and Thermal Radiation". Heat Transfer Research 48, no. 2 (2017): 139-159.

[20] Ashraf M., and Ashraf M. M., "MHD stagnation point flow of a micropolar fluid towards a heated surface". Applied Mathematics and Mechanics 32, no. 1 (2011): 45-54.

[21] Pal D., and Gopinath M. "Thermal radiation and MHD effects on boundary layer flow of micropolar nanofluid past a stretching sheet with non-uniform heat source/sink". International Journal of Mechanical Sciences 126, (2017): 308-318.

[22] Sui J., Peng Z., Zhengdong C., Liancun Z., and Xinxin Z., "A novel investigation of a micropolar fluid characterized by nonlinear constitutive diffusion model in boundary layer flow and heat transfer". Physics of Fluids 29, no. 2 (2017): 023105.

[23] Asad M., Bin C., and Abuzar G., "Hydromagnetic Hiemenz flow of micropolar fluid over a nonlinearly stretching/shrinking sheet: Dual solutions by using Chebyshev Spectral Newton Iterative Scheme". Journal of Magnetism and Magnetic Materials 416, (2016): 329-334.

[24] Gibanov N. S., Sheremet M. A., and Pop I., "Natural convection of micropolar fluid in a wavy differentially heated cavity ". Journal of Molecular Liquids 221, (2016): 518-525.

[25] Muthtamilselvan M., Periyadurai K., and Deog H. D., "Impact of nonuniform heated plate on double-diffusive natural convection of micropolar fluid in a square cavity with Soret and Dufour effects". Advanced Powder Technology 29, no. 1 (2018): 66-77.

[26] Miroshnichenko I. V., Sheremet M. A., Pop I., and Anuar I., "Convective heat transfer of micropolar fluid in a horizontal wavy channel under the local heating ". International Journal of Mechanical Sciences 128, (2017): 541-549.

[27] Chang C. L., "Numerical simulation for natural convection of micropolar fluids flow along slender hollow circular cylinder with wall conduction effect ". Communications in Nonlinear Science and Numerical Simulation 13, no. 3 (2008): 624-636.

[28] Cheng C. Y., "Natural convection boundary layer flow of a micropolar fluid over a vertical permeable cone with variable wall temperature ". International Communications in Heat and Mass Transfer 38, no. 4 (2011): 429-433.

[29] Kelson N. A., and Farrell T. W., "Micropolar flow over a porous stretching sheet with strong suction or injection". International Communications in Heat and Mass Transfer 28, no. 4 (2001): 479-488.

[30] Kelson N. A., and Andre D., "Effect of surface conditions on flow of a micropolar fluid driven by a porous stretching sheet". International Journal of Engineering Science 39, no. 16 (2001): 1881-1897.

[31] Bhargava R., Lokendra K., and Harmindar S. T., "Finite element solution of mixed convection micropolar flow driven by a porous stretching sheet". International Journal of Engineering Science 41, no. 18 (2003): 2161-2178.

[32] Ahmed S. E., Ahmed K. H., Mohammed H. A., and Sivasankaran S., "Boundary layer flow and heat transfer due to permeable stretching tube in the presence of heat source/sink utilizing nanofluids ". Applied Mathematics and Computation 238, (2014): 149-162.

[33] Turkyilmazoglu M., "A note on micropolar fluid flow and heat transfer over a porous shrinking sheet". International Journal of Heat and Mass Transfer 72, (2014): 388-391.

[34] Turkyilmazoglu M., "Flow of a micropolar fluid due to a porous stretching sheet and heat transfer". International Journal of Non-Linear Mechanics 83, (2016): 59-64.

[35] Rahman, M. M. and Sattar M. A., "Magnetohydrodynamic convective flow of a micropolar fluid past a continuously moving vertical porous plate in the presence of heat generation/absorption." Journal of Heat Transfer 128, no. 2 (2006): 142-152.

[36] Vajravelu, K., and Hadjinicolaou A., "Heat transfer in a viscous fluid over a stretching sheet with viscous dissipation and internal heat generation." International Communications in Heat and Mass Transfer 20, no. 3 (1993): 417-430.

[37] Ziabakhsh, Z., Domairry G., and Bararnia H., "Analytical solution of non-Newtonian micropolar fluid flow with uniform suction/blowing and heat generation ". Journal of the Taiwan Institute of Chemical Engineers 40, no. 4 (2009): 443-451.

[38] Damseh, Rebhi A., Al-Odat M. Q., Chamkha A. J., and Benbella Shannak A., "Combined effect of heat generation or absorption and first-order chemical reaction on micropolar fluid flows over a uniformly stretched permeable surface ". International Journal of Thermal Sciences 48, no. 8 (2009): 1658-1663.

[39] Mohamed, R. A., and Abo-Dahab S. M., "Influence of chemical reaction and thermal radiation on the heat and mass transfer in MHD micropolar flow over a vertical moving porous plate in a porous medium with heat generation". International Journal of Thermal Sciences 48, no. 9 (2009): 1800-1813.

[40] Olajuwon, B. I., and Oahimire J. I., "Effect of thermal diffusion and chemical reaction on heat and mass transfer in an MHD micropolar fluid with heat generation". Afrika Matematika 25, no. 4 (2014): 911-931.

[41] Mishra, S. R., Pattnaik P. K., and Dash G. C., "Effect of heat source and double stratification on MHD free convection in a micropolar fluid ". Alexandria Engineering Journal 54, no. 3 (2015): 681-689.

[42] Ikbal M. A., Santabrata Chakravarty, and Prashanta Kumar Mandal, "Two-layered micropolar fluid flow through stenosed artery: effect of peripheral layer thickness ". Computers & Mathematics with Applications 58, no. 7 (2009): 1328-1339.

[43] Shit G. C., and Roy M., "Pulsatile flow and heat transfer of a magneto-micropolar fluid through a stenosed artery under the influence of body acceleration ". Journal of Mechanics in Medicine and Biology 11, no. 03 (2011): 643-661.

[44] Shit G. C., and Roy M., "Effect of induced magnetic field on blood flow through a constricted channel: An analytical approach ". Journal of Mechanics in Medicine and Biology 16, no. 3 (2016): 1650030.

[45] Lee J. D., and Eringen, A. C., "Boundary effects of orientation of nematic liquid crystals". The Journal of Chemical Physics 55, no. 9 (1971): 4509-4512.

[46] Chaudhary R. C., and Jain P., "Combined heat and mass transfer in magneto-micropolar fluid flow from radiate surface with variable permeability in slip-flow regime". ZAMM-Journal of Applied Mathematics and Mechanics, 87, no. 8-9 (2007): 549-563.

[47] Ishak A., Nazar R., and Pop I., "Magnetohydrodynamics (MHD) flow of a micropolar fluid towards a stagnation point on a vertical surface". Computers & Mathematics with Applications 56, no. 12s (2008): 3188-3194.

[48] Borrelli A., Giantesio G., and Patria M. C., "MHD orthogonal stagnation-point flow of a micropolar fluid with the magnetic field parallel to the velocity at infinity ". Applied Mathematics and Computation 264, (2015): 44-60.

[49] Siddiqa S., Faryad A., Begum N., Hossain M. A., and Gorla R. S. R., "Periodic magnetohydrodynamic natural convection flow of a micropolar fluid with radiation ". International Journal of Thermal Sciences 111, (2017): 215-222.

[50] Turkyilmazoglu M., "Mixed convection flow of Magnetohydrodynamics micropolar fluid due to a porous heated/cooled deformable plate: exact solutions ". International Journal of Heat and Mass Transfer 106, (2017): 127-134.

[51] Malga B. S., and Naikoti K., "Finite element analysis for unsteady MHD heat and mass transfer free convection flow of polar fluids past a vertical moving porous plate in a porous medium with heat generation and thermal diffusion."Journal of Naval Architecture and Marine Engineering 11, no. 1 (2014): 69-82.

[52] Bakr, A. A., Raizah Z. A. S., and Ahmed Elaiw M., "MHD micropolar fluid near a vertical plate with newtonian heating and thermal radiation in the presence of mass diffusion ". Pure and Applied Mathematics Journal 4, no. 3 (2015): 80-89.

[53] Naveed, M., Abbas Z., and Sajid M., "MHD Flow of Micropolar Fluid due to a Curved Stretching Sheet with Thermal Radiation". Journal of Applied Fluid Mechanics 9, no. 1 (2016): pp. 131-138.

[54] Khan Sabeel M., Hammad M., and Sunny D. A., "Chemical reaction, thermal relaxation time and internal material parameter effects on MHD viscoelastic fluid with internal structure using the Cattaneo-Christov heat flux equation". The European Physical Journal Plus 132, no. 8 (2017): 338.

[55] Amirat Y., and Kamel H., "Global weak solutions to the equations of thermal convection in micropolar fluids subjected to Hall current ". Nonlinear Analysis: Theory, Methods & Applications 102, (2014): 186-207.

[56] Eldahab A., Emad M., and El Aziz M. A., "Hall current and ohmic heating effects on mixed convection boundary layer flow of a micropolar fluid from a rotating cone with power-law variation in surface temperature ". International Communications in Heat and Mass Transfer 5, no. 31 (2004): 751-762.

[57] Neela R., and Tomar S. K., "Thermal convection problem of micropolar fluid subjected to hall current ". Applied Mathematical Modelling 34, no. 2 (2010): 508-519.

[58] Pal D., Babulal T., Shivakumara I. S., and Vajravelu K., "Effects of hall current and chemical reaction on oscillatory mixed convection-radiation of a micropolar fluid in a rotating system ". Chemical Engineering Communications 199, no. 8 (2012): 943-965.

[59] Yang X., and Lei W., "Multiple-relaxation-time lattice Boltzmann study of the magnetic field effects on natural convection of non-Newtonian fluids ". International Journal of Modern Physics C 28, no. 11 (2017): 1750138.

[60] Anika N. N., Hoque M. M., Hossain S. I., and Alam M. M, "Thermal diffusion effect on unsteady viscous MHD micropolar fluid flow through an infinite vertical plate with Hall and ion-slip current."Procedia Engineering 105 (2015): 160-166.

[61] Othman M. I. A., Ramadan Tantawi S., and Hilal M. I. M., "Hall current and gravity effect on magnetomicropolar thermoelastic medium with microtemperatures ". Journal of Thermal Stresses 39, no. 7 (2016): 751-771.

[62] Abdel-Wahed M., and Akl M., "Effect of hall current on MHD flow of a nanofluid with variable properties due to a rotating disk with viscous dissipation and nonlinear thermal radiation". AIP Advances 6, no. 9 (2016): 095308.

154

[63] Bilal M., Hussain S., and Sagheer M., "Boundary layer flow of magneto-micropolar nanofluid flow with Hall and ion-slip effects using variable thermal diffusivity". Bulletin of the Polish Academy of Sciences Technical Sciences 65, no. 3 (2017): 383-390.

[64] Mohamed R. A., and Abo-Dahab S. M., "Influence of chemical reaction and thermal radiation on the heat and mass transfer in MHD micropolar flow over a vertical moving porous plate in a porous medium with heat generation ". International Journal of Thermal Sciences 48, no. 9 (2009): 1800-1813.

[65] Chamkha A. J., Mohamed R. A., and Sameh E. A., "Unsteady MHD natural convection from a heated vertical porous plate in a micropolar fluid with Joule heating, chemical reaction and radiation effects". Meccanica 46, no. 2 (2011): 399-411.

[66] Bakr A. A., "Effects of chemical reaction on MHD free convection and mass transfer flow of a micropolar fluid with oscillatory plate velocity and constant heat source in a rotating frame of reference ". Communications in Nonlinear Science and Numerical Simulation 16, no. 2 (2011): 698-710.

[67] Hayat T., Shehzad S. A., and Qasim M., "Mixed convection flow of a micropolar fluid with radiation and chemical reaction ". International Journal for Numerical Methods in Fluids 67, no. 11 (2011): 1418-1436.

[68] Eldabe N. T., and Ouaf M. E., "Chebyshev finite difference method for heat and mass transfer in a hydromagnetic flow of a micropolar fluid past a stretching surface with Ohmic heating and viscous dissipation ". Applied Mathematics and Computation 177, no. 2 (2006): 561-571.

[69] Anuar I., Roslinda N., and Pop I., "Boundary-layer flow of a micropolar fluid on a continuously moving or fixed permeable surface". International Journal of Heat and Mass Transfer 50, no. 23-24 (2007): 4743-4748.

[70] Anuar I., "Thermal boundary layer flow over a stretching sheet in a micropolar fluid with radiation effect ". Meccanica 46, (2010): 367-373.

[71] Bachok N., Anuar I., and Roslinda N., "Flow and heat transfer over an unsteady stretching sheet in a micropolar fluid". Meccanica 46, no. 5 (2011): 935-942.

[72] Zheng L., Niu J., Zhang X., and Ma L., "Dual solutions for flow and radiative heat transfer of a micropolar fluid over stretching/shrinking sheet ". International Journal of Heat and Mass Transfer 55, no. 25-26 (2012): 7577-7586.

[73] Sherief H. H., Faltas M. S., and Shreen E. S., "Pipe flow of magneto-micropolar fluids with slip". Canadian Journal of Physics 95, no. 10 (2017): 885-893.

[74] Ezzat M. A., and Shreen E. S., "State space approach to magnetohydrodynamic flow of perfectly conducting micropolar fluid with stretch". International Journal for Numerical Methods in Fluids 70, no. 1 (2012): 114-134.

[75] Burgdorfer A., "The influence of the molecular mean free path on the performance of hydrodynamic gas lubricated bearings ". ASME Journal of Basic Engineering 81, (1959): 94–100.

[76] Hsia Y.T., and Domoto G.A., "An experimental investigation of molecular rarefaction effects in gas lubricated bearings at ultra-low clearances ". Journal of Lubrication Technology 105, no. 1 (1983): 120–129.

[77] Mitsuya Y., "Modified Reynolds equation for ultra-thin film gas lubrication using 1.5-order slip-flow model and considering surface accommodation coefficient". Journal of Tribology 115, no.2 (1993): 289–289.

[78] Fukui S, and Kaneko R., "A database for interpolation of Poiseuille flow rates for high Knudsen number lubrication problems ". Journal of Tribology 112, no. 1 (1990): 78–83.

[79] Fang T., Yao S., Zhang J., and Aziz A., "Viscous flow over a shrinking sheet with a second order slip flow model ". Communications in Nonlinear Science and Numerical Simulation 15, no. 7 (2010): 1831–1842.

[80] Nandeppanavar M. M., Vajravelu K., Abel M. S., and Siddalingappa M.N., "Second order slip flow and heat transfer over a stretching sheet with nonlinear Navier boundary condition ". International Journal of Thermal Sciences 58, (2012): 143–150.

[81] Singh, G., and Chamkha A. J., "Dual solutions for second-order slip flow and heat transfer on a vertical permeable shrinking sheet". Ain Shams Engineering Journal 4, no. 4 (2013): 911-917.

[82] Rosca N. C., and Pop I., "Mixed convection stagnation point flow past a vertical flat plate with a second order slip: heat flux case". International Journal of Heat and Mass Transfer 65, (2013): 102-109.

[83] Turkyilmazoglu M. "Heat and mass transfer of MHD second order slip flow ". Computers & Fluids 71, (2013): 426-434.

[84] Rosca, N. C., and Pop I., "Boundary layer flow past a permeable shrinking sheet in a micropolar fluid with a second order slip flow model". European Journal of Mechanics-B/Fluids 48, (2014): 115-122.

[85] Sharma R., Anuar I., and Pop I., "Stagnation point flow of a micropolar fluid over a stretching/shrinking sheet with second-order velocity slip ". Journal of Aerospace Engineering 29, no. 5 (2016): 04016025.

[86] Ibrahim W., "MHD boundary layer flow and heat transfer of micropolar fluid past a stretching sheet with second order slip". Journal of the Brazilian Society of Mechanical Sciences and Engineering 39, no. 3 (2017): 791-799.

[87] Kamran M., and Benchawan W., "Chemical reaction and Newtonian heating effects on steady convection flow of a micropolar fluid with second order slip at the boundary". European Journal of Mechanics-B/Fluids 71, (2018): 138-150.

[88] Ibrahim W., "Passive control of nanoparticle of micropolar fluid past a stretching sheet with nanoparticles, convective boundary condition and second-order slip". Journal of Process Mechanical Engineering 231, no. 4 (2017): 704-719.

[89] Merkin J. H., "Natural-convection boundary-layer flow on a vertical surface with Newtonian heating ". International Journal of Heat and Fluid Flow 15, no. 5 (1994): 392–398.

[90] Salleh M. Z., Nazar R., and Pop I., "Boundary layer flow and heat transfer over a stretching sheet with Newtonian heating ". Journal of the Taiwan Institute of Chemical Engineers 41, no. 6 (2010): 651-655.

[91] Salleh M. Z., Nazar R., Arifin N. M., Pop I., and Merkin J. H., "Forced-convection heat transfer over a circular cylinder with Newtonian heating."Journal of Engineering Mathematics 69, no. 1 (2011): 101-110.

[92] Chaudhary, R. C., and Preeti Jain, "An exact solution to the unsteady free-convection boundary-layer flow past an impulsively started vertical surface with Newtonian heating". Journal of Engineering Physics and Thermophysics 80, no. 5 (2007): 954-960.

[93] Salleh, M. Z., Nazar R., and Pop I., "Modeling of free convection boundary layer flow on a solid sphere with Newtonian heating."Acta Applicandae Mathematicae 112, no. 3 (2010): 263-274.

[94] Rajesh, V., and Ali C. J., "Unsteady convective flow past an exponentially accelerated infinite vertical porous plate with Newtonian heating and viscous

dissipation". International Journal of Numerical Methods for Heat & Fluid Flow 24, no. 5 (2014): 1109-1123.

[95] Liao S.J., The proposed homotopy analysis technique for the solution of nonlinear problems, Ph.D. thesis, Shanghai Jiao Tong University, 1992.

[96] Liao S. J., Beyond perturbation: Introduction to the Homotopy Analysis Method. CRC Press 2003.

[97] Liao S.J., *Homotopy analysis method in nonlinear differential equations.* Beijing: Higher education press, 2012.

[98] Liao S. J., "Notes on the homotopy analysis method: some definitions and theorems". Communications in Nonlinear Science and Numerical Simulation 14, no. 4 (2009): 983-997.

[99] Abbasbandy, S., Shivanian E., and Vajravelu K., "Mathematical properties of $\hbar$-curve in the frame work of the homotopy analysis method". Communications in Nonlinear Science and Numerical Simulation 16, no. 11 (2011): 4268-4275.

[100] Abbasbandy S., and Jalili M., "Determination of optimal convergence-control parameter value in homotopy analysis method". Numerical Algorithms 64, no. 4 (2013): 593-605.

[101] Robert A. V. G., and Vajravelu K., "On the selection of auxiliary functions, operators, and convergence control parameters in the application of the homotopy analysis method to nonlinear differential equations: a general approach". Communications in Nonlinear Science and Numerical Simulation 14, no. 12 (2009): 4078-4089.

[102] Ramazannia T. S. J., and Saeidian J., "Comments on "RA Van Gorder and K. Vajravelu, Commun. Nonlinear Sci. Numer. Simul. 14 (2009) 4078-4089"."Communications in Nonlinear Science and Numerical Simulations 17 (2012): 1085-1088.

[103] Odibat Z. M., "A study on the convergence of homotopy analysis method". Applied Mathematics and Computation 217, no. 2 (2010): 782-789.

[104] Ahmadi G., "Self-similar solution of incompressible micropolar boundary layer flow over a semi-infinite plate ". International Journal of Engineering Science 14, no. 7 (1976): 639–646.

[105] Bhattacharyya K., Swati M., Layek G. C., and Pop I., "Effects of thermal radiation on micropolar fluid flow and heat transfer over a porous shrinking

sheet ". International Journal of Heat and Mass Transfer 55, no. 11-12 (2012): 2945-2952.

[106] Ramesh Chand, Rana G. C., and Ahmed Hussein, "Effect of suspended particles on the onset of thermal convection in a nanofluid layer for more realistic boundary conditions". International Journal of Fluid Mechanics Research 42, no. 5 (2015): 375–390.

[107] Narahari M., and Kamran M., "MHD natural convection flow past an impulsively started infinite vertical porous plate with Newtonian heating in the presence of radiation ". International Journal of Numerical Methods for Heat & Fluid Flow 26, no. 6 (2016): 1932–1953.

[108] Siddiqui, A. M., Irum S., and Ansari A. R., "Unsteady squeezing flow of a viscous MHD fluid between parallel plates, a solution using the homotopy perturbation method". Mathematical Modelling and Analysis 13, no. 4 (2008): 565-576.

[109] Brewster M. Q., Thermal radiative transfer and properties. John Wiley & Sons 1992.

[110] Pop I., and Watanabe T., "Hall effects on magnetohydrodynamic free convection about a semi-infinite vertical flat plate". International Journal of Engineering Science 32, no. 12 (1994): 1903-1911.

[111] Sutton G.W., and Sherman A., *Engineering Magnetohydrodynamics* (McGraw-Hill, New York, 1965).

[112] Hughes W., John B., and Nicholas W., *Schaum's Outline of Fluid Dynamics* (McGraw Hill, 1999).

[113] Shampine L.F., Gladwell I., and Thompson S., Solving ODEs with MATLAB, (Cambridge University Press, 2003).

[114] Shampine L.F., Reichelt M.W., and Kierzenka J., Solving boundary value problems for ordinary differential equations in Matlab with bvp4c, 2010. https://de.mathworks.com/help/matlab/ref/bvp4c.html